ISSN: 2153-1196 Volume 10, Number 7, June 2019

Scientific Research Publishing

Journal of Modern Physics

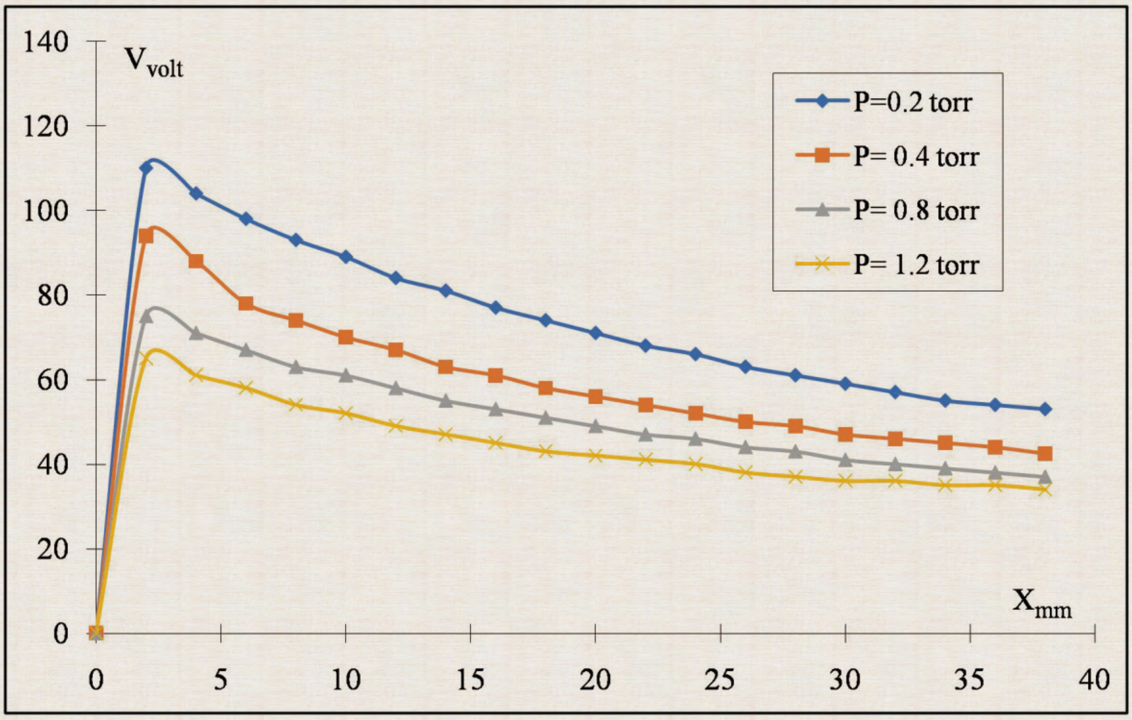

ISSN: 2153-1196

www.scirp.org/journal/jmp

Journal Editorial Board

ISSN: 2153-1196 (Print) ISSN: 2153-120X (Online)
http://www.scirp.org/journal/jmp

Journal of Modern Physics, 2019, 10, 687-880
http://www.scirp.org/journal/jmp
ISSN Online: 2153-120X
ISSN Print: 2153-1196

Table of Contents

Volume 10 Number 7 June 2019

The figure on the front cover is from the article published in Journal of Modern Physics, 2019, Vol. 10, No. 7, pp. 699-716 by Ahmed Rida Galaly, Guido Van Oost.

Journal of Modern Physics (JMP)
Journal Information

SUBSCRIPTIONS

The *Journal of Modern Physics* (Online at Scientific Research Publishing, www.SciRP.org) is published monthly by Scientific Research Publishing, Inc., USA.

Subscription rates:
Print: $89 per issue.
To subscribe, please contact Journals Subscriptions Department, E-mail: sub@scirp.org

SERVICES

Advertisements
Advertisement Sales Department, E-mail: service@scirp.org

Reprints (minimum quantity 100 copies)
Reprints Co-ordinator, Scientific Research Publishing, Inc., USA.
E-mail: sub@scirp.org

COPYRIGHT

PRODUCTION INFORMATION

For manuscripts that have been accepted for publication, please contact:
E-mail: jmp@scirp.org

Journal of Modern Physics, 2019, 10, 687-698
http://www.scirp.org/journal/jmp
ISSN Online: 2153-120X
ISSN Print: 2153-1196

Statistical Induced Dynamic of Self-Gravitating System

B. I. Lev

Bogolyubov Institute for Theoretical Physics, NAS of Ukraine, Metrolohichna, Ukraine
Email: bohdan.lev@gmail.com

How to cite this paper: Lev, B.I. (2019) Statistical Induced Dynamic of Self-Gravitating System. *Journal of Modern Physics*, **10**, 687-698.
https://doi.org/10.4236/jmp.2019.107049

Received: April 29, 2019
Accepted: June 3, 2019
Published: June 6, 2019

Abstract

The self-gravitating systems *a priory* are non-equilibrium. The new approach, based on non-equilibrium statistical operator, which allows taking into account inhomogeneous distribution of particles and temperature, has been proposed. Such method employs a saddle point procedure to find dominant contributions to the partition function and permits to obtain all thermodynamic parameters of the system. Statistical induced dynamic and behavioral peculiarities of self-gravitating systems for different conditions have been predicted.

Keywords

Nonequilibrium Statistical Operator, Self-Gravitating System, Inhomogeneous

1. Introduction

The statistical description of a system of interacting particles has a fundamental physical interest. In that context, the interacting system provides a model of fundamental interest for which ideas of statistical mechanics and thermodynamics can be tested and developed. For self-gravitating system the thermodynamical ensemble can be nonequivalent [1] [2]. In particular, since energy is not-additive, and cannot use the canonical ensemble to study the system with long-range interaction. Since equilibrium states are only local entropy maximum.

Two type approaches (statistical and thermodynamic) have been developed to determine the equilibrium states of the interacting system and describe possible phase transition. It is generally believed that mean field theory is exact for systems. Since in mean field theory any thermodynamical function depends on the thermodynamical variables only through the dimensionless combinations and the system is thermodynamically stable but the thermodynamical limit does exist [3].

Formation of the spatially inhomogeneous distribution of interaction particles is a typical problem in condensed matter physics and requires non-conventional methods of the statistical description of the system tailored to gravitational interacting particles with regard for an arbitrary spatially inhomogeneous particles distribution. Statistical description must employ the procedure to find dominant contributions to the partition function and to avoid entropy divergences for infinite system volume. Formation of the inhomogeneous distribution of interaction particles requires a non-conventional method, which was proposal in [4] [5] [6] [7] [8]. This method is based on Hubbard-Stratonovich representation of statistical sum [9] which is now extended and applied to the self-gravitating system to find solution for particles distribution without using spatial box restrictions. It is important that this solution has no divergences in thermodynamic limits. For this goal using the saddle point approximation took into account the conservation number of particles in limiting space and provided to nonlinear equation. The partition function in the case of homogeneous distribution of the particles, and in case of inhomogeneous distribution was obtained in [5] [6] [10], but in this approach described only condition in the formation of the possible inhomogeneous distribution of the interacting particles.

Systems with long-range interactions, such as self-gravitating system do not relax to the usual Boltzmann-Gibbs thermodynamic equilibrium, but become trapped in quasi-stationary states, the lifetime of which diverges with the number of particles. The instability threshold was predicted for spontaneous symmetry breaking for a class of d-dimensional systems [11]. Non-equilibrium stationary states of systems were described in article [12] where concluded that three-dimensional systems do not evolve to thermodynamic equilibrium but trap in non-equilibrium quasi-stationary states.

Mostly due to the fact that self-gravitating system exist in a states that far from equilibrium and the relaxation time to equilibrium state is very long. The homogeneous particle distribution in a self-gravitating system is not stable. The particles distribution in such a system is inhomogeneous in space, from the beginning. There is standardized behavior of the interacting system, it is described differently for different equilibrium ensembles. That approach does not seem to be very consistent, due to the fact that, the state equation has to come from the definition of partition function, but the definition of it is unknown for the space inhomogeneous systems [13] [14]. Therefore, there is a dilemma, either to take the postulates of equilibrium statistical mechanics to obtain only instability criteria or not to try to account for the space in homogeneity using different approach. Such inhomogeneous distribution of the particles, temperature and chemical potential can be accounted for in non-equilibrium statistical operator approach [15], where possibility of local change of thermodynamic parameters is included. This system is non-equilibrium and inhomogeneous distribution of particle can motivate the inhomogeneous distribution of temperature and chemical potential and other thermodynamic parameter.

In this article are proposed the new approach, based on non-equilibrium statistic operator [15], which are more suitable for the description of a self-gravitating systems. The equation of state and all thermodynamic characteristics needed are defined by the equations which contribute the most to the partition function. Therefore, there is no need to introduce additional hypothesis about temperature on density dependence. This dependence is an outcome of solving corresponding thermodynamic relations, which describe extreme of non-equilibrium partition function. The possible space inhomogeneous distributions of particles and temperature have been obtained for the simple cases. For the equilibrium case the well-known result [16] [17] of partition function has been reproduced. Has been shown, that used this approach can describe inhomogeneous distribution of particle and determine necessary parameter in the self -gravitating system. The main idea of this paper is to provide a possible detailed description of self -gravitating system based on the principles of non-equilibrium statistical mechanics and obtain possible distribution particle by fixed number of particle and energy of the system. After that we can determine the dynamic of self -gravitating system which induced the statistical principles and low increasing the entropy in the case existence the thermodynamic limit.

2. Nonequilibrium Statistical Operator

Phenomenological thermodynamic based on the conservation lows for average value of physical parameter as number of particles, energy and impulse. Statistical thermodynamic non-equilibrium system based too on conservation lows not the average value dynamic variables but in particular for this dynamic variable. It present local conservation lows for dynamic variables. For the determination thermodynamic function of non- equilibrium system are teed use the presentation of corresponding statistical ensembles which take into account the non-equilibrium states of this systems. The conception of Gibbs ensembles can brings to description non-equilibrium stationary states of system. In this case can determine non-equilibrium ensemble as totality of system which be contained in same stationary external action. This system has same character of contact with thermostat and possess all possible value macroscopic parameters which compatibility present conditions. In system, which are in same stationary external condition will are formed local equilibrium stationary distribution. If external condition will be depend from time that local equilibrium distribution are not stationary. For exactly determination local equilibrium ensemble must accordingly determine the distribution function or statistical operator of the system [15], finally, can recall that the stable states on the series of equilibrium of classical self-gravitating particles are only metastable because they correspond to local maximal of entropy from which can determine behavior of the system.

If assume that non-equilibrium states of system can determine through inhomogeneous distribution energy $H(\boldsymbol{r})$ and number of particles (density) $n(\boldsymbol{r})$ the local equilibrium distribution function for classical system can write in the form [15]:

$$f_l = Q_l^{-1}\exp\left\{-\int\left(\beta(\boldsymbol{r})H(\boldsymbol{r})-\eta(\boldsymbol{r})n(\boldsymbol{r})\right)\mathrm{d}\boldsymbol{r}\right\} \tag{1}$$

where

$$Q_l = \int D\Gamma\exp\left\{-\int\left(\beta(\boldsymbol{r})H(\boldsymbol{r})-\eta(\boldsymbol{r})n(\boldsymbol{r})\right)\mathrm{d}\boldsymbol{r}\right\} \tag{2}$$

present determination of statistical operator local equilibrium distribution. The integration in present formula must take over all phase space of system. Must note, that in the case local equilibrium distribution Lagrange multipliers $\beta(\boldsymbol{r})$ and $\eta(\boldsymbol{r})$ are function of spatial point. The microscopic density of particles can present in standard form:

$$n(\boldsymbol{r}) = \sum_i \delta(\boldsymbol{r}-\boldsymbol{r}_i) \tag{3}$$

The introduction local equilibrium distribution are possible if relaxation time in all system is more as relaxation time on local macroscopically area as part of this system.

After determination of non-equilibrium statistical operator can obtain all thermodynamic parameter non-equilibrium system. For this can determine thermodynamic relation for inhomogeneous systems. The variation of statistical operator by Lagrange multipliers can write necessary thermodynamic relation in the form [15]: $-\frac{\delta\ln Q_l}{\delta\beta(\boldsymbol{r})} = \langle H(\boldsymbol{r})\rangle_l$ and $\frac{\delta\ln Q_l}{\delta\eta(\boldsymbol{r})} = \langle n(\boldsymbol{r})\rangle_l$. This relation is natural general prolongation well-known relation which take place in the case equilibrium systems, on the case inhomogeneous system. The conservation number of particles and energy in system can present in form natural relations $\int n(\boldsymbol{r})\mathrm{d}\boldsymbol{r} = N$ and $\int H(\boldsymbol{r})\mathrm{d}\boldsymbol{r} = E$

For further statistical description of non-equilibrium system is necessary determine Hamiltonian of system. In general case Hamiltonian of system interacting particle can present as:

$$H = \sum_i \frac{p_i^2}{2m} - \frac{1}{2}\sum_{i,j} W(\boldsymbol{r}_i\boldsymbol{r}_j) \tag{4}$$

where $W(\boldsymbol{r}_i\boldsymbol{r}_j)$ determine the attractive interaction energy. Further will be use only density of energy which for self-gravitating system can write in the following form:

$$H(\boldsymbol{r}) = \frac{p^2(\boldsymbol{r})}{2m}n(\boldsymbol{r}) - \frac{1}{2}\int W(\boldsymbol{r},\boldsymbol{r}')n(\boldsymbol{r})n(\boldsymbol{r}')\mathrm{d}\boldsymbol{r}' \tag{5}$$

This density energy of a system is possible to use if we smash to equal bits all space with equal mass and consider moving in phase space not compressed gravitational fluid. In our case interacting system can write are non-equilibrium statistical operator in the form:

$$Q_l = \int D\Gamma\exp\left\{-\int\left(\beta(\boldsymbol{r})\frac{p^2(\boldsymbol{r})}{2m}-\eta(\boldsymbol{r})\right)n(\boldsymbol{r})\mathrm{d}\boldsymbol{r} + \frac{1}{2}\int\beta(\boldsymbol{r})W(\boldsymbol{r},\boldsymbol{r}')n(\boldsymbol{r})n(\boldsymbol{r}')\right\} \tag{6}$$

The integration over phase space can present as $D\Gamma = \frac{1}{(2\pi\hbar)^3}\prod_i \mathrm{d}r_i \mathrm{d}p_i$.

In order to perform a formal integration in second part of this presentation, additional field variables can be introduced making use of the theory of Gaussian integrals [8] [9]:

$$\exp\left\{-\frac{\nu^2}{2}\int \beta(\boldsymbol{r})\omega(\boldsymbol{r},\boldsymbol{r}')n(\boldsymbol{r})n(\boldsymbol{r}')\mathrm{d}\boldsymbol{r}\mathrm{d}\boldsymbol{r}'\right\}$$
$$= \int D\sigma \exp\left\{-\frac{\nu^2}{2}\int(\beta(\boldsymbol{r})\omega(\boldsymbol{r}))^{-1}\sigma(\boldsymbol{r})\sigma(\boldsymbol{r}')\mathrm{d}\boldsymbol{r}\mathrm{d}\boldsymbol{r}' - \nu\int\sqrt{\beta(\boldsymbol{r})}\sigma(\boldsymbol{r})n(\boldsymbol{r})\mathrm{d}\boldsymbol{r}\right\} \tag{7}$$

where $D\sigma = \frac{\prod_s \mathrm{d}\sigma_s}{\sqrt{\det 2\pi\beta\omega(\boldsymbol{r},\boldsymbol{r}')}}$ and $\omega^{-1}(\boldsymbol{r},\boldsymbol{r}')$ is the inverse operator which satisfies the condition $\omega^{-1}(\boldsymbol{r},\boldsymbol{r}')\omega(\boldsymbol{r}',\boldsymbol{r}'') = \delta(\boldsymbol{r}-\boldsymbol{r}'')$, that means: the interaction energy presented the Green function for this operator and $\nu^2 = \pm 1$ depending on the sign of the interaction or the potential energy. After present manipulation the field variable $\sigma(\boldsymbol{r})$ contains the same information as original distribution function, *i.e.* all information about possible spatial states of the systems.

After this manipulation the statistical operator can rewrite in the form:

$$Q_l = \int D\Gamma \int D\psi \exp\left\{-\int\left(\beta(\boldsymbol{r})\frac{p^2(\boldsymbol{r})}{2m} - \eta(\boldsymbol{r}) - \sqrt{\beta(\boldsymbol{r})}\psi(\boldsymbol{r})\right)n(\boldsymbol{r})\mathrm{d}\boldsymbol{r}\right\}Q_{int} \tag{8}$$

where part which cam from interaction

$$Q_{int} = \exp\left\{-\frac{1}{2}\int(\beta(\boldsymbol{r})W(\boldsymbol{r},\boldsymbol{r}'))^{-1}\psi(\boldsymbol{r})\psi(\boldsymbol{r}')\mathrm{d}\boldsymbol{r}\mathrm{d}\boldsymbol{r}'\right\} \tag{9}$$

In this general functional integral can be provide the integration on phase space. If use the definition of density we can rewrite the non-equilibrium statistical operator as:

$$Q_l = \int D\psi \int \frac{1}{(2\pi\hbar)^3 N!}\prod_i \mathrm{d}r_i \mathrm{d}p_i \xi(\boldsymbol{r}_i)\exp\left\{-\left(\beta(\boldsymbol{r}_i)\frac{p_i^2}{2m} - \sqrt{\beta(\boldsymbol{r}_i)}\psi(\boldsymbol{r}_i)\right)\right\}Q_{int} \tag{10}$$

where introduce the new variable $\xi(\boldsymbol{r}) \equiv \exp\eta(\boldsymbol{r})$ which can interpreter as chemical activity. Now can make integration over impulse. Real part of non-equilibrium statistical operator take the form:

$$Q_l = \int D\varphi \int D\psi Q_{int}\frac{1}{N!}\prod_i \int \mathrm{d}r_i \xi(\boldsymbol{r}_i)\left(\frac{2\pi m}{\hbar^3\beta(\boldsymbol{r}_i)}\right)^{\frac{3}{2}}\exp\left(\sqrt{\beta(\boldsymbol{r}_i)}\psi(\boldsymbol{r}_i)\right) \tag{11}$$

$$Q_l = \int D\varphi \int D\psi Q_{int}\sum_N \frac{1}{N!}\left(\int \mathrm{d}\boldsymbol{r}\xi(\boldsymbol{r})\left(\frac{2\pi m}{\hbar^3\beta(\boldsymbol{r})}\right)^{\frac{3}{2}}\exp\left(\sqrt{\beta(\boldsymbol{r})}\psi(\boldsymbol{r})\right)\right)^N \tag{12}$$

After that the non-equilibrium statistical operator take the simple form:

$$Q_l = \int D\varphi \int D\psi Q_{int} \exp\left\{ \int \left[\xi(\boldsymbol{r}) \left(\frac{2\pi m}{\hbar^3 \beta(\boldsymbol{r})} \right)^{\frac{3}{2}} \exp \sqrt{\beta(r)} \psi(\boldsymbol{r}) \right] \mathrm{d}\boldsymbol{r} \right\} \tag{13}$$

In definition Q_{int} are the reverse operator of interaction energy. For further description we must determine this inverse operator. For general case of long range interaction as Coulomb like or Newtonian gravitational interaction in continuum limit should be treated in the operator sense, *i.e.*

$$W^{-1}(\boldsymbol{r}, \boldsymbol{r}') = -\frac{1}{4\pi G m^2} \Delta_{\boldsymbol{r}} \delta(\boldsymbol{r} - \boldsymbol{r}') \tag{14}$$

where Δ_r is Laplace operator in real space. Gravitation interaction energy in three dimensional case can write in well-known form

$$W(\boldsymbol{r}, \boldsymbol{r}') = \frac{G m^2}{|\boldsymbol{r} - \boldsymbol{r}'|} \tag{15}$$

G is gravitational constant and m is mass of separate area. For long range interaction between particle we can rewrite the non-equilibrium statistical operator in the form:

$$Q_l = \int D\psi \exp - \left\{ \int \left[\frac{1}{2 r_\psi} \left[(\nabla \psi)^2 \right] - \xi \Lambda^{-3} \exp \sqrt{\beta} \psi \right] \mathrm{d}\boldsymbol{r} \right\} \tag{16}$$

where all function β, φ, ψ are dependence from spatial point. In this presentation was using the definition thermal de-Broglie wavelength and definition of interaction length as

$$\Lambda^{-1}(\boldsymbol{r}) = \left(\frac{2m}{\hbar^2 \beta(\boldsymbol{r})} \right), r_\psi(\boldsymbol{r}) = 4\pi G m^2 \beta(r), \tag{17}$$

In general case the non-equilibrium statistical operator can rewrite in the form:

$$Q_l = \int D\psi \exp\left\{ -S(\psi(\boldsymbol{r}), \xi(\boldsymbol{r}), \beta(\boldsymbol{r})) \right\} \tag{18}$$

where effective non-equilibrium "local entropy" take the form:

$$S = \int \left[\frac{1}{2 r_\psi} (\nabla \psi(\boldsymbol{r}))^2 - \xi(\boldsymbol{r}) \Lambda^{-3} \exp \sqrt{\beta(r)} \psi(\boldsymbol{r}) \right] \mathrm{d}\boldsymbol{r} \tag{19}$$

The statistical operator allows obtain use the of efficient methods developed in the quantum field theory without imposing additional restrictions of integration over field variables or the perturbation theory. The functional $S(\varphi(\boldsymbol{r}), \xi(\boldsymbol{r}), \beta(r))$ depends on the distribution of the field variables $\varphi(\boldsymbol{r})$, the chemical activity $\xi(\boldsymbol{r})$ and inverse temperature $\beta(\boldsymbol{r})$. The saddle point method can now be further employed to find the asymptotic value of the statistical operator Q_l for increasing number of particles N to ∞. The dominant contribution is given by the states which satisfy the extreme condition for the functional. It's easy to see that saddle point equation present thermodynamic relation and it can write in the other form as: equation for field variable $\frac{\delta S}{\delta\psi(\boldsymbol{r})}=0$ for the normalization condition $\frac{\delta S}{\delta(\eta(\boldsymbol{r}))}=-\int\frac{\delta S}{\delta(\xi(\boldsymbol{r}))}\xi(\boldsymbol{r})\mathrm{d}\boldsymbol{r}=N$ and for the conservation the energy of the system $-\int\frac{\delta S}{\delta(\beta(\boldsymbol{r}))}\xi(\boldsymbol{r})\mathrm{d}\boldsymbol{r}=E$ Solution of this equation fully determine all thermodynamic parameter and describe general behavior of interacting system, whether this distribution of particles is spatially inhomogeneous or not. The above set of equations in principle solves the many-particle problem in thermodynamic limit. The spatially inhomogeneous solution of this equations correspondent the distribution of the interacting particles. Such inhomogeneous behavior is associated with the nature and intensity of the interaction. In other words, accumulation of particles in a finite spatial region (formation of a cluster) reflects the spatial distribution of the fields, the activity and temperature. Very important note, that only in this approach can take into account the inhomogeneous distribution temperature, which can depend from spatial distribution of particle in system.

3. Saddle-Point Equation for Self-Gravitating System

The solution of saddle-point equation completely determines all the thermodynamic parameters and describes the general behavior of a self-gravitating system both for spatially homogeneous and inhomogeneous particle distributions. The above set of equations in principle solves the many-particle problem in the thermodynamic limit. The spatially inhomogeneous solution of these equations corresponds to the distribution of the interacting particles. Such inhomogeneous behavior is associated with the nature and intensity of the interaction. In other words, accumulation of the particles in a finite spatial region (cluster formation) reflects the spatial distribution of the field, activity, and temperature. It is very important to note that only this approach makes it possible to take into account the inhomogeneity of temperature distribution that may depend on the spatial distribution of the particles in the system. In other approaches [2] the dependence of the temperature on a spatial point is introduced through the polytrophic dependence of temperature on particle density in the equation of state [18]. In the present approach, such dependence follows from the necessary thermodynamic condition, and can be found for various particle distributions. Now we derive the saddle-point equation for the extreme of the local entropy functional $S(\psi,\xi,\beta)$. The equation for the field variable $\frac{\delta S}{\delta\psi}=0$ in the case $\lambda=0$ and absent repulsive interaction $\varphi=0$ yields.

$$\frac{1}{r_m}\Delta\psi(\boldsymbol{r})+\xi(\boldsymbol{r})\left(\frac{2\pi m}{\hbar^2\beta(\boldsymbol{r})}\right)^{\frac{3}{2}}\sqrt{\beta(r)}\exp\left(\sqrt{\beta(r)}\psi(\boldsymbol{r})\right)=0, \tag{20}$$

where the notation $r_m\equiv 4\pi Gm^2$ is introduced. The normalization condition may be written as

$$\int \xi(\boldsymbol{r})\left(\frac{2m}{\hbar^2\beta(\boldsymbol{r})}\right)^{\frac{3}{2}} \exp\left(\sqrt{\beta(r)}\psi(\boldsymbol{r})\right)\mathrm{d}\boldsymbol{r} = N \tag{21}$$

and the equation for the energy conservation in the system is given by

$$\frac{1}{2}\int\left(\frac{2\pi m}{\hbar^2\beta(\boldsymbol{r})}\right)^{\frac{3}{2}} \frac{\xi(\boldsymbol{r})}{\beta(\boldsymbol{r})}\left(3-\sqrt{\beta(r)}\psi(\boldsymbol{r})\right)\exp\left(\sqrt{\beta(r)}\psi(\boldsymbol{r})\right)\mathrm{d}\boldsymbol{r} = E. \tag{22}$$

To draw more information on the behavior of a self-gravitating system, we introduce new variables. The normalization condition $\int \rho(\boldsymbol{r})\mathrm{d}\boldsymbol{r} = N$ yields the definition for the density function, *i.e.*,

$$\rho(\boldsymbol{r}) \equiv \left(\frac{2\pi m}{\hbar^2\beta(\boldsymbol{r})}\right)^{\frac{3}{2}} \xi(\boldsymbol{r})\exp\left(\sqrt{\beta(r)}\psi(\boldsymbol{r})\right), \tag{23}$$

which reduces the equations to a simpler form. The equation for the field variable is given by

$$\Delta\psi(\boldsymbol{r}) + r_m\sqrt{\beta(\boldsymbol{r})}\rho(\boldsymbol{r}) = 0. \tag{24}$$

In the case constant temperature and chemical activity, this equation transform into an equation for gravitational potential $\psi = \sqrt{\beta(\boldsymbol{r})}\psi$ in the well-known form:

$$\Delta\psi(\boldsymbol{r}) = -4\pi G m^2 \beta\rho(\boldsymbol{r}). \tag{25}$$

The equation for energy conservation takes the form

$$\frac{1}{2}\int \frac{\rho(\boldsymbol{r})}{\beta(\boldsymbol{r})}\left(3-\sqrt{\beta(r)}\psi(\boldsymbol{r})\right)\mathrm{d}\boldsymbol{r} = E. \tag{26}$$

Hereinafter we obtain the chemical activity in terms of chemical potential $\xi(\boldsymbol{r}) = \exp\left(\mu(\boldsymbol{r})\beta(\boldsymbol{r})\right)$. Having differentiated the equation for energy conservation over the volume, we obtain interesting relation for the chemical potential

$$\frac{1}{2}\frac{\rho(\boldsymbol{r})}{\beta(\boldsymbol{r})}\left(3-\sqrt{\beta(r)}\psi(\boldsymbol{r})\right) = \frac{\delta E}{\delta V}\frac{\delta V}{\delta N} = \mu(\boldsymbol{r})\rho(\boldsymbol{r}), \tag{27}$$

which yields the chemical potential to be given by

$$\mu(\boldsymbol{r})\beta(\boldsymbol{r}) = \frac{3}{2} - \frac{1}{2}\sqrt{\beta(r)}\psi(\boldsymbol{r}). \tag{28}$$

and the equation for the energy conservation reduces to very simple form: $\int \rho(\boldsymbol{r})\mu(\boldsymbol{r}) = E$. The equation thus obtained cannot be solved in the general case, but it is possible to analyze many cases of the behavior of a self-gravitating system under various external conditions. Within the context of the expression for density, and the definition of reduced thermal de-Broglie wavelength, and the gravitation length, *i.e.*,

$$\Lambda(\boldsymbol{r}) = \left(\frac{\hbar^2\beta(\boldsymbol{r})}{2me}\right)^{\frac{1}{2}}, R_g(\boldsymbol{r}) = 2\pi G m^2 \beta(\boldsymbol{r}), \tag{29}$$

we can rewrite all the equations and the normalization condition in terms of density and temperature. Thus we have general equation in the term of concentration and temperature in the form:

$$\Delta\left(\frac{\ln\left(\Lambda^3(\boldsymbol{r})\rho(\boldsymbol{r})\right)}{\sqrt{\beta(\boldsymbol{r})}}\right)+\frac{R_g(\boldsymbol{r})}{\sqrt{\beta(\boldsymbol{r})}}\rho(\boldsymbol{r})=0. \tag{30}$$

The chemical potential reduces to

$$\mu(\boldsymbol{r})\beta(\boldsymbol{r})=\frac{3}{2}-\ln\left(\Lambda^3(\boldsymbol{r})\rho(\boldsymbol{r})\right). \tag{31}$$

In this way we can obtain the equation of state for self-gravitating system if we use the thermodynamic relation for conservation energy E,

$$P=-\frac{1}{\beta}\frac{\delta S}{\delta V}. \tag{32}$$

Using the definition of the density of particles, one can obtain the local entropy in the form

$$S=\int\left[-\rho(\boldsymbol{r})\ln\left(\Lambda^3(\boldsymbol{r})\rho(\boldsymbol{r})\right)-\rho(\boldsymbol{r})\right]\mathrm{d}\boldsymbol{r}, \tag{33}$$

from which the local equation of state can present as

$$P(\boldsymbol{r})\beta(\boldsymbol{r})=\rho(\boldsymbol{r})\left(1-\ln\left(\Lambda^3(\boldsymbol{r})\rho(\boldsymbol{r})\right)\right)=\rho(\boldsymbol{r})\left(\mu(\boldsymbol{r})\beta(\boldsymbol{r})-\frac{1}{2}\right) \tag{34}$$

In general case this equation of state has a multiplier which logarithmically depends on the density of the particles. Only in the case $\Lambda^3(\boldsymbol{r})\rho(\boldsymbol{r})=1$ we obtain the equation of state for an ideal gas $P\beta\equiv\rho$. We have a sense to talk about pressure in classical cases only. If the concentration is large, and takes place the reverse relation $1\ll\Lambda^3(\boldsymbol{r})\rho(\boldsymbol{r})$, the determination of pressure are not correct. In the classical case $\Lambda^3(\boldsymbol{r})\rho(\boldsymbol{r})\ll 1$. As shown below there is a natural limit of our approach. We cannot describe the processes which can be realize within short distances since because in a system with large concentration quantum effects would take place. In the case of the ideal gas we obtain usual equation of state, because in this case $\varphi(\boldsymbol{r})=0$ and $P\beta=\rho$ as result absent of interaction. In the case on ideal gas $\mu(\boldsymbol{r})\beta(\boldsymbol{r})=\frac{3}{2}$ and equation of state reproduce to the equilibrium relation for the ideal gas. In this case the energy of the system $E=\frac{3}{2}NkT$ which corresponds to the previously obtained results [16] [17]. In the next section, we find the classical distributions of particles for various inner and external conditions.

4. Statistical Induced Dynamic for Self-Gravitating System

In system not far from equilibrium, patterns may form as results of the competition long-range interactions operating of different length scales [19]. The latter is countered by a long range gravitation attractive interaction. This is often accompanied by the macroscopical separation transition which leads to spontaneous formation of patterns in ideally homogeneous system upon variation of control parameter. An important class of system with competing interaction is the system in which the long-range interaction is gravitational. The fundamental nature of the gravitational interaction makes this class of system extremely diverse. We stop on the point statistical induced dynamics of self-gravitating system taking into account the possible spatial distribution of particle. For this goal we must determine the dynamic equation for field variable or density of particle. In this sense we can use the Ginsburg-Landau equation for density

$$\frac{\partial\rho(\boldsymbol{r},t)}{\partial t}=-\nabla^{2}\gamma\frac{\delta S}{\delta\rho(\boldsymbol{r})},\tag{35}$$

where γ is dynamic gravitational viscous coefficient [20]. In self-gravitating system we have not any other viscous process without dynamic influence of gravitational action, all systems on local spatial point. This evolution equation is, in fact applicable to a number of systems with non-conserved order parameter. Taking into account the presentation of local entropy in the terms of density, we can write the dynamic equation for density in the form:

$$\frac{\partial\rho(\boldsymbol{r},t)}{\partial t}=-\nabla^{2}\gamma\ln\left(\Lambda^{3}(\boldsymbol{r})\rho(\boldsymbol{r},t)\right)\tag{36}$$

The evolution of patterns in non-equilibrium will generate to be guided by the local entropy landscape and the morphological instabilities of the parameter. The dynamic of the system is dissipative, it will result in decrease of the local entropy of the patterns with time. To mimic this behavior we can use the simple gradient, descent dynamic defined with chemical potential may be considered as generalization of Cahn equation for non-uniform system with an arbitrary concentration gradient which becomes Cahn nonlinear diffusion equation [21]:

$$\frac{\partial\rho(\boldsymbol{r},t)}{\partial t}=\nabla\gamma\nabla\beta\mu(\boldsymbol{r})=-\nabla^{2}\gamma\ln\left(\Lambda^{3}(\boldsymbol{r})\rho(\boldsymbol{r},t)\right)\tag{37}$$

which is fully equivalent previous dynamic equation in Ginsburg-Landau approach. If we take the solution of this dynamic equation in the form $\rho(\boldsymbol{r},t)=\exp(\gamma r_m t)\rho(\boldsymbol{r})$ the solution of problem reduces to solve the previous equation

$$\Delta\left(\ln\Lambda^{3}\rho(\boldsymbol{r})\right)+R_g\rho(\boldsymbol{r})=0\tag{38}$$

and can be transformed to

$$\Delta\left(\ln\rho(\boldsymbol{r})\right)+R_g\rho(\boldsymbol{r})=0.\tag{39}$$

for constant temperature, that means, the obtained spatial solution will be existed in all time increasing the density of particles. If we determine the possible structure in distribution of density, this pattern will be conserved in all-time decrease of density. In this approach [7], the probable behavior of a self-gravitating system can be predicted for any external conditions. On much longer timescales, an evolution towards the true thermal equilibrium is postulated. In this way we can solve the complicated problem of statistical description of self-gravitating systems. Moreover, this method can also be applied for the further development of the physics of self-gravitational and similar systems that are not far from the equilibrium.

Acknowledgements

The paper is prepared with the financial support of the National Academy of Sciences of Ukraine (the project "Dynamics of structure formation in many-particle systems") PK 0118U003535.

Conflicts of Interest

The author declares no conflicts of interest regarding the publication of this paper.

References

[1] Thirring, W. (1970) *Zeitschrift für Physik*, **235**, 339. https://doi.org/10.1007/BF01403177

[2] Chavanis, P.-H., Rosier, C. and Sire, C. (2002) *Physical Review E*, **66**, Article ID: 036105. https://doi.org/10.1103/PhysRevE.66.036105

[3] Laliena, V. (2003) *Nuclear Physics B*, **668**, 403. https://doi.org/10.1016/j.nuclphysb.2003.07.005

[4] Bilotsky, Y.D. and Lev, B.I. (1984) *Teoreticheskaya i Matematicheskaya Fizika*, **60**, 120.

[5] Lev, B.I. and Ya, A. (1998) *Physical Review E*, **57**, 6460-6469. https://doi.org/10.1103/PhysRevE.57.6460

[6] Lev, B.I. (2011) *International Journal of Modern Physics B*, **25**, 2237-2249. https://doi.org/10.1142/S0217979211100771

[7] Lev, S.B. and Lev, B.I. (2017) *The European Physical Journal B*, **90**, 3. https://doi.org/10.1140/epjb/e2016-70386-9

[8] Kleinert, H. (1989) Gauge Field in Condensed Matter. Word Scientific, Singapore.

[9] Stratonovich, R.L. (1958) *Sov. Phys. Dokl.*, 2, 416-419.

Hubbard, J. (1958) *Phys. Rev. Lett.*, 3, 77. https://doi.org/10.1103/PhysRevLett.3.77

[10] Grigorishin, K.V. and Lev, B.I. (2005) *Physical Review*, **71**, Article ID: 066105. https://doi.org/10.1103/PhysRevE.71.066105

[11] Pakter, R., Marcos, B. and Levin, Y. (2013) *Physical Review Letters*, **111**, Article ID: 230603. https://doi.org/10.1103/PhysRevLett.111.230603

[12] Benetti, F.P.C., Ribeiro-Teixeira, A.C., Pakter, R. and Levin, Y. (2014) *Physical Review Letters*, **113**, Article ID: 100602. https://doi.org/10.1103/PhysRevLett.113.100602

[13] Baxter, R. (1980) Exactly Solved Models in Statistical Mechanics. Academic Press, New York.

[14] Ruelle, D. (1969) Statistical Mechanics. Rigorous Results, New York, Amsterdam.

[15] Zubarev, D.N. (1974) Non-Equilibrium Statistical Thermodynamics. Consultants Bureau, New York.

[16] Huang, K. (1963) Statistical Mechanics. J. Wiley and Sons, New York.

[17] Isihara, A. (1971) Statistical Mechanics. State University of New York, New York.

[18] Sire, C. and Chavanis, P.-H. (2002) *Physical Review E*, **66**, Article ID: 046133. https://doi.org/10.1103/PhysRevE.66.046133

[19] Muratov, C.B. (2002) *Physical Review E*, **66**, Article ID: 066108. https://doi.org/10.1103/PhysRevE.66.066108

[20] Chandrasekhar, S. (1942) An Introduction to the Study of Stellar Structure. Dover Publications, New York.

[21] Onuki, A. (1989) *Journal of the Physical Society of Japan*, **58**, 3065-3068. https://doi.org/10.1143/JPSJ.58.3065

Journal of Modern Physics, 2019, 10, 699-716
http://www.scirp.org/journal/jmp
ISSN Online: 2153-120X
ISSN Print: 2153-1196

Comparison between Theoretical and Experimental Radial Electron Temperature Profiles in a Low Density Weakly Ionized Plasma

Ahmed Rida Galaly[1,2*], **Guido Van Oost**[3,4,5]

[1]Department of Physics, Faculty of Science, Beni-Suef University, Beni Suef, Egypt
[2]Department of Engineering Science, Faculty of Community, Umm Al_Qura University, Mecca, Mecca Province, KSA
[3]Department of Applied Physics, Ghent University, Technicum B4, Ghent, Belgium
[4]National Research Nuclear University "MEPHI", Moscow, Russia
[5]National Research University "Moscow Power Engineering Institute", Moscow, Russia
Email: *ahmed_galaly@yahoo.com

How to cite this paper: Galaly, A.R. and Van Oost, G. (2019) Comparison between Theoretical and Experimental Radial Electron Temperature Profiles in a Low Density Weakly Ionized Plasma. *Journal of Modern Physics*, **10**, 699-716.
https://doi.org/10.4236/jmp.2019.107050

Received: May 15, 2019
Accepted: June 11, 2019
Published: June 14, 2019

Abstract

Experimental and theoretical studies of the radial distribution function of the electron temperature (RDFT) in a low-density plasma and weakly ionized gas for the abnormal glow region are presented. Experimentally, the electron temperatures and densities are measured by a Langmuir probe moved radially from the center to the edge of the cathode electrode for helium gas at different pressures in the low-pressure glow discharge. The comparison of the final experimental data for the radial distribution of electron temperatures and densities for different low pressures ranging from 0.2 to 1.2 torr, with the final proved equation of RDFT confirms that the electron temperatures decrease with increasing product of radial distance and gas pressures, showing a radial decrement dependence of the electron temperature from the center to the edge of the electrode. This is attributed to the increase of the number of electron-atom collisions at higher gas pressures and consequently of the rate of ionization. For the axial distance (L) from the tip of the probe to cathode electrode and the cathode electrode radius (R), a theoretical and experimental comparison for the two conditions $L < R$ and $L > R$, for both cases the produced plasma temperatures decrease and densities increase. It is concluded that the RDFT accurately shows a dramatic decrease for $L < R$ by 60% less than RDFT values for $L > R$ similar as for conditions of magnetized and unmagnetized effect for DC plasma. This means that the rate of plasma loss by diffusion decreased for $L < R$, agrees well with the applied of magnetic field behavior.

Keywords

Radial Distribution, Electron Temperature, Ambipolar Diffusion, Low Pressure, Weakly Ionized Plasma

1. Introduction

Plasma is the fourth state of matter, considered to be a quasi-neutral medium. However, when a diagnostic such as probe (a small metallic electrode) is inserted into a weakly ionized plasma, a very thin sheath is formed around the conducting surface of the probe due to the redistribution of charges. The amplitude and the polarity of the probe potential control the motion of electrons and ions near the probe. When the probe potential is sufficiently negative, only the ions can reach the probe surface. The probe current is thus equal to the ion random current (I_{ri}) [1] [2] [3].

Ambipolar diffusion is the most important process taking place within a weakly ionized plasma and considered as a vital process for the distribution of the plasma parameters. Assuming a Maxwellian velocity distribution [4], the plasma parameters especially electron temperature and electron density can be determined from the current-voltage characteristic curves of the probe [5]. Diffusion phenomena occur in a plasma when a spatial gradient of the charged species is present [6]. Furthermore, it is caused by the differently charged species having different diffusivities, hence there is a loss of neutrality [7] due to plasma rapidly diffusion for some of charged species more than the others. Furthermore, a minor loss of neutrality, however, induces an ambipolar electric field which, if the Debye length is sufficiently small, slows down the fast-diffusing species and speeds up the slow-diffusing species in such a way that the plasma remains quasi-neutral [8].

The experimental and numerical radial distribution of electron temperature and density from the axis of the tube up to the tube wall have been amply investigated [9] [10], but not the theoretical derivation in terms of the effect of Schottky condition and ambipolar diffusion due to the recurrence relation of the Bessel condition.

In the present work, an experimental study of the radial dependence of the electron temperature in a low-density plasma using a single probe as diagnostic technique was performed. Theoretically, it was proven that the ambipolar diffusion is an important factor in the weakly-ionized gas. Furthermore, a theoretical physical model for the radial distribution of the temperature was derived. The theoretical considerations are compatible with the experimental data of the temperatures at different pressures in a low-pressure glow discharge of a DC (cold cathode) magnetron sputtering unit.

2. Experimental Study

2.1. Experimental Set-Up

Figure 1 shows the experimental setup of DC (cold cathode) magnetron sputtering unit to generate a glow discharge in a glass tube between two circular, parallel and movable metallic discs acting as electrodes. Two parallel electrodes made of aluminum, are enclosed in the discharge cell, one of the two electrodes is grounded represented cathode electrode and the other is movable to change the axial distance represented the anode electrode, where the axial distance (L) between tip of the probe and the cathode electrode, 5 cm and with 3 cm in radius (R) taking into account that we will deal with two conditions $R > L$ and $R < L$. The discharge unit is evacuated using a rotary pump to a base pressure of 7 mtorr. A pressure gauge is connected to the discharge tube to measure the inside gas pressure. A stationary DC-glow discharge was generated between two both electrodes, for different parameters as shown in **Table 1**.

Figure 1 also shows the schematic diagram of the spherical single Langmuir probe circuit. The probe made of molybdenum wire (diameter 3.0-mm and length 0.5 mm) and the tip of a probe is inside the glow discharge plasma. The single probe (between the cathode fixed at the ground potential, and the anode) move axially to measure the axial potential distribution between the two electrodes. Also, it moves radially from the center to the edge of the cathode electrode, and a potential V_P is applied to the probe.

2.2. Experimental Study of Axial Potential and Electric Field Distribution Measurements

The potential distribution was measured at discharge currents of 10 mA and gas pressure of (0.2 - 1.2 torr) for He as shown in **Figure 2**, shows that the potential

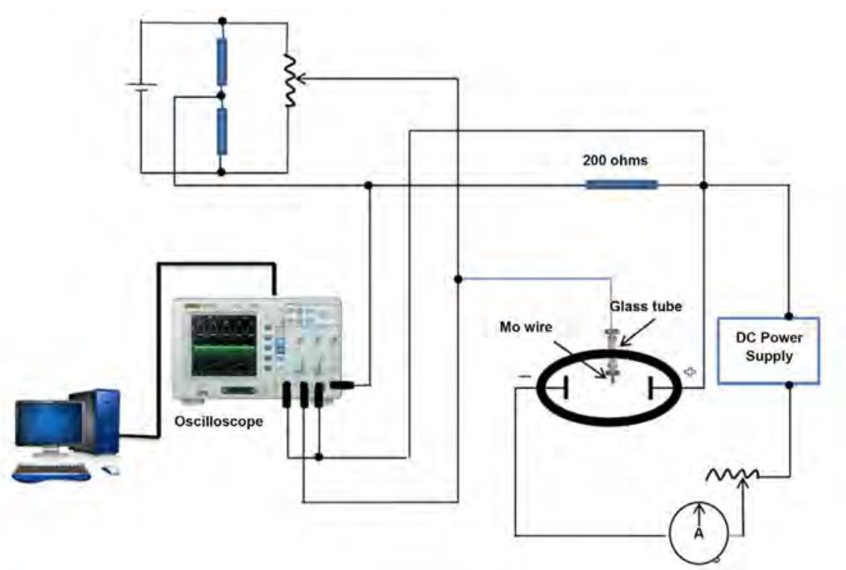

Figure 1. Schematic diagram of the experimental setup and the single Langmuir probe circuit.

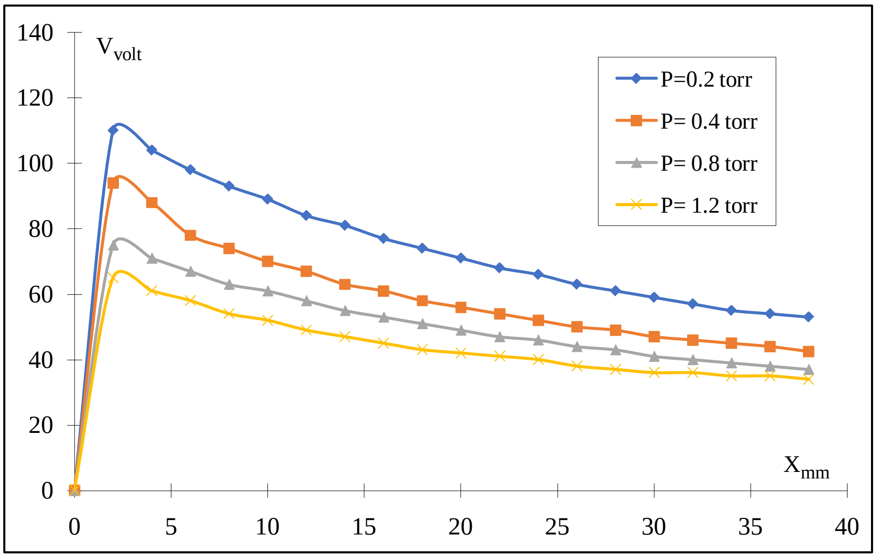

Figure 2. Axial potential distribution at constant current (I = 10 mA).

Table 1. Shows the values of operating parameters.

Parameters	Values
Discharge Current (I_a)	4 - 30 mA
Gas Pressure (P)	0.1 - 1.5 torr
Discharge Voltage (V_a)	200 - 1200 V DC
Current Density	2 - 15 mA/m^2
Working Gas	He

distribution can be divided into three regions. In region I (AB) (cathode fall), the potential increases sharply within a small discharge length. Whenever, gas breakdown takes place in the tube, a rapid growth in the rate of ionization, near the cathode is detected. Meanwhile the electrons transfer in the electric field much more faster than positive ions (due to their masses), electrons are swept rapidly towards the anode leaving a dense positive space charge near the cathode. Thus, the electric field is distorted and most of the applied potential is dropped across a narrow space in front of the cathode. Region II (BC) (negative glow) indicates that the potential decreases slightly and hence the electric field will be weak, since this region contains many free electrons. In region III (CD) (positive column), the potential distribution is nearly constant and linear since the positive and negative carriers densities are closely, equal. The positive column can be extended to any length to fill the remaining space between the end of the negative glow and the anode.

Values of the electric field distribution are obtained by differentiating the measured potential distribution of Figure 2. Figure 3 and Figure 4 show the electric field distribution for He discharge. In the cathode fall region at edge and center, high electric field is observed which is decreased sharply away from the

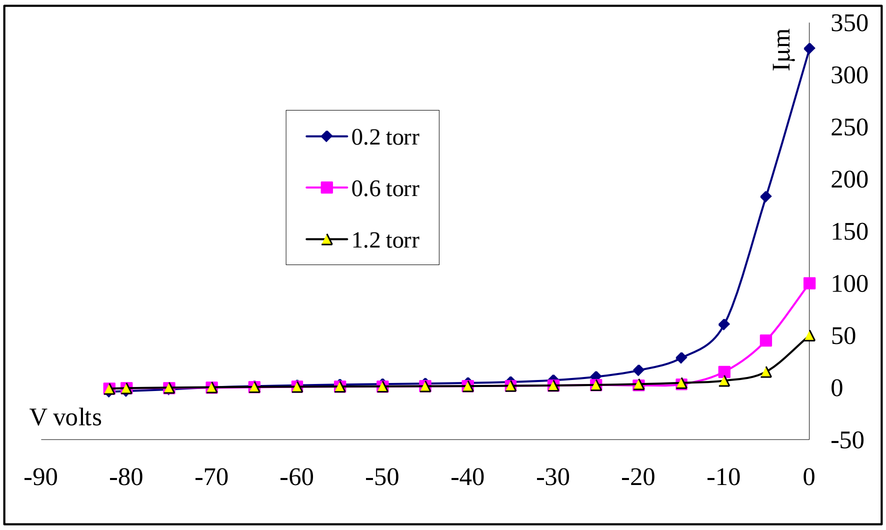

Figure 3. I-V curves of the single probe for cathode fall region at different He pressures at the edge.

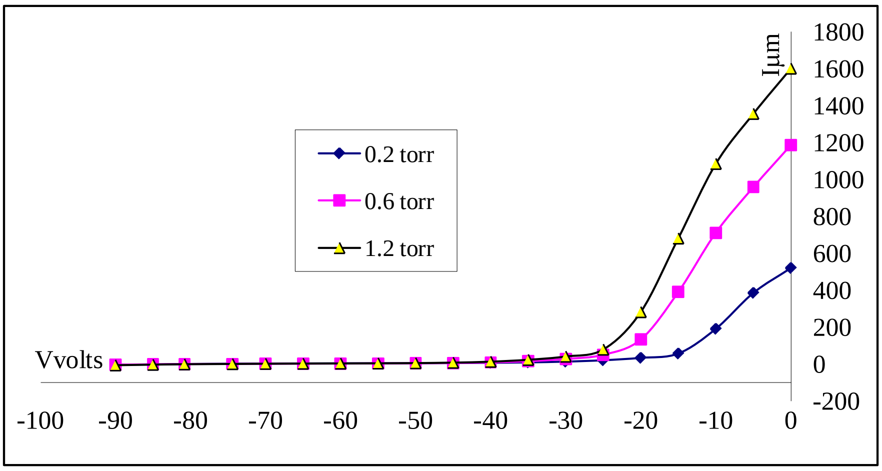

Figure 4. Measured I-V curves of the single probe for cathode fall region at different He pressures at the center.

cathode. This is related to the intense positive space charge which lies in front of the cathode. This acts as an accelerator for the electrons towards anode. Thus, the electrons emitted from the cathode are then accelerated away, until they reach the negative glow region where the electric field becomes weak (zero and sometimes it reaches a negative value). In this region, the gained kinetic energy of the electrons is dissipated in collisions with the atoms of the gas and thus secondary electrons would be produced. In the positive column region constant and linear electric field is needed to maintain discharge along the large length of the column which is required to carry the discharge current.

2.3. Experimental Study of Radial Dependence of the Electron Temperature

The region investigated in the present work is the abnormal region. The radial dependence of the electron temperature in low-density plasma at edge and center of the cathode electrode has been studied for different He pressures.

The plasma parameters like the electron temperature and electron density can be determined from the current-voltage (I-V) characteristic curve of the single Langmuir probe, based on the theory and the fundamental technique discussed in detail in many articles [10] [11].

Figure 3 and Figure 4 show I-V characteristic curves of the single probe at different He pressures at edge and center of the cathode electrode for the abnormal glow region [12]. The probe was moved to investigate the radial distribution from the center to the edge of the cathode, in the direction perpendicular to the direction of the electric field lines. Figure 5 and Figure 6 show the radial temperatures and densities distributions at different pressures from center to the edge. T_e is decreased and n_e increased due to the general trend that values of T_e and n_e are inversely proportional [13].

Increasing the helium working pressures from 0.2 to 1.2 torr, the temperature T_e decreases at the center from 9.7 eV to 5.5 eV and at the edge from 4.1 to 1.15 eV. Values of densities n_e increased at center n_e from 0.6×10^9 cm^{-3} to 1.3×10^9 cm^{-3} and at the edge from 2.5 to 3.95×10^9 cm^{-3}.

3. Theoretical Consideration of the Radial Dependence of the Electron Temperature

Conductivity at the tube axis, and charge density of plasma according to the following expression [14] [15]

$$D_s = D_a \left[1 - \mu_e \frac{\rho}{\sigma} \right] \tag{1}$$

where D_a is the ambipolar diffusion coefficient as follows:

The flow of ions and electrons are the same, hence

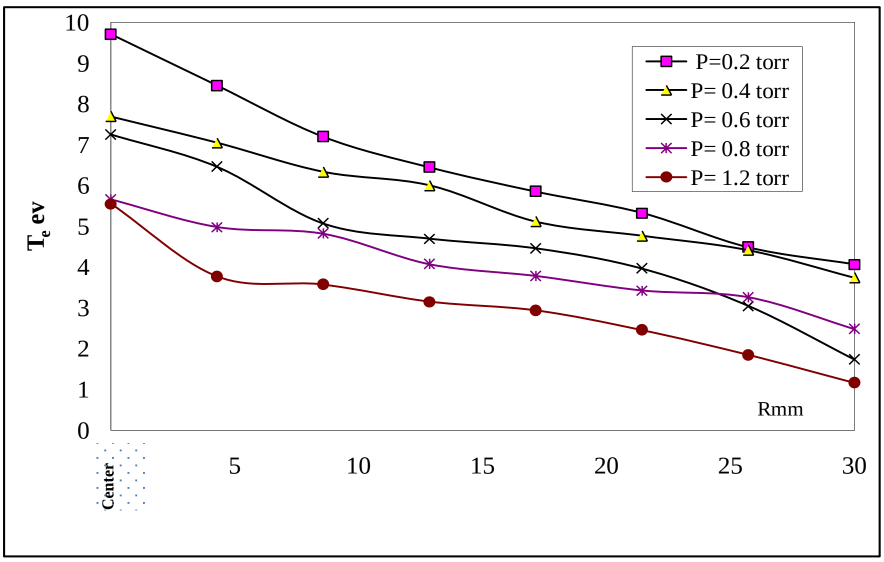

Figure 5. The Experimental radial temperature distribution of abnormal region for helium at different pressures.

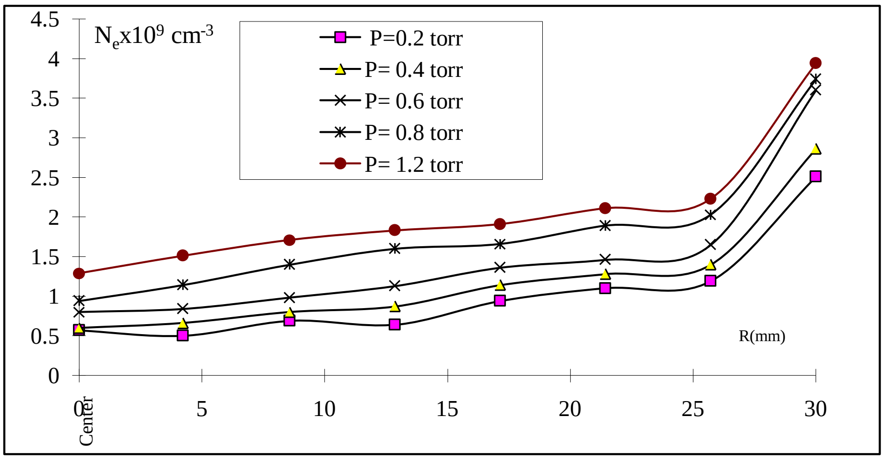

Figure 6. Measured radial density distribution of abnormal region for helium at different pressures.

$$\Gamma = \Gamma_i = \Gamma_e$$

(Congruence approximation). If there is no external electric field, the fluxes of ions and electrons (drift-diffusion model) can be expressed as:

$$\Gamma_i = -D_i \nabla n_i + \mu_i n_i E_D$$

$$\Gamma_e = -D_e \nabla n_e + \mu_e n_e E_D$$

where E_D follows Poisson's equation. If we multiply the first equation by $\mu_e n_e$ and the second one by $\mu_i n_i$ and then subtract them, we get:

$$\mu_i n_i \Gamma_e - \mu_e n_e \Gamma_i = \mu_e n_e D_i \nabla n_i - \mu_e n_e \mu_i n_i E_D - \mu_i n_i D_e \nabla n_e + \mu_i n_i \mu_e n_e E_D$$

Since $\Gamma = \Gamma_i = \Gamma_e$, the terms with E_D cancel each other out and using $n_e = n_i$, the expression for the flow of particles becomes:

$$\Gamma = \frac{-\left(D_e \mu_i - D_i \mu_e\right)}{\mu_i - \mu_e} \nabla n_i$$

With the ambipolar diffusion coefficient being

$$D_a = \frac{D_e \mu_+ - D_+ \mu_e}{\mu_+ - \mu_e} \tag{2}$$

and ρ is the charge density in the plasma given by:

$$\rho = e\left[n_+ - n_e\right] \tag{3}$$

and σ is the conductivity at the tube axis given by:

$$\sigma = e\left[\mu_+ n_+ - \mu_e n_e\right] \tag{4}$$

Considering that diffusion coefficient D given by:

$$D = \frac{kT}{m\nu} \text{ m/s}^2 \tag{5}$$

where $\mu_{\varepsilon,+}$ are the mobility of electrons (e) and ions (+), kT (ev) is the particle temperature, ν is the collision frequency between electrons and neutral atoms in Hz. By substituting with Equations (2, 3 and 4) into Equation (1), then we get

$$D_s = \frac{D_e\mu_+ - D_+\mu_e}{\mu_+ - \mu_e}\left[1 - \mu_e \frac{n_+ - n_e}{\mu_+ n_+ - \mu_e n_e}\right] \tag{6}$$

But by substituting by the Einstein relation [16] [17]:

$$\mu = \frac{\lceil q \rceil D}{kT} \tag{7}$$

into Equation (6) by the value of D, then we get

$$D_s = \frac{\mu_e\mu_+ KT_e - \mu_e\mu_+ KT_+}{q(\mu_+ - \mu_e)}\left[1 - \mu_e \frac{n_+ - n_e}{\mu_+ n_+ - \mu_e n_e}\right] \tag{8}$$

or

$$D_s = \frac{\mu_e\mu_+ (KT_e - KT_+)}{e(\mu_+ - \mu_e)}\left[\frac{\mu_+ n_+ - \mu_e n_e - \mu_e n_+ + \mu_e n_e}{\mu_+ n_+ - \mu_e n_e}\right] \tag{9}$$

Neglecting kT_+, where $kT_e \gg kT_+$ finally results in

Then

$$D_s = \frac{n_+\mu_e\mu_+ (kT_e)}{e(\mu_+ - \mu_e)}\left[\frac{\mu_+ - \mu_e}{\mu_+ n_+ - \mu_e n_e}\right] \tag{10}$$

$$D_s = \frac{n_+\mu_e\mu_+ (kT_e)}{e}\left[\frac{1}{\mu_+ n_+ - \mu_e n_e}\right]$$

Then

$$D_s = \frac{kT_e}{e}\left[\frac{\mu_e\mu_+}{\mu_+ - \mu_e \frac{n_e}{n_+}}\right] \tag{11}$$

or

$$D_s = \frac{kT_e}{e}\left[\frac{\mu_e}{1 - \frac{\mu_e}{\mu_+}\frac{n_e}{n_+}}\right] \tag{12}$$

Substituting $\mu_e = \frac{e}{m_e \nu_e}$ and $\mu_i = \frac{e}{m_i \nu_i}$ from Equations (5) and (7) into Equation (12) results in

$$D_S = \frac{kT_e}{e}\left[\frac{\left(\frac{e}{m_e\nu_e}\right)}{1 - \frac{\left(\frac{e}{m_e\nu_e}\right) n_e}{\left(\frac{e}{m_i\nu_i}\right) n_+}}\right] \tag{13}$$

or

$$D_S = kT_e \left[\frac{\dfrac{1}{m_e \nu_e}}{1 - \dfrac{m_i \nu_i n_e}{m_e \nu_e n_+}} \right] \tag{14}$$

or

$$D_S = kT_e \left[\frac{n_+}{m_e \nu_e n_+ - m_i \nu_i n_e} \right] \tag{15}$$

$$\frac{D_S}{\nu_i} = \frac{kT_e}{m_e \nu_e \nu_i - \dfrac{m_i \nu_i^2 n_e}{n_+}} \tag{16}$$

Experimentally, due to the diffusion process during plasma formation an interesting process occur in the plasma formation stage of the basil discharge. Theoretically, basil discharge process related with the recurrence relation for Bessel condition as shown in appendix A, where from the recurrence relation for the Bessel condition, the Schottky condition can be derived and proofed [18] [19] stating that:

3.1. In the Case of *L* (Axial Distance) > *R* (Radial Distance)

$$\frac{D_S}{\nu_i} = \left(\frac{R}{2.405} \right)^2 \tag{17}$$

A proof of the Schottky condition will be discussed briefly by two methods in **Appendix A**, where (R cm) represents the radial distance from the center to the edge through the cathode electrode measured by the Langmuir probe moved radially, and by substituting Equation (17) into (16), then

$$\left(\frac{R}{2.4} \right)^2 = \frac{kT_e}{m_e \nu_e \nu_i - \dfrac{m_i \nu_i^2 n_e}{n_+}} \tag{18}$$

Substituting the following equation into Equation (18)

$$\nu_e = N_n \left\langle Q_{e\text{-}n} \upsilon_{e\text{-}n} \right\rangle \tag{19a}$$

$$\nu_e = \left(3.55 \times 10^{16} P \right) \left\langle Q_{e\text{-}n} \right\rangle \left(\frac{2kT_e}{m_e} \right)^{1/2} \tag{19b}$$

$$\nu_i = \left(3.55 \times 10^{16} P \right) \left\langle Q_{i\text{-}n} \right\rangle \left(\frac{2kT_i}{m_i} \right)^{1/2} \tag{19c}$$

where P in torr, $Q_{e\text{-}n}$ and $Q_{i\text{-}n}$ are the cross sections of electron-neutral and ion-neutral collisions, respectively results in

$$\left(\frac{R}{2.4} \right)^2 = \frac{kT_e}{\left[m_e \left(\frac{2kT_e}{m_e} \right)^{1/2} \left(\frac{2kT_i}{m_i} \right)^{1/2} \left(3.55 \times 10^{16} P \right)^2 \left\langle Q_i \right\rangle \left\langle Q_e \right\rangle \right] - \left[\frac{n_e}{n_+} m_i \left[\left(3.55 \times 10^{16} P \right)^2 \left\langle Q_i \right\rangle \right]^2 \left(\frac{2kT_i}{m_i} \right) \right]} \tag{20}$$

then

$$\left(\frac{RP}{2.4}\right)^2 = \frac{1}{\left[\left(\frac{4m_e kT_i}{m_i kT_e}\right)^{1/2}\left(3.55\times10^{16}\right)^2\langle Q_i\rangle\langle Q_e\rangle\right]-\left[\frac{n_e}{n_+}\left(3.55\times10^{16}\langle Q_i\rangle\right)^2\left(\frac{2kT_i}{m_i kT_e}\right)\right]} \tag{21}$$

But from [20] [21] $\frac{\mu_e}{\mu_i}\cong 7.64\left(m_i\right)^{0.5}$

Or

$$m_i \cong \left(\frac{1}{7.64}\frac{\mu_e}{\mu_i}\right)^2 \tag{22a}$$

Then substituting (7) into (22a) gives

$$\frac{1}{m_i}\cong\left(7.64\frac{kT_i}{kT_e}\right)^2 \tag{22b}$$

Moreover, substituting (22b), $\frac{m_i}{m_e}\cong 2000$ and $\frac{\nu_i}{\nu_e}\cong 10^{-2}$ into (21) gives

$$\left(\frac{RP}{2.4}\right)^2 = \frac{1}{\left[\left(7.64\frac{kT_i}{kT_e}\right)\left(\frac{4m_e kT_i}{kT_e}\right)^{1/2}\left(3.55\times10^{16}\right)^2\langle Q_i\rangle\langle Q_e\rangle\right]-\left[\frac{n_e}{n_+}\left(3.55\times10^{16}\langle Q_i\rangle\right)^2\left(7.64\frac{kT_i}{kT_e}\right)^2\left(\frac{2kT_i}{kT_e}\right)\right]} \tag{23}$$

$$\left(RP\right)^2 = \frac{2.4^2}{\left[\left(7.64\frac{kT_i}{kT_e}\right)\left(\frac{4m_e kT_i}{kT_e}\right)^{1/2}\left(3.55\times10^{16}\right)^2\langle Q_i\rangle\langle Q_e\rangle\right]-\left[\frac{n_e}{n_+}\left(3.55\times10^{16}\langle Q_i\rangle\right)^2\left(7.64\frac{kT_i}{kT_e}\right)^2\left(\frac{2kT_i}{kT_e}\right)\right]} \tag{24}$$

Substituting the values of the cross sections, masses of ions and electrons into (24) gives

$$\left(RP\right)^2 = \frac{2.4^2}{(3.55)^2(7.64)(2)\left[\left[\left(\frac{kT_i}{kT_e}\right)\left(\frac{m_e kT_i}{kT_e}\right)^{1/2}\right]-\left[\frac{n_e}{n_+}7.64\left(\frac{kT_i}{kT_e}\right)^2\left(\frac{kT_i}{kT_e}\right)\right]\right]} \tag{25}$$

or

$$\left(RP\right)^2 = \frac{2.4^2}{(3.55)^2(7.64)(2)\left(\frac{kT_i}{kT_e}\right)^{3/2}\left[m_e^{1/2}-7.64\frac{n_e}{n_+}\left(\frac{kT_i}{kT_e}\right)^{3/2}\right]} \tag{26}$$

Then finally

$$RP = 0.1729\frac{1}{\left(\frac{kT_i}{kT_e}\right)^{3/4}\left[m_e^{1/2}-7.64\frac{n_e}{n_+}\left(\frac{kT_i}{kT_e}\right)^{3/2}\right]^{1/2}} \tag{27}$$

Using the data of the electron temperatures and densities shown in **Figure 4** and **Figure 5** respectively, into the Equation (27), taking into account that $T_e \gg T_i$ ($T_i = 0.1T_e$), $\frac{m_e}{m_i} \cong 2000$ [22] and for the spherical probe, the ion density is given by [23]:

$$n_+ = \frac{I_+}{0.6}\left(\frac{kT_e}{m_i}\right)^{1/2} A_p \tag{28}$$

Knowing T_e, ($A_p = 4\pi r_p^2$) area of spherical probe) and calculating positive ion current I_+ from the I-V characteristic curve of the spherical single probe [24], n_+ can be determined.

Figure 7 shows the radial distribution of the electron temperature (RDFT) theoretically using Equation (27), in the abnormal cathode fall region from the center to the edge of the electrode as a function of He as an inert gas. The RDFT from the theoretical method presented above accurately shows a dramatic radial reduction of the electron temperature for any region (cathode fall or negative glow or positive column) and for any applied pressure. Furthermore, the decrements of T_e at the edge of the electrode are more pronounced at the center due to edge effect [25].

3.2. In the Case of *L* (Axial Distance) < *R* (Radial Distance)

$$\frac{D_S}{\nu_i} = \left(\frac{R}{2.405}\right)^2 + \left(\frac{L}{\pi}\right)^2 \tag{29}$$

and by substituting Equation (29) into (16), then

$$\left(\frac{R}{2.4}\right)^2 + \left(\frac{L}{\pi}\right)^2 = \frac{kT_e}{m_e \nu_e \nu_i - \frac{m_i \nu_i^2 n_e}{n_+}} \tag{30}$$

Substituting by Equations (19a, b and c) into Equation (30), respectively results in

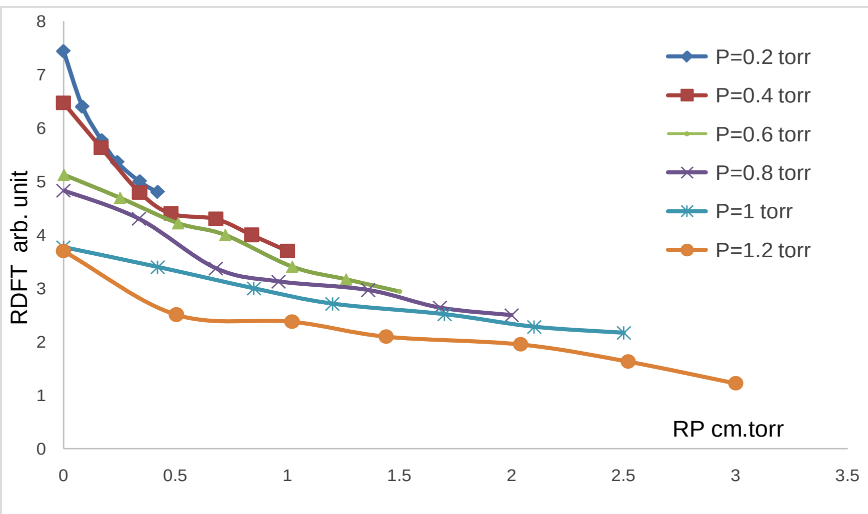

Figure 7. Theoretical radial distribution of the electron temperature (RDFT).

$$\left(\frac{R}{2.4}\right)^2+\left(\frac{L}{\pi}\right)^2=\frac{kT_e}{\left[m_e\left(\frac{2kT_e}{m_e}\right)^{1/2}\left(\frac{2kT_i}{m_i}\right)^{1/2}\left(3.55\times10^{16}P\right)^2\langle Q_i\rangle\langle Q_e\rangle\right]-\left[\frac{n_e}{n_+}m_i\left[\left(3.55\times10^{16}P\right)^2\langle Q_i\rangle\right]^2\left(\frac{2kT_i}{m_i}\right)\right]} \tag{31}$$

then

$$\left(\frac{R}{2.4}\right)^2+\left(\frac{L}{\pi}\right)^2=\frac{1}{\left[\left(\frac{4m_ekT_i}{m_ikT_e}\right)^{1/2}\left(3.55\times10^{16}\right)^2\langle Q_i\rangle\langle Q_e\rangle\right]-\left[\frac{n_e}{n_+}\left(3.55\times10^{16}\langle Q_i\rangle\right)^2\left(\frac{2kT_i}{m_ikT_e}\right)\right]} \tag{32}$$

Substitution from (22a and b) into (32) gives

$$\left(\frac{RP}{2.4}\right)^2+\left(\frac{L}{\pi}\right)^2=\frac{1}{\left[\left(7.64\frac{kT_i}{kT_e}\right)\left(\frac{4m_ekT_i}{kT_e}\right)^{1/2}\left(3.55\times10^{16}\right)^2\langle Q_i\rangle\langle Q_e\rangle\right]-\left[\frac{n_e}{n_+}\left(3.55\times10^{16}\langle Q_i\rangle\right)^2\left(7.64\frac{kT_i}{kT_e}\right)^2\left(\frac{2kT_i}{kT_e}\right)\right]} \tag{33}$$

$$(RP)^2=\frac{2.4^2}{\left[\left(7.64\frac{kT_i}{kT_e}\right)\left(\frac{4m_ekT_i}{kT_e}\right)^{1/2}\left(3.55\times10^{16}\right)^2\langle Q_i\rangle\langle Q_e\rangle\right]-\left[\frac{n_e}{n_+}\left(3.55\times10^{16}\langle Q_i\rangle\right)^2\left(7.64\frac{kT_i}{kT_e}\right)^2\left(\frac{2kT_i}{kT_e}\right)\right]}-2.4^2\left(\frac{L}{\pi}\right)^2 \tag{34}$$

Substituting the values of the cross sections, masses of ions and electrons into (34) gives finally

$$RP=\sqrt{\left(\frac{0.0299}{\left(\frac{kT_i}{kT_e}\right)^{3/2}\left[m_e^{1/2}-7.64\frac{n_e}{n_+}\left(\frac{kT_i}{kT_e}\right)^{3/2}\right]}-5.76\left(\frac{L}{\pi}\right)^2\right)} \tag{35}$$

For 1.2 torr of applied pressure, **Figure 8** shows comparison between the radial distribution of the electron temperature (RDFT) for $L < R$ using Equation (35) and for $L > R$ using Equation (27), in the abnormal cathode fall region from the center to the edge of the electrode as a function of He as an inert gas.

The reasons for the radial distribution of the electron temperatures for both cases.

$L < R$ and $L > R$ are the following:

a) The temperature decreases for increasing pressure may be due to the relation between the temperature and the pressure given by [26]:

$$|T_e|=6.5\left|P^{-0.066}\right| \tag{36}$$

b) As the pressure increase leads to a further increase in the breakdown voltage, a sharp increase in electron density and a higher electron-electron collision frequency, leads to the decrease of the electron temperatures [27].

c) The present theoretical and experimental results are compatible and agree fairly well with the behavior of the data of von Engel [28] [29] [30] for the radial distribution of the electron temperature.

For $L < R$, RDFT accurately shows a dramatic decrease by 60% *less than RDFT values for $L > R$. This may be attributed to*:

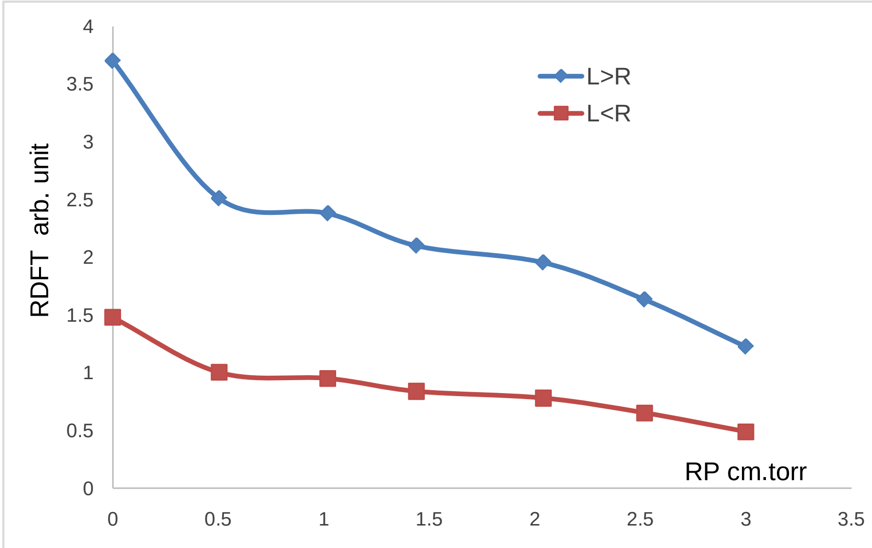

Figure 8. Comparison between the radial distribution of the electron temperature (RDFT) for L < R and for L > R, at P = 1.2 torr.

The cathode fall, negative glow and positive column regions are compressed when $L < R$, *i.e.* the cathode fall region is compressed in thickness and henceforth higher potentials are expected. Thus, strong electric field is produced and therefore ions would accelerate, and more efficient sputtering processes take place. The produced plasma temperatures decrease, and densities increases; this means that the rate of plasma loss by diffusion decreased similarly as in the applied of magnetized DC plasma [23], therefore the current and current density are increased.

4. Conclusion

Theoretically, using the Einstein relation of ambipolar diffusion, charge density of the plasma, conductivity at the axis of the tube, the Schottky condition, and the cross sections of ion-neutral and electron-neutral collisions, the decrease of the radial distribution function of the electron temperature with increasing product of the radial distance and gas pressures can be determined. The theoretical study agrees well with experimental data of electron and ion temperatures and gives the radial decrement dependence of the electron temperatures from the center to the edge of the electrode.

Acknowledgements

GVO acknowledges for the partial financial support from MEPhI and NRU MPEI in the framework of the Russian Academic Excellence Project.

Conflicts of Interest

The authors declare no conflicts of interest regarding the publication of this paper.

References

[1] Chen, F.F. (1965) Plasma Diagnostic Techniques. Academic Press, New York.

[2] Radmilovic-Radjenovic, M. and Radjenovic, B. (2006) *Journal of Physics D: Applied Physics*, **39**, 3002. https://doi.org/10.1088/0022-3727/39/14/019

[3] Kagan, Y. and Paskalev, K.K. (1975) *Soviet Physics. Technical Physics*, **19**, 1604.

[4] Kagan, Y. and Perel, V.I. (1964) *Soviet Physics Uspekhi*, **6**, 767. https://doi.org/10.1070/PU1964v006n06ABEH003611

[5] Mott-Smith and Langmuir (1926) *Physical Review*, **28**, 727. https://doi.org/10.1103/PhysRev.28.727

[6] Parent, B., Macheret, S.O. and Shneider, M.N. (2011) *Journal of Computational Physics*, **230**, 8010-8027. https://doi.org/10.1016/j.jcp.2011.07.006

[7] Holt, E.H. and Haskell, R.E. (1965) Foundations of Plasma Dynamics. 2nd Edition, MacMillan Company, New-York.

[8] Huang, P.G., Shang, J.S. and Stanfield, S.A. (2011) *AIAA Journal*, **49**, 119. https://doi.org/10.2514/1.J050463

[9] Bisek, N.J., Boyd, I.D. and Poggie (2009) *Journal of Spacecraft and Rockets*, **46**, 568. https://doi.org/10.2514/1.39032

[10] Galaly, A.R. and Khedr, M.A. (2015) *British Journal of Applied Science & Technology*, **11**, 1-14. https://doi.org/10.9734/BJAST/2015/17663

[11] Galaly, A.R. (2016) *British Journal of Applied Science & Technology*, **13**, 1.

[12] Galaly, A.R. and El Akshar, F.F. (2013) *Physica Scripta*, **88**, Article ID: 065503. https://doi.org/10.1088/0031-8949/88/06/065503

[13] Yasuda, H.K., Tao, W.H. and Prelas, M.A. (1996) *Journal of Vacuum Science & Technology A: Vacuum, Surfaces, and Films*, **14**, 2113. https://doi.org/10.1116/1.580089

[14] Nasser, E. (1971) Fundamentals of Gaseous Ionization and Plasma Electronics. Wiley-Interscience, New York.

[15] Raizer, Y.P. (1999) Gas Discharge Physics. Springer, New York.

[16] Von Engel, A.H. (1964) Ionized Gases. Oxford University Press, Oxford.

[17] Franklin, R.N. (1977) Plasma Phenomena in Gas Discharges. Oxford University Press, Oxford.

[18] Lieberman, M.A. and Lichtenberg, A.J. (1994) Principles of Plasma Discharges for Materials Processing. Wiley Interscience, New York.

[19] Braithwaite, N.St.J. (2000) *Plasma Sources Science and Technology*, **9**, 517. https://doi.org/10.1088/0963-0252/9/4/307

[20] Piel, A. (2011) Plasma Physics. Springer, Berlin.

[21] Kolobov, V.I. (2013) *Physics of Plasmas*, **20**, Article ID: 101610. https://doi.org/10.1063/1.4823472

[22] Fruchtman, A. (2009) *Plasma Sources Science and Technology*, **18**, Article ID: 025033. https://doi.org/10.1088/0963-0252/18/2/025033

[23] Simon, A. (1955) *Physical Review*, **98**, 317. https://doi.org/10.1103/PhysRev.98.317

[24] Galaly, A.R. (2014) *Physical Science International Journal*, **4**, 930-939. https://doi.org/10.9734/PSIJ/2014/9604

[25] Hutchinson (1990) Principles of Plasma Diagnostics. Cambridge University Press, Cambridge.

[26] Huba, J.D. (2011) Plasma Formulary. Naval Research Laboratory Report NRL/PU/6790-94-265.

[27] Druyvesteyn, M.J. and Penning, F.M. (1940) *Reviews of Modern Physics*, **12**, 87. https://doi.org/10.1103/RevModPhys.12.87

[28] Von Engel, A. and Corrigan, S.J.B. (1958) *Proceedings of the Physical Society*, **72**, 786. https://doi.org/10.1088/0370-1328/72/5/314

[29] Von Engel, A. and Cozens, J.R. (1965) *International Journal of Electronics*, **19**, 61-68. https://doi.org/10.1080/00207216508937799

[30] Von Engel, A. (1956) *Proceedings of the Physical Society*, **59**, 468.

[31] Bowman, F. (1958) Introduction to Bessel Conditions. Dover, New York.

[32] Korenev, B.G. (2002) Bessel Condition and Their Applications. CRC Press Company, Boca Raton, London, New York, Washington DC.

[33] Arfken, G. (1985) Bessel Conditions. In: *Mathematical Methods for Physicists*, 3rd Edition, Academic Press, Orlando, Ch. 11, 573-636. https://doi.org/10.1016/B978-0-12-059820-5.50019-7

[34] Gray, A. and Mathews, G.B. (1966) A Treatise on Bessel Conditions and Their Applications to Physics. 2nd Edition, Dover, New York.

[35] Watson, G.N. (1966) A Treatise on the Theory of Bessel conditions. 2nd Edition, Cambridge University Press, Cambridge.

Appendix: Proofing of the Schottky Condition

There are two classes of Schottky condition models using.

Appendix A: the recurrence relation for the Bessel condition

Appendix B: the boundary conditions

$$\frac{D_S}{\nu_i} = \frac{KT_e}{\frac{m_i \nu_i^2 n_e}{n_+} + m_e \nu_e \nu_i} \tag{36}$$

Due to the diffusion process during plasma formation an interesting process occur in the plasma formation stage of the basil discharge. The Schottky condition stating that

$\frac{D_S}{\nu_i} = \left(\frac{R}{2.4}\right)^2$ can be demonstrated as follows:

Appendix A: From the Recurrence Relation for Bessel Condition [31] [32] [33]

$$2J_n'(x) = J_{n-1}(x) - J_{n+1}(x) \tag{37}$$

and

$$\frac{2n}{x} J_n(x) = J_{n-1}(x) + J_{n+1}(x) \tag{38}$$

Subtracting equation (37) from (38), gives

$$\frac{2n}{x} J_n(x) - 2J_n'(x) = J_{n-1}(x) + J_{n+1}(x) - J_{n-1}(x) + J_{n+1}(x) \tag{39}$$

Or

$$\frac{n}{x} J_n(x) - J_n'(x) = J_{n+1}(x)$$

Or

$$nJ_n(x) - xJ_n'(x) = xJ_{n+1}(x)$$

This results in

$$xJ_n'(x) = n\,J_n(x) - xJ_{n+1}(x) \tag{40}$$

Differentiating (40) with respect to x, gives:

$$xJ_n''(x) + J_n'(x) = nJ_n'(x) - xJ_{n+1}'(x) - J_{n+1}(x) \tag{41}$$

Multiplying Equation (40) in n/x gives:

$$nJ_n'(x) = \frac{n^2}{x} J_n(x) - nJ_{n+1}(x) \tag{42}$$

Adding Equations (37) and (38) gives

$$xJ_n'(x) = xJ_{n-1}(x) - nJ_n(x) \tag{43}$$

Putting $n = n + 1$ in Equation (43) gives

$$xJ'_{n+1}(x) = xJ_n(x) - (n+1)J_{n+1}(x) \tag{44}$$

Substituting (39) and (40) into (38), results in

$$xJ''_n(x) + J'_n(x) = \frac{n^2}{x}J_n(x) - xJ_n(x)$$

Then

$$J''_n(x) + \frac{1}{x}J'_n(x) + \left(1 - \frac{n^2}{x^2}\right)J_n(x) = 0 \tag{45}$$

Finally

$$J'' + \frac{1}{x}J' + \left(\lambda - \frac{n^2}{x^2}\right)J = 0 \tag{46}$$

For $n = 0$

$$J'' + \frac{1}{x}J' + (\lambda)J = 0 \tag{47}$$

For the Bessel condition in cylindrical coordinate

$$x = Kr = \left(\frac{1}{D_a\tau}\right)^{1/2} R = \left(\frac{\lambda}{D_a}\right)^{1/2} R$$

with the solution $J_n(x) = \sqrt{\frac{2}{\pi}}\cos\left(x - \frac{n\pi}{2} - \frac{\pi}{4}\right)$, and $J_0 = 0$ for $n = 0$, gives $0 = \cos\left(x - \frac{\pi}{4}\right)$ with the solution $x = \frac{3\pi}{4} \approx 2.4$

$x = Kr = \frac{R}{(D\tau)^{1/2}} \approx 2.4$ or $\frac{R}{2.4} = (D\tau)^{1/2}$

Then

$$\frac{R}{2.4} = \left(\frac{D_S}{\nu_i}\right)^{1/2}$$

or

$$\frac{D_S}{\nu_i} = \left(\frac{R}{2.4}\right)^2$$

Appendix B: From the Boundary Conditions [34] [35]

$$n_e\upsilon_e = -D_S\nabla n_e$$

Then

$$D_S = -\frac{n_e\upsilon_e}{\nabla n_e} \tag{48}$$

But

$$\nu_i = \frac{\nabla\cdot n_e\upsilon_e}{n_e}$$

Then

$$\frac{D_S}{\nu_i} = -\left(\frac{n_e}{\nabla n_e}\right)^2 \tag{49}$$

For boundary conditions $r = R$, $n_e = n_{e0}$, and $J_0 = 2.4$, then

$$\nabla n_e = -\frac{2.4 n_e}{R} \tag{50}$$

Substituting from (50) into (49) then we get

$$\frac{D_S}{\nu_i} = \left(\frac{R}{2.4}\right)^2$$

Journal of Modern Physics, 2019, 10, 717-724
http://www.scirp.org/journal/jmp
ISSN Online: 2153-120X
ISSN Print: 2153-1196

Zero Strength of the Lorentz Force and Lack of a Classical Energy Radiation in the Bohr's Hydrogen Atom

Stanislaw Olszewski

Institute of Physical Chemistry, Polish Academy of Sciences, Warsaw, Poland
Email: olsz@ichf.edu.pl

How to cite this paper: Olszewski, S. (2019) Zero Strength of the Lorentz Force and Lack of a Classical Energy Radiation in the Bohr's Hydrogen Atom. *Journal of Modern Physics*, **10**, 717-724.

https://doi.org/10.4236/jmp.2019.107051

Received: May 21, 2019
Accepted: June 16, 2019
Published: June 19, 2019

Abstract

It is demonstrated that the Lorentz force acting on the electron particle in the Bohr's hydrogen atom, as well as the classical radiation energy of that atom, tends to be zero on condition both the electric and magnetic fields in the atom are considered in a definite quantum state. The ratio of the mentioned fields becomes of importance for discussion of the occurence of the electron spin.

Keywords

Bohr's Hydrogen Atom, Lorentz Force, Classical Electron Radiation Energy, Electron Spin

1. Introduction

The Bohr model of the hydrogen atom can be still a useful tool in considering the electron properties in that atom. The point - which was neglected by Bohr and was planned to be discussed in the present paper - concerns mainly the influence of the presence of the magnetic field in the atom on the physical processes which can be examined.

In general the Bohr model is based on the equivalence of the attractive electrostatic force between the electron and atomic nucleus and the repulsive centrifugal force due to the velocity of the circulating electron along its orbit [1–5]. This assumption is supplemented by the quantization requirement concerning the electron angular momentum. In effect it is obtained the well-known set of the electron states of a definite energy, the differences of which remain in a perfect agreement with experiment.

This semiclassical model was formally objected mainly because of the fact that the motion of the electron particle should be accompanied by a continuous emission of its energy which makes the particle motion to be only a very temporary effect. In practice, however, the electron motion in the electron's ground state is never stopped, and in case of an excited atom we observe only a very short-time spontaneous transition of the electron from a higher to a lower quantum energy level. The emitted energy in course of such transition is strictly connected with the energy difference existent between the levels.

Our idea is to re-examine the Bohr model first by taking into account the magnetic field created in the atom due to the electron circulation. This field was fully neglected in the original Bohr's approach. But in effect of the magnetic supplement the electron is moving not in one but in two fields, *i.e.* the electric and magnetic together. For a combination of such fields the Lorentz force acting on the atomic electron can be easily calculated [6].

We find that the Lorentz force for the hydrogen electron becomes exactly zero. A similar calculation can be done for the classical radiation intensity of the electron particle. This provides us also with a zero result for that intensity. It should be noted that both zero effects are strictly connected with the quantization properties exhibited by the electric and magnetic fields entering the atom.

2. A Look on the Electron Properties in the Hydrogen Atom

A specific situation of the Bohr hydrogen atom is that all discrete states of that atom are the bound states, so they have a negative energy. Since the electron energy in the atom obeys the virial theorem [7], viz.

$$2E_{\mathrm{kin}} + E_{\mathrm{pot}} = 0, \tag{1}$$

where E_{kin} and E_{pot} are respectively the kinetic and potential energy parts, the total energy of a quantum state n becomes

$$E_{\mathrm{tot}} = E_{\mathrm{kin}} + E_{\mathrm{pot}} = -E_{\mathrm{kin}} \tag{2}$$

which is a negative kinetic electron energy in the n state. The kinetic energy can be written as

$$E_{\mathrm{kin}} = \left(\frac{1}{2}\right) m v_n^2 = \frac{1}{2} m \left(\frac{e^2}{n\hbar}\right)^2 \tag{3}$$

since [7]

$$v_n = \frac{e^2}{n\hbar} \tag{4}$$

and m is the electron mass. Evidently the lowest quantum state $n = 1$ entering (2) should have the largest velocity

$$v_1 = \frac{e^2}{\hbar} \tag{4a}$$

because this makes (2) of the lowest value for any $n \geq 1$. On the other hand the velocity v_n decreases gradually to zero at infinitely high n; see (4).

Classically the circulating electron in the atom is submitted to the well-known attractive electric field of the atomic nucleus having the charge $Ze = e$, the property applied widely by Bohr. This gives the well-known electric field acting on the electron [7]:

$$\vec{E}_n = -\frac{e}{r_n^2}\frac{\vec{r}_n}{r_n} = -\frac{e^5 m^2}{n^4 \hbar^4}\frac{\vec{r}_n}{r_n}. \tag{5}$$

But the circular electron motion along an orbit creates also the magnetic field the size of which is dictated by the speed v_n in (4). The quanta of this field - neglected by Bohr - are derived below; see also [8].

First, it can be easily verified that v_n is coupled with the orbit radius

$$r_n = \frac{n^2\hbar^2}{me^2} \tag{6}$$

and the time period T_n necessary for the electron travel along the orbit having the radius r_n, viz.

$$T_n = \frac{2\pi n^3\hbar^3}{me^4}, \tag{7}$$

by the formula

$$v_n = \frac{2\pi r_n}{T_n}. \tag{8}$$

In effect the electron motion has its circular frequency

$$\Omega_n = \frac{2\pi}{T_n} \tag{9}$$

and this quantity is induced by the magnetic field B_n coupled with (9) by the formula [6] [8] [9]

$$\Omega_n = \frac{eB_n}{mc}. \tag{10}$$

In result be obtain the size of the magnetic field B_n due to the electron orbital motion equal to:

$$B_n = \frac{cm^2e^3}{n^3\hbar^3}. \tag{11}$$

Our aim is to examine a classical expression for the particle acceleration in the presence of the electric field $\vec{E}$ and magnetic field $\vec{B}$ represented by [6]:

$$\dot{\vec{v}}_n = \frac{e}{m}\sqrt{1-\frac{v^2}{c^2}}\left\{\vec{E}_n + \frac{1}{c}\left[\vec{v}_n \times \vec{B}_n\right] - \frac{1}{c^2}\vec{v}_n(\vec{v}_n\vec{E}_n)\right\}. \tag{12}$$

3. Calculation of the Acceleration in (12) with the Aid of $\vec{E}_n$, $\vec{B}_n$, and $\vec{v}_n$

First we note that the electron velocity vector $\vec{v}_n$ is normal to the vector $\vec{E}_n$, so the dot product

$$\vec{v}_n \cdot \vec{E}_n = 0. \tag{13}$$

In this way the last expression on the right-hand side of (12) is equal to zero. The next point, rather evident, is that

$$v_n < c. \tag{14}$$

A maximal v_n holds for $n = 1$ and this gives approximately the ratio

$$\frac{v_1}{c} = \frac{e^2}{c\hbar} \cong \frac{1}{137}. \tag{15}$$

This provides us with the right-hand side of (12) reduced to

$$\left(\frac{e}{m}\right)\left\{\vec{E}_n + \left(\frac{1}{c}\right)[\vec{v}_n \times \vec{B}_n]\right\}. \tag{16}$$

But the second vector component in (16) contains $\vec{v}_n$ which is normal to $\vec{B}_n$. The resulted vector product lies in the orbit plane and is normal to the electron track, as it does also the vector $\vec{E}_n$. In effect $\vec{E}_n$ and the vector combining $\vec{v}_n$ and $\vec{B}_n$ can add together. We find:

$$\left(\frac{1}{c}\right)[\vec{v}_n \times \vec{B}_n] = \frac{1}{c}\frac{e^2}{n\hbar}\frac{cm^2e^3}{n^3\hbar^3}\frac{\vec{r}_n}{r_n} = \frac{e^5m^2}{n^4\hbar^4}\frac{\vec{r}_n}{r_n} \tag{17}$$

because the sizes of both vectors entering (17) which are normal each to other are constant in time. In the next step let us note that the size of (17) is equal to the size of $\vec{E}_n$ in (5).

Since the results obtained in (5) and (17) have opposite signs, the sum in (16) becomes equal to zero. In effect we obtain a vanishing Lorentz force due to (12) acting on the electron for any quantum number n.

4. The Energy Radiated by the Electron in State n

This energy is obtained for the electron particle being in the quantum state n in the form of the integral [6]:

$$\Delta E_n = \frac{2e^4}{3m^2c^3}\int_{-\infty}^{+\infty} \frac{\left(\vec{E}_n + \frac{1}{c}[\vec{v}_n \times \vec{B}_n]\right)^2 - \frac{1}{c^2}(\vec{E}_n \cdot \vec{v}_n)^2}{1 - \frac{v_n^2}{c^2}}\,dt. \tag{18}$$

Evidently the expression entering the numerator of the fraction under the integral is equal to zero because of the result in (13) and

$$\vec{E}_n + \left(\frac{1}{c}\right)[\vec{v}_n \times \vec{B}_n] = 0 \tag{19}$$

entering equally (16) and (18). Therefore no energy is radiated classically by the electron being in state n.

5. Reference of the Field Strengths E_n and B_n to the Electron Spin

The spin of the electron particle has been fully neglected in the Bohr atomic model. Nevertheless it can be considered in that model on the basis of the papers [10] [11] [12].

The approach done in references [10] [11] [12] concerned mainly the spin property of electron on the Bohr quantum level $n = 1$. Our aim is to extend the spin discussion to the orbits having $n > 1$. First, the assumption that the spinning electron particle is circulating with velocity close to the light speed c along a circle having its radius equal to the shortest distance acceptable between two electron particles, viz.

$$\Delta x_{\min} = r_c = \frac{\hbar}{mc} \approx \frac{c}{\Omega_c} \tag{20}$$

remains unchanged. The Ω_c is the angular velocity of the spinning electron.

The motion chracterized by the radius r_c in (20) induces the magnetic field of the strength B_c which is coupled with Ω_c by the formula

$$\Omega_c = \frac{eB_c}{mc}. \tag{21}$$

This expression, together with (20), implies the relation

$$\frac{\hbar}{mc} \approx \frac{mc^2}{eB_c} \tag{22}$$

so

$$B_c = \frac{m^2c^3}{e\hbar}. \tag{23}$$

Simultaneously a minimal distance between the proton being at rest and the moving electron particle should approach also the distance (20) because the proton contribution to that distance is negligible due to a large proton mass. In effect the absolute value of the electrostatic force between the proton and the spinning electron becomes [11] [12]:

$$eE_c = \frac{e^2}{(\Delta x_{\min})^2} = \frac{e^2m^2c^2}{\hbar^2}. \tag{24}$$

Since the force eB_c is normal to eE_c, the driving electron velocity due to the joint action of eB_c and eE_c is given by [13]:

$$v_c = c\frac{|\vec{E}_c \times \vec{B}_c|}{B_c^2} = c\frac{E_c}{B_c} = c\frac{e^2}{\hbar c} = \frac{e^2}{\hbar}. \tag{25}$$

Therefore the driving velocity (25) is equal to the orbital Bohr electron velocity existent in the case of $n = 1$; see (4a).

But the ratio $\frac{E_c}{B_c}$ entering (25) is exactly equal to $\frac{E_1}{B_1}$, so we have

$$c\frac{E_c}{B_c} = c\frac{E_1}{B_1} = v_1. \tag{26}$$

This is a maximal driving velocity along the Bohr orbit. The other orbit velocities like

$$v_2, v_3, v_4, \ldots < v_1 \tag{27}$$

are smaller than v_1 and can be attained successively by the ratios:

$$c\frac{E_2}{B_2} = c\frac{e^2}{2\hbar c} = \frac{e^2}{2\hbar} = v_2, \tag{26a}$$

$$c\frac{E_3}{B_3} = c\frac{e^2}{3\hbar c} = v_3, \tag{26b}$$

$$c\frac{E_4}{B_4} = c\frac{e^2}{4\hbar c} = v_4, \tag{26c}$$

etc. This means that the driving electron velocities along successive orbits n can be provided by the ratios $\frac{E_n}{B_n}$ characteristic for these orbits, with no reference to the ratio $\frac{E_c}{B_c}$ excepting for the case of $n = 1$.

The parameters entering E_c and B_c define the electron spin frequency which is the same for all Bohr orbits n. Since the time of circulation along the spin orbit having the radius r_c is equal to

$$T_c \cong \frac{2\pi r_c}{c} = \frac{2\pi\hbar}{mc^2} = \frac{h}{mc^2}, \tag{28}$$

the number of spin circulations in course of the time T_n necessary to travel along the nth Bohr orbit becomes [see (7)]:

$$\frac{T_n}{T_c} = \frac{2\pi\hbar^3 n^3}{me^4}\frac{mc^2}{h} = n^3\frac{\hbar^2 c^2}{e^4} = \frac{n^3}{\alpha^2}. \tag{29}$$

Here α is the well-known atomic constant:

$$\alpha = \frac{e^2}{\hbar c}. \tag{30}$$

The angular frequency of a single spin circulation equal to

$$\Omega_c = \frac{2\pi}{T_c} = \frac{mc^2}{\hbar} \tag{31}$$

is evidently independent of n.

6. Adiabatic Invariants for the Electron Orbital Motion and Spin Motion in the Bohr Atom

Having the B_n for the electron orbital motion and B_c for the spin motion [see Equations (11) and (23) respectively] it is easy to calculate the adiabatic invariant in each motion case according to the formula [6]:

$$I = \frac{3\pi c p_n^2}{eB_n}. \tag{32}$$

The symbol p_n in (32) represents the size of momentum along the electron path which is

$$p_n = mv_n = m\frac{e^2}{n\hbar} \tag{33}$$

in the case of circulation along the nth Bohr orbit with the velocity v_n [see (4)], and instead of p_n the expression

$$p_c = mc \tag{34}$$

approximates the momentum of a spinning electron particle; see the inferences above (20).

The formula (33) substituted to (32) together with B_n from (11) gives the invariant equal to

$$I = I_n = \frac{3\pi c}{e^4 cm^2} n^3\hbar^3 \frac{m^2 e^4}{n^2\hbar^2} = 3\pi n\hbar, \tag{35}$$

whereas (34) substituted to (32) instead of p_n and B_c of (23) instead of B_n lead to the invariant formula:

$$I = \frac{3\pi c p_c^2}{eB_c} = \frac{3\pi cm^2c^2}{m^2c^3}\hbar = 3\pi\hbar. \tag{36}$$

Evidently (35) and (36) are much similar: they differ solely by an integer factor n indicating the orbit number present in (35).

7. Summary

The Lorentz force acting on the electron in the Bohr's hydrogen atom, and classical radiation energy of that electron which is assumed to occupy a definite quantum state n, are examined. It is found that both the Lorentz force and radiation energy tend to be zero, on condition the magnetic field induced by the electron motion in the atom, neglected in the former Bohr's theory, is taken into account.

The electric and magnetic field strengths (E_n and B_n respectively) entering the Lorentz force are useful in deriving the drift velocity of the electron along the orbit n. For $n = 1$ the drift velocity obtained from E_n and B_n is equal to that obtained from the ratio of E_c and B_c characteristic for the spinning electron particle. But for $n > 1$ the driving velocity, equal to $v_n < v_1$, is defined solely by the ratio of E_n and B_n.

A characteristic feature concerns the adiabatic invariants of the orbital and spin motion calculated respectively in Section 6: both invariants differ solely by the integer factor n present in the orbital case.

Conflicts of Interest

The author declares no competing financial interests.

References

[1] Bohr, N. (1913) *The London, Edinburgh, and Dublin Philosophical Magazine and Journal of Science*, **26**, 857-875. https://doi.org/10.1080/14786441308635031

[2] Bohr, N. (1914) *The London, Edinburgh, and Dublin Philosophical Magazine and Journal of Science*, **27**, 506-524. https://doi.org/10.1080/14786440308635119

[3] Bohr, N. (1915) *Philosophical Magazine*, **29**, 332.

[4] Bohr, N. (1915) *The London, Edinburgh, and Dublin Philosophical Magazine and Journal of Science*, **30**, 394-415. https://doi.org/10.1080/14786440908635413

[5] Bohr, N. (1922) The Theory of Spectra and the Atomic Constitution. Cambridge University Press, Cambridge, UK.

[6] Landau, L.D. and Lifshitz, E.M. (1948) The Field Theory. 2nd Edition, OGIZ, Moscow. (In Russian)

[7] Sommerfeld, A. (1931) Atombau und Spektrallinien. Vol. 1, 5th Edition, Vieweg, Braunschweig.

[8] Olszewski, S. (2016) *Quantum Matter*, **5**, 641-644. https://doi.org/10.1166/qm.2016.1357

[9] Olszewski, S. (2016) *Reviews in Theoretical Science*, **4**, 336-352. https://doi.org/10.1166/rits.2016.1066

[10] Olszewski, S. (2014) *Journal of Modern Physics*, **5**, 1254.

[11] Olszewski, S. (2014) *Journal of Modern Physics*, **5**, 2022-2029. https://doi.org/10.4236/jmp.2014.518198

[12] Olszewski, S. (2014) *Journal of Modern Physics*, **5**, 2030-2040. https://doi.org/10.4236/jmp.2014.518199

[13] Matveev, A.N. (1964) Electrodynamics and the Theory of Relativity. Izd. Wyzszaja Szkola, Moscow. (In Russian)

Journal of Modern Physics, 2019, 10, 725-728
http://www.scirp.org/journal/jmp
ISSN Online: 2153-120X
ISSN Print: 2153-1196

On the Final State of Black Holes

Bo Lehnert

Alfvén Laboratory, Royal Institute of Technology, Stockholm, Sweden
Email: bo.lehnert@ee.kth.se

How to cite this paper: Lehnert, B. (2019) On the Final State of Black Holes. *Journal of Modern Physics*, **10**, 725-728.

https://doi.org/10.4236/jmp.2019.107052

Received: May 10, 2019
Accepted: June 17, 2019
Published: June 20, 2019

Abstract

The final state of a black hole and its force balance is considered, in the limit where all available energy is radiated away and all matter remains in the lowest form of Zero Point Energy (ZPE). In conventional theory without the concept of ZPE, the gravitational contraction would transfer the system into a mass point, being questionable from the theoretical point of view. But the inclusion of ZPE makes a force balance possible, resulting in a finite characteristic radius of a black hole mass distribution. This radius is of the same order as that of the so-called Schwarzschild radius, but is not related to the physics of the latter, which is due to particle trapping in the gravitational field.

Keywords

Black Holes, Zero Point Energy

1. Introduction

The black hole concept was first discovered by Schwarzschild [1] in an analysis of a simplified system having no electric charge and no angular momentum. The result was at that time merely considered as a curiosity. But a star which collapses into a black hole under the compressive action of its own gravitational field is now a subject of ever increasing interest. In its most generalized form the related physics includes both gravitational and electromagnetic fields as well as problems of General Relativity, to account for its mass, electric charge, and its intrinsic angular momentum. The associated theoretical analysis and related astronomical observations have been described in a review by Misner, Thorne and Wheeler [2]. It is thereby to be noticed that no black hole has so far been associated with a substantial electric charge.

The present investigation is limited to the Schwarzschild case of a final state of a star collapsing into a black hole. Section 2 first describes the applied physics being similar to that of the Standard Model for a vacuum state of empty space. This is followed in Section 3 by the extended analysis of a vacuum state including the Zero Point Energy

(ZPE) discovered by Planck [3].

2. Black Hole in a Vacuum of Empty Space

The final state of a collapsing star and its black hole will first be considered in terms being similar to those of the Standard Model, *i.e.* where the vacuum is treated as an empty space where there are no sources of electric charge and current, and there is no ZPE. In this state all available energy has been radiated away. The gravitational contraction is then unbalanced, and it will continue all the way to a mathematical point. The reality of a mass point is, however, questionable from the physical point of view.

3. Black Hole in a Vacuum Including Zero Point Energy

When all energy of the collapsing star has been radiated away, its temperature tends to the limit $T = 0$, and all matter turns into that of ZPE. The resulting mass m of the black hole then corresponds to a density ρ distributed inside a radius r_0 and within the volume $V = \frac{4}{3}\pi r_0^3$. The average mass density is $\bar{\rho} = m/V$. We further restrict the analysis to a system without electric charge and angular momentum.

3.1. The Inwards Pointing Gravitational Pressure

Following Bergmann [4] a steady curl-free gravitational field strength

$$\mathbf{g} = -\nabla\phi = \left(-\frac{d\phi}{dr}, 0, 0\right) \qquad (\mathrm{m/s^2}) \tag{1}$$

is considered which originates from the potential $\phi(r)$ in a spherically symmetric frame (r, θ, φ) where r is the only independent variable. The mass density ρ is the source of $\mathbf{g}$ as given by

$$-\mathrm{div}\,\mathbf{g} = 4\pi G\rho = \nabla^2\phi = \frac{1}{r^2}\frac{d}{dr}\left(r^2\frac{d\phi}{dr}\right) \tag{2}$$

where the constant of gravitation $G = 6.6726 \times 10^{-11}$ $\mathrm{m^3/kg\,s^2}$. The associated local force density becomes

$$\mathbf{f} = \rho\,\mathbf{g} \tag{3}$$

The analysis is now restricted by assuming a form

$$\phi(r) = \phi_0 (r/r_0)^\alpha \tag{4}$$

with positive values of α. Equation (2) then yields

$$4\pi G\rho = (\phi_0/r_0^\alpha)\,\alpha\,(\alpha+1)\,r^{\alpha-2} > 0 \tag{5}$$

When aiming at orders of magnitude, a further restriction to $\alpha = 2$ leads to a homogeneous density $\rho = \bar{\rho}$ within the volume $0 < r < r_0$. Then Equation (5) results in

$$4\pi G\rho = 6\,\phi_0/r_0^2 \tag{6}$$

From Equation (3)

$$f_r = -2\rho\left(\phi_0 r_0^2\right) r = -3\left(\phi_0/r_0^2\right)^2 (1/\pi G)\,r \qquad (\mathrm{N/m^3}) \tag{7}$$

in combination with Equation (6). The inwards pointing gravitational pressure then becomes

$$p_G = \int_0^{r_0} f_r dr = -\frac{3}{2}\left(\phi_0/r_0^2\right)^2 (1/\pi G)\, r_0^2 \qquad (\mathrm{N/m^2}) \tag{8}$$

With

$$\phi_0/r_0^2 = \frac{2}{3}\pi G\rho = \frac{2}{3}\pi G(m/V) \qquad (\mathrm{s^{-2}}) \tag{9}$$

the pressure (8) takes the form

$$p_G = -\frac{2}{3}(m/V)^2 \pi G\, r_0^2 \qquad (\mathrm{N/m^2}) \tag{10}$$

The values of the parameters α, ϕ_0 and r_0 represent various chosen forms for the radial distribution of mass. This freedom does not affect the order of magnitude of the results obtained here.

3.2. The Outwards Pointing Zero Point Energy Pressure

At the final state there is only gravitationally compressed mass m at the density $\bar{\rho}$ within the region $0 < r < r_0$ and in the form of ZPE. In the outer vacuum region $r > r_0$, where r_0 represents the boundary of the black hole mass, there remains a ZPE density being much lower than $\bar{\rho}$, i.e. that which would exist in the vacuum in absence of a black hole. With $\alpha = 2$ and $\rho = \bar{\rho} = const.$ there is a jump in ZPE density at the boundary $r = r_0$. This generates an outward pointing pressure

$$p_Z = mc^2/V \qquad (\mathrm{N/m^2}) \tag{11}$$

Even if ZPE represents the lowest energy level, its spatial gradient can thus generate a force [5].

3.3. The Pressure Balanced Black Hole

A pressure balance at a finite characteristic radius r_0 becomes possible through the condition $p_G = -p_Z$. Equations (10) and (11) combine to

$$r_0 = mG/2\,c^2 \tag{12}$$

With a solar mass of about 1.893×10^{30} kg and a black hole of n_Z such masses, this radius becomes

$$r_0 = 0.7383 \times 10^3 n_Z \tag{13}$$

An example can be given of the black hole of the Milky Way, with a mass of about $n_Z = 4 \times 10^6$. It leads to $r_0 = 3 \times 10^9$ m, *i.e.* about 4 solar radii.

It should be observed that the physics of the present pressure balance differs considerably from that underlying the so called Schwarzschild radius

$$R = 2Gm/c^2 = 4\,r_0 \tag{14}$$

The latter is obtained from the work which is required to "lift" a massive particle out of a black hole. The particle thereby gets trapped within the hole when being inside the radius R.

Equation (12) also holds approximately when not all of the gravitationally trapped matter has had time to approach zero absolute temperature T.

4. Conclusion

Conventional physics is faced by difficulties in the treatment of black holes, in the form of an unbalanced gravitational contraction, all the way to a point mass which is questionable from the physical point of view. This can be overcome by including the effects of Zero Point Energy, the expanding force of which can outbalance that of the gravitational contraction. It results in a finite characteristic radius of the black hole configuration. This radius is of the order of the Schwarzschild radius, but not related to the physics of particle trapping in the gravitational field.

Conflicts of Interest

The author declares no conflicts of interest regarding the publication of this paper.

References

[1] Schwarzschild, K. (1916) *Sitzungsber.Preuss.Akad.Wiss.Berlin (Math.Phys.)*, 189-196.

[2] Misner, C.W., Thorne, K.S. and Wheeler, J.A. (1973) Gravitation. Chap. 33, W.H. Freeman and Co., San Francisco and Reading.

[3] Planck, M. (1900) *Verh. Dtsch Phys. Ges.*, **2**, 237.

[4] Bergmann, P.G. (1942) Introduction to the Theory of Relativity. Chap. X, Prentice Hall, Inc., New York.

[5] Lehnert, B. (2019) *Journal of Modern Physics*, **10**, 663-672. https://doi.org/10.4236/jmp.2019.106047

Journal of Modern Physics, 2019, 10, 729-794
http://www.scirp.org/journal/jmp
ISSN Online: 2153-120X
ISSN Print: 2153-1196

The Solution Cosmological Constant Problem

Jaykov Foukzon[1], Elena Men'kova[2], Alexander Potapov[3]

[1]Department of Mathematics, Israel Institute of Technology, Haifa, Israel
[2]All-Russian Research Institute for Optical and Physical Measurement, Moscow, Russia
[3]Kotel'nikov Institute of Radioengineering and Electronics, Russian Academy of Sciences, Moscow, Russia
Email: jaykovfoukzon@list.ru, e_menkova@mail.ru, potapov@cplire.ru

How to cite this paper: Foukzon, J., Men'kova, E. and Potapov, A. (2019) The Solution Cosmological Constant Problem. *Journal of Modern Physics*, **10**, 729-794.
https://doi.org/10.4236/jmp.2019.107053

Received: February 5, 2019
Accepted: June 17, 2019
Published: June 20, 2019

Abstract

The cosmological constant problem arises because the magnitude of vacuum energy density predicted by the Quantum Field Theory is about 120 orders of magnitude larger then the value implied by cosmological observations of accelerating cosmic expansion. We pointed out that the fractal nature of the quantum space-time with negative Hausdorff-Colombeau dimensions can resolve this tension. The canonical Quantum Field Theory is widely believed to break down at some fundamental high-energy cutoff Λ_* and therefore the quantum fluctuations in the vacuum can be treated classically seriously only up to this high-energy cutoff. In this paper we argue that the Quantum Field Theory in fractal space-time with negative Hausdorff-Colombeau dimensions gives high-energy cutoff on natural way. We argue that there exists hidden physical mechanism which cancels divergences in canonical QED_4, QCD_4, Higher-Derivative-Quantum gravity, etc. In fact we argue that corresponding supermassive Pauli-Villars ghost fields really exist. It means that there exists the ghost-driven acceleration of the universe hidden in cosmological constant. In order to obtain the desired physical result we apply the canonical Pauli-Villars regularization up to Λ_*. This would fit in the observed value of the dark energy needed to explain the accelerated expansion of the universe if we choose highly symmetric masses distribution between standard matter and ghost matter below the scale Λ_*, *i.e.*, $f_{s.m}(\mu) \simeq -f_{g.m}(\mu), \mu = mc, \mu \leq \mu_{\text{eff}}, \mu_{\text{eff}} c < \Lambda_*$ The small value of the cosmological constant is explained by tiny violation of the symmetry between standard matter and ghost matter. Dark matter nature is also explained using a common origin of the dark energy and dark matter phenomena.

Keywords

Cosmological Constant Problem, Quantum Field Theory, Vacuum Energy Density, Quantum Space-Time, Hausdorff-Colombeau Dimension, Quantum

Fluctuations, High-Energy Cutoff, Canonical Pauli-Villars Regularization, Universe

1. Introduction

1.1. The Formulation of the Cosmoloigical Constant Problem

The cosmological constant problem arises at the intersection between general relativity and quantum field theory, and is regarded as a fundamental unsolved problem in modern physics. A peculiar and truly quantum mechanical feature of the quantum fields is reminded that they exhibit zero-point fluctuations everywhere in space, even in regions which are otherwise "empty" (*i.e.* devoid of matter and radiation). This vacuum energy density is believed to act as a contribution to the cosmological constant λ appearing in Einstein's field equations from 1917,

$$R_{\mu\nu} - \frac{1}{2} g_{\mu\nu} R = \frac{8\pi G}{c^4} T'_{\mu\nu} \tag{1}$$

where $R_{\mu\nu}$ and R refer to the curvature of space-time, $g_{\mu\nu}$ is the metric, $T'_{\mu\nu}$ is the the energy-momentum tensor,

$$T'_{\mu\nu} = T_{\mu\nu} + \frac{c^4 \lambda}{8\pi G} \begin{pmatrix} 1 & 0 & 0 & 0 \\ 0 & -1 & 0 & 0 \\ 0 & 0 & -1 & 0 \\ 0 & 0 & 0 & 1 \end{pmatrix} \tag{2}$$

where $T_{\mu\nu}$ is the energy-momentum tensor of matter. Thus $T'_{00} = T_{00} + \varepsilon_\lambda$, $T'_{\alpha\beta} = T_{\alpha\beta} + \delta_{\alpha\beta} P_\lambda$, where

$$\varepsilon_\lambda = -P_\lambda = c^4 \lambda / 8\pi G. \tag{3}$$

Reminding that under Lorentz transformations $(\varepsilon_\lambda, P_\lambda) \to \varepsilon'_\lambda, (\varepsilon_\lambda, P_\lambda) \to P'_\lambda$ the quantities ε_λ and P_λ are changes by the law

$$\varepsilon'_\lambda = \frac{\varepsilon_\lambda + \beta^2 P_\lambda}{1-\beta^2}, P'_\lambda = \frac{P_\lambda + \beta^2 \varepsilon_\lambda}{1-\beta^2}. \tag{4}$$

Thus for the quantities ε_λ and P_λ Lorentz invariance holds by Equation (3) [1].

In modern cosmology it is assumed that the observable universe was initially vacuumlike, *i.e.*, the cosmological medium was non-singular and Lorentz invariant. In the earlier, non-singular Friedmann cosmology, the Friedmann universe comes into being during the phase transition of an initial vacuumlike state to the state of "ordinary" matter [2] [3].

The Friedmann equations start with the simplifying assumption that the universe is spatially homogeneous and isotropic, *i.e.* the cosmological principle; empirically, this is justified on scales larger than ~100 Mpc. The cosmological principle implies that the metric of the universe must be of the form Robertson-Walker metric [2]. Robertson-Walker metric reads

$$\mathrm{d}s^2 = \mathrm{d}t^2 - a^2(t)\left[\frac{\mathrm{d}r^2}{1-kr^2} + r^2\left(\mathrm{d}\theta^2 + \sin^2\theta \mathrm{d}\varphi^2\right)\right]. \tag{5}$$

For such a metric, the Ricci curvature scalar is $R = -6k$ and it is said that space has the curvature *k*. The scaling factor $a(t)$ rescales this curvature for a given time *t*, producing a curvature $k(t) = k/a(t)$. The scaling factor $a(t)$ is given by two independent Friedmann equations for modeling a homogeneous, isotropic universe reads

$$\dot{a}^2 = \frac{G}{3}\varepsilon a^2 - k, \ddot{a} = -\frac{G}{6}(\varepsilon + 3p) \tag{6}$$

and the equation of state

$$p = p(\varepsilon), \tag{7}$$

where p is pressure and ε is a density of the cosmological medium. For the case of the vacuumlike cosmological medium equation of state reads [2] [3] [4]:

$$p = -\varepsilon. \tag{8}$$

By virtue of Friedman's Equation (6) in the Universe filled with a vacuum-like medium, the density of the medium is preserved, *i.e.* $\varepsilon = const$, but the scale factor $a(t)$ grows exponentially. By virtue of continuity, it can be assumed that the admixture of a substance does not change the nature of the growth of the latter, and the density of the medium hardly changes. This growth, interpreted by analogy with the Friedmann models as an expansion of the universe, but almost without changing the density of the medium! was named inflation. The idea of inflation is the basis of inflation scenarios [2].

Non-singular cosmology [2] [4] suggests that the initial state of the observable universe was vacuum-like, but unstable with respect to the phase transition to the ordinary non-Lorentz-invariant medium. This, for example, takes place if, by virtue of the equations of state of the medium, a fluctuation decrease in its density d violates the condition of vacuum-like degeneration, $p = -\varepsilon$ or, which is the same, $3p + \varepsilon = -2\varepsilon < 0$, replacing it with

$$-2\varepsilon < 3p + \varepsilon < 0. \tag{9}$$

According to Friedman's equations, it corresponds to an accelerated expansion of the cosmological medium, accompanied by a drop in its density, which makes the process irreversible [2]. The impulse for expansion in this scenario, the vacuum-like environment, is not reported to itself (bloating), but to the emerging Friedmann environment.

In review [5], Weinberg indicates that the first published discussion of the contribution of quantum fluctuations to the cosmological constant was a 1967 paper by Zel'dovich [6]. In his article [1] Zel'dovich emphasizes that zeropoint energies of particle physics theories cannot be ignored when gravitation is taken into account, and since he explicitly discusses the discrepancy between estimates of vacuum energy and observations, he is clearly pointing to a cosmological constant problem. As well known zeropoint energy density of scalar quantum field, etc. is divergent

$$\varepsilon_{\text{vac}}(m) = \frac{2\pi c}{(2\pi\hbar)^3}\int_0^\infty \sqrt{p^2 + m^2c^2}\, p^2 \mathrm{d}p = \infty. \tag{10}$$

In order to avoid difficulties mentioned above, in article [1] Zel'dovich has applied canonical Pauli-Villars regularization [7] [8] and formally has obtained a finite result (his formulas [1], Eqs. (VIII.12)-(VIII.13) p. 228)

$$\varepsilon_{\text{vac}} = -p_{\text{vac}} = \frac{1}{8}\int_0^\infty f(\mu)\mu^4(\ln\mu)\mathrm{d}\mu = \frac{c^4\lambda}{8\pi G}, \tag{11}$$

where

$$\int_0^\infty f(\mu)\mathrm{d}\mu = \int_0^\infty f(\mu)\mu^2\mathrm{d}\mu = \int_0^\infty f(\mu)\mu^4\mathrm{d}\mu = 0. \tag{12}$$

Remark 1.1.1. Unfortunately, Equation (11) and Equation (12) give nothing in order to obtain desired numerical values of the zero-point energy density ε.

In his paper [1], Zel'dovich arrives at a zero-point energy (his formula (IX.1))

$$\varepsilon_{\text{vac}} = m\left(\frac{mc}{\hbar}\right)^3 \sim 10^{17}\ \mathrm{g/cm^3}, \lambda \sim 10^{-10}\ \mathrm{cm^{-2}}, \tag{13}$$

where m (the ultra-violet cut-of) is taken equal to the proton mass. Zel'dovich notes that since this estimate exceeds observational bounds by 46 orders of magnitude it is clear that "... such an estimate has nothing in common with reality".

In his paper [1], Zel'dovich wrote: Recently A. D. Sakharov proposed a theory of gravitation, or, more precisely, a justification GR equation based on consideration of vacuum fluctuations. In this theory, the essential assumption is that there is some elementary length L or the corresponding limiting momentum $p_0 = \hbar/L$. Shorter lengths or for large impulses theory is not applicable. Sakharov gets the expression of gravitational constant G through L or p_0 (his formula (IX.6))

$$G = \frac{c^3L^2}{\hbar} = \frac{\hbar c^3}{p_0^2}. \tag{14}$$

This expression has been known since the days of Planck, but it was read "from right to left": gravity determines the length L and the momentum p_0. According to Sakharov, L and p_0 are primary. Substitute (IX. 6) in the expression (IX. 4), we get

$$\rho_{\text{vac}} = \frac{m^6c^5}{p_0^2\hbar^3}, \varepsilon_{\text{vac}} = \frac{m^6c^7}{p_0^2\hbar^3}. \tag{15}$$

That is expressions that the first members (in the formulas (VIII.10), (VIII. 11)) which are vanishes (with $p_0 \to \infty$). Thus, we can suggest the following interpretation of the cosmological constant: there is a theory of elementary particles, which would give (according to the mechanism that has not been revealed at the present time) identically zero vacuum energy, if this theory is applicable infinitely, up to arbitrarily large momentum; there is a momentum p_0, beyond which the theory is non applicable; along with other implications, modifying the theory gives different from zero vacuum energy; general considerations make it likely that the effect is portional p_0^{-2}. Clarification of the question of the existence and magnitude of the cosmological constant will also be of fundamental importance for the theory of elementary particles.

Nonclassical Assumptions

(I) In contrast with Zel'dovich paper [1] we assume that Poincaré group is deformed at some fundamental high-energy cutoff Λ_* [9] [10] [11] in accordance with the basis of the following deformed Poisson brackets

$$\begin{gathered}\left\{x^\mu, x^\nu\right\} = \varkappa^{-1}\left(x^\mu \eta^{0\nu} - x^\nu \eta^{\mu 0}\right), \left\{p^\mu, p^\nu\right\} = 0, \\ \left\{x^\mu, p^\nu\right\} = -\eta^{\mu\nu} + \varkappa^{-1}\eta^{\mu 0} p^\nu\end{gathered} \tag{16}$$

where $\mu,\nu = 0,1,2,3$, $\eta^{\mu\nu} = (+1,-1,-1,-1)$ and is a parameter identified as the ratio between the high-energy cutoff Λ_* and the light speed. The corresponding to (16) momentum transformation reads [11]

$$\begin{gathered}p_0' = \frac{\gamma\left(p_0 - up_x\right)}{1+(c\varkappa)^{-1}\left[(\gamma-1)p_0 - \gamma up_x\right]}, p_x' = \frac{\gamma\left(p_x - up_0/c^2\right)}{1+(c\varkappa)^{-1}\left[(\gamma-1)p_0 - \gamma up_x\right]}, \\ p_y' = \frac{p_y}{1+(c\varkappa)^{-1}\left[(\gamma-1)p_0 - \gamma up_x\right]}, p_z' = \frac{p_z}{1+(c\varkappa)^{-1}\left[(\gamma-1)p_0 - \gamma up_x\right]},\end{gathered} \tag{17}$$

and coordinate transformation reads [11]

$$\begin{gathered}t' = \frac{\gamma\left(t - ux/c^2\right)}{1+(c\varkappa)^{-1}\left[(\gamma-1)p_0 - \gamma up_x\right]}, x' = \frac{\gamma\left(x - ut\right)}{1+(c\varkappa)^{-1}\left[(\gamma-1)p_0 - \gamma up_x\right]}, \\ y' = \frac{y}{1+(c\varkappa)^{-1}\left[(\gamma-1)p_0 - \gamma up_x\right]}, z' = \frac{z}{1+(c\varkappa)^{-1}\left[(\gamma-1)p_0 - \gamma up_x\right]},\end{gathered} \tag{18}$$

where $\gamma = \sqrt{1-u^2/c^2}$. It is easy to check that the energy $E = c\varkappa$, identified as the high-energy cutoff Λ_*, is an invariant as it is also the case for the fundamental length $l_{\Lambda_*} = \hbar c/E = \hbar/\varkappa$.

Remark 1.1.2. Note that the transformation (17) defined in *p*-space and the transformation (1.1.18) defined in *x*-space becomes Lorentz for small energies and momenta and defines a large invariant energy $l_{\Lambda_*}^{-1}$. The high-energy cutoff Λ_* is preserved by the modified action of the Lorentz group [9] [10].

This meant that the canonical concept of metric as quadratic invariant collapses at high energies, being replaced by the non-quadratic invariant [9]:

$$\|p\|^2 = \frac{\eta^{ab} p_a p_b}{\left(1 + l_{\Lambda_*} p_0\right)}, \tag{19}$$

or by the non-quadratic invariant

$$\|p\|^2 = \frac{\eta^{ab} p_a p_b}{\left(1 - l_{\Lambda_*} p_0\right)}, \tag{20}$$

where $l_{\Lambda_*} = \Lambda_*^{-1}, a,b = 0,1,2,3$.

Remark 1.1.3. Note that:

1) the invariant (16) is infinite for the new negative invariant energy scale of the theory $\Lambda_* = -l_{\Lambda_*}^{-1}$, and it's not quadratic for energies close or above and

2) the invariant (17) is infinite for the new positive invariant energy scale of the theory $\Lambda_* = l_{\Lambda_*}^{-1}$.

Remark 1.1.4. It is also clear from Equation (16) and Equation (17) that the symmetry of positive and negative values of the energy is broken. The two theories with the two signs of l_Λ obviously are physically distinct; and we know of no theoretical argument which fixes the signs of Λ

The massive particles have a positive invariant $\|p\|^2 > 0$ which can be identified with the square of the mass $\|p\|^2 = m^2$, ($c = 1$). Thus in the case of the invariant (16) we obtain

$$\frac{p_0^2 - p^2}{\left(1 + l_{\Lambda_*} p_0\right)^2} = m^2, p_0 \in \left(-l_{\Lambda_*}^{-1}, \infty\right) \tag{21}$$

From Equation (18) we obtain

$$p_0 = \frac{m^2 l_{\Lambda_*}}{1 - m^2 l_{\Lambda_*}^2} + \frac{1}{\sqrt{1 - m^2 l_{\Lambda_*}^2}} \sqrt{\frac{m^4 l_{\Lambda_*}^2}{1 - m^2 l_{\Lambda_*}^2} + \left(p^2 + m^2\right)}. \tag{22}$$

In the case of the invariant (17) we obtain

$$\frac{p_0^2 - p^2}{\left(1 - l_{\Lambda_*} p_0\right)^2} = m^2, p_0 \in \left(-\infty, l_{\Lambda_*}^{-1}\right). \tag{23}$$

From Equation (20) we obtain

$$p_0 = -\frac{m^2 l_{\Lambda_*}}{1 - m^2 l_{\Lambda_*}^2} - \frac{1}{\sqrt{1 - m^2 l_{\Lambda_*}^2}} \sqrt{\frac{m^4 l_{\Lambda_*}^2}{1 - m^2 l_{\Lambda_*}^2} + \left(p^2 + m^2\right)}. \tag{24}$$

The action for a scalar field φ must be invariant under the deformed Lorentz transformations. The invariant action reads [10]

$$S = \frac{1}{2} \int \mathrm{d}^4 x \frac{\eta^{ab} (\partial_a \varphi)(\partial_b \varphi)}{\left[1 + l_{\Lambda_*} \partial_0 \varphi\right]} + \frac{m^2}{2} \varphi^2. \tag{25}$$

Thus there is no linear field equation.

Remark 1.1.5. Throughout this paper, we use below high-energy cutoff Λ_* the perturbative expansion

$$S = \frac{1}{2} \int \mathrm{d}^4 x \left(\eta^{ab} (\partial_a \varphi)(\partial_b \varphi) + \frac{m^2}{2} \varphi^2 \right) + O\left(l_{\Lambda_*}\right). \tag{26}$$

and dealing in Lorentz invariant approximation

$$S \simeq \frac{1}{2} \int \mathrm{d}^4 x \left(\eta^{ab} (\partial_a \varphi)(\partial_b \varphi) + \frac{m^2}{2} \varphi^2 \right). \tag{27}$$

since for $l_{\Lambda_*} \ll 1$ the expansion (26) holds.

(**II**) The canonical concept of Minkowski space-time collapses at a small distance $l_{\Lambda_*} = \Lambda_*^{-1}$ to fractal space-time with Hausdorff-Colombeau negative dimension and therefore the canonical Lebesgue measure $\mathrm{d}^4 x$ being replaced by the Colombeau-Stieltjes measure with negative Hausdorff-Colombeau dimension D^-:

$$\left(\mathrm{d}\eta(x,\varepsilon)\right)_\varepsilon = \left(v_\varepsilon\left(s(x)\right)\mathrm{d}^4 x\right)_\varepsilon, \tag{28}$$

where $\left(v_\varepsilon\left(s(x)\right)\right)_\varepsilon = \left(\left(\left|s(x)\right|^{\left|D^-\right|}+\varepsilon\right)^{-1}\right)_\varepsilon$ and $s(x)=\sqrt{x_\mu x^\mu}$, see Section 3 and [12].

(**III**) The canonical concept of momentum space collapses at fundamental high-energy cutoff Λ_* to fractal momentum space with Hausdorff-Colombeau negative dimension and therefore the canonical Lebesgue measure $\mathrm{d}^3\mathbf{k}$, where $\mathbf{k}=\left(k_x,k_y,k_z\right)$ being replaced by the Hausdorff-Colombeau measure

$$\mathrm{d}^{D^+,D^-}\mathbf{k} \triangleq \frac{\Delta\left(D^-\right)\mathrm{d}^{D^+}\mathbf{k}}{\left(\left|\mathbf{k}\right|^{\left|D^-\right|}+\varepsilon\right)_\varepsilon} = \frac{\Delta\left(D^+\right)\Delta\left(D^-\right)p^{D^+-1}\mathrm{d}p}{\left(p^{\left|D^-\right|}+\varepsilon\right)_\varepsilon}, \tag{29}$$

where $\Delta\left(D^\pm\right)=2\pi^{D^\pm/2}\big/\Gamma\left(D^\pm/2\right)$ and $p=\left|\mathbf{k}\right|=\sqrt{k_x+k_y+k_z}$ and where $D^+-\left|D^-\right|\leq -6$, see Section 3 and ref. [9]. Hausdorff-Colombeau measure (29) avoids classical divergence (10) of the zeropoint energy $\varepsilon_{\mathrm{vac}}(m)$ and instead Equation (10) one obtains

$$\varepsilon_{\mathrm{vac}}\left(p_*,m\right)=\int_0^{p_*}\mathrm{d}^3 p\sqrt{p^2+m^2}+\Delta\left(D^+\right)\Delta\left(D^-\right)\int_{p_*}^{\infty}\mathrm{d}pp^2\frac{\sqrt{p^2+m^2}}{\left(p^{\left|D^-\right|}+\varepsilon\right)_\varepsilon}\simeq p_*^4. \tag{30}$$

See Section 5 and ref. [12].

Remark 1.1.6. If we take the Planck scale (*i.e.* the Planck mass) as a cut-off, the vacuum energy density $\varepsilon_{\mathrm{vac}}\left(p_*,m\right)$ is 10^{121} times larger than the observed dark energy density $\varepsilon_{\mathrm{de}}$. Several possible approaches to the problem of vacuum energy have been discussed in the contemporary literature, for the review see [5], [12]. They can be roughly devided into five different groups: 1) Modification of gravity on large scales. 2) Anthropic principle.

3) Symmetry leading to $\varepsilon_{\mathrm{vac}}=0$. 4) Adjustment mechanism, see. 5) Hidden nonstandard dark matter sector and corresponding hidden symmetry leading to $\varepsilon_{\mathrm{vac}}\simeq 0$, see [12].

(**IV**) We assume that there exists the nonstandard dark matter sector formed by ghost particles, see [12].

1.2. Zel'dovich Approach by Using Pauli-Villars Regularization Revisited. Ghosts as Physical Dark Matter

Remind that vacuum energy density for free scalar quantum field is

$$\varepsilon(\mu)=\frac{1}{2}\frac{c}{(2\pi\hbar)^3}\int_0^\infty 4\pi\sqrt{p^2+\mu^2}\,p^2\mathrm{d}p=K\int_0^\infty\sqrt{p^2+\mu^2}\,p^2\mathrm{d}p=KI(\mu), \quad (31)$$

where $\mu=m_0c$. From Equation (31) one obtains [1]

$$p(\mu)=\frac{K}{3}\int_0^\infty\frac{p^4\mathrm{d}p}{\sqrt{p^2+\mu^2}}=KF(\mu). \quad (32)$$

For fermionic quantum field one obtains

$$\varepsilon(\mu)=KI(\mu),\, p(\mu)=-4KF(\mu). \quad (33)$$

Thus free vacuum energy density ε and corresponding pressure p is

$$\varepsilon=\sum_i C_iI(\mu_i),P=\sum_i C_iF(\mu_i). \quad (34)$$

From Equation (34) by using Pauli-Willars regularization [7] [8] in general case one obtains [1]

$$\varepsilon=\int f(\mu)I(\mu)\mathrm{d}\mu,P=\int f(\mu)F(\mu)\mathrm{d}\mu. \quad (35)$$

In order to obtain asymptotical expansion on the parameter p_0 of the quantity $\varepsilon_{\text{vac}}(p_0,m)=\int_0^{p_0}\mathrm{d}^3p\sqrt{p^2+m^2}$ let us evaluate now the following integral

$$\begin{aligned}I(\mu,p_0)&=\int_0^{p_0}p^2\sqrt{p^2+\mu^2}\,\mathrm{d}p=\int_0^{p_\mu}p^2\sqrt{p^2+\mu^2}\,\mathrm{d}p+\int_{p_\mu}^{p_0}p^2\sqrt{p^2+\mu^2}\,\mathrm{d}p\\&=\int_0^{p_\mu}p^2\sqrt{p^2+\mu^2}\,\mathrm{d}p=\int_{p_\mu}^{p_\mu}p^3\sqrt{1+\frac{\mu^2}{p^2}}\mathrm{d}p+\int_{p_\mu}^{p_0}p^3\sqrt{1+\frac{\mu^2}{p^2}}\mathrm{d}p\end{aligned} \quad (36)$$

and

$$\begin{aligned}F(\mu,p_0)&=\frac{1}{3}\int_0^{p_0}\frac{p^4\mathrm{d}p}{\sqrt{p^2+\mu^2}}=\frac{1}{3}\int_0^{p_\mu}\frac{p^4\mathrm{d}p}{\sqrt{p^2+\mu^2}}+\frac{1}{3}\int_{p_\mu}^{p_0}\frac{p^4\mathrm{d}p}{\sqrt{p^2+\mu^2}}\\&=\frac{1}{3}\int_0^{p_\mu}\frac{p^4\mathrm{d}p}{\sqrt{p^2+\mu^2}}+\frac{1}{3}\int_{p_\mu}^{p_0}\frac{p^3\mathrm{d}p}{\sqrt{1+\frac{\mu^2}{p^2}}},\end{aligned} \quad (37)$$

where $p_\mu=r\mu, r>1, \mu/p<1/r<1$. Note that

$$\begin{aligned}&\sqrt{1+\frac{\mu^2}{p^2}}=1+\frac{1}{2}\frac{\mu^2}{p^2}-\frac{1}{8}\frac{\mu^4}{p^4}+\frac{1}{16}\frac{\mu^6}{p^6}+\cdots\\&p^2\sqrt{p^2+\mu^2}=p^3\sqrt{1+\frac{\mu^2}{p^2}}=p^3+\frac{1}{2}\mu^2p-\frac{1}{8}\frac{\mu^4}{p}+\frac{1}{16}\frac{\mu^6}{p^3}+\cdots\end{aligned} \quad (38)$$

By inserting Equation (38) into Equations (36) one obtains

$$I(\mu,p_0)=C_1\mu^4+\frac{1}{4}p_0^4+\frac{1}{4}\mu^2p_0^2-\frac{1}{8}\mu^4\ln\left(\frac{p_0}{\mu}\right)-\frac{1}{32}\frac{\mu^6}{p_0^2}+p_0^{-5}O(\mu^8), \quad (39)$$

where $C_1\mu^4=\int_0^{p_\mu}p^2\sqrt{p^2+\mu^2}\mathrm{d}p$. Note that

$$\left(\sqrt{1+\frac{\mu^2}{p^2}}\right)^{-1} = 1-\frac{1}{2}\frac{\mu^2}{p^2}+\frac{3}{8}\frac{\mu^4}{p^4}-\frac{5}{16}\frac{\mu^6}{p^6}+\cdots \tag{40}$$

By inserting Equation (40) into Equation (37) one obtains

$$F(\mu, p_0) = C_2\mu^4 + \frac{1}{12}p_0^4 - \frac{1}{12}\mu^2 p_0^2 + \frac{1}{8}\mu^4 \ln\left(\frac{p_0}{\mu}\right) + \frac{5}{32}\frac{\mu^6}{p_0^2} + p_0^{-5}O(\mu^8). \tag{41}$$

By inserting Equation (39) and Equation (41) into Equations (35) one obtains

$$\begin{aligned}
\varepsilon &= \frac{1}{4}p_0^4\int_0^{\mu_{\text{eff}}} f(\mu)\mathrm{d}\mu + \frac{1}{4}p_0^2\int_0^{\mu_{\text{eff}}} f(\mu)\mu^2\mathrm{d}\mu + \left(C_1 - \frac{1}{8}\ln p_0\right)\int_0^{\mu_{\text{eff}}} f(\mu)\mu^4\mathrm{d}\mu \\
&\quad + \frac{1}{8}\int_0^{\mu_{\text{eff}}} f(\mu)\mu^4(\ln\mu)\mathrm{d}\mu - \left(\frac{1}{p_0^2}\right)\frac{1}{32}\int_0^{\mu_{\text{eff}}} f(\mu)\mu^6\mathrm{d}\mu + O\left(\int_0^{\mu_{\text{eff}}} f(\mu)\mu^8\right)p_0^{-5}, \\
p &= \frac{1}{12}p_0^4\int_0^{\mu_{\text{eff}}} f(\mu)\mathrm{d}\mu - \frac{1}{12}p_0^2\int_0^{\mu_{\text{eff}}} f(\mu)\mu^2 d\mu + \left(C_2 + \frac{1}{8}\ln p_0\right)\int_0^{\mu_{\text{eff}}} f(\mu)\mu^4\mathrm{d}\mu \\
&\quad - \frac{1}{8}\int_0^{\mu_{\text{eff}}} f(\mu)\mu^4(\ln\mu)\mathrm{d}\mu + \left(\frac{5}{p_0^2}\right)\frac{1}{32}\int_0^{\mu_{\text{eff}}} f(\mu)\mu^6\mathrm{d}\mu + O\left(\int_0^{\mu_{\text{eff}}} f(\mu)\mu^8\right)p_0^{-5}.
\end{aligned} \tag{42}$$

We choose now

$$\int_0^{\mu_{\text{eff}}} f(\mu)\mathrm{d}\mu = \int_0^{\mu_{\text{eff}}} f(\mu)\mu^2\mathrm{d}\mu = \int_0^{\mu_{\text{eff}}} f(\mu)\mu^4\mathrm{d}\mu = 0. \tag{43}$$

By inserting Equation (43) into Equations (42) one obtains

$$\begin{aligned}
\varepsilon(\mu_{\text{eff}}) &= \frac{1}{8}\int_0^{\mu_{\text{eff}}} f(\mu)\mu^4(\ln\mu)\mathrm{d}\mu + O(p_0^{-2}), \\
p(\mu_{\text{eff}}) &= -\frac{1}{8}\int_0^{\mu_{\text{eff}}} f(\mu)\mu^4(\ln\mu)\mathrm{d}\mu + O(p_0^{-2}).
\end{aligned} \tag{44}$$

Taking the limit $p \to \infty$ in Equation (44) gives

$$\begin{aligned}
\varepsilon(\mu_{\text{eff}}) &= \frac{1}{8}\int_0^{\mu_{\text{eff}}} f(\mu)\mu^4(\ln\mu)\mathrm{d}\mu, \\
p(\mu_{\text{eff}}) &= -\frac{1}{8}\int_0^{\mu_{\text{eff}}} f(\mu)\mu^4(\ln\mu)\mathrm{d}\mu.
\end{aligned} \tag{45}$$

Thus finally we obtain [3]

$$\varepsilon(\mu_{\text{eff}}) = -p(\mu_{\text{eff}}) = \frac{1}{8}\int_0^{\mu_{\text{eff}}} f(\mu)\mu^4(\ln\mu)\mathrm{d}\mu = \frac{c^4\Lambda}{8\pi G}. \tag{46}$$

Remark 1.2.1. Remind that Pauli-Villars regularization consists of introducing a fictitious mass term. For example, we would replace a propagator $1/(k^2 - m_0^2 + i\epsilon)$, by the regulated propagator

$$\Delta(k^2) = \sum_{i=0}^{N}\frac{a_i}{k^2 - m_i^2 + i\epsilon} = \frac{1}{k^2 - m_0^2 + i\epsilon} - \sum_{i=0}^{N}\frac{a_i}{k^2 - m_i^2 + i\epsilon}, \tag{47}$$

where $a_0 = 1$ and $m_i, i = 1, 2, \cdots, N$ can be thought of as the mass of a fictitious heavy particle, whose contribution is subtracted from that of an ordinary particle. Assume that $m_i^2/k^2 < 1$, if we expand each term of this sum (46) as a power series in $k^2+i\epsilon$ we get

$$\Delta\left(k^2\right)=\sum_{i=0}^{N}\frac{a_i}{k^2+i\epsilon}+\sum_{i=0}^{N}\frac{a_i m_i^2}{\left(k^2+i\epsilon\right)^2}+\sum_{i=0}^{N}O\left(\frac{1}{\left(k^2+i\epsilon\right)^3}\right). \tag{48}$$

For a renormalizable theory the maximum supercriticial power of divergence of any integral is quadratic, so that the $O\left(1/k^6\right)$ terms are ultraviolet finite. The finiteness of the regulated integral is then guaranteed by requiring that

$$\sum_{i=0}^{N}a_i=0,\sum_{i=0}^{N}a_i m_i^2=0. \tag{49}$$

Remark 1.2.2. Note that in order to apply Pauli-Villars regularization to QFT with Lagrangian $\mathcal{L}\left(\varphi,\psi,\partial_\mu\varphi,\partial_\mu\psi\right)$ we would replace the Lagrangian $\mathcal{L}\left(\varphi,\psi,\partial_\mu\varphi,\partial_\mu\psi\right)$ by Lagrangian $\underline{\mathcal{L}}\left(\underline{\varphi},\underline{\psi},\partial_\mu\underline{\varphi},\partial_\mu\underline{\psi}\right)$, where [7]:

$$\underline{\varphi}(x)=\varphi(x)+\sum_n b_n\breve{\varphi}_n\left(x,\mu_n^2\right),\underline{\psi}(x)=\psi(x)+\sum_n c_n\breve{\psi}_n\left(x,\varkappa_n^2\right), \tag{50}$$

where commutator for $\breve{\varphi}_n$ and anticommutator for $\breve{\psi}_n$ reads

$$\left[\breve{\varphi}_m\left(x,\mu_m^2\right),\breve{\varphi}_n\left(x',\mu_n^2\right)\right]=-i\rho_n\Delta\left(x-x',\mu_n^2\right)\delta_{mn},$$
$$\left\{\breve{\psi}_m\left(x,\varkappa_m^2\right),\breve{\psi}_n\left(x',\varkappa_n^2\right)\right\}=-i\varepsilon_n S\left(x-x',\varkappa_n^2\right)\delta_{mn}.$$

From Equations (50)-Equations (51) one obtains

$$\begin{aligned}&\left[\underline{\varphi}(x),\underline{\varphi}(x')\right]=i\sum_{n=0}^{N}\rho_n b_n^2\Delta\left(x-x',\mu_n^2\right),\\&\left[\underline{\psi}(x),\underline{\psi}(x')\right]=-i\sum_{n=0}^{N}\varepsilon_n\bar{c}_n c_n S\left(x-x',\varkappa_n^2\right).\end{aligned} \tag{52}$$

Assume now that

$$\sum_{n=0}^{N}\rho_n b_n^2=0,\sum_{n=0}^{N}\rho_n b_n^2\mu_n^2=0,\sum_{n=0}^{N}\varepsilon_n\bar{c}_n c_n=0,\sum_{n=0}^{N}\varepsilon_n\bar{c}_n c_n\varkappa_n^2=0. \tag{53}$$

From Equations (53) it follows directly that QFT with Lagrangian $\underline{\mathcal{L}}\left(\underline{\varphi},\underline{\psi},\partial_\mu\underline{\varphi},\partial_\mu\underline{\psi}\right)$ is finite QFT with indefinite metric [4], see Remark 1.2.1.

Remark 1.2.3. Note that "bad ghosts" represent general meaning of the word "ghost" in theoretical physics: states of negative norm [7] or fields with the wrong sign of the kinetic term, such as Pauli--Villars ghosts φ, whose existence allows the probabilities to be negative thus violating unitarity. The quadratic lagrangian $\mathcal{L}_\varphi^2$ for φ begins with a wrong sign kinetic term [in $(+---)$ signature]

$$\mathcal{L}_\varphi^2=-\frac{1}{2}\partial^\mu\varphi\partial_\mu\varphi+\cdots \tag{54}$$

Remark 1.2.4. Note that in order to obtain Equations (44), the standard quantum fields do not need to couple directly to the ghost sector. In this paper the ghost sector is considered as physical mechanism which acts only on a function $f(\mu)$ in Equations (43). It means that there exists the ghost-driven acceleration of the universe hidden in cosmological constant Λ.

Remark 1.2.5. As pointed out in paper [13] even if the standard model fields have no direct couplings to the ghost sector, they will indirectly interact with it through gravity, and the propagation of gravity through the ghost condensate gives rise to a fascinating modification of gravity in the IR. However, no modifications of gravity can be seen directly, and no cosmological experiment can distinguish the ghost-driven acceleration from a cosmological constant.

Remark 1.2.6. In order to obtain desired physical result from Equations (45), *i.e.*,

$$\varepsilon_{\text{vac}} = 0.7\times10^{-29}\,\text{g}\cdot\text{cm}^{-3} = 2.8\times10^{-47}\,\text{GeV}^4/\hbar^3c^5 \tag{55}$$

we assume that

$$f(\mu) = f_{s.m.}(\mu) + f_{g.m.}(\mu), \tag{56}$$

where $f_{s.m.}(\mu)$ corresponds to standard matter and where $f_{g.m.}(\mu)$ corresponds to a physical ghost matter.

Remark 1.2.7. We assume now that

$$|f(\mu)| = \begin{cases} O(\mu^{-n}), n > 1 & \mu \le \mu_{\text{eff}} \\ 0 & \mu > \mu_{\text{eff}} \end{cases} \tag{57}$$

From Equation (57) and Equation (45) it follows directly that

$$|p(\mu_{\text{eff}})| = |\varepsilon(\mu_{\text{eff}})| = \frac{1}{8}\left|\int_0^{\mu_{\text{eff}}} f(\mu)\mu^4(\ln\mu)\,\mathrm{d}\mu\right| \le O\left(\mu_{\text{eff}}^{-n+5}\ln\mu_{\text{eff}}\right). \tag{58}$$

Remark 1.2.8. However serious problem arises from non-renormalizability of canonical quantum gravity with Einstein-Hilbert action

$$S_{EH} = \frac{1}{16\pi G}\int \mathrm{d}^4x\sqrt{-g}R. \tag{59}$$

For example taking Λ^3 particles of energy a per unit volume gives the gravitational self-energy density of order Λ^6, *i.e.*, the density ε_Λ diverges as Λ^6

$$\varepsilon_\Lambda \simeq G\Lambda^6, \tag{60}$$

where Λ is a high-energy cutoff [5].

In order to avoid these difficulties we apply instead Einstein-Hilbert action (59) the gravitational action which includes terms quadratic in the curvature tensor

$$\Im = -\int \mathrm{d}^4x\sqrt{-g}\left(\alpha R_{\mu\nu}R^{\mu\nu} - \beta R^2 + 2\kappa^{-2}R\right), \tag{61}$$

Remark 1.2.9. Gravitational actions (61) which include terms quadratic in the curvature tensor are renormalizable [14]. The requirement that the graviton propagator behaves like p^{-4} for large momenta makes it necessary to choose the indefinite-metric vector space over the negative-energy states. These negative-norm states cannot be excluded from the physical sector of the vector space without destroying the unitarity of the $\mathbf{S}$ matrix, however, for their unphysical behavior may be restricted to arbitrarily large energy scales Λ_* by an appropriate limitation on the renormalized masses m_2 and m_0.

Remark 1.2.10. We assume that $m_0c \gg \mu_{\text{eff}}, m_2c \gg \mu_{\text{eff}}$.

Remark 1.2.11. The canonical Quantum Field Theory is widely believed to break down at some fundamental high-energy cutoff Λ_* and therefore the quantum fluctuations in the vacuum can be treated classically seriously only up to this high-energy cutoff, see for example [15]. In this paper we argue that Quantum Field Theory in fractal space-time with negative Hausdorff-Colombeau dimensions [12] gives high-energy cutoff on natural way.

2. Ghosts as Physical Dark Matter

2.1. Paulu-Villars Ghosts As Physical Dark Matter

Before explaining the role of PV ghosts, etc. as physical dark matter remind the idea of PV regularization as a conventional UV regularization. We consider, as an example, the scalar field theory with the interaction $\lambda\varphi^4$. Lagrangian density of this theory reads

$$\mathcal{L} = \frac{1}{2}\partial^\mu\varphi\partial_\mu\varphi - \frac{m_0^2}{2}\varphi^2 + \lambda\varphi^4. \tag{62}$$

This theory requires UV regularization (e.g. in (2+1) and (3+1) dimensions). Let us show that it is sufficient to introduce N extra fields with large mass playing the role of the regularization parameter. Lagrangian density can be rewritten as follows

$$\begin{gathered}\mathcal{L} = \sum_{i=0}^{N}(-1)^i\left(\frac{1}{2}\partial^\mu\varphi\partial_\mu\varphi - \frac{m_i^2}{2}\varphi_i^2\right) + \lambda : \varphi^4 :, \\ \varphi = \varphi_0 + \breve{\varphi} = \sum_{i=0}^{N}\varphi_i, \breve{\varphi} = \sum_{i=0}^{N}a_i\varphi_i.\end{gathered} \tag{63}$$

Here the symbol "::" means that in perturbation theory we drop Feynman diagrams with loops containing only one vertex. The φ_0 is usual field with mass m_0 and the $\varphi_i, i = 1,\cdots,N$ is the extra field with mass $m_i, i = 1,\cdots,N$. It can be shown that in (3+1)-dimensional theory the introduction of one PV field is sufficient for the ultraviolet regularization of perturbation theory in λ. One can show that momentum space Feynman diagrams in the original theory with Lagrangian density (62) diverge no more than quadratically [16] [17] [18] (beside of vacuum diagrams) shown in **Figure 1**.

If we consider now Feynman diagrams in the theory with Lagrangian density (63) we see that propagators of fields φ_0 and $\breve{\varphi}$ sum up in corresponding diagrams so that we obtain the following expression which plays the role of regularized propagator

$$\Delta\left(k^2\right) = \sum_{j=0}^{N}\frac{a_j}{k^2 - m_j^2 + i0} = \frac{1}{k^2 - m_0^2 + i0} - \sum_{j=0}^{N}\frac{a_j}{k^2 - m_j^2 + i0}, \tag{64}$$

where $k^2 = k_0^2 - k_1^2 + k_2^2 + k_3^2$. Integral corresponding to vacuum diagram is

$$\Im = \int\frac{\mathrm{d}^4k}{(2\pi)^4}\Delta\left(k^2\right) = \int\frac{\mathrm{d}^4k}{(2\pi)^4}\sum_{j=0}^{N}\frac{a_j}{k^2 - m_j^2 + i0}. \tag{65}$$

To do this integral, since it is convergent, we can Wick rotate.

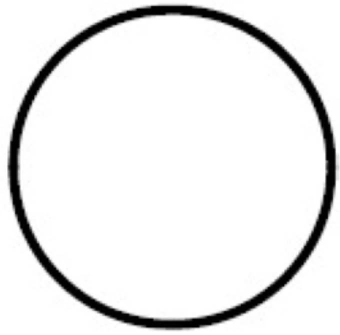

Figure 1. One-loop massive vacuum diagram.

Remark 2.1.1. All the integrals in quantum field theory are written in Minkowski space, however, the ultraviolet divergence appears for large values of modulus of momentum and it is useful to regularise it in Euclidean space [17]. Transition to Euclidean space can be achieved by replacing thr zeroth component of momentum $k_0 \to ik_4$, where the integration over the fourth component of momenta goes along the imaginary axis. To go to the integration along the real axis, one has to perform the (Wick) rotation of the integration contour by 90° (see **Figure 2**). This is possible since the integral over the big circle vanishes and during the transformation of the contour it does not cross the poles.

Then we get

$$\Im_E = \frac{i}{8\pi^2}\int_0^{\infty} \mathrm{d}k_E \sum_{j=0}^{N} \frac{a_j k_E^3}{k_E^2 + m_j^2}. \tag{66}$$

To do this integral, since it is convergent, we can deal with regularized integral

$$\Im(\varepsilon,\Lambda) = \frac{i}{8\pi^2}\int_{\varepsilon}^{\Lambda} \mathrm{d}k_E \sum_{j=0}^{N} \frac{a_j k_E^3}{k_E^2 + m_j^2}, \tag{67}$$

where $\varepsilon \asymp 0, \Lambda \asymp \infty$, *i.e.* $\Im(\varepsilon,\Lambda) \approx \Im_E$. We assume now that Pauli-Villars conditions given by Equations (48) holds. Let us consider now the quantity

$$\Im_\eta \triangleq \Im_\eta(\varepsilon,\Lambda) = \frac{i}{8\pi^2}\int_{\varepsilon}^{\Lambda} \mathrm{d}k_E \sum_{j=0}^{N} \frac{a_j k_E^3}{k_E^2 + \eta m_j^2}, \tag{68}$$

where $\eta \in (0,1]$, and therefore from Equation (68) we obtain

$$\Im_\eta\big|_{\eta=0} = \frac{i}{8\pi^2}\int_{\varepsilon}^{\Lambda} \mathrm{d}k_E \sum_{j=0}^{N} a_j k_E = \frac{i}{8\pi^2}\sum_{j=0}^{N} a_j \int_{\varepsilon}^{\Lambda} k_E \mathrm{d}k_E \equiv 0, \tag{69}$$

since Equations (48) holds. From Equation (68) by differentiation we obtain

$$\frac{\mathrm{d}}{\mathrm{d}\eta}\Im_\eta = \frac{i}{8\pi^2}\int_{\varepsilon}^{\Lambda} \mathrm{d}k_E \sum_{j=0}^{N} \frac{a_j m_j^2 k_E^3}{\left(k_E^2 + \eta m_j^2\right)^2}, \tag{70}$$

and therefore from Equation (39) we obtain

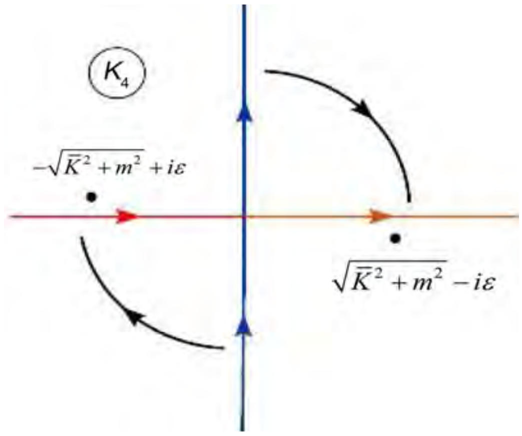

Figure 2. The Wick rotation of the integration contour.

$$\begin{aligned}\left.\frac{\mathrm{d}}{\mathrm{d}\eta}\Im_\eta\right|_{\eta=0} &= \frac{i}{8\pi^2}\int_\varepsilon^\Lambda \mathrm{d}k_E \sum_{j=0}^N \left.\frac{a_j m_j^2 k_E^3}{\left(k_E^2+\eta m_j^2\right)^2}\right|_{\eta=0} \\ &= \frac{i}{8\pi^2}\sum_{j=0}^N a_j m_j^2 \int_\varepsilon^\Lambda k_E^{-1}\mathrm{d}k_E \equiv 0,\end{aligned} \tag{71}$$

since Equations (48) holds. From Equation (70) by differentiation we obtain

$$\begin{aligned}&\frac{\mathrm{d}^2}{\mathrm{d}\eta^2}\Im_\eta = \sum_{j=0}^N \Re_j(\eta) = \frac{i}{4\pi^2}\int_\varepsilon^\Lambda \mathrm{d}k_E \sum_{j=0}^N \frac{a_j m_j^4 k_E^3}{\left(k_E^2+\eta m_j^2\right)^3}, \\ &\Re_j(\eta) = \frac{i a_j m_j^4}{4\pi^2}\int_\varepsilon^\Lambda \mathrm{d}k_E \frac{k_E^3}{\left(k_E^2+\eta m_j^2\right)^3}.\end{aligned} \tag{72}$$

Note that

$$\Re_j(\eta) \simeq \frac{i a_j m_j^4}{4\pi^2}\int_0^\infty \mathrm{d}k_E \frac{k_E^3}{\left(k_E^2+\eta m_j^2\right)^3} = \frac{i a_j m_j^4}{4\pi^2}\frac{-i}{4\eta m_j^2} = \frac{a_j m_j^2}{16\pi^2\eta}. \tag{73}$$

Thus

$$\frac{\mathrm{d}}{\mathrm{d}\eta}\Im_\eta = \sum_{j=0}^N \int_0^1 \Re_j(\eta)\mathrm{d}\eta = \sum_{j=0}^N \frac{a_j m_j^2}{16\pi^2}\ln\eta \tag{74}$$

and

$$\Im_\eta = \sum_{j=0}^N \frac{a_j m_j^2}{16\pi^2}(\eta\ln\eta-\eta), \tag{75}$$

Therefore

$$\Im(\varepsilon,\Lambda) = \Im_\eta\big|_{\eta=1} = -\sum_{j=0}^N \frac{a_j m_j^2}{16\pi^2} \equiv 0, \tag{76}$$

since Equations (48) holds. Thus integral (65) corresponding to vacuum diagram by using Pauli-Villars renormalization identically equal zero, *i.e.*

$$\mathrm{Ren}_{PV}(\Im) = \frac{\mathrm{d}^4k}{(2\pi)^4}\Delta\left(k^2\right) = \frac{\mathrm{d}^4k}{(2\pi)^4}\sum_{j=0}^N \frac{a_j}{k^2-m_j^2+i0} \equiv 0. \tag{77}$$

Let us consider now how this method works in the case of the simplest scalar diagram shown in Figure 3. The corresponding Feinman integral has the form

$$\Im\left(p^2\right)=\frac{1}{(2\pi)^4}\int\frac{\mathrm{d}^4k}{\left(k^2-m_0^2+i0\right)\left[\left(p^2-k^2\right)-m_0^2+i0\right]}. \tag{78}$$

Regularized Feinman integral (78) reads

$$\Im_{reg}\left(p^2\right)=\frac{1}{(2\pi)^4}\int\sum_{j=0}^{N}\frac{a_j\mathrm{d}^4k}{\left(k^2-m_j^2+i0\right)\left[\left(p^2-k^2\right)-m_j^2+i0\right]}, \tag{79}$$

where $N=1$. To do this integral, since it is convergent, we can Wick rotate. Then we get

$$\Im_{reg}\left(p^2\right)=\frac{i}{(2\pi)^4}\int\sum_{j=0}^{N}\frac{a_j\mathrm{d}^4k}{\left(k^2+m_j^2\right)\left[\left(p^2-k^2\right)+m_j^2\right]}. \tag{80}$$

The integral (80) can be written as

$$\begin{aligned}\Im_{reg}\left(p^2\right)&=\frac{i}{(2\pi)^4}\int_0^1\mathrm{d}x\int\sum_{j=0}^{N}\frac{a_j\mathrm{d}^4k}{\left[k^2+p^2x(1-x)+m_j^2\right]^2}\\&=\frac{i}{8\pi^2}\int_0^1\mathrm{d}x\int\sum_{j=0}^{N}\frac{a_jk_E^3\mathrm{d}k_E}{\left[k_E^2+p^2x(1-x)+m_j^2\right]^2}.\end{aligned} \tag{81}$$

To do this integral, since it is convergent, we can deal with regularized integral

$$\Im_{reg}\left(p^2,\varepsilon,\Lambda\right)=\frac{i}{8\pi^2}\int_0^1\mathrm{d}x\int_\varepsilon^\Lambda\sum_{j=0}^{N}\frac{a_jk_E^3\mathrm{d}k_E}{\left[k_E^2+p^2x(1-x)+m_j^2\right]^2}. \tag{82}$$

Let us consider now the quantity

$$\Im_\eta\left(p^2,\varepsilon,\Lambda\right)=\frac{i}{8\pi^2}\int_0^1\mathrm{d}x\int_\varepsilon^\Lambda\sum_{j=0}^{N}\frac{a_jk_E^3\mathrm{d}k_E}{\left[k_E^2+p^2x(1-x)+\eta m_j^2\right]^2}. \tag{83}$$

where $\eta\in(0,1]$, and therefore from Equation (83) we obtain $\Im_0\left(p^2,\varepsilon,\Lambda\right)\equiv 0$, since Equations (48) holds. From Equation (83) by differentiation we obtain

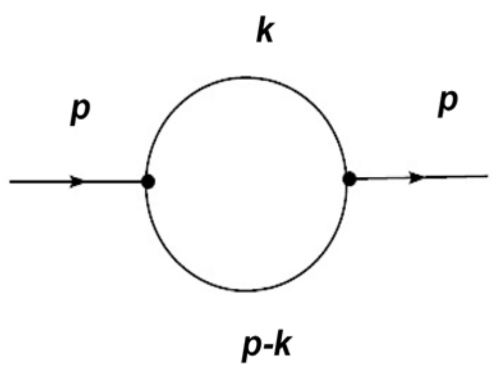

Figure 3. The simplest scalar diagram.

$$\begin{aligned}\frac{\mathrm{d}}{\mathrm{d}\eta}\Im_{\eta}\left(p^{2},\varepsilon,\Lambda\right) &= -\frac{i}{4\pi^{2}}\int_{0}^{1}\mathrm{d}x\int_{\varepsilon}^{\Lambda}\sum_{j=0}^{N}\frac{a_{j}m_{j}^{2}k_{E}^{3}\mathrm{d}k_{E}}{\left[k_{E}^{2}+p^{2}x(1-x)+\eta m_{j}^{2}\right]^{3}} \\ &\simeq -\frac{i}{4\pi^{2}}\sum_{j=0}^{N}a_{j}m_{j}^{2}\Re_{j}\left(p^{2},\eta,\Lambda,\varepsilon\right), \\ \Re_{j}\left(p^{2},\eta,\Lambda,\varepsilon\right) &\simeq \int_{0}^{1}\mathrm{d}x\int\frac{k_{E}^{3}\mathrm{d}k_{E}}{\left[k_{E}^{2}+p^{2}x(1-x)+\eta m_{j}^{2}\right]^{3}} \\ &= \frac{1}{4}\int_{0}^{1}\frac{\mathrm{d}x}{p^{2}x(1-x)+\eta m_{j}^{2}}.\end{aligned} \tag{84}$$

From Equation (84) we obtain

$$\begin{aligned}\frac{\mathrm{d}}{\mathrm{d}\eta}\Im_{\eta}\left(p^{2},\varepsilon,\Lambda\right) &\simeq -\frac{i}{4\pi^{2}}\sum_{j=0}^{N}a_{j}m_{j}^{2}\Re_{j}\left(p^{2},\eta,\varepsilon,\Lambda\right) \\ &= -\frac{i}{16\pi^{2}}\sum_{j=0}^{N}a_{j}\int_{0}^{1}\frac{\mathrm{d}x}{m_{j}^{-2}p^{2}x(1-x)+\eta}.\end{aligned} \tag{85}$$

From Equation (85) we obtain

$$\Im_{reg}\left(p^{2}\right) = -\frac{i}{16\pi^{2}}\sum_{j=0}^{N}a_{j}\int_{0}^{1}\mathrm{d}x\int_{0}^{1}\frac{\mathrm{d}\eta}{m_{j}^{-2}p^{2}x(1-x)+\eta}. \tag{86}$$

Note that

$$\begin{aligned}\int_{0}^{1}\frac{\mathrm{d}\eta}{m_{j}^{-2}p^{2}x(1-x)+\eta} &= \left[m_{j}^{-2}p^{2}x(1-x)+\eta\right]\ln\left[m_{j}^{-2}p^{2}x(1-x)+\eta\right]\Big|_{0}^{1}-1 \\ &= \left[m_{j}^{-2}p^{2}x(1-x)+1\right]\ln\left[m_{j}^{-2}p^{2}x(1-x)+1\right] \\ &\quad -\left[m_{j}^{-2}p^{2}x(1-x)\right]\ln\left[m_{j}^{-2}p^{2}x(1-x)\right]-1.\end{aligned} \tag{87}$$

Thus

$$\begin{aligned}\Im_{reg}\left(p^{2}\right) &= -\frac{i}{16\pi^{2}}\sum_{j=0}^{N=1}a_{j}\int_{0}^{1}\mathrm{d}x\int_{0}^{1}\frac{\mathrm{d}\eta}{m_{j}^{-2}p^{2}x(1-x)+\eta} \\ &= -\frac{i}{16\pi^{2}}\sum_{j=0}^{N=1}a_{j}\int_{0}^{1}\mathrm{d}x\Big\{\left[m_{j}^{-2}p^{2}x(1-x)+1\right]\ln\left[m_{j}^{-2}p^{2}x(1-x)+1\right] \\ &\quad -\left[m_{j}^{-2}p^{2}x(1-x)\right]\ln\left[m_{j}^{-2}p^{2}x(1-x)\right]\Big\}+\frac{i}{16\pi^{2}}\sum_{j=0}^{N=1}a_{j} \\ &= -\frac{i}{16\pi^{2}}\sum_{j=0}^{N=1}a_{j}\int_{0}^{1}\mathrm{d}x\Big\{\left[m_{j}^{-2}p^{2}x(1-x)+1\right]\ln\left[m_{j}^{-2}p^{2}x(1-x)+1\right] \\ &\quad -\left[m_{j}^{-2}p^{2}x(1-x)\right]\ln\left[m_{j}^{-2}p^{2}x(1-x)\right]\Big\} \\ &= -\frac{i}{16\pi^{2}}\int_{0}^{1}\mathrm{d}x\Big\{\left[m_{0}^{-2}p^{2}x(1-x)+1\right]\ln\left[m_{0}^{-2}p^{2}x(1-x)+1\right] \\ &\quad -\left[m_{0}^{-2}p^{2}x(1-x)\right]\ln\left[m_{0}^{-2}p^{2}x(1-x)\right]\Big\} \\ &\quad +\frac{i}{16\pi^{2}}\int_{0}^{1}\mathrm{d}x\Big\{\left[m_{1}^{-2}p^{2}x(1-x)+1\right]\ln\left[m_{1}^{-2}p^{2}x(1-x)+1\right] \\ &\quad -\left[m_{1}^{-2}p^{2}x(1-x)\right]\ln\left[m_{1}^{-2}p^{2}x(1-x)\right]\Big\}.\end{aligned} \tag{88}$$

From Equation (88) we obtain

$$\begin{aligned}\Im_{reg}\left(p^2\right) = & -\frac{i}{16\pi^2}\int_0^1 \mathrm{d}x\Big\{\left[m_0^{-2}p^2x(1-x)+1\right]\ln\left[m_0^{-2}p^2x(1-x)+1\right] \\ & -\left[m_0^{-2}p^2x(1-x)\right]\ln\left[m_0^{-2}p^2x(1-x)\right]\Big\} \\ & +\frac{i}{16\pi^2}\int_0^1 \mathrm{d}x\Big\{\left[m_1^{-2}p^2x(1-x)+1\right]\ln\left[m_1^{-2}p^2x(1-x)+1\right] \\ & -\left[m_1^{-2}p^2x(1-x)\right]\ln\left[m_1^{-2}p^2x(1-x)\right]\Big\}.\end{aligned} \tag{89}$$

We assume now that $m_1^{-2}p^2 \ll 1$ and from Equation (89) finally we obtain

$$\begin{aligned}\Im_{reg}\left(p^2\right) = & -\frac{i}{16\pi^2}\int_0^1 \mathrm{d}x\Big\{\left[m_0^{-2}p^2x(1-x)+1\right]\ln\left[m_0^{-2}p^2x(1-x)+1\right] \\ & -\left[m_0^{-2}p^2x(1-x)\right]\ln\left[m_0^{-2}p^2x(1-x)\right]\Big\}+O\left(m_1^{-2}p^2\right).\end{aligned} \tag{90}$$

Remark 2.1.2. The simple renormalizable models with finite masses $m_i, i=1,\cdots,N$ which we have considered in the section many years regarded only as constructs for a study of the ultraviolet problem of QFT. The difficulties with unitarity appear to preclude their direct acceptability as canonical physical theories in locally Minkowski space-time. However, for their unphysical behavior may be restricted to arbitrarily large energy scales Λ_* mentioned above by an appropriate limitation on the finite masses m_i.

2.2. Renormalizability of Higher Derivative Quantum Gravity

Gravitational actions which include terms quadratic in the curvature tensor are renormalizable. The necessary Slavnov identities are derived from Becchi-Rouet-Stora (BRS) transformations of the gravitational and Faddeev-Popov ghost fields. In general, non-gauge-invariant divergences do arise, but they may be absorbed by nonlinear renormalizations of the gravitational and ghost fields and of the BRS transformations [14]. The geneic expression of the action reads

$$I_{sym} = -\int \mathrm{d}^4x\sqrt{-g}\left(\alpha R_{\mu\nu}R^{\mu\nu} - \beta R^2 + 2\kappa^{-2}R\right), \tag{91}$$

where the curvature tensor and the Ricci is defined by $R^{\lambda}_{\mu\alpha\nu} = \partial_\nu \Gamma^{\lambda}_{\mu\alpha}$ and $R_{\mu\nu} = R^{\lambda}_{\mu\lambda\nu}$ correspondingly, $\kappa^2 = 32\pi G$. The convenient definition of the gravitational field variable in terms of the contravariant metric density reads

$$\kappa h^{\mu\nu} = g^{\mu\nu}\sqrt{-g} - \eta^{\mu\nu}. \tag{92}$$

Analysis of the linearized radiation shows that there are eight dynamical degrees of freedom in the field. Two of these excitations correspond to the familiar massless spin-2 graviton. Five more correspond to a massive spin-2 particle with mass m_2. The eighth corresponds to a massive scalar particle with mass m_0. Although the linearized field energy of the massless spin-2 and massive scalar excitations is positive definite, the linearized energy of the massive spin-2 excitations is negative definite. This feature is characteristic of higher-derivative models, and poses the major obstacle to their physical interpretation.

In the quantum theory, there is an alternative problem which may be substituted for the negative energy. It is possible to recast the theory so that the massive spin-2 eigenstates of the free-fieid Hamiltonian have positive-definite energy, but also negative norm in the state vector space.

These negative-norm states cannot be excluded from the physical sector of the vector space without destroying the unitarity of the $\mathbf{S}$ matrix. The requirement that the graviton propagator behaves like p^{-4} for large momenta makes it necessary to choose the indefinite-metric vector space over the negative-energy states.

The presence of massive quantum states of negative norm which cancel some of the divergences due to the massless states is analogous to the Pauli-Villars regularization of other field theories. For quantum gravity, however, the resulting improvement in the ultraviolet behavior of the theory is sufficient only to make it renormalizable, but not finite.

The gauge choice which we adopt in order to define the quantum theory is the canonical harmonic gauge: $\partial_\nu h^{\mu\nu}=0$. Corresponding Green's functions are then given by a generating functional

$$\begin{aligned} Z\left(T_{\mu\nu}\right) &= N\int\left[\prod\nolimits_{\mu\le\nu}\mathrm{d}h^{\mu\nu}\right]\left[\mathrm{d}C^{\sigma}\right]\left[\mathrm{d}\bar{C}_{\tau}\right]\delta^4\left(F^{\tau}\right) \\ &\times\exp\left[i\left(I_{sym}+\int\mathrm{d}^4x\bar{C}_{\tau}\vec{F}^{\tau}_{\mu\nu}D^{\mu\nu}_{\alpha}C^{\alpha}+\kappa\int\mathrm{d}^4xT_{\mu\nu}h^{\mu\nu}\right)\right]. \end{aligned} \tag{93}$$

Here $F^{\tau}=\vec{F}^{\tau}_{\mu\nu}h^{\mu\nu},\vec{F}^{\tau}_{\mu\nu}=\delta^{r}_{\mu}\vec{\partial}_{\nu}$ and the arrow indicates the direction in which the derivative acts. N is a normalization constant. C^{σ} is the Faddeev-Popov ghost field, and $\bar{C}_{\tau}$ is the antighost field. Notice that both C^{σ} and $\bar{C}_{\tau}$ are anticommuting quantities. $D^{\mu\nu}_{\alpha}$ is the operator which generates gauge transformations in $h^{\mu\nu}$, given an arbitrary spacetime-dependent vector $\xi^{\alpha}(x)$ corresponding to $x^{\mu'}=x^{\mu}+\kappa\xi^{\mu}$ and where

$$\begin{aligned} D^{\mu\nu}_{\alpha}\xi^{\alpha}(x) &= \partial^{\mu}\xi^{\nu}+\partial^{\nu}\xi^{\mu}-\eta^{\mu\nu}\partial_{\alpha}\xi^{\alpha} \\ &+\kappa\left(\partial_{\alpha}\xi^{\mu}h^{\alpha\nu}+\partial_{\alpha}\xi^{\nu}h^{\alpha\mu}-\xi^{\alpha}\partial_{\alpha}h^{\mu\nu}-\partial_{\alpha}\xi^{\alpha}h^{\mu\nu}\right) \end{aligned} \tag{94}$$

In the functional integral (93), we have written the metric for the gravitational field as $\left[\prod\nolimits_{\mu\le\nu}\mathrm{d}h^{\mu\nu}\right]$ without any local factors of $g=\det\left(g_{\mu\nu}\right)$. Such factors do not contribute to the Feynman rules because their effect is to introduce terms proportional to $\delta^4(0)\int\mathrm{d}^4x\ln(-g)$ into the effective action and $\delta^4(0)$ is set equal to zero in dimensional regularization.

In calculating the generating functional (93) by using the loop expansion, one may represent the δ function which fixes the gauge as the limit of a Gaussian, discarding an infinite normalization constant

$$\delta^4\left(F^{\tau}\right)\sim\lim_{\Delta\to0}\exp\left[i\left(\frac{1}{2}\Delta^{-1}\int\mathrm{d}^4xF_{\tau}F^{\tau}\right)\right]. \tag{95}$$

In this expression, the index τ has been lowered using the flat-space metric tensor $\eta_{\mu\nu}$. For the remainder of this paper, we shall adopt the standard approach to the covariant quantization of gravity, in which only Lorentz tensors occur, and all raising and lowering of indices is done with respect to flat space.

The graviton propagator may be calculated from $I_{sym}+\frac{1}{2}\Delta^{-1}\int \mathrm{d}^4xF_\tau F^\tau$ in the usual fashion, letting $\Delta\to 0$ after inverting. The expression $\frac{1}{2}\Delta^{-1}\int \mathrm{d}^4xF_\tau F^\tau$ contains only two derivatives. Consequently, there are parts of the graviton propagator which behave like p^{-2} for large momenta. Specifically, the p^{-2} terms consist of everything but those parts of the propagator which are transverse in all indices. These terms give rise to unpleasant infinities already at the one-loop order. For example, the graviton self-energy diagram shown in **Figure 4** has a divergent part with the general structure $\left(\partial^4 h\right)^2$. Such divergences do cancel when they are connected to tree diagrams whose outermost lines are on the mass shell, as they must if the $\mathbf{S}$ matrix is to be made finite without introducing counterterms for them. However, they greatly complicate the renormalization of Green's functions.

We may attempt to extricate ourselves from the situation described in the last paragraph by picking a different weighting functional. Keeping in mind that we want no part of the graviton propagator to fall off slower than p^{-4} for large momenta, we now choose the weighting functional [14]

$$\omega_4\left(e^\tau\right)=\exp\left[i\left(\frac{1}{2}\Delta^{-1}\int \mathrm{d}^4xe_\tau\Box^2e^\tau\right)\right], \tag{96}$$

where e^τ is any four-vector function. The corresponding gauge-fixing term in the effective action is

$$-\frac{1}{2}\kappa^2\Delta^{-1}\int \mathrm{d}^4xF_\tau\Box^2F^\tau. \tag{97}$$

The graviton propagator resulting from the gauge-fixing term (97) is derived in [14]. For most values of the parameters α and β in I_{sym} it satisfies the requirement that all its leading parts fall off like p^{-4} for large momenta. There are, however, specific choices of these parameters which must be avoided. If $\alpha=0$, the massive spin-2 excitations disappear, and inspection of the graviton propagator shows that some terms then behave like k^{-2}. Likewise, if $3\beta-\alpha=0$, the massive scalar excitation disappears, and there are again terms in the propagator which behave like p^{-2}. However, even if we avoid the special cases $\alpha=0$ and $3\beta-\alpha=0$, and if we use the propagator derived from (97), we still do not obtain a clean renormalization of the Green's functions. We now turn to the implications of gauge invariance. Before we write down the BRS transformations for gravity, let us first establish the commutation relation for gravitational gauge transformations, which reveals the group structure of the theory. Take the gauge transformation (94) of $h^{\mu\nu}$, generated by ξ^μ and

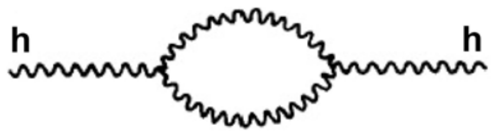

Figure 4. The one-loop graviton self-energy diagram.

perform a second gauge transformation, generated by η^{μ}, on the $h^{\mu\nu}$ fields appearing there. Then antisymmetrize in ξ^{μ} and η^{μ}. The result is

$$\frac{\delta D_{\alpha}^{\mu\nu}}{\delta h^{\rho\sigma}} D_{\beta}^{\rho\sigma}\left(\xi^{\alpha}\eta^{\beta}-\eta^{\alpha}\xi^{\beta}\right)=\kappa D_{\lambda}^{\mu\nu}\left(\partial_{\alpha}\xi^{\lambda}\eta^{\alpha}-\partial_{\alpha}\xi^{\alpha}\eta^{\lambda}\right), \tag{98}$$

where the repeated indices denote both summation over the discrete values of the indices and integration over the spacetime arguments of the functions or operators indexed.

The BRS transformations for gravity appropriate for the gauge-fixing term (96) are [13]

$$\begin{aligned}&(\mathrm{a})\ \delta_{\mathrm{BRS}} h^{\mu\nu}=\kappa D_{\alpha}^{\mu\nu} C^{\alpha}\delta\lambda,\\&(\mathrm{b})\ \delta_{\mathrm{BRS}} C^{\alpha}=-\kappa^{2}\partial_{\beta} C^{\alpha} C^{\beta}\delta\lambda,\\&(\mathrm{c})\ \delta_{\mathrm{BRS}}\bar{C}_{\tau}=-\kappa^{3}\Delta^{-1}\square^{2} F_{\tau}\delta\lambda,\end{aligned} \tag{99}$$

where $\delta\lambda$ is an infinitesimal anticommuting constant parameter. The importance of these transformations resides in the quantities which they leave invariant. Note that

$$\delta_{\mathrm{BRS}}\left(\partial_{\beta} C^{\sigma} C^{\beta}\right)=0 \tag{100}$$

and

$$\delta_{\mathrm{BRS}}\left(D_{\alpha}^{\mu\nu} C^{\alpha}\right)=0. \tag{101}$$

As a result of Equation (101), the only part of the ghost action which varies under the BRS transformations is the antighost $\bar{C}_{\tau}$. Accordingly, the transformation (99c) has been chosen to make the variation of the ghost action just cancel the variation of the gauge-fixing term. Therefore, the entire effective action is BRS invariant:

$$\delta_{\mathrm{BRS}}\left(I_{sim}-\frac{1}{2}\kappa^{2}\Delta^{-1}F_{\tau}\square^{2}F^{\tau}+\bar{C}_{\tau}F_{\mu\nu}^{\tau}D_{\alpha}^{\mu\nu}C^{\alpha}\right)=0. \tag{102}$$

Equations (99), (100), and (102) now enable us to write the Slavnov identities in an economical way. In order to carry out the renormalization program, we will need to have Slavnov identities for the proper vertices.

A) Slavnov identities for Green's functions

First consider the Slavnov identities for Green's functions.

$$\begin{aligned}&Z\left(T_{\mu\nu},\bar{\beta}_{\sigma},\beta^{\tau},K_{\mu\nu},L_{\sigma}\right)\\&=N\int\left[\prod\nolimits_{\mu\le\nu}\mathrm{d}h^{\mu\nu}\right]\left[\mathrm{d}C^{\sigma}\right]\left[\mathrm{d}\bar{C}_{\tau}\right]\\&\quad\times\exp\left[i\tilde{\Sigma}\left(h^{\mu\nu},C^{\sigma},\bar{C}_{\tau},K_{\mu\nu},L_{\sigma},\bar{\beta}_{\sigma}C^{\sigma}\right)+\bar{\beta}_{\sigma}C^{\sigma}+\bar{C}_{\tau}\beta^{\tau}+\kappa T_{\mu\nu}h^{\mu\nu}\right].\end{aligned} \tag{103}$$

Anticommuting sources have been included for the ghost and antighost fields, and the effective action $\tilde{\Sigma}$ has been enlarged by the inclusion of BRS invariant couplings of the ghosts and gravitons to some external fields $K_{\mu\nu}$ (anticommuting) and L_{σ} (commuting),

$$\tilde{\Sigma}=I_{sim}-\frac{1}{2}\kappa^{2}\Delta^{-1}F_{\tau}\square^{2}F^{\tau}+\bar{C}_{\tau}\vec{F}_{\mu\nu}^{\tau}D_{\alpha}^{\mu\nu}C^{\alpha}+\kappa K_{\mu\nu}D_{\alpha}^{\mu\nu}+\kappa^{2}L_{\sigma}\partial_{\beta}C^{\sigma}C^{\beta}. \tag{104}$$

$\tilde{\Sigma}$ is BRS invariant by virtue of Equation (99), Equation (100), and Equation (102). We may use the new couplings to write this invariance as

$$\frac{\delta\tilde{\Sigma}}{\delta K_{\mu\nu}}\frac{\delta\tilde{\Sigma}}{\delta h^{\mu\nu}}+\frac{\delta\tilde{\Sigma}}{\delta L_{\sigma}}\frac{\delta\tilde{\Sigma}}{\delta C^{\sigma}}+\kappa^{3}\Delta^{-1}\Box^{2}F_{\tau}\frac{\delta\tilde{\Sigma}}{\delta\bar{C}_{\tau}}. \tag{105}$$

In this equation, and throughout this subsection, we use left variational derivatives with respect to anticommuting quantities: $\delta f\left(C^{\sigma}\right)=\delta C^{\tau}\delta f/\delta C^{\tau}$. Equation (105) may be simplified by rewriting it in terms of a reduced effective action,

$$\Sigma=\tilde{\Sigma}+\frac{1}{2}\kappa^{2}\Delta^{-1}F_{\tau}\Box^{2}F^{\tau}. \tag{106}$$

Substitution of (106) into (105) gives

$$\frac{\delta\Sigma}{\delta K_{\mu\nu}}\frac{\delta\Sigma}{\delta h^{\mu\nu}}+\frac{\delta\Sigma}{\delta L_{\sigma}}\frac{\delta\Sigma}{\delta C^{\sigma}}=0, \tag{107}$$

where we have used the relation

$$\kappa^{-1}\vec{F}^{\tau}_{\mu\nu}\frac{\delta\Sigma}{\delta K_{\mu\nu}}-\frac{\delta\Sigma}{\delta\bar{C}_{\tau}}=0. \tag{108}$$

Note that a measure

$$\left[\prod\nolimits_{\mu\leq\nu}\mathrm{d}h^{\mu\nu}\right]\left[\mathrm{d}C^{\sigma}\right]\left[\mathrm{d}\bar{C}_{\tau}\right] \tag{109}$$

is BRS invariant since for infinitesimal transformations, the Jacobian is 1, because of the trace relations

$$\begin{aligned}&(\mathrm{a})\ \frac{\delta^{2}\tilde{\Sigma}}{\delta K_{(\mu\nu)}\delta h^{(\mu\nu)}}=0,\\&(\mathrm{b})\ \frac{\delta^{2}\tilde{\Sigma}}{\delta C^{\sigma}\delta L_{\sigma}}=0,\end{aligned} \tag{110}$$

both of which follow from $\int\mathrm{d}^{4}x\partial_{\alpha}C^{\alpha}=0$. The parentheses surrounding the indices in (110a) indicate that the summation is to be carried out only for $\mu\leq\nu$.

Remark 2.2.1. Note that the Slavnov identity for the generating functional of Green's functions is obtained by performing the BRS transformations (99) on the integration variables in the generating functional (103). This transformation does not change the value of the generating functional and therefore we obtain

$$\begin{aligned}&N\int\left[\prod\nolimits_{\mu\leq\nu}\mathrm{d}h^{\mu\nu}\right]\left[\mathrm{d}C^{\sigma}\right]\left[\mathrm{d}\bar{C}_{\tau}\right]\left(\kappa^{2}T_{\mu\nu}D^{\mu\nu}_{\alpha}-\kappa^{2}\bar{\beta}_{\sigma}\partial_{\beta}C^{\sigma}C^{\beta}\right.\\&\left.+\kappa^{3}\Delta^{-1}\beta^{\tau}\Box^{2}\vec{F}_{\tau\mu\nu}h^{\mu\nu}\right)\exp\left[i\left(\tilde{\Sigma}+\kappa T_{\mu\nu}h^{\mu\nu}+\bar{\beta}_{\sigma}C^{\sigma}+\bar{C}_{\tau}\beta^{\tau}\right)\right]=0.\end{aligned} \tag{111}$$

Another identity which we shall need is the ghost equation of motion. To derive this equation, we shift the antighost integration variable $\bar{C}_{\tau}$ to $\bar{C}_{\tau}+\delta\bar{C}_{\tau}$, again with no resulting change in the value of the generating functional:

$$N\int\left[\prod_{\mu\le\nu}\mathrm{d}h^{\mu\nu}\right]\left[\mathrm{d}C^{\sigma}\right]\left[\mathrm{d}\bar{C}_{\tau}\right]\left(\frac{\delta\tilde{\Sigma}}{\delta C^{\sigma}}+\beta^{\tau}\right)$$
$$\times\exp\left[i\left(\tilde{\Sigma}+\kappa T_{\mu\nu}h^{\mu\nu}+\bar{\beta}_{\sigma}C^{\sigma}+\bar{C}_{\tau}\beta^{\tau}\right)\right] \tag{112}$$

We define now the generating functional of connected Green's functions as the logarithm of the functional (103),

$$W\left[T_{\mu\nu},\bar{\beta}_{\sigma},\beta^{\tau},K_{\mu\nu},L_{\sigma}\right]=-i\ln Z\left[T_{\mu\nu},\bar{\beta}_{\sigma},\beta^{\tau},K_{\mu\nu},L_{\sigma}\right]. \tag{113}$$

and make use of the couplings to the external fields $K_{\mu\nu}$ and L_{σ} to rewrite (112) in terms of W

$$\kappa T_{\mu\nu}\frac{\delta W}{\delta K_{\mu\nu}}-\bar{\beta}_{\sigma}\frac{\delta W}{\delta L_{\sigma}}+\kappa^{2}\Delta^{-1}\beta^{\tau}\square^{2}\vec{F}_{\tau\mu\nu}\frac{\delta W}{\delta T_{\mu\nu}}=0. \tag{114}$$

Similarly, we get the ghost equation of motion:

$$\kappa^{-1}\vec{F}^{\tau}_{\mu\nu}\frac{\delta W}{\delta K_{\mu\nu}}+\beta^{\tau}=0. \tag{115}$$

B) Proper vertices

A Legendre transformation takes us from the generating functional of connected Green's functions (113) to the generating functional of proper vertices. First, we define the expectation values of the gravitational, ghost, and antighost fields in the presence of the sources $T_{\mu\nu},\bar{\beta}_{\sigma}$, and β^{τ} and the external fields $K_{\mu\nu}$ and L_{σ}

$$\begin{aligned}&(\mathrm{a})\,h^{\mu\nu}(x)=\frac{\delta W}{\kappa\delta T_{\mu\nu}(x)},\\&(\mathrm{b})\,C^{\sigma}(x)=\frac{\delta W}{\delta\bar{\beta}_{\sigma}(x)},\\&(\mathrm{c})\,\bar{C}_{\tau}(x)=\frac{\delta W}{\delta\beta^{\tau}(x)}.\end{aligned} \tag{116}$$

We have chosen to denote the expectation values of the fields by the same symbols which were used for the fields in the effective action (104).

The Legendre transformation can now be performed, giving us the generating functional of proper vertices as a functional of the new variables (116) and the external fields $K_{\mu\nu}$ and L_{σ}

$$\begin{aligned}&\tilde{\Gamma}\left[h^{\mu\nu},C^{\sigma},\bar{C}_{\tau},K_{\mu\nu},L_{\sigma}\right]\\&=W\left[T_{\mu\nu},\bar{\beta}_{\sigma},\beta^{\tau},K_{\mu\nu},L_{\sigma}\right]-\kappa T_{\mu\nu}h^{\mu\nu}-\bar{\beta}_{\sigma}C^{\sigma}-\bar{C}_{\tau}\beta^{\tau}.\end{aligned} \tag{117}$$

In this equation, the quantities $T_{\mu\nu}$, $\bar{\beta}_{\sigma}$, and β^{τ} are given implicitly in terms of $h^{\mu\nu},C^{\sigma},\bar{C}_{\tau},K_{\mu\nu}$, and L_{σ} by Equation (116). The relations dual to (116) are

$$\begin{aligned}&(\mathrm{a})\,\kappa T_{\mu\nu}(x)=-\frac{\delta\tilde{\Gamma}}{\delta h^{\mu\nu}(x)},\\&(\mathrm{b})\,\bar{\beta}_{\sigma}(x)=\frac{\delta\tilde{\Gamma}}{\delta C^{\sigma}(x)},\\&(\mathrm{c})\,\beta_{\tau}(x)=-\frac{\delta\tilde{\Gamma}}{\delta\bar{C}_{\tau}(x)}.\end{aligned} \tag{118}$$

Since the external fields $K_{\mu\nu}$ and L_σ do not participate in the Legendre transformation (116), for them we have the relations

$$\begin{aligned}
&(\mathrm{a})\ \frac{\delta\tilde{\Gamma}}{\delta K_{\mu\nu}(x)}=\frac{\delta W}{\delta K_{\mu\nu}(x)},\\
&(\mathrm{b})\ \frac{\delta\tilde{\Gamma}}{\delta L_\sigma(x)}=\frac{\delta W}{\delta L_\sigma(x)}.
\end{aligned} \tag{119}$$

Finally, the Slavnov identity for the generating functional of proper vertices is obtained by transcribing (114) using the relations (116), (118), and (119)

$$\frac{\delta\tilde{\Gamma}}{\delta K_{\mu\nu}}\frac{\delta\tilde{\Gamma}}{\delta h^{\mu\nu}}+\frac{\delta\tilde{\Gamma}}{\delta L_\sigma}\frac{\delta\tilde{\Gamma}}{\delta C^\sigma}+\kappa^3\Delta^{-1}\Box^2\vec{F}_{\tau\mu\nu}h^{\mu\nu}\frac{\delta\tilde{\Gamma}}{\delta C^\sigma}=0. \tag{120}$$

We also have the ghost equation of motion,

$$\kappa^{-1}\vec{F}^{\tau}_{\mu\nu}\frac{\delta\tilde{\Gamma}}{\delta K_{\mu\nu}}-\frac{\delta\tilde{\Gamma}}{\delta C^\sigma}=0. \tag{121}$$

Since Equation (120) has exactly the same form as (105), we follow the example set by (106) and define a reduced generating functional of the proper vertices,

$$\Gamma=\tilde{\Gamma}+\frac{1}{2}\kappa^2\Delta^{-1}\left(\vec{F}_{\tau\mu\nu}h^{\mu\nu}\right)\Box^2\left(\vec{F}^{\tau}_{\rho\sigma}h^{\rho\sigma}\right). \tag{122}$$

Substituting this into (120) and (121), the Slavnov identity becomes

$$\frac{\delta\Gamma}{\delta K_{\mu\nu}}\frac{\delta\Gamma}{\delta h^{\mu\nu}}+\frac{\delta\Gamma}{\delta L_\sigma}\frac{\delta\Gamma}{\delta C^\sigma}=0. \tag{123}$$

and the ghost equation of motion becomes

$$\kappa^{-1}\vec{F}^{\tau}_{\mu\nu}\frac{\delta\Gamma}{\delta K_{\mu\nu}}-\frac{\delta\Gamma}{\delta\bar{C}_\tau}=0. \tag{124}$$

Equations (123) and (124) are of exactly the same form as (107) and (108). This is as it should be, since at the zero-loop order

$$\Gamma^{(0)}=\Sigma. \tag{125}$$

C) Structure of the divergences and renormalization equation

The Slavnov identity (123) is quadratic in the functional Γ. This nonlinearity is reflected in the fact that the renormalization of the effective action generally also involves the renormalization of the BRS transformations which must leave the effective action invariant.

The canonical approach uses the Slavnov identity for the generating functional of proper vertices to derive a linear equation for the divergent parts of the proper vertices. This equation is then solved to display the structure of the divergences. From this structure, it can be seen how to renormalize the effective action so that it remains invariant under a renormalized set of BRS transformations [14].

Suppose that we have successfully renormalized the reduced effective action up to $n-1$ loop order; that is, suppose we have constructed a quantum extension of Σ which satisfies Equations (107) and (108) exactly, and which leads to finite proper vertices when calculated up to order $n-1$. We will denote this renormalized quantity by $\Sigma^{(n-1)}$. In general, it contains terms of many different orders in the loop expansion, including orders greater than $n-1$. The $n-1$ loop part of the reduced generating functional of proper vertices will be denoted by $\Gamma^{(n-1)}$.

When we proceed to calculate $\Gamma^{(n)}$, we find that it contains divergences. Some of these come from n-loop Feynman integrals. Since all the subintegrals of an n-loop Feynman integral contain less than w loops, they are finite by assumption. Therefore, the divergences which arise from w-Ioop Feynman integrals come only from the overall divergences of the integrals, so the corresponding parts of $\Gamma^{(n)}$ are local in structure. In the dimensional regularization procedure, these divergences are of order $\epsilon^{-1}=(d-4)^{-1}$, where d is the dimensionality of space-time in the Feynman integrals.

There may also be divergent parts of $\Gamma^{(n)}$ which do not arise from loop integrals, and which contain higher-order poles in the regulating parameter ϵ. Such divergences come from n-loop order parts of $\Sigma^{(n-1)}$ which are necessary to ensure that (107) is satisfied. Consequently, they too have a local structure. We may separate the divergent and finite parts of $\Gamma^{(n)}$:

$$\Gamma^{(n)}=\Gamma^{(n)}_{\text{div}}+\Gamma^{(n)}_{\text{finite}}. \tag{126}$$

If we insert this breakup into Equation (123), and keep only the terms of the equation which are of n-loop order, we get

$$\begin{aligned}&\frac{\delta\Gamma^{(n)}_{\text{div}}}{\delta K_{\mu\nu}}\frac{\delta\Gamma^{(0)}}{\delta h^{\mu\nu}}+\frac{\delta\Gamma^{(0)}}{\delta K_{\mu\nu}}\frac{\delta\Gamma^{(n)}_{\text{div}}}{\delta h^{\mu\nu}}+\frac{\delta\Gamma^{(n)}_{\text{div}}}{\delta L_{\sigma}}\frac{\delta\Gamma^{(0)}}{\delta C^{\sigma}}+\frac{\delta\Gamma^{(0)}}{\delta L_{\sigma}}\frac{\delta\Gamma^{(n)}_{\text{div}}}{\delta C^{\sigma}}\\&=-\sum\nolimits_{i=0}^{n}\left[\frac{\delta\Gamma^{(n-i)}_{\text{finite}}}{\delta K_{\mu\nu}}\frac{\delta\Gamma^{(i)}_{\text{finite}}}{\delta h^{\mu\nu}}+\frac{\delta\Gamma^{(n-i)}_{\text{finite}}}{\delta L_{\sigma}}\frac{\delta\Gamma^{(i)}_{\text{finite}}}{\delta C^{\sigma}}\right].\end{aligned} \tag{127}$$

Since each term on the right-hand side of (127) remains finite as $\epsilon\to 0$, while each term on the left-hand side contains a factor with at least a simple pole in e, each side of the equation must vanish separately. Remembering the Equation (125), we can write the following equation, called the renormalization equation:

$$\Re\Gamma^{(n)}_{\text{div}}=0, \tag{128}$$

where

$$\Re=\frac{\delta\Sigma}{\delta h^{\mu\nu}}\frac{\delta}{\delta K_{\mu\nu}}+\frac{\delta\Sigma}{\delta C^{\sigma}}\frac{\delta}{\delta L_{\sigma}}+\frac{\delta\Sigma}{\delta K_{\mu\nu}}\frac{\delta}{\delta h^{\mu\nu}}+\frac{\delta\Sigma}{\delta L_{\sigma}}\frac{\delta}{\delta C^{\sigma}}. \tag{129}$$

Similarly by collecting the n-loop order divergences in the ghost equation of motion (124) we get

$$\kappa^{-1}\vec{F}^{\tau}_{\mu\nu}\frac{\delta\Gamma^{(n)}_{\text{div}}}{\delta K_{\mu\nu}}-\frac{\delta\Gamma^{(n)}_{\text{div}}}{\delta\bar{C}_{\tau}}=0. \tag{130}$$

In order to construct local solutions to Equations. (128) and (130) remind that the operator $\Re$ defined in (129) is nilpotent [14]:

$$\Re^2 = 0. \tag{131}$$

Equation (131) gives us the local solutions to Equation (128) of the form

$$\Gamma_{\text{div}}^{(n)} = \Im\left(h^{\mu\nu}\right) + \Re\left[X\left(h^{\mu\nu}, C^{\sigma}, \bar{C}_{\tau}, K_{\mu\nu}, L_{\sigma}\right)\right], \tag{132}$$

where $\Im$ is an arbitrary gauge-invariant local functional of $h^{\mu\nu}$ and its derivatives, and X is an arbitrary local functional of $h^{\mu\nu}, C_{\sigma}, \bar{C}_{\tau}, K_{\mu\nu}$ and L^{σ} and their derivatives. In order to satisfy the ghost equation of motion (130) we require that

$$\Gamma_{\text{div}}^{(n)} = \Gamma_{\text{div}}^{(n)}\left(h^{\mu\nu}, C^{\sigma}, K_{\mu\nu} - \kappa^{-1}\bar{C}_{\pi}\vec{F}_{\mu\nu}^{\tau}, L_{\sigma}\right). \tag{133}$$

D) Ghost number and power counting

Structure of the effective action (104) shows that we may define the following conserved quantity, called ghost number [14]:

$$\begin{gathered} N_{\text{ghost}}\left[h^{\mu\nu}\right] = 0, N_{\text{ghost}}\left[C_{\sigma}\right] = +1, N_{\text{ghost}}\left[\bar{C}_{\tau}\right] = -1, \\ N_{\text{ghost}}\left[K_{\mu\nu}\right] = -1, N_{\text{ghost}}\left[L_{\sigma}\right] = -2. \end{gathered} \tag{134}$$

From Equations (134) follows that

$$N_{\text{ghost}}\left[\Sigma\right] = N_{\text{ghost}}\left[\Gamma\right] = 0. \tag{135}$$

Since

$$N_{\text{ghost}}\left[\Re\right] = +1, \tag{136}$$

we require of the functional $X(\cdot)$ that

$$N_{\text{ghost}}\left[X\right] = -1. \tag{137}$$

In order to complete analysis of the structure of $\Gamma_{\text{div}}^{(n)}$, we must supplement the symmetry Equations (132), (133), and (137) with the constraints on the divergences which arise from power counting. Accordingly, we introduce the following notations:

n_E = number of graviton vertices with two derivatives,
n_G = number of antighost-graviton-ghost vertices,
n_K = number of K-graviton-ghost vertices,
n_L = number of L-ghost-ghost vertices,
I_G = number of internal-ghost propagators,
E_C = number of external ghosts,
$E_{\bar{C}}$ = number of external antighosts.

Since graviton propagators behave like p^{-4}, and ghost propagators like p^{-2}, we are led by standard power counting to the degree of divergence of an arbitrary diagram,

$$D = 4 - 2n_E + 2I_G - 2n_G - 3n_L - 3n_K - E_{\bar{C}}. \tag{138}$$

The last term in (2.2.48) arises because each external antighost line carries with it a factor of external momentum. We can make use of the topological relation

$$2I_G - 2n_G = 2n_L + n_K - E_C - E_{\bar{C}} \tag{139}$$

to write the degree of divergence as

$$D = 4 - 2n_E - n_L - 2n_K - E_C - 2E_{\bar{C}}. \tag{140}$$

Together with conservation of ghost number, Equation (140) enables us to catalog three different types of divergent structures involving ghosts. These are illustrated in **Figure 5**. Each of the three types has degree of divergence $D = 1 - 2n_E$. Consequently, all the divergences which involve ghosts have $n_E = 0$. Since the degree of divergence is then 1, the associated divergent structures in $\Gamma_{\text{div}}^{(n)}$ have an extra derivative appearing on one of the fields. Diagrams whose external lines are all gravitons have degree of divergence $D = 4 - 2n_E$. Combining (140) with (137), (133), and (132), we can finally write the most general expression for $\Gamma_{\text{div}}^{(n)}$ which satisfies all the constraints of symmetries and power counting:

$$\Gamma_{\text{div}}^{(n)} = \Im\left(h^{\mu\nu}\right) + \Re\left[\left(K_{\mu\nu} - \kappa^{-1}\bar{C}_\tau \vec{F}_{\mu\nu}^{\tau}\right)P^{\mu\nu}\left(h^{\alpha\beta}\right) + L_\sigma Q_\tau^\sigma\left(h^{\alpha\beta}\right)C^\tau\right], \tag{141}$$

where $P^{\mu\nu}\left(h^{\alpha\beta}\right)$ and $Q_\tau^\sigma\left(h^{\alpha\beta}\right)$ are arbitrary Lorentz-covariant functions of the gravitational field $h^{\mu\nu}$, but not of its derivatives, at a single spacetime point. $\Im\left(h^{\mu\nu}\right)$ is a local gauge-invariant functional of $h^{\mu\nu}$ containing terms with four, two, and zero derivatives. Expanding (141), we obtain an array of possible divergent structures:

$$\begin{aligned}\Gamma_{\text{div}}^{(n)} = {} & \Im\left(h^{\mu\nu}\right) + \frac{\delta I_{\text{sym}}}{\delta h^{\mu\nu}}P^{\mu\nu} + \left(\kappa K_{\rho\sigma} - \bar{C}_\tau \vec{F}_{\rho\sigma}^{\tau}\right)\left(\frac{\delta D_\alpha^{\rho\sigma}}{\delta h^{\mu\nu}}C^\alpha\right)P^{\mu\nu} \\ & - \left(\kappa K_{\rho\sigma} - \bar{C}_\tau \vec{F}_{\rho\sigma}^{\tau}\right)\frac{\delta P^{\rho\sigma}}{\delta h^{\mu\nu}}D_\alpha^{\mu\nu}C^\alpha - \left(\kappa K_{\mu\nu} - \bar{C}_\tau \vec{F}_{\mu\nu}^{\tau}\right)D_\sigma^{\mu\nu}\left(Q_\varepsilon^\sigma C^\varepsilon\right) \\ & - \kappa^2 L_\sigma \partial_\beta\left(Q_\tau^\sigma C^\tau\right)C^\beta - \kappa^2 L_\sigma \partial_\beta C^\sigma Q_\tau^\beta C^\tau \\ & - \kappa L_\sigma \frac{\delta Q_\tau^\sigma}{\delta h^{\mu\nu}}C^\tau D_\alpha^{\mu\nu}C^\alpha + \kappa^2 L_\sigma Q_\tau^\sigma \partial_\beta C^\tau C^\beta.\end{aligned} \tag{142}$$

The breakup between the gauge-invariant divergences S and the rest (142) is determined only up to a term of the form [14].

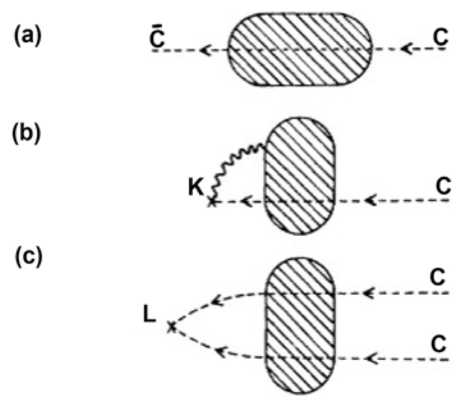

Figure 5. The three types of divergent diagram which involve external ghost lines. Arbitrarily many gravitons may emerge from each of the central regions,(a) Ghost action type,(b) K type, (c) L type.

The breakup between the gauge-invariant divergences S and the rest of (142)

$$\int \mathrm{d}^4 x\left(\eta^{\mu\nu}+\kappa h^{\mu\nu}\right)\frac{\delta I_{sym}}{\kappa\delta h^{\mu\nu}}, \tag{143}$$

which can be generated by adding to $P^{\mu\nu}$ a term proportional to $\eta^{\mu\nu}+\kappa h^{\mu\nu}=\sqrt{g}g^{\mu\nu}$. The profusion of divergences allowed by (142) appears to make the task of renormalizing the effective action rather complicated. Although the many divergent structures do pose a considerable nuisance for practical calculations, the situation is still reminiscent in principle of the renormalization of Yang-Mills theories. There, the non-gauge-invariant divergences may be eliminated by a number of field renormalizations. We shall find the same to be true here, but because the gravitational field $h^{\mu\nu}$ carries no weight in the power counting, there is nothing to prevent the field renormalizations from being nonlinear, or from mixing the gravitational and ghost fields. The corresponding renormalizations procedure considered in [14].

Remark 2.2.2. We assume now that:

1) The local Poincaré group of momentum space is deformed at some fundamental high-energy cutoff Λ_* [9] [10].

2) The canonical quadratic invariant $\|p\|^2=\eta^{ab}p_a p_b$ collapses at high-energy cutoff Λ_* and being replaced by the non-quadratic invariant:

$$\|p\|^2=\frac{\eta^{ab}p_a p_b}{\left(1+l_{\Lambda_*}p_0\right)}. \tag{144}$$

3) The canonical concept of Minkowski space-time collapses at a small distance $l_{\Lambda_*}=\Lambda_*^{-1}$ to fractal space-time with Hausdorff-Colombeau negative dimension and therefore the canonical Lebesgue measure d^4x being replaced by the Colombeau-Stieltjes
measure

$$\left(\mathrm{d}\eta(x,\varepsilon)\right)_\varepsilon=\left(v_\varepsilon\left(s(x)\right)\mathrm{d}^4x\right)_\varepsilon, \tag{145}$$

where

$$\begin{gathered}\left(v_\varepsilon\left(s(x)\right)\right)_\varepsilon=\left(\left(\left|s(x)\right|^{|D^-|}+\varepsilon\right)^{-1}\right)_\varepsilon,\\ s(x)=\sqrt{x_\mu x^\mu},\end{gathered} \tag{146}$$

see subsection IV.2.

4) The canonical concept of local momentum space collapses at fundamental high-energy cutoff Λ_* to fractal momentum space with Hausdorff-Colombeau negative dimension and therefore the canonical Lebesgue measure $\mathrm{d}^3\mathbf{k}$, where $\mathbf{k}=\left(k_x,k_y,k_z\right)$ being replaced by the Hausdorff-Colombeau measure

$$\mathrm{d}^{D^+,D^-}\mathbf{k}\triangleq\frac{\Delta\left(D^-\right)\mathrm{d}^{D^+}\mathbf{k}}{\left(\left|\mathbf{k}\right|^{|D^-|}+\varepsilon\right)_\varepsilon}=\frac{\Delta\left(D^+\right)\Delta\left(D^-\right)p^{D^+-1}\mathrm{d}p}{\left(p^{|D^-|}+\varepsilon\right)_\varepsilon}, \tag{147}$$

see Subsection 3.4. Note that the integral over measure $\mathrm{d}^{D^+,D^-}\mathbf{k}$ is given by formula (185).

Remark 2.2.3. (I) The renormalizable models which we have considered in this section many years regarded only as constructs for a study of the ultraviolet problem of quantum gravity. The difficulties with unitarity appear to preclude their direct acceptability as canonical physical theories in locally Minkowski space-time. In canonical case they do have only some promise as phenomenological models.

(II) However, for their unphysical behavior may be restricted to *arbitrarily large energy scales* Λ_* mentioned above by an appropriate limitation on the renormalized masses m_2 and m_0. Actually, it is only the massive spin-two excitations of the field which give the trouble with unitarity and thus require a very large mass. The limit on the mass m_0 is determined only by the observational constraints on the static field.

3. Hausdorff-Colombeau Measure and Associated Negative Hausdorff-Colombeau Dimension

3.1. Fractional Integration in Negative Dimensions

Let $\mu_H^{D_+}$ be a Hausdorff measure [19] and $X \subset \mathbb{R}^n$ is measurable set. Let $s(x)$ be a function $s: X \to \mathbb{R}$ such that is symmetric with respect to some centre $x_0 \in X$, *i.e.* $s(x)$ = constant for all x satisfying $d(x, x_0) = r$ for arbitrary values of r. Then the integral in respect to Hausdorff measure over n-dimensional metric space X is then given by [19]:

$$\int_X s(x)\,\mathrm{d}\mu_H^{D_+} = \frac{2\pi^{D_+/2}}{\Gamma(D_+/2)} \int_0^\infty s(r) r^{D_+ - 1} \mathrm{d}r. \tag{148}$$

The integral in RHS of the Equation (148) is known in the theory of the Weyl fractional calculus where, the Weyl fractional integral $W^D f(x)$, is given by

$$W^D f(x) = \frac{1}{\Gamma(D)} \int_0^\infty (t - x)^{D-1} f(t)\,\mathrm{d}t. \tag{149}$$

Remark 3.1.1. In order to extend the Weyl fractional integral (148) in negative dimensions we apply the Colombeau generalized functions [20] and Colombeau generalized numbers [21].

Recall that Colombeau algebras $\mathcal{G}(\Omega)$ of the Colombeau generalized functions defined as follows. Let Ω be an open subset of $\mathbb{R}^n$. Throughout this paper, for elements of the space $C^\infty(\Omega)^{(0,1]}$ of sequences of smooth functions indexed by $\varepsilon \in (0,1]$ we shall use the canonical notations $(\zeta_\varepsilon(x))_\varepsilon$ and $(u_\varepsilon)_\varepsilon$ so $u_\varepsilon \in C^\infty(\Omega)$, $\varepsilon \in (0,1]$.

Definition 3.1.1. We set $\mathcal{G}(\Omega) = \mathcal{E}_M(\Omega) / \mathcal{N}(\Omega)$, where

$$\begin{aligned} \mathcal{E}_M(\Omega) = \Big\{ (u_\varepsilon)_\varepsilon \in C^\infty(\Omega)^{(0,1]} \,\Big|\, & \forall K \subset\subset \Omega, \forall \alpha \in \mathbb{N}^n\ \exists p \in \mathbb{N} \text{ with} \\ & \sup\nolimits_{x\in K} |u_\varepsilon(x)| = O(\varepsilon^{-p}) \text{ as } \varepsilon \to 0 \Big\}, \\ \mathcal{N}(\Omega) = \Big\{ (u_\varepsilon)_\varepsilon \in C^\infty(\Omega)^{(0,1]} \,\Big|\, & \forall K \subset\subset \Omega, \forall \alpha \in \mathbb{N}^n\ \forall q \in \mathbb{N} \\ & \sup\nolimits_{x\in K} |u_\varepsilon(x)| = O(\varepsilon^{q}) \text{ as } \varepsilon \to 0 \Big\}. \end{aligned} \tag{150}$$

Notice that $\mathcal{G}(\Omega)$ is a differential algebra. Equivalence classes of sequences $(u_\varepsilon)_\varepsilon$ will be denoted by $\mathrm{cl}\left[(u_\varepsilon)_\varepsilon\right]$ is a differential algebra containing $D'(\Omega)$ as a linear subspace and $C^\infty(\Omega)$ as subalgebra.

Definition 3.1.2. Weyl fractional integral $\left(W_\varepsilon^{D^{--}} f(x)\right)_\varepsilon$ in negative dimensions $D^- < 0$, $D^- \neq 0,-1,\cdots,-n,\cdots,n\in\mathbb{N}$ is given by

$$W^{D^-} f(x) = \frac{1}{\Gamma(D^-)}\left(\int_\varepsilon^\infty (t-x)^{D^- -1} f(t)\,\mathrm{d}t\right)_\varepsilon$$

or (151)

$$\left(W_\varepsilon^{D^-} f(x)\right)_\varepsilon = \frac{1}{\Gamma(D^-)}\left(\int_0^\infty \frac{1}{\varepsilon+(t-x)^{|D^-|+1}} f(t)\,\mathrm{d}t\right)_\varepsilon,$$

where $\varepsilon\in(0,1]$ and $\int_0^\infty |f(t)\mathrm{d}t| < \infty$. Note that $\left(W_\varepsilon^{D^{--}} f(x)\right)_\varepsilon \in \mathcal{G}(\mathbb{R})$. Thus in order to obtain appropriate extension of the Weyl fractional integral $W^{D^+} f(x)$ on the negative dimensions $D_- < 0$ the notion of the Colombeau generalized functions is essentially important.

Remark 3.1.2. Thus in negative dimensions from Equation (148) we formally obtain

$$\left(\int_X s(x)\,\mathrm{d}\mu_{HC,\varepsilon}^{D^{--}}\right)_\varepsilon = \frac{2\pi^{D^-/2}}{\Gamma(D^-/2)}\left(\int_0^\infty \frac{s(r)}{\varepsilon + r^{|D^-|+1}}\,\mathrm{d}r\right)_\varepsilon = \left(I_\varepsilon^{D_-}\right)_\varepsilon, \tag{152}$$

where $\varepsilon\in(0,1]$ and $D^-\neq 0,-2,\cdots,-2n,\cdots,n\in\mathbb{N}$ and where $\left(\mu_{HC,\varepsilon}^{D^-}\right)_\varepsilon$ is appropriate generalized Colombeau outer measure. Namely Hausdorff-Colombeau outer measure.

Remark 3.1.3. Note that: if $s(0)\neq 0$ the quantity $\left(I_\varepsilon^{D^+,D^-}\right)$ takes infinite large value in sense of Colombeau generalized numbers, *i.e.*, $\left(I_\varepsilon^{D^+,D^-}\right)_\varepsilon =_{\tilde{\mathbb{R}}} \tilde{\infty}$, see Definition 3.3.2 and Definition 3.3.3.

Remark 3.1.4. We apply through this paper more general definition then (3.1.4):

$$\left(\int_X s(x)\,\mathrm{d}\mu_{HC,\varepsilon}^{D^+,D^-}\right)_\varepsilon = \frac{4\pi^{D^+/2}\pi^{D^-/2}}{\Gamma(D^+/2)\Gamma(D^-/2)}\left(\int_0^\infty \frac{r^{D^+-1}s(r)}{\varepsilon + r^{|D^-|}}\,\mathrm{d}r\right)_\varepsilon = \left(I_\varepsilon^{D^+,D_-}\right)_\varepsilon, \tag{153}$$

where $\varepsilon\in(0,1]$ and $D^+\geq 1$, $D^-\neq 0,-2,\cdots,-2n,\cdots,n\in\mathbb{N}$ and where $\left(\mu_{HC,\varepsilon}^{D^+,D^-}\right)_\varepsilon$ is appropriate generalized Colombeau outer measure. Namely Hausdorff-Colombeau outer measure. In Subsection 3.3 we pointed out that there exists Colombeau generalized measure $\left(\mathrm{d}\mu_{HC,\varepsilon}^{D^+,D^-}\right)_\varepsilon$ and therefore Equation (151) gives appropriate extension of the Equation (148) on the negative Hausdorff-Colombeau dimensions.

3.2. Hausdorff Measure and Associated Positive Hausdorff Dimension

Recall that the classical Hausdorff measure [19] [22] originate in Caratheodory's construction, which is defined as follows: for each metric space *X*, each set $F=\{E_i\}_{i\in\mathbb{N}}$ of subsets E_i of *X*, and each positive function $\zeta^+(E)$, such that

$0 \le \zeta^{+}(E_i) \le \infty$ whenever $E_i \in F$, a preliminary measure $\phi_{\delta}^{+}(E)$ can be constructed corresponding to $0 < \delta \le +\infty$, and then a final measure $\mu^{+}(E)$, as follows: for every subset $E \subset X$, the preliminary measure $\phi_{\delta}^{+}(E)$ is defined by

$$\phi_{\delta}^{+}(E) = \inf_{\{E_i\}_{i\in\mathbb{N}}} \left\{ \sum\nolimits_{i\in\mathbb{N}} \zeta^{+}(E_i) \mid E \subset \bigcup\nolimits_{i\in\mathbb{N}} E_i, diam(E_i) \le \delta \right\}. \tag{154}$$

Since $\phi_{\delta_1}^{+}(E) \ge \phi_{\delta_2}^{+}(E)$ for $0 < \delta_1 < \delta_2 \le +\infty$, the limit

$$\mu^{+}(E) = \lim_{\delta \to 0_{+}} \phi_{\delta}^{+}(E) = \sup_{\delta > 0} \phi_{\delta}^{+}(E) \tag{155}$$

exists for all $E \subset X$. In this context, $\mu^{+}(E)$ can be called the result of Caratheodory's construction from $\zeta^{+}(E)$ on *F*. $\phi_{\delta}^{+}(E)$ can be referred to as the size δ approximating positive measure. Let $\zeta^{+}(E_i, d^{+})$ be for example

$$\zeta^{+}(E_i, d^{+}) = \Theta(d^{+}) \left[diam(E_i) \right]^{d^{+}}, 0 < \Theta(d^{+}), \tag{156}$$

for non-empty subsets $E_i, i \in \mathbb{N}$ of *X*. Where $\Theta(d^{+})$ is some geometrical factor, depends on the geometry of the sets E_i, used for covering. When *F* is the set of all non-empty subsets of *X*, the resulting measure $\mu_H^{+}(E, d^{+})$ is called the d^{+}-dimensional Hausdorff measure over *X*; in particular, when *F* is the set of all (closed or open) balls in *X*,

$$\Theta(d^{+}) \triangleq \Omega(d^{+}) = \pi^{\frac{d^{+}}{2}} \left(2^{-d^{+}} \right) \Gamma\left(1 + \frac{d^{+}}{2} \right). \tag{157}$$

Consider a measurable metric space $(X, \mu_H(d)), X \subseteqq \mathbb{R}^n, d \in (-\infty, +\infty)$. The elements of *X* are denoted by $x, y, z, \cdots$, and represented by *n*-tuples of real numbers $x = (x_1, x_2, \cdots, x_n)$

The metric $d(x, y)$ is a function $d : X \times X \to R_{+}$ is defined in *n* dimensions by

$$d(x, y) = \sum_{ij} \left[\delta_{ij} (y_i - x_i)(y_j - x_j) \right]^{1/2} \tag{158}$$

and the diameter of a subset $E \subset X$ is defined by

$$diam(E) = \sup \left\{ d(x, y) \mid x, y \in E \right\}. \tag{159}$$

Definition 3.2.1. The Hausdorff measure $\mu_H^{+}(E, D^{+})$ of a subset $E \subset X$ with the associated Hausdorff positive dimension $D^{+} \in \mathbb{R}_{+}$ is defined by canonical way

$$\begin{gathered} \mu_H^{+}(E, D^{+}) = \lim_{\delta \to 0} \left[\inf_{\{E_i\}_{i\in\mathbb{N}}} \left\{ \sum\nolimits_{i\in\mathbb{N}} \zeta^{+}(E_i, D^{+}) \mid E \subset \bigcup\nolimits_i E_i, \forall i \left(diam(E_i) < \delta \right) \right\} \right], \\ D^{+}(E) = \sup \left\{ d^{+} \in \mathbb{R}_{+} \mid d^{+} > 0, \mu_H^{+}(E, d^{+}) = +\infty \right\}. \end{gathered} \tag{160}$$

Definition 3.2.2. Remind that a function $f : X \to \mathbb{R}$ defined in a measurable space (X, Σ, μ), is called a simple function if there is a finite disjoint set of sets $\{E_1,, \cdots, E_n\}$ of measurable sets and a finite set $\{\alpha_1, \cdots, \alpha_n\}$ of real numbers such that $f(x) = \alpha_i$ if $x \in E_i$ and $f(x) = 0$ if $x \notin E_i$. Thus $f(x) = \sum\nolimits_{i=1}^{n} \alpha_i \chi_{E_i}(x)$, where $\chi_{E_i}(x)$ is the characteristic function of E_i. A simple function f on a measurable space (X,Σ,μ) is integrable if $\mu(E_i)<\infty$ for every index i for which $\alpha_i \neq 0$. The Lebesgue-Stieltjes integral of f is defined by

$$\int f\mathrm{d}\mu = \sum_{i=1}^{n}\alpha_i\mu(E_i). \tag{161}$$

A continuous function is a function for which $\lim_{x\to y} f(x)=f(y)$ whenever $\lim_{x\to y} d(x,y)=0$.

The Lebesgue-Stieltjes integral over continuous functions can be defined as the limit of infinitesimal covering diameter: when $\{E_i\}_{i\in\mathbb{N}}$ is a disjoined covering and $x_i\in E_i$ by definition (3.2.12) one obtains

$$\begin{aligned}&\int_X f(x)\mathrm{d}\mu_H^+(x,D^+)\\ &=\lim_{diam(E_i)\to 0}\left[\sum_{\bigcup E_i=X} f(x_i)\inf_{\{E_{ij}\}\text{ with }\bigcup_j E_{ij}\supset E_i}\sum_j \zeta^+\left(E_{ij},D^+\left(E_{ij}\right)\right)\right].\end{aligned} \tag{162}$$

From now on, X is assumed metrically unbounded, *i.e.* for every $x\in X$ and $r>0$ there exists a point y such that $d(x,y)>r$. The standard assumption that D^+ is uniquely defined in all subsets E of X requires X to be regular (homogeneous, uniform) with respect to the measure, *i.e.* $\mu_H^+(B_r(x),D^+)=\mu_H^+(B_r(y),D^+)$ for all elements $x,y\in X$ and (convex) balls $B_r(x)$ and $B_r(y)$ of the form $B_{r>0}(x)=\{z\mid d(x,z)\le r; x,z\in X\}$. In the limit $diam(E_i)\to 0$, the infimum is satisfied by the requirement that the variation overall coverings $\{E_{ij}\}_{ij\in\mathbb{N}}$ is replaced by one single covering E_i, such that $\bigcup_j E_{ij}\to E_i\ni x_i$. Hence

$$\int_X f(x)\mathrm{d}\mu_H^+(x,D^+)=\lim_{diam(E_i)\to 0}\sum_{\bigcup E_i=X} f(x_i)\zeta^+(E_i,D^+). \tag{163}$$

The range of integration X may be parametrized by polar coordinates with $r=d(x,0)$ and angle Ω. $\{E_{r_i,\Omega_i}\}_{i\in\mathbb{N}}$ can be thought of as spherically symmetric covering around a centre at the origin. In the limit, the function $\zeta^+(E_{r,\Omega},D^+)$ defined by Equation (156) is given by

$$\mathrm{d}\mu_H^+(x,D^+)=\lim_{diam(E_{r,\omega})\to 0}\zeta^+(E_{r,\Omega},D^+)=\mathrm{d}\Omega^{D^+-1}r^{D^+-1}\mathrm{d}r. \tag{164}$$

Let us assume now for simplification that $f(x)=f(\|x\|)=f(r)$ and $\lim\limits_{r\to\infty} f(r)=0$. The integral over a D^+-dimensional metric space X is then given by

$$\int_X f(x)\mathrm{d}\mu_H^+(x,D^+)=\int_X f(x)\mathrm{d}^{D^+}x=\frac{2\pi^{\frac{D^+}{2}}}{\Gamma\left(1+\frac{D^+}{2}\right)}\int_0^\infty f(r)r^{D^+-1}\mathrm{d}r. \tag{165}$$

The integral defined in (163) satisfies the following conditions.

1) Linearity:

$$\begin{aligned}&\int_X\left[a_1 f_1(x)+a_2 f_2(x)\right]\mathrm{d}\mu_H^+(x,D^+)\\ &=a_1\int_X f_1(x)\mathrm{d}\mu_H^+(x,D^+)+a_2\int_X f_2(x)\mathrm{d}\mu_H^+(x,D^+).\end{aligned} \tag{166}$$

2) Translational invariance:

$$\int_X f(x+x_0)\,\mathrm{d}\mu_H^+(x,D^+) = \int_X f(x)\,\mathrm{d}\mu_H^+(x,D^+) \tag{167}$$

since $\mathrm{d}\mu_H^+(x-x_0,D^+) = \mathrm{d}\mu_H^+(x,D^+)$.

3) Scaling property:

$$\int_X f(ax)\,\mathrm{d}\mu_H^+(x,D^+) = a^{-D^+}\int_X f(x)\,\mathrm{d}\mu_H^+(x,D^+) \tag{168}$$

since $\mathrm{d}\mu_H^+(x/a,D^+) = a^{-D^+}\,\mathrm{d}\mu_H^+(x,D^+)$.

4) The generalized $\delta^{D^+}(x)$ function:

The generalized $\delta^{D^+}(x)$ function for sets with non-integer Hausdorff dimension exists and can be defined by formula

$$\int_X f(x)\delta^{D^+}(x-x_0)\,\mathrm{d}\mu_H^+(x,D^+) = f(x_0). \tag{169}$$

3.3. Hausdorff-Colombeau Measure and Associated Negative Hausdorff-Colombeau Dimensions

During last 20 years the notion of negative dimension in geometry was many developed, see [12] [23] [24] [25] [26] [27].

Remind that canonical definitions of noninteger positive dimension always equipped with a measure. Hausdorff-Besicovich dimension equipped with Hausdorff measure $\mathrm{d}\mu_H^+(x,D^+)$.

Let us consider example of a space of noninteger positive dimension equipped with the Haar measure. On the closed interval $0 \le x \le 1$ there is a scale $0 \le \sigma \le 1$ of Cantor dust with the Haar measure equal to x^σ for any interval $(0,x)$ similar to the entire given set of the Cantor dust. The direct product of this scale by the Euclidean cube of dimension $k-1$ gives the entire scale $k+\sigma$, where $k \in \mathbb{Z}$ and $\sigma \in (0,1)$ [24].

In this subsection we define generalized Hausdorff-Colombeau measure. In subsection III.4 we will prove that negative dimensions of fractal equipped with the Hausdorff-Colombeau measure in natural way.

Let Ω be an open subset of $\mathbb{R}^n$, let X be metric space $X \subsetneqq \mathbb{R}^n$ and let F be a set $F = \{E_i\}_{i\in\mathbb{N}}$ of subsets E_i of X. Let $\zeta(E,x,\breve{x})$ be a function $\zeta: F\times\Omega\times\Omega \to \mathbb{R}$. Let $C_F^\infty(\Omega)$ be a set of the all functions $\zeta(E,x)$ such that $\zeta(E,x) \in C^\infty(\Omega)$ whenever $E \in F$. Throughout this paper, for elements of the space $C_F^\infty(\Omega)^{(0,1]}$ of sequences of smooth functions indexed by $\varepsilon \in (0,1]$ we shall use the canonical notations $(\zeta_\varepsilon(E,x))_\varepsilon$ and $(\zeta_\varepsilon)_\varepsilon$ so $\zeta_\varepsilon \in C_F^\infty(\Omega)$, $\varepsilon \in (0,1]$.

Definition 3.3.1. We set $\mathcal{G}_F(\Omega) = \mathcal{E}_M(F,\Omega)/\mathcal{N}(F,\Omega)$, where

$$\begin{aligned}
\mathcal{E}_M(F,\Omega) = \Big\{&(\zeta_\varepsilon)_\varepsilon \in C_F^\infty(\Omega)^{(0,1]} \,\Big|\, \forall K \subset\subset \Omega, \forall \alpha \in \mathbb{N}^n\ \exists p \in \mathbb{N} \text{ with} \\
&\sup_{E\in F;x\in K}\left|\zeta_\varepsilon(E,x)\right| = O\left(\varepsilon^{-p}\right) \text{ as } \varepsilon \to 0\Big\}, \\
\mathcal{N}(F,\Omega) - \Big\{&(\zeta_\varepsilon)_\varepsilon \in C_F^\infty(\Omega)^{(0,1]} \,\Big|\, \forall K \subset\subset \Omega, \forall \alpha \in \mathbb{N}^n\ \forall q \in \mathbb{N} \\
&\sup_{E\in F;x\in K}\left|\zeta_\varepsilon(E,x)\right| = O\left(\varepsilon^{q}\right) \text{ as } \varepsilon \to 0\Big\}.
\end{aligned} \tag{170}$$

Notice that $\mathcal{G}_F(\Omega)$ is a differential algebra. Equivalence classes of sequences

$(\zeta_\varepsilon)_\varepsilon$ will be denoted by $\mathrm{cl}\left[(\zeta_\varepsilon)_\varepsilon\right]$ or simply $\left[(\zeta_\varepsilon)_\varepsilon\right]$.

Definition 3.3.2. We denote by $\tilde{\mathbb{R}}$ the ring of real, Colombeau generalized numbers. Recall that by definition $\tilde{\mathbb{R}} = \mathcal{E}_M(\mathbb{R})/\mathcal{N}(\mathbb{R})$ [21], where

$$\begin{aligned}\mathcal{E}_M(\mathbb{R}) &= \left\{(x_\varepsilon)_\varepsilon \in \mathbb{R}^{(0,1]} \middle| (\exists\alpha\in\mathbb{R})(\exists\varepsilon_0\in(0,1])\forall\varepsilon\le\varepsilon_0\left[|x_\varepsilon|\le\varepsilon^\alpha\right]\right\},\\ \mathcal{N}(\mathbb{R}) &= \left\{(x_\varepsilon)_\varepsilon \in \mathbb{R}^{(0,1]} \middle| (\forall\alpha\in\mathbb{R})(\exists\varepsilon_0\in(0,1])\forall\varepsilon\le\varepsilon_0\left[|x_\varepsilon|\le\varepsilon^\alpha\right]\right\}.\end{aligned} \tag{171}$$

Notice that the ring $\tilde{\mathbb{R}}$ arises naturally as the ring of constants of the Colombeau algebras $\mathcal{G}(\Omega)$. Recall that there exists natural embedding $\tilde{r}:\mathbb{R}\hookrightarrow\tilde{\mathbb{R}}$ such that for all $r\in\mathbb{R}$, $\tilde{r}=(r_\varepsilon)_\varepsilon$ where $r_\varepsilon\equiv r$ for all $\varepsilon\in(0,1]$. We say that r is standard number and abbreviate $r\in\mathbb{R}$ for short. The ring $\tilde{\mathbb{R}}$ can be endowed with the structure of a partially ordered ring: for $r,s\in\tilde{\mathbb{R}}$ $\eta\in\mathbb{R}_+,\eta\le1$ we abbreviate $r\le_{\tilde{\mathbb{R}},\eta}s$ or simply $r\le_{\tilde{\mathbb{R}}}s$ if and only if there are representatives $(r_\varepsilon)_\varepsilon$ and $(s_\varepsilon)_\varepsilon$ with $r_\varepsilon\le s_\varepsilon$ for all $\varepsilon\in(0,\eta]$. Colombeau generalized number $r\in\tilde{\mathbb{R}}$ with representative $(r_\varepsilon)_\varepsilon$ we abbreviate $\mathrm{cl}\left[(r_\varepsilon)_\varepsilon\right]$.

Definition 3.3.3. 1) Let $\delta\in\tilde{\mathbb{R}}$. We say that δ is infinite small Colombeau generalized number and abbreviate $\delta\approx_{\tilde{\mathbb{R}}}\tilde{0}$ if there exists representative $(\delta_\varepsilon)_\varepsilon$ and some $q\in\mathbb{N}$ such that $|\delta_\varepsilon|=O(\varepsilon^q)$ as $\varepsilon\to0$. 2) Let $\Delta\in\tilde{\mathbb{R}}$. We say that Δ is infinite large Colombeau generalized number and abbreviate $\Delta=_{\tilde{\mathbb{R}}}\tilde{\infty}$ if $\Delta^{-1}_{\tilde{\mathbb{R}}}\approx_{\tilde{\mathbb{R}}}\tilde{0}$. 3) Let $\mathbb{R}_\infty$ be $\mathbb{R}\cup\{\infty\}$ We say that $\Theta\in\tilde{\mathbb{R}}_\infty$ is infinite Colombeau generalized number and abbreviate $\Theta=_{\tilde{\mathbb{R}}}\infty_{\tilde{\mathbb{R}}}$ if there exists representative $(\Theta_\varepsilon)_\varepsilon$ where $\Theta_\varepsilon=\infty$ for all $\varepsilon\in(0,1]$. Here we set $\mathcal{E}_M(\mathbb{R}_\infty)=\mathcal{E}_M(\mathbb{R})\cup\{(\Theta_\varepsilon)_\varepsilon\}$, $\mathcal{N}(\mathbb{R}_\infty)=\mathcal{N}(\mathbb{R})$ and $\tilde{\mathbb{R}}_\infty=\mathcal{E}_M(\mathbb{R}_\infty)/\mathcal{N}(\mathbb{R}_\infty)$.

Definition 3.3.4. The singular Hausdorff-Colombeau measure originate in Colombeau generalization of canonical Caratheodory's construction, which is defined as follows: for each metric space X, each set $F=\{E_i\}_{i\in\mathbb{N}}$ of subsets E_i of X, and each Colombeau generalized function $(\zeta_\varepsilon(E,x,\breve{x}))_\varepsilon$, such that: 1) $0\le(\zeta_\varepsilon(E,x,\breve{x}))_\varepsilon$, 2) $(\zeta_\varepsilon(E,\breve{x},\breve{x}))_\varepsilon=_{\tilde{\mathbb{R}}}\tilde{\infty}$, whenever $E\in F$, a preliminary Colombeau measure $(\phi_\delta(E,x,\breve{x},\varepsilon))_\varepsilon$ can be constructed corresponding to $0<\delta\le+\infty$, and then a final Colombeau measure $(\mu_\varepsilon(E,x,\breve{x}))_\varepsilon$, as follows: for every subset $E\subset X$, the preliminary Colombeau measure $(\phi_\delta(E,x,\breve{x},\varepsilon))_\varepsilon$ is defined by

$$\phi_\delta(E,x,\breve{x},\varepsilon)=\sup_{\{E_i\}_{i\in\mathbb{N}}}\left\{\sum\nolimits_{i\in\mathbb{N}}\zeta_\varepsilon(E_i,x,\breve{x})\,|\,E\subset\bigcup\nolimits_{i\in\mathbb{N}}E_i,\mathit{diam}(E_i)\le\delta\right\}. \tag{172}$$

Since for all $\varepsilon\in(0,1]$: $\phi^-_{\delta_1}(E,x,\breve{x},\varepsilon)\ge\phi^-_{\delta_2}(E,x,\breve{x},\varepsilon)$ for $0<\delta_1<\delta_2\le+\infty$, the limit

$$(\mu(E,x,\breve{x},\varepsilon))_\varepsilon=\left(\lim_{\delta\to0_+}\phi_\delta(E,x,\breve{x},\varepsilon)\right)_\varepsilon=\left(\inf_{\delta>0}\phi_\delta(E,x,\breve{x},\varepsilon)\right)_\varepsilon \tag{173}$$

exists for all $E\subset X$. In this context, $(\mu(E,x,\breve{x},\varepsilon))_\varepsilon$ can be called the result of Caratheodory's construction from $(\zeta_\varepsilon(E,x,\breve{x}))_\varepsilon$ on F and $(\phi_\delta(E,x,\breve{x},\varepsilon))_\varepsilon$ can be referred to as the size δ approximating Colombeau measure.

Definition 3.3.5. Let $(\zeta_\varepsilon(E_i,D^+,D^-,x,\breve{x}))_\varepsilon$ be

$$\left(\zeta_{\varepsilon}\left(E_i, D^+, D^-, x, \breve{x}\right)\right)_{\varepsilon} = \begin{cases} \left(\dfrac{\Theta_1\left(D^+\right)\Theta_2\left(D^-\right)\left[diam\left(E_i\right)\right]^{D^+}}{\left[d\left(x, \breve{x}\right)\right]^{\left|D^-\right|} + \varepsilon}\right)_{\varepsilon} & \text{if } x \in E_i \\ 0 & \text{if } x \notin E_i \end{cases} \quad (174)$$

where $\varepsilon \in (0,1], \Theta_1\left(D^+\right), \Theta_2\left(D^-\right) > 0$. In particular, when F is the set of all (closed or open) balls in X,

$$\Theta_1\left(D^+\right) = \frac{2^{-D^+}\pi^{\frac{D^+}{2}}}{\Gamma\left(1+\frac{D^+}{2}\right)} \quad (175)$$

and

$$\Theta_2\left(D^-\right) = \frac{2^{-D^-}\pi^{\frac{D^-}{2}}}{\left|\Gamma\left(1+\frac{D^-}{2}\right)\right|}, \quad (176)$$

$$D^- \neq -2, -4, -6, \cdots, -2(n+1), \cdots$$

Definition 3.3.6. The Hausdorff-Colombeau singular measure $\left(\mu_H\left(E, D^+, D^-, x, \breve{x}, \varepsilon\right)\right)_{\varepsilon}$ of a subset $E \subset X$ with the associated Hausdorff-Colombeau dimension $\breve{D}^+\left(D^-\right) \in \mathbb{R}_+, D^- \in \mathbb{R}_+$ is defined by

$$\begin{aligned} &\left(\mu_{HC}\left(E, \breve{D}^+, D^-, x, \breve{x}, \varepsilon\right)\right)_{\varepsilon} \\ &= \left(\lim_{\delta \to 0}\left[\sup_{\{E_i\}_{i\in\mathbb{N}}}\left\{\sum\nolimits_{i\in\mathbb{N}}\left(\zeta_{\varepsilon}\left(E_i, \breve{D}^+, D^-, x, \breve{x}\right)\right)_{\varepsilon} \mid E \subset \bigcup\nolimits_i E_i, \forall i\left(diam\left(E_i\right) < \delta\right)\right\}\right]\right)_{\varepsilon}, \\ &\breve{D}^+ = \sup\left\{D^+ > 0 \mid \left(\mu_{HC}\left(E, D^+, D^-, x, \breve{x}, \varepsilon\right)\right)_{\varepsilon} = \infty_{\widetilde{\mathbb{R}}}\right\}, \end{aligned} \quad (177)$$

The Colombeau-Lebesgue-Stieltjes integral over continuous functions $f : X \to \mathbb{R}$ can be evaluated similarly as in Subsection III.3, (but using the limit in sense of Colombeau generalized functions) of infinitesimal covering diameter when $\{E_i\}_{i\in\mathbb{N}}$ is a disjoined covering and $x_i \in E_i$:

$$\begin{aligned} &\left(\int_X f(x)\,\mathrm{d}\mu_{HC}\left(E, D^+, D^-, x, \breve{x}, \varepsilon\right)\right)_{\varepsilon} \\ &= \left(\lim_{diam(E_i)\to 0}\left[\sum\nolimits_{\bigcup E_i = X} f\left(x_i\right) \inf_{\{E_{ij}\} \text{ with } \bigcup_j E_{ij} \supset E_i} \sum\nolimits_j \zeta_{\varepsilon}\left(E_i, D^+, D^-, x_i, \breve{x}\right)\right]\right)_{\varepsilon}. \end{aligned} \quad (178)$$

We assume now that X is metrically unbounded, *i.e.* for every $x \in X$ and $r > 0$ there exists a point y such that $d(x, y) > r$. The standard assumption that $\breve{D}^+$ and $\breve{D}^-$ is uniquely defined in all subsets E of X requires X to be regular (homogeneous, uniform) with respect to the measure, *i.e.* $\left(\mu_{HC}^-\left(B_r\left(\breve{x}\right), \breve{D}^+, \breve{D}^-, x, \breve{x}, \varepsilon\right)\right)_{\varepsilon} = \left(\mu_{HC}^-\left(B_r\left(\breve{y}\right), \breve{D}^+, \breve{D}^-, x', \breve{y}, \varepsilon\right)\right)_{\varepsilon}$, where $d\left(x, \breve{x}\right) = d\left(x', \breve{y}\right)$ for all elements $\breve{x}, \breve{y}, x, x' \in X$ and convex balls $B_r\left(\breve{x}\right)$ and $B_r\left(\breve{y}\right)$ of the form $B_r\left(\breve{x}\right) = \left\{z \mid d\left(\breve{x}, z\right) \leq r; \breve{x}, z \in X\right\}$ and $B_r\left(\breve{y}\right) = \left\{z \mid d\left(\breve{y}, z\right) \leq r; \breve{y}, z \in X\right\}$. In the limit $diam\left(E_i\right) \to 0$, the infimum is satisfied by the requirement that the variation over all coverings $\{E_{ij}\}_{ij\in\mathbb{N}}$ is replaced by one single covering E_i, such that $\bigcup_j E_{ij} \to E_i \ni x_i$. Therefore

$$\begin{aligned}&\left(\int_X f(x)\mathrm{d}\mu_{HC}\left(E,\breve{D}^+,\breve{D}^-,x,\breve{x},\varepsilon\right)\right)_\varepsilon\\&=\left(\lim_{diam(E_i)\to 0}\sum_{\bigcup E_i=X} f(x_i)\zeta_\varepsilon\left(E_i,\breve{D}^+,\breve{D}^-,x_i,\breve{x}\right)\right)_\varepsilon.\end{aligned}\tag{179}$$

Assume that $f(x)=f(r), r=\|r\|$. The range of integration X may be parametrized by polar coordinates with $r=d(x,0)$ and angle ω. $\{E_{r_i,\omega_i}\}$ can be thought of as spherically symmetric covering around a centre at the origin. Thus

$$\begin{aligned}&\left(\int_X f(r)\mathrm{d}\mu_{HC}\left(E,\breve{D}^+,\breve{D}^-,x,\breve{x},\varepsilon\right)\right)_\varepsilon\\&=\left(\lim_{diam(E_i)\to 0}\sum_{\bigcup E_i=X} f(r_i)\zeta_\varepsilon\left(E_i,\breve{D}^+,\breve{D}^-,x_i,\breve{x}\right)\right)_\varepsilon.\end{aligned}\tag{180}$$

Notice that the metric set $X\subset\mathbb{R}^n$ can be tesselated into regular polyhedra; in particular it is always possible to divide $\mathbb{R}^n$ into parallelepipeds of the form

$$\Pi_{i_1,\cdots,i_n}=\left\{x=(x_1,\cdots,x_n)\in X \mid x_j=(i_j-1)\Delta x_j+\gamma_j, 0\le\gamma_j\le\Delta x_j, j=1,\cdots,n\right\}.\tag{181}$$

For $n=2$ the polyhedra Π_{i_1,i_2} is shown in **Figure 6**. Since X is uniform

$$\begin{aligned}\left(\mathrm{d}\mu_{HC}\left(x,\breve{D}^+,\breve{D}^-,x,\breve{x},\varepsilon\right)\right)_\varepsilon&=\left(\lim_{diam(\Pi_{i_1,\cdots,i_n})}\zeta_\varepsilon\left(\Pi_{i_1,\cdots,i_n},\breve{D}^+,\breve{D}^-,x,\breve{x}\right)\right)_\varepsilon\\&=\left(\lim_{diam(\Pi_{i_1,\cdots,i_n})}\prod_{j=1}^n\left(\frac{\Delta x_j}{\left|x_j-\breve{x}_j\right|^{\left|\breve{D}^-\right|}+\varepsilon}\right)^{\frac{\breve{D}^+}{n}}\right)_\varepsilon\\&\triangleq\left(\prod_{j=1}^n\frac{\mathrm{d}^{\frac{\breve{D}^+}{n}}x_j}{\left(\left|x_j-\breve{x}_j\right|^{\left|\breve{D}^-\right|}+\varepsilon\right)^{\frac{\breve{D}^+}{n}}}\right)_\varepsilon.\end{aligned}\tag{182}$$

Notice that the range of integration X may also be parametrized by polar coordinates with $r=d(x,0)$ and angle Ω. $E_{r,\Omega}$ can be thought of as spherically symmetric covering around a centre at the origin (see **Figure 7** for the two-dimensional case). In the limit, the Colombeau generalized function $\left(\zeta_\varepsilon\left(E_{r,\Omega},\breve{D}^+,\breve{D}^-,r,0\right)\right)_\varepsilon$ is given by

$$\begin{aligned}&\left(\mathrm{d}\mu_{HC}\left(r,\Omega,\breve{D}^+,\breve{D}^-,\varepsilon\right)\right)_\varepsilon\\&=\left(\lim_{diam(\Pi_{i_1,\cdots,i_n})}\zeta_\varepsilon\left(E_{r,\Omega},\breve{D}^+,\breve{D}^-,\{r,\Omega\},0\right)\right)_\varepsilon\triangleq\frac{\mathrm{d}\Omega^{\breve{D}^+-1}r^{\breve{D}^+-1}\mathrm{d}r}{\left(r^{\left|\breve{D}^-\right|}+\varepsilon\right)_\varepsilon}\end{aligned}\tag{183}$$

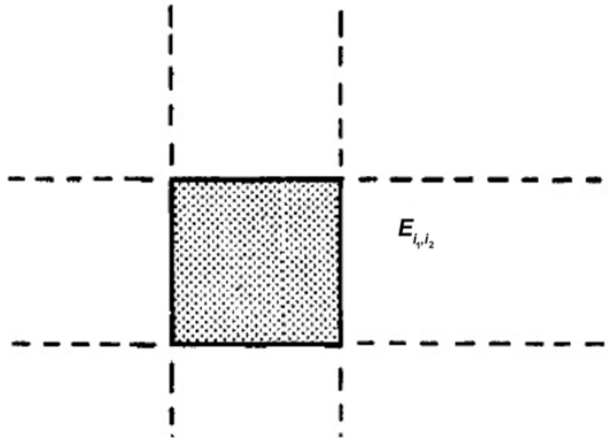

Figure 6. The polyhedra covering for $n = 2$.

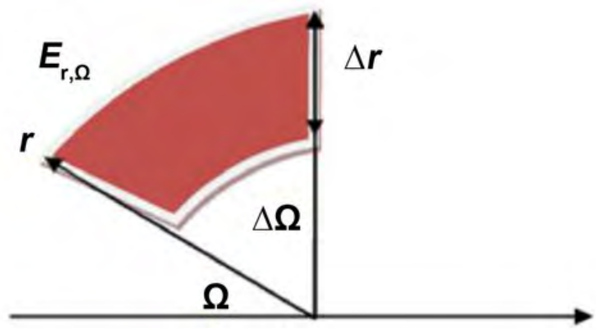

Figure 7. The spherical covering $E_{r,\Omega}$.

When $f(x)$ is symmetric with respect to some centre $\breve{x} \in X$, *i.e.* $f(x) =$ constant for all x satisfying $d(x, \breve{x}) = r$ for arbitrary values of r, then change of the variable

$$x \to z = x - \breve{x} \tag{184}$$

can be performed to shift the centre of symmetry to the origin (since X is not a linear space, (184) need not be a map of X onto itself and (184) is measure presuming). The integral over metric space X is then given by formula

$$\begin{aligned}&\left(\int_X f(x)\mathrm{d}\mu_{HC}\left(E, \breve{D}^+, \breve{D}^-, x, \breve{x}, \varepsilon\right)\right)_\varepsilon \\ &= \frac{4\pi^{D^+/2}\pi^{D^-/2}}{\Gamma\left(D^+/2\right)\Gamma\left(D^-/2\right)}\left(\int_0^\infty \frac{r^{D^+-1} f(r)}{\varepsilon + r^{\left|D^-\right|}}\mathrm{d}r\right)_\varepsilon.\end{aligned} \tag{185}$$

3.4. Main Properties of the Hausdorff-Colombeau Metric Measures with Associated Negative Hausdorff-Colombeau Dimensions

Definition 3.4.1. An outer Colombeau metric measure on a set $X \subseteq \mathbb{R}^n$ is a Colombeau generalized function $\left[\left(\phi_\varepsilon(E)\right)_\varepsilon\right] \in \mathcal{G}_F(\Omega)$ (see Definition 3.3.1) defined on all subsets of X satisfies the following properties.

1) Null empty set: The empty set has zero Colombeau outer measure

$$\left[\left(\phi_{\varepsilon}(\varnothing)\right)_{\varepsilon}\right]=0. \tag{186}$$

2) Monotonicity: For any two subsets A and B of X

$$A\subseteq B\left[\left(\phi_{\varepsilon}(A)\right)_{\varepsilon}\right]\leq_{\tilde{\mathbb{R}}}\left[\left(\phi_{\varepsilon}(B)\right)_{\varepsilon}\right]. \tag{187}$$

3) Countable subadditivity: For any sequence $\{A_j\}$ of subsets of X pairwise disjoint or not

$$\left[\left(\phi_{\varepsilon}\left(\bigcup_{j=1}^{\infty}A_j\right)\right)_{\varepsilon}\right]\leq_{\tilde{\mathbb{R}}}\left[\left(\sum_{j=1}^{\infty}\phi_{\varepsilon}(A_j)\right)_{\varepsilon}\right]. \tag{188}$$

4) Whenever $d(A,B)=\inf\{d_n(x,y)\mid x\in A, y\in B\}>0$

$$\left[\left(\phi_{\varepsilon}(A\cup B)\right)_{\varepsilon}\right]=\left[\left(\phi_{\varepsilon}(A)\right)_{\varepsilon}\right]+\left[\left(\phi_{\varepsilon}(B)\right)_{\varepsilon}\right], \tag{189}$$

where $d_n(x,y)$ is the usual Euclidean metric: $d_n(x,y)=\sqrt{\sum(x_i-y_i)^2}$.

Definition 3.4.2. We say that outer Colombeau metric measure $(\mu_{\varepsilon})_{\varepsilon},\varepsilon\in(0,1]$ is a Colombeau measure on σ-algebra of subests of $X\subseteq\mathbb{R}^n$ if $(\mu_{\varepsilon})_{\varepsilon}$ satisfies the following property:

$$\left[\left(\phi_{\varepsilon}\left(\bigcup_{j=1}^{\infty}A_j\right)\right)_{\varepsilon}\right]=\left[\left(\sum_{j=1}^{\infty}\phi_{\varepsilon}(A_j)\right)_{\varepsilon}\right]. \tag{190}$$

Definition 3.4.3. If U is any non-empty subset of n-dimensional Euclidean space, $\mathbb{R}^n$, the diamater $|U|$ of U is defined as

$$|U|=\sup\{d(x,y)\mid x,y\in U\} \tag{191}$$

If $F\subseteq\mathbb{R}^n$, and a collection $\{U_i\}_{i\in\mathbb{N}}$ satisfies the following conditions:

1) $|U_i|<\delta$ for all $i\in\mathbb{N}$, 2) $F\subseteq\bigcup_{i\in\mathbb{N}}U_i$, then we say the collection $\{U_i\}_{i\in\mathbb{N}}$ is a δ-cover of *F*.

Definition 3.4.4. If $F\subseteq\mathbb{R}^n$ and $s,q,\delta>0$, we define Hausdorff-Colombeau content:

$$\left(H_{\delta}^{s,q}(F,\varepsilon)\right)_{\varepsilon}=\left(\inf\left\{\sum_{i=1}^{\infty}\frac{|U_i|^s}{\|x_i\|^q+\varepsilon}\right\}\right)_{\varepsilon} \tag{192}$$

where the infimum is taken over all δ-covers of F and where $x_i=(x_{i,1},\cdots,x_{i,n})\in U_i$ for all $i\in\mathbb{N}$ and $\|x\|$ is the usual Euclidean norm: $\|x\|=\sqrt{\sum_{j=1}^{n}x_j^2}$.

Note that for $0<\delta_1<\delta_2<1,\varepsilon\in(0,1]$ we have

$$H_{\delta_1}^{s,q}(F,\varepsilon)\geq H_{\delta_2}^{s,q}(F,\varepsilon) \tag{193}$$

since any δ_1 cover of F is also a δ_2 cover of *F*, *i.e.* $H_{\delta_1}^{s,q}(F,\varepsilon)$ is increasing as δ decreases.

Definition 3.4.5. We define the (s,q)-dimensional Hausdorff-Colombeau (outer) measure as:

$$\left(H^{s,q}(F,\varepsilon)\right)_{\varepsilon}=\left(\lim_{\delta\to 0}H_{\delta}^{s,q}(F,\varepsilon)\right)_{\varepsilon}. \tag{194}$$

Theorem 3.4.1. For any δ-cover, $\{U_i\}_{i\in\mathbb{N}}$ of *F*, and for any $\varepsilon\in(0,1]$, $t>s$:

$$H^{t,q}(F,\varepsilon) \le \delta^{t-s} H^{s,q}(F,\varepsilon). \tag{195}$$

Proof. Consider any δ-cover $\{U_i\}_{i\in\mathbb{N}}$ of *F*. Then each $|U_i|^{t-s} \le \delta^{t-s}$ since $|U_i| \le \delta$, so:

$$|U_i|^t = |U_i|^{t-s}|U_i|^s \le \delta^{t-s}|U_i|^s. \tag{196}$$

From (196) it follows that

$$\frac{|U_i|^t}{\|x_i\|^q + \varepsilon} \le \frac{\delta^{t-s}|U_i|^s}{\|x_i\|^q + \varepsilon} \tag{197}$$

and summing (196) over all $i \in \mathbb{N}$ we obtain

$$\sum_{i=1}^{\infty} \frac{|U_i|^t}{\|x_i\|^q + \varepsilon} \le \delta^{t-s} \sum_{i=1}^{\infty} \frac{|U_i|^s}{\|x_i\|^q + \varepsilon}. \tag{198}$$

Thus (195) follows by taking the infimum.

Theorem 3.4.2. 1) If $\left(H^{s,q}(F,\varepsilon)\right)_\varepsilon <_{\tilde{\mathbb{R}}} \infty_{\tilde{\mathbb{R}}}$, and if $t > s$, then $\left(H^{t,q}(F,\varepsilon)\right)_\varepsilon = 0_{\tilde{\mathbb{R}}}$.

2) If $0_{\tilde{\mathbb{R}}} <_{\tilde{\mathbb{R}}} \left(H^{s,q}(F,\varepsilon)\right)_\varepsilon$, and if $t < s$, then $\left(H^{t,q}(F,\varepsilon)\right)_\varepsilon = \infty_{\tilde{\mathbb{R}}}$.

Proof. 1) The result follows from (195) after taking limits, since $\forall \varepsilon \in (0,1]$ by definitions follows that $H^{s,q}(F,\varepsilon) < \infty$.

2) From (3.4.10) $\forall \varepsilon \in (0,1], \forall \delta > 0$ follows that

$$\frac{1}{\delta^{s-t}} H^{s,q}(F,\varepsilon) \le H^{t,q}(F,\varepsilon). \tag{199}$$

After taking limit $\delta \to 0$, we obtain $H^{t,q}(F,\varepsilon) = \infty$, since $\lim_{\delta\to 0}\left(\delta^{s-t}\right)^{-1} = \infty$ and $\lim_{\delta\to 0} H^{s,q}_\delta(F,\varepsilon) = H^{s,q}(F,\varepsilon) > 0$.

Definition 3.4.6. We define now the Hausdorff-Colombeau dimension $\dim_{HC}(F,q)$ of a set *F* (relative to $q > 0$) as

$$\begin{aligned} \dim_{HC}(F,q) &= \sup\left\{ s = s(q) \mid \left(H^{s,q}(F,\varepsilon)\right)_\varepsilon = \infty_{\tilde{\mathbb{R}}} \right\} \\ &= \inf\left\{ s = s(q) \mid \left(H^{s,q}(F,\varepsilon)\right)_\varepsilon = 0_{\tilde{\mathbb{R}}} \right\}. \end{aligned} \tag{200}$$

Remark 3.4.1. From theorem 3.4.2 it follows that for any fixed $q = \breve{q}$:

$\left(H^{s,\breve{q}}(F,\varepsilon)\right)_\varepsilon = 0_{\tilde{\mathbb{R}}}$ or $\left(H^{s,\breve{q}}(F,\varepsilon)\right)_\varepsilon = \infty_{\tilde{\mathbb{R}}}$ everywhere except at a unique value *s*, where this value may be finite. As a function of *s*, $H^{s,\breve{q}}(F,\varepsilon)$ is decreasing function. Therefore, the graph of $H^{s,\breve{q}}(F,\varepsilon)$ will have a unique value where it jumps from ∞ to 0.

Remark 3.4.2. Note that the graph of $\left(H^{s,\breve{q}}(F,\varepsilon)\right)_\varepsilon$ for a fixed $q = \breve{q}$ is

$$\left(H^{s,\breve{q}}(F,\varepsilon)\right)_\varepsilon = \begin{cases} \infty_{\tilde{\mathbb{R}}} & \text{if } s > \dim_{HC}(F,\breve{q}) \\ 0_{\tilde{\mathbb{R}}} & \text{if } s > \dim_{HC}(F,\breve{q}) \\ \text{undetermined} & \text{if } s = \dim_{HC}(F,\breve{q}) \end{cases} \tag{201}$$

Definition 3.4.7. We say that fractal $\mathcal{F} \subseteq \mathbb{R}^n$ has a negative dimension relative to $q>0$

if $\dim_{HC}(F,q)-q<0$.

4. Scalar Quantum Field Theory in Spacetime with Hausdorff-Colombeau Negative Dimensions

4.1. Equation of motion and Hamiltonian

Scalar quantum field theory and quantum gravity in spacetime with noninteger positive Hausdorff dimensions developed in papers [28] [29] [30] [31]. Quantum mechanics in negative dimensions developed in papers [32] [33] Scalar quantum field theory and quantum gravity in spacetime with Hausdorff-Colombeau negative dimensions originally developed in paper [12]. In this section only free scalar quantum field in spacetime with negative dimensions briefly is considered.

A negative-dimensional spacetime structure is a desirable feature of superrenormalizable spacetime models of quantum gravity, and the most simply way to obtain it is to let the effective dimensionality of the multifractal universe to change at different scales. A simple realization of this feature is via suitable extended fractional calculus and the definition of a fractional action. Note that below we use canonical isotropic scaling such that:

$$\left[x^{\mu}\right]=-1,\mu=0,1,\cdots,D_t-1 \tag{202}$$

while replacing the standard measure with a nontrivial Colombeau-Stieltjes measure,

$$\begin{gathered}\mathrm{d}^{D_{\mathrm{t}}}x\to\mathrm{d}^{D_{\mathrm{f}}}x=\left(\mathrm{d}\eta\left(x,\varepsilon\right)\right)_{\varepsilon},\\ \left[\eta\right]=D_{\mathrm{t}}\cdot\alpha,\alpha\in\left[1,-\infty\right).\end{gathered} \tag{203}$$

Here D_{t} is the topological (positive integer) dimension of embedding spacetime and α is a parameter. Any Colombeau integrals on net multifractals can be approximated by the left-sided Colombeau-Riemann--Liouville complex milti-fractional integral of a function $\mathcal{L}(t)$:

$$\begin{gathered}\left(\int_0^{\bar{t}}\mathrm{d}\eta\left(x,\varepsilon\right)\mathcal{L}\left(t\right)\right)_{\varepsilon}\propto\left(I_{\bar{t},\varepsilon}^{\{z_i(\bar{t})\}}\right)_{\varepsilon}\triangleq\left(\sum_{i=1}^{m}\int_{\varepsilon}^{\bar{t}}\frac{\left[\left(\bar{t}-t\right)+i\varepsilon\right]^{z_i(\bar{t})-1}}{\Gamma\left(z_i\left(\bar{t}\right)\right)}\mathcal{L}\left(t\right)\mathrm{d}t\right)_{\varepsilon},\\ \left(\eta\left(t,\varepsilon\right)\right)_{\varepsilon}=\left(\frac{\bar{t}^{z_i(\bar{t})}-\left[\left(\bar{t}-t\right)+i\varepsilon\right]^{z_i(\bar{t})}}{\Gamma\left(z_i\left(\bar{t}\right)+1\right)}\right)_{\varepsilon},\end{gathered} \tag{204}$$

where $\varepsilon\in(0,1]$, $\bar{t}$ is fixed and the order $z(\bar{t})$ is (related to) the complex Hausdorff-Colombeau dimensions of the set. In particular if $z_i\in\mathbb{C},i=1,2,\cdots,m$ is a complex parameter an integral on net multifractals can be approximated by finite sum of the left-sided Colombeau-Riemann-Liouville complex fractional integral of a function $\mathcal{L}(t)$

$$\left(\int_0^{\bar{t}} \mathrm{d}\eta(x,\varepsilon)\mathcal{L}(t)\right)_\varepsilon \propto \left(I_{\bar{t},\varepsilon}^{\{z_i\}_{i=1}^m}\right)_\varepsilon$$

$$= \sum_{i=1}^m \left(I_{\bar{t},\varepsilon}^{z_i}\right)_\varepsilon \triangleq \sum_{i=1}^m \left(\frac{1}{\Gamma(z_i)}\int_\varepsilon^{\bar{t}} \mathrm{d}\left[\left(\bar{t}-t\right)+i\varepsilon\right]^{z_i-1}\mathcal{L}(t)\right)_\varepsilon, \tag{205}$$

$$\left(\eta(t,\varepsilon)\right)_\varepsilon = \sum_{i=1}^m \left(\frac{\bar{t}^{z_i}-\left[\left(\bar{t}-t\right)+i\varepsilon\right]^{z_i}}{\Gamma(z_i+1)}\right)_\varepsilon.$$

Note that a change of variables $t \to \bar{t}-t$ transforms Equation (205) into the form

$$\left(\int_0^{\bar{t}} \mathrm{d}\eta(x,\varepsilon)\mathcal{L}(t)\right)_\varepsilon = \sum_{i=1}^m \left(\int_0^{\bar{t}} \mathrm{d}t \frac{\left[t+i\varepsilon\right]^{z_i-1}}{\Gamma\left(z(\bar{t})\right)}\mathcal{L}\left(\bar{t}-t\right)\right)_\varepsilon. \tag{206}$$

The Colombeau-Riemann-Liouville multifractional integral (206) can be mapped onto a Colombeau-Weyl multifractional integral in the formal limit $\bar{t} \to +\infty$. We assume otherwise, so that there exists $\lim_{\bar{t}\to+\infty} z(\bar{t})$ and $\lim_{\bar{t}\to+\infty} \mathcal{L}\left(\bar{t}-t\right) = \mathcal{L}\left[q(t),\dot{q}(t)\right]$. In particular if $z \in \mathbb{C}$ is a complex parameter a change of variables $t \to \bar{t}-t$ transforms Equation (206) into the form

$$\sum_{i=1}^m \left(I_{\bar{t},\varepsilon}^{z_i}\right)_\varepsilon = \sum_{i=1}^m \left(\int_\varepsilon^{\bar{t}} \mathrm{d}t \frac{\left[t+i\varepsilon\right]^{z_i-1}}{\Gamma(z_i)}\mathcal{L}\left[q(t),\dot{q}(t)\right]\right)_\varepsilon. \tag{207}$$

This form will be the most convenient for defining a Colombeau-Stieltjes field theory action. In D_{t} dimensions, we consider now the action

$$\left(\mathbf{S}_\varepsilon\right)_\varepsilon = \left(\int_M \mathrm{d}\eta(x,\varepsilon)\mathcal{L}\left[\varphi_\varepsilon(x),\partial_\mu\varphi_\varepsilon(x)\right]\right)_\varepsilon, \tag{208}$$

where $\mathcal{L}\left[\varphi,\partial_\mu\varphi\right]$ is the Lagrangian density of the scalar field $\left(\varphi_\varepsilon(x)\right)_\varepsilon$ and where

$$\left(\mathrm{d}\eta(x,\varepsilon)\right)_\varepsilon = \sum_{i=1}^m \prod_{\mu=0}^{D_{\mathrm{t}}-1}\left(f_{\mu,i}(x,\varepsilon)\right)_\varepsilon \mathrm{d}x^\mu, \left(f_{\mu,i}(x,\varepsilon)\right)_\varepsilon : M \to \tilde{\mathbb{R}}, \tag{209}$$

is some Colombeau-Stieltjes measure. We denote with pair $\left(M,\left(\mathrm{d}\eta(x,\varepsilon)\right)_\varepsilon\right)$ the metric spacetime M equipped with Colombeau-Stieltjes measure $\left(\mathrm{d}\eta(x,\varepsilon)\right)_\varepsilon$. The former can be taken to be the canonical scalar field Lagrangian,

$$\left(\mathcal{L}\left[\varphi_\varepsilon(x),\partial_\mu\varphi_\varepsilon(x)\right]\right)_\varepsilon = -\frac{1}{2}\left(\partial_\mu\varphi_\varepsilon\partial^\mu\varphi_\varepsilon\right)_\varepsilon - \left(V(\varphi_\varepsilon)\right)_\varepsilon, \tag{210}$$

where $V(\varphi)$ is a potential and contraction of Lorentz indices is done via the Minkowski metric $\eta_{\mu\nu} = (-,+,\cdots,+)_{\mu\nu}$. As for the Colombeau-Stieltjes measure, we make the multifractal spacetime isotropic choice

$$\left(f_{(\mu,i),\varepsilon}\right)_\varepsilon = \left(f_{i,\varepsilon}\right)_\varepsilon, \mu = 1,\cdots,D_{\mathrm{t}}-1; i = 1,\cdots,m. \tag{211}$$

Hence the scalar field action (208) reads

$$\begin{aligned}\left(\mathbf{S}_\varepsilon\right)_\varepsilon &= \left(\int_M \mathrm{d}\eta(x,\varepsilon)\left[\varphi_\varepsilon(x),\partial_\mu\varphi_\varepsilon(x)\right]\right)_\varepsilon \\ &= \sum_{j=1}^m \left(\int \mathrm{d}^{D_{\mathrm{t}}} x v_{\varepsilon,j}(x)\left[\frac{1}{2}\partial_\mu\varphi_\varepsilon\partial^\mu\varphi_\varepsilon + V(\varphi_\varepsilon)\right]\right)_\varepsilon,\end{aligned} \tag{212}$$

where $\left(v_\varepsilon(x)\right)_\varepsilon$ is a coordinate-dependent

Lorentz scalar

$$\left(v_{\varepsilon,j}(x)\right)_{\varepsilon}=\left(\frac{1}{\left[s_j(x)\right]^{D_{\mathrm{t}}(|\alpha-1|)}+\varepsilon}\right)_{\varepsilon}. \tag{213}$$

We define now the Dirac distribution as Colombeau generalized function by equation

$$\sum_{j=1}^{m}\left(\int \mathrm{d}\eta_j(x,\varepsilon)\delta_{\{v_j\}}^{(D_{\mathrm{f},j})}(x,\varepsilon)\right)_{\varepsilon}=m. \tag{214}$$

In particular for the case $m=1$

$$\left(\int \mathrm{d}\eta(x,\varepsilon)\delta_{\{v\}}^{(D_{\mathrm{f}})}(x,\varepsilon)\right)_{\varepsilon}=1. \tag{215}$$

Invariance of the action under the infinitesimal shift $\varphi(x)\to\varphi(x)+\delta\varphi(x)$ gives the equation of motion for a generic weight $\left(v_{i,\varepsilon}\right)_{\varepsilon}, i=1,\cdots,m$:

$$\left(\frac{\partial\mathcal{L}}{\partial\varphi_{\varepsilon}}\right)_{\varepsilon}-\sum_{i=1}^{m}\left(\left[\left(\frac{\partial_{\mu}v_{i,\varepsilon}}{v_{i,\varepsilon}}\right)+\frac{\mathrm{d}}{\mathrm{d}x^{\mu}}\right]\frac{\partial\mathcal{L}}{\partial\left(\partial_{\mu}\varphi_{\varepsilon}\right)}\right)_{\varepsilon}=0. \tag{216}$$

In particular for the case $m=1$ we obtain

$$\left(\frac{\partial\mathcal{L}}{\partial\varphi_{\varepsilon}}\right)_{\varepsilon}-\left(\left[\frac{\partial_{\mu}v_{\varepsilon}}{v_{\varepsilon}}+\frac{\mathrm{d}}{\mathrm{d}x^{\mu}}\right]\frac{\partial\mathcal{L}}{\partial\left(\partial_{\mu}\varphi_{\varepsilon}\right)}\right)_{\varepsilon}=0. \tag{217}$$

From Equation (212) and Equation (216) we obtain

$$\left(\Box\varphi_{\varepsilon}\right)_{\varepsilon}+\sum_{i=1}^{m}\left\{\left(\left[\frac{\partial_{\mu}v_{i,\varepsilon}}{v_{i,\varepsilon}}\right]\partial^{\mu}\varphi_{\varepsilon}\right)_{\varepsilon}\right\}-\left(\frac{\mathrm{d}}{\mathrm{d}\varphi_{\varepsilon}}V\left(\varphi_{\varepsilon}\right)\right)_{\varepsilon}=0. \tag{218}$$

where $\Box=\partial_{\mu}\partial^{\mu}$. In particular for the case $m=1$ we obtain

$$\left(\Box\varphi_{\varepsilon}\right)_{\varepsilon}+\left(\left[\frac{\partial_{\mu}v_{\varepsilon}}{v_{\varepsilon}}\right]\partial^{\mu}\varphi_{\varepsilon}\right)_{\varepsilon}-\left(\frac{\mathrm{d}}{\mathrm{d}\varphi_{\varepsilon}}V\left(\varphi_{\varepsilon}\right)\right)_{\varepsilon}=0. \tag{219}$$

4.2. Propagator in Configuration Space with Negative-Dimensions

We define the canonical vacuum-to-vacuum amplitude by

$$\left(Z[J,\varepsilon]\right)_{\varepsilon}=\left(\int \mathbf{D}\varphi_{\varepsilon}\exp\left[i\sum_{j=1}^{m}\int \mathrm{d}\eta_{j,\varepsilon}\left(\mathcal{L}+\varphi_{\varepsilon}J\right)\right]\right)_{\varepsilon}, \tag{220}$$

where J is a source. Integration by parts in the exponent leads to the Lagrangian density for a free field as

$$\left(\mathcal{L}_{\varepsilon}\right)_{\varepsilon}=\frac{1}{2}\left(\varphi_{\varepsilon}\left(\Box+\sum_{j=1}^{m}\frac{\partial_{\mu}v_{j,\varepsilon}}{v_{j,\varepsilon}}\partial^{\mu}-m^2\right)\varphi_{\varepsilon}\right)_{\varepsilon}=\frac{1}{2}\left(\varphi_{\varepsilon}\mathfrak{I}_{\varepsilon}\varphi_{\varepsilon}\right)_{\varepsilon}, \tag{221}$$

where

$$\mathfrak{I}_{\varepsilon}=\Box+\sum_{j=1}^{m}\frac{\partial_{\mu}v_{j,\varepsilon}}{v_{j,\varepsilon}}\partial^{\mu}-m^2;\ j=1,\cdots,m. \tag{222}$$

In particular for the case $m=1$ we obtain

$$\Im_\varepsilon = \Box + \frac{\partial_\mu v_\varepsilon}{v_\varepsilon}\partial^\mu - m^2. \tag{223}$$

The propagator is the Green function $(G_\varepsilon(x))_\varepsilon$ solving the equation

$$\left(\Im_\varepsilon G_\varepsilon(x)\right)_\varepsilon = \left(\delta_v^{D^-}(x,\varepsilon)\right)_\varepsilon, \tag{224}$$

where $D^- = D_t(\alpha-1) < 0$. By virtue of Lorentz covariance, the Green function $G_\varepsilon(x)$ must depend only on the Lorentz interval $s^2 = x_\mu x^\mu = x_i x^i - t^2$, where $x^0 = t$ and $i = 1,\cdots,D_t - 1$. In particular, $(v_\varepsilon)_\varepsilon = \left(v_\varepsilon(s(x))\right)_\varepsilon$ with the correct scaling property is

$$\left(v_\varepsilon(s(x))\right)_\varepsilon = \left(\left(\left|s(x)\right|^{\left|D^-\right|} + \varepsilon\right)^{-1}\right)_\varepsilon, s(x) = \sqrt{x_\mu x^\mu}. \tag{225}$$

Note that

$$\partial_\mu = \frac{x_\mu}{(s+\varepsilon)_\varepsilon}\partial_s, \Box = \partial_s^2 + \frac{D_t - 1}{(s+\varepsilon)_\varepsilon}\partial_s. \tag{226}$$

Hence the inhomogeneous Equation (224) reads

$$\left(\partial_s^2 + \frac{D_t\alpha - 1}{(s+\varepsilon)_\varepsilon}\partial_s - m^2\right)\left(G_\varepsilon(x)\right)_\varepsilon = \left(\delta_v^{D^-}(x,\varepsilon)\right)_\varepsilon. \tag{227}$$

We first consider the Euclidean propagator and denote with $r = \sqrt{x_i x^i + t^2}$ the Wick-rotated Lorentz invariant. In the massless case, the solution of the homogeneous equations for any $\alpha < 0$ is

$$\left(G_\varepsilon(r)\right)_\varepsilon = Cr^{2\beta}, \beta = \frac{2 + D_t|\alpha|}{2}. \tag{228}$$

Let us now consider the massive case.The solution of the homogeneous equation $\left(\Im_\varepsilon G_\varepsilon(r)\right)_\varepsilon = 0$ for any $\alpha < 0$ is

$$\left(G_\varepsilon(r)\right)_\varepsilon = \left(\frac{r}{m}\right)^{\frac{2+D_t|\alpha|}{2}}\left[C_1\mathbf{K}_{-\frac{2+D_t\cdot|\alpha|}{2}}(mr) + C_2\mathbf{I}_{-\frac{2+D_t\cdot|\alpha|}{2}}(mr)\right], \tag{229}$$

where C_1, C_2 are constants and $\mathbf{K}_\lambda$ and $\mathbf{I}_\lambda$ are the modified Bessel functions. The function $\mathbf{I}_\nu(z)$ is

$$\mathbf{I}_\nu(z) = \sum_{k=0}^\infty \frac{(z/2)^{\nu+2k}}{k!\Gamma(\nu+k+1)}. \tag{230}$$

Formula (230) is valid providing $\nu \neq -1,-2,-3,\cdots$

$$\mathbf{I}_{-|\nu|}(z) = \sum_{k=0}^\infty \frac{(z/2)^{-|\nu|+2k}}{k!\Gamma(-|\nu|+k+1)} \tag{231}$$

Formula (231) is obtained by replacing ν in (232) with a $-\nu$.

$$\mathbf{K}_{-|\nu|}(z) = -\frac{\pi}{2\sin|\nu|\pi}\left[\mathbf{I}_{|\nu|}(z) - \mathbf{I}_{-|\nu|}(z)\right]. \tag{232}$$

The modified Bessel functions $\mathbf{I}_{-|\nu|}(z)$ and

$\mathbf{K}_{-|\nu|}(z)$ have the following asymptotic forms for $z \to 0$:

$$\mathbf{K}_{-|\nu|}(z) \simeq \frac{1}{2}\Gamma(-|\nu|)\left(\frac{2}{z}\right)^{-|\nu|}, \mathbf{I}_{-|\nu|}(z) \simeq \frac{1}{\Gamma(-|\nu|+1)}\left(\frac{z}{2}\right)^{-|\nu|}, \nu \neq -1,-2,-3,\cdots \quad (233)$$

Since for small $m \simeq 0$ the solution must agree with the massless case (228), we can set $C_2 = 0$. To find the solution of the inhomogeneous equation, one exploits the fact that the mass term does not contribute near the origin. Expanding Equation (229) at $mr \simeq 0$ when $\alpha < 0$ ($C_2 = 0$), we find

$$\left(G_\varepsilon(r)\right)_\varepsilon = C_1 2^{-\frac{4+D_t\cdot|\alpha_i|}{2}}\Gamma\left(-\frac{2+D_t\cdot|\alpha_i|}{2}\right)\left(r^2\right)^{\frac{2+D_t\cdot|\alpha_i|}{2}} \quad (234)$$

which must coincide with Equation (228). This gives the coefficient C_1 and the propagator reads

$$G(r) = -\frac{1}{2\pi^{\frac{D_t}{2}}}\frac{\Gamma\left(\frac{D_t}{2}\right)}{\Gamma\left(-\frac{D_t|\alpha|}{2}\right)}\left(\frac{m}{2r}\right)^{-\frac{2+D_{t,i}\cdot|\alpha_i|}{2}}\mathbf{K}_{-\frac{2+D_t|\alpha|}{2}}(mr). \quad (235)$$

5. The Solution Cosmological Constant Problem

5.1. Einstein-Gliner-Zel'dovich Vacuum with Tiny Lorentz Invariance Violation

We assume now that:

1) Poincaré group of momentum space is deformed at some fundamental high-energy cutoff Λ_* [9] [10].

2) The canonical quadratic invariant $\|p\|^2 = \eta^{ab}p_a p_b$ collapses at high-energy cutoff Λ_* and being replaced by the non-quadratic invariant:

$$\|p\|^2 = \frac{\eta^{ab}p_a p_b}{\left(1 + l_{\Lambda_*}p_0\right)}. \quad (236)$$

3) The canonical concept of Minkowski space-time collapses at a small distance $l_{\Lambda_*} = \Lambda_*^{-1}$ to fractal space-time with Hausdorff-Colombeau negative dimension and therefore the canonical Lebesgue measure d^4x being replaced by the Colombeau-Stieltjes measure

$$\left(\mathrm{d}\eta(x,\varepsilon)\right)_\varepsilon = \left(v_\varepsilon(s(x))\mathrm{d}^4x\right)_\varepsilon, \quad (237)$$

where

$$\begin{gathered}\left(v_\varepsilon(s(x))\right)_\varepsilon = \left(\left(|s(x)|^{|D^-|} + \varepsilon\right)^{-1}\right)_\varepsilon, \\ s(x) = \sqrt{x_\mu x^\mu},\end{gathered} \quad (238)$$

see subsection IV.2.

4) The canonical concept of momentum space collapses at fundamental

high-energy cutoff Λ_* to fractal momentum space with Hausdorff-Colombeau negative dimension and therefore the canonical Lebesgue measure $\mathrm{d}^3\mathbf{k}$, where $\mathbf{k}=(k_x,k_y,k_z)$ being replaced by the Hausdorff-Colombeau measure

$$d^{D^+,D^-}\mathbf{k} \triangleq \frac{\Delta(D^-)\mathrm{d}^{D^+}\mathbf{k}}{\left(|\mathbf{k}|^{|D^-|}+\varepsilon\right)_\varepsilon} = \frac{\Delta(D^+)\Delta(D^-)p^{D^+-1}\mathrm{d}p}{\left(p^{|D^-|}+\varepsilon\right)_\varepsilon}, \tag{239}$$

where $\Delta(D^\pm)=\dfrac{2\pi^{D^\pm/2}}{\Gamma(D^\pm/2)}$ and $p=|\mathbf{k}|=\sqrt{k_x+k_y+k_z}$.

Remark 5.1.1. Note that the integral over measure $\mathrm{d}^{D^+,D^-}\mathbf{k}$ is given by formula (185). Thus vacuum energy density $\varepsilon(D^+,D^-,\mu_{\text{eff}},p_*)$ for free quantum fields is

$$\varepsilon(D^+,D^-,\mu_{\text{eff}},p_*)=\varepsilon(\mu_{\text{eff}})+\varepsilon(\mu_{\text{eff}},p_*)+\breve{\varepsilon}(D^+,D^-,\mu_{\text{eff}},p_*). \tag{240}$$

Here the quantity $\varepsilon(\mu_{\text{eff}})$ is given by formula

$$\begin{aligned}\varepsilon(\mu_{\text{eff}}) &= \frac{1}{2(2\pi\hbar)^3}\int_0^{\mu_{\text{eff}}}\mathrm{d}\mu f(\mu)\int_{\|\mathbf{k}\|\le\mu}\sqrt{\mathbf{k}^2+\mu^2}\,\mathrm{d}^3\mathbf{k}\\ &= K\int_0^{\mu_{\text{eff}}}\mathrm{d}\mu f(\mu)\int_{p\le\mu}\sqrt{p^2+\mu^2}\,p^2\mathrm{d}p\\ &= K\int_0^{\mu_{\text{eff}}}\mathrm{d}\mu f(\mu)\int_0^{\mu}\sqrt{p^2+\mu^2}\,p^2\mathrm{d}p\end{aligned} \tag{241}$$

where $K=\dfrac{2\pi}{(2\pi\hbar)^3}, c=1$. The quantity $\varepsilon(\mu_{\text{eff}},p_*)$ is given by formula

$$\begin{aligned}\varepsilon(\mu_{\text{eff}},p_*) &= \frac{1}{2(2\pi\hbar)^3}\int_0^{\mu_{\text{eff}}}\mathrm{d}\mu f(\mu)\int_{\mu<\|\mathbf{k}\|<p_*}\sqrt{\mathbf{k}^2+\mu^2}\,\mathrm{d}^3\mathbf{k}\\ &= K\int_0^{\mu_{\text{eff}}}\mathrm{d}\mu f(\mu)\int_{\mu<\|\mathbf{k}\|<p_*}\sqrt{p^2+\mu^2}\,p^2\mathrm{d}p.\end{aligned} \tag{242}$$

The quantity $\breve{\varepsilon}(D^+,D^-,\mu_{\text{eff}},p_*)$ (since Equation (22) holds) is given by formula

$$\begin{aligned}&\breve{\varepsilon}(D^+,D^-,\mu_{\text{eff}},p_*)\\ &= K\int_0^{\mu_{\text{eff}}}\mathrm{d}\mu f(\mu)\int_{\|\mathbf{k}\|\ge p_*}\left[\frac{\mu^2 l_{\Lambda_*}}{1-\mu^2 l_{\Lambda_*}^2}+\frac{1}{\sqrt{1-\mu^2 l_{\Lambda_*}^2}}\sqrt{\frac{\mu^4 l_{\Lambda_*}^2}{1-\mu^2 l_{\Lambda_*}^2}+\left(|\mathbf{k}|^2+\mu^2\right)}\right]\mathrm{d}^{D^+,D^-}\mathbf{k},\end{aligned} \tag{243}$$

where $K'=\dfrac{1}{2(2\pi\hbar)^3}, c=1$.

Remark 5.1.2. We assume now that $\mu^2 l_{\Lambda_*}^2 \ll 1, \mu^4 l_{\Lambda_*}^2 \ll 1$ and therefore from Equation (243)
we obtain

$$\begin{aligned}&\varepsilon\left(D^{+},D^{-},\mu_{\mathbf{eff}},p_{*}\right)\\&=K'l_{\Lambda}\int\limits_{0}^{\mu_{\text{eff}}}f\left(\mu\right)\mu^{2}\mathrm{d}\mu\int\limits_{\|\mathbf{k}\|\geq p_{*}}\mathrm{d}^{3,D_{-}}\mathbf{k}+K'\int\limits_{0}^{\mu_{\text{eff}}}\mathrm{d}\mu f\left(\mu\right)\int\limits_{\|\mathbf{k}\|\geq p_{*}}\sqrt{\mathbf{k}^{2}+\mu^{2}}\mathrm{d}^{D^{+},D^{-}}\mathbf{k}.\end{aligned}\tag{244}$$

From Equation (244) and Equation (239) we obtain

$$\begin{aligned}&\varepsilon\left(D^{+},D^{-},\mu_{\text{eff}},p_{*}\right)\\&=K'l_{\Lambda}\int_{0}^{\mu_{\text{eff}}}f\left(\mu\right)\mu^{2}\mathrm{d}\mu\int\limits_{\|\mathbf{k}\|\geq p_{*}}\mathrm{d}^{D^{+},D^{-}}\mathbf{k}+K'\int_{0}^{\mu_{\text{eff}}}\mathrm{d}\mu f\left(\mu\right)\int\limits_{\|\mathbf{k}\|\geq p_{*}}\sqrt{\mathbf{k}^{2}+\mu^{2}}\mathrm{d}^{D^{+},D^{-}}\mathbf{k}\\&=\left(K'l_{\Lambda}\Delta\left(D^{+}\right)\Delta\left(D^{-}\right)\int_{0}^{\mu_{\text{eff}}}f\mathrm{d}\mu\left(\mu\right)\mu^{2}\right)\int_{p_{*}}^{\infty}\frac{p^{D^{+}-1}\mathrm{d}p}{\left(p^{\left|D^{-}\right|}+\varepsilon\right)_{\varepsilon}}\\&\quad+K'\Delta\left(D^{+}\right)\Delta\left(D^{-}\right)\int_{0}^{\mu_{\text{eff}}}\mathrm{d}\mu f\left(\mu\right)\int_{p_{*}}^{\infty}\frac{\sqrt{p^{2}+\mu^{2}}\,p^{D^{+}-1}\mathrm{d}p}{\left(p^{\left|D^{-}\right|}+\varepsilon\right)_{\varepsilon}}\\&=\left(K'l_{\Lambda}\Delta\left(D^{+}\right)\Delta\left(D^{-}\right)\int_{0}^{\mu_{\text{eff}}}f\left(\mu\right)\mu^{2}\mathrm{d}\mu\right)\int_{p_{*}}^{\infty}p^{D^{-}+D^{+}-1}\mathrm{d}p\\&\quad+K'\Delta\left(D^{+}\right)\Delta\left(D^{-}\right)\int_{0}^{\mu_{\text{eff}}}\mathrm{d}\mu f\left(\mu\right)\int_{p_{*}}^{\infty}\sqrt{p^{2}+\mu^{2}}\,p^{D^{-}+D^{+}-1}\mathrm{d}p.\end{aligned}\tag{245}$$

Remark 5.1.2. We assume now that:

$$D^{-}+D^{+}+2\leq-6.\tag{246}$$

Note that

$$\begin{aligned}&\int_{0}^{\mu_{\text{eff}}}\mathrm{d}\mu f\left(\mu\right)\int_{p_{*}}^{\infty}\sqrt{p^{2}+\mu^{2}}\,p^{D^{-}+D^{+}-1}\mathrm{d}p\\&=\int_{0}^{\mu_{\text{eff}}}\mathrm{d}\mu f\left(\mu\right)\int_{p_{*}}^{\infty}\sqrt{1+\frac{\mu^{2}}{p^{2}}}\,p^{D^{-}+D^{+}}\mathrm{d}p\\&=\int_{0}^{\mu_{\text{eff}}}f\left(\mu\right)\mathrm{d}\mu\int_{p_{*}}^{\infty}p^{D^{-}+D^{+}}\mathrm{d}p+\frac{1}{2}\int_{0}^{\mu_{\text{eff}}}f\left(\mu\right)\mu^{2}\mathrm{d}\mu\int_{p_{*}}^{\infty}p^{D^{-}+D^{+}-1}\mathrm{d}p\\&\quad-\frac{1}{8}\int_{0}^{\mu_{\text{eff}}}f\left(\mu\right)\mu^{4}\mathrm{d}\mu\int_{p_{*}}^{\infty}p^{D^{-}+D^{+}-3}\mathrm{d}p+O\left(p_{*}^{D^{-}+D^{+}-4}\right)\\&=\frac{p_{*}^{D^{-}+D^{+}+1}}{D^{-}+D^{+}+1}\int_{0}^{\mu_{\text{eff}}}f\left(\mu\right)\mathrm{d}\mu+\frac{p_{*}^{D^{-}+D^{+}}}{2\left(D^{-}+D^{+}\right)}\int_{0}^{\mu_{\text{eff}}}f\left(\mu\right)\mu^{2}\mathrm{d}\mu\\&\quad-\frac{p_{*}^{D^{-}+D^{+}-1}}{8\left(D^{-}+D^{+}-1\right)}\int_{0}^{\mu_{\text{eff}}}f\left(\mu\right)\mu^{4}\mathrm{d}\mu+O\left(p_{*}^{D^{-}+D^{+}-4}\right).\end{aligned}\tag{247}$$

Thus finally we obtain

$$\begin{aligned}&\varepsilon\left(D^{+},D^{-},\mu_{\text{eff}},p_{*}\right)\\&=\frac{K'p_{*}^{D^{-}+D^{+}+1}}{D^{-}+D^{+}+1}\int_{0}^{\mu_{\text{eff}}}f\left(\mu\right)\mathrm{d}\mu\\&\quad+\left(\left[K'l_{\Lambda}\Delta\left(D^{+}\right)\Delta\left(D^{-}\right)+0.5\right]\int_{0}^{\mu_{\text{eff}}}f\left(\mu\right)\mu^{2}\mathrm{d}\mu\right)\frac{p_{*}^{D^{-}+D^{+}}}{D^{-}+D^{+}}\\&\quad-\frac{K'p_{*}^{D^{-}+D^{+}-2}}{8\left(D^{-}+D^{+}-1\right)}\int_{0}^{\mu_{\text{eff}}}f\left(\mu\right)\mu^{4}\mathrm{d}\mu+O\left(p_{*}^{D^{-}+D^{+}-4}\right).\end{aligned}\tag{248}$$

Remark 5.1.3. Note that (see Equations (42)):

$$\begin{aligned}&\tilde{\varepsilon}(\mu_{\text{eff}},p_*)=\varepsilon(\mu_{\text{eff}})+\varepsilon(\mu_{\text{eff}},p_*)\\&=\frac{1}{4}p_*^4\int_0^{\mu_{\text{eff}}}f(\mu)\mathrm{d}\mu+\frac{1}{4}p_*^2\int_0^{\mu_{\text{eff}}}f(\mu)\mu^2\mathrm{d}\mu+\left(C_1-\frac{1}{8}\ln p_*\right)\int_0^{\mu_{\text{eff}}}f(\mu)\mu^4\mathrm{d}\mu\\&\quad+\frac{1}{8}\int_0^{\mu_{\text{eff}}}f(\mu)\mu^4(\ln\mu)\mathrm{d}\mu-\left(\frac{1}{p_*^2}\right)\frac{1}{32}\int_0^{\mu_{\text{eff}}}f(\mu)\mu^6\mathrm{d}\mu+O\left(\int_0^{\mu_{\text{eff}}}f(\mu)\mu^8\right)p_*^{-5}.\end{aligned}\tag{249}$$

From Equation (240), Equation (248) and Equation (249) finally we obtain

$$\begin{aligned}&\varepsilon(D^+,D^-,\mu_{\text{eff}},p_*)=\varepsilon(\mu_{\text{eff}})+\varepsilon(\mu_{\text{eff}},p_*)+\breve{\varepsilon}(D^+,D^-,\mu_{\text{eff}},p_*)\\&=\frac{1}{4}p_*^4\int_0^{\mu_{\text{eff}}}f(\mu)\mathrm{d}\mu+\frac{1}{4}p_*^2\int_0^{\mu_{\text{eff}}}f(\mu)\mu^2\mathrm{d}\mu+\left(C_1-\frac{1}{8}\ln p_*\right)\int_0^{\mu_{\text{eff}}}f(\mu)\mu^4\mathrm{d}\mu\\&\quad+\frac{1}{8}\int_0^{\mu_{\text{eff}}}f(\mu)\mu^4(\ln\mu)\mathrm{d}\mu-\left(\frac{1}{p_*^2}\right)\frac{1}{32}\int_0^{\mu_{\text{eff}}}f(\mu)\mu^6\mathrm{d}\mu+O\left(\int_0^{\mu_{\text{eff}}}f(\mu)\mu^8\right)p_*^{-5}\\&\quad+O\left(p_*^{D^-+D^++2}\right).\end{aligned}\tag{250}$$

The pressure $p(D^+,D^-,\mu_{\text{eff}},p_*)$ for free scalar quantum field is

$$p(D^+,D^-,\mu_{\text{eff}},p_*)=p(\mu_{\text{eff}})+p(\mu_{\text{eff}},p_*)+\breve{p}(D^+,D^-,\mu_{\text{eff}},p_*).\tag{251}$$

Here the quantity $p(\mu_{\text{eff}})$ is given by formula

$$p(\mu_{\text{eff}})=\frac{K}{3}\int_0^{\mu_{\text{eff}}}\mathrm{d}\mu f(\mu)\int_{\|p\|<\mu}\frac{p^4}{\sqrt{p^2+\mu^2}}\mathrm{d}p.\tag{252}$$

The quantity $p(\mu_{\text{eff}},p_*)$ is given by formula

$$p(\mu_{\text{eff}},p_*)=\frac{K}{3}\int_0^{\mu_{\text{eff}}}\mathrm{d}\mu f(\mu)\int_{\mu\le\|p\|\le p_*}\frac{p^4}{\sqrt{p^2+\mu^2}}\mathrm{d}p.\tag{253}$$

The quantity $\breve{p}(D^+,D^-,\mu_{\text{eff}},p_*)$ is given by formula

$$\breve{p}(D^+,D^-,\mu_{\text{eff}},p_*)\simeq\frac{K'}{3}\int_0^{\mu_{\text{eff}}}\mathrm{d}\mu\int_{\|p\|>p_*}f(\mu)\frac{p^4}{\sqrt{p^2+\mu^2}}\mathrm{d}p,\tag{254}$$

where $K'=\dfrac{1}{2(2\pi\hbar)^3},c=1$.

Remark 5.1.4. Note that (see Equations (42):

$$\begin{aligned}\tilde{p}(\mu_{\text{eff}},p_*)&=p(\mu_{\text{eff}})+p(\mu_{\text{eff}},p_*)\\&=\frac{1}{12}p_*^4\int_0^{\mu_{\text{eff}}}f(\mu)\mathrm{d}\mu-\frac{1}{12}p_*^2\int_0^{\mu_{\text{eff}}}f(\mu)\mu^2\mathrm{d}\mu\\&\quad+\left(C_2+\frac{1}{8}\ln p_*\right)\int_0^{\mu_{\text{eff}}}f(\mu)\mu^4\mathrm{d}\mu-\frac{1}{8}\int_0^{\mu_{\text{eff}}}f(\mu)\mu^4(\ln\mu)\mathrm{d}\mu\\&\quad+\left(\frac{5}{p_*^2}\right)\frac{1}{32}\int_0^{\mu_{\text{eff}}}f(\mu)\mu^6\mathrm{d}\mu+O\left(\int_0^{\mu_{\text{eff}}}f(\mu)\mu^8\right)p_*^{-5}.\end{aligned}\tag{255}$$

From Equation (250), Equation (254) and Equation (255) similarly as above finally we get

$$\begin{aligned}&p\left(D^{+},D^{-},\mu_{\text{eff}},p_{*}\right)\\&=\frac{1}{12}p_{*}^{4}\int_{0}^{\mu_{\text{eff}}}f(\mu)\mathrm{d}\mu-\frac{1}{12}p_{*}^{2}\int_{0}^{\mu_{\text{eff}}}f(\mu)\mu^{2}\mathrm{d}\mu\\&+\left(C_{2}+\frac{1}{8}\ln p_{*}\right)\int_{0}^{\mu_{\text{eff}}}f(\mu)\mu^{4}\mathrm{d}\mu-\frac{1}{8}\int_{0}^{\mu_{\text{eff}}}f(\mu)\mu^{4}(\ln\mu)\mathrm{d}\mu\\&+\left(\frac{5}{p_{*}^{2}}\right)\frac{1}{32}\int_{0}^{\mu_{\text{eff}}}f(\mu)\mu^{6}\mathrm{d}\mu+O\left(\int_{0}^{\mu_{\text{eff}}}f(\mu)\mu^{8}\right)p_{*}^{-5}+O\left(p_{*}^{D^{-}+D^{+}+2}\right).\end{aligned} \tag{256}$$

Remark 5.1.5. We assume now that:

$$\int_{0}^{\mu_{\text{eff}}}f(\mu)\mathrm{d}\mu=\int_{0}^{\mu_{\text{eff}}}f(\mu)\mu^{2}\mathrm{d}\mu=\int_{0}^{\mu_{\text{eff}}}f(\mu)\mu^{4}\mathrm{d}\mu=0. \tag{257}$$

From Equation (250), Equation (256) and Equation (257) finally we get

$$\begin{aligned}&\varepsilon\triangleq\varepsilon\left(D^{+},D^{-},\mu_{\text{eff}},p_{*}\right)=\frac{1}{8}\int_{0}^{\mu_{\text{eff}}}f(\mu)\mu^{4}(\ln\mu)\mathrm{d}\mu+O\left(p_{*}^{-2}\right),\\&p\triangleq\left(D^{+},D^{-},\mu_{\text{eff}},p_{*}\right)=-\frac{1}{8}\int_{0}^{\mu_{\text{eff}}}f(\mu)\mu^{4}(\ln\mu)\mathrm{d}\mu+O\left(p_{*}^{-2}\right).\end{aligned} \tag{258}$$

Remark 5.1.6. Note that the Equation (258) can be obtained without fine-tuning (257) which was assumed in Zel'dovich paper [1].

In order to obtain Equation (5.1.23) and strictly weaker conditions we assume now that:

1)

$$\left|f(\mu)\right|=\left|f_{s.m.}(\mu)+f_{g.m.}(\mu)\right|=\mu_{\text{eff}}^{-n}, \tag{259}$$

where $n>0$ is an parameter, $f_{s.m.}(\mu)$ corresponds to standard matter and where $f_{g.m.}(\mu)$ corresponds to physical ghost matter, see Equation (32).

2)

$$\begin{aligned}&I_{1}=p_{*}^{4}\int_{0}^{\mu_{\text{eff}}}f(\mu)\mathrm{d}\mu\approx 0,\\&I_{2}=p_{*}^{2}\int_{0}^{\mu_{\text{eff}}}f(\mu)\mu^{2}\mathrm{d}\mu\approx 0,\\&I_{3}=\ln p_{*}\int_{0}^{\mu_{\text{eff}}}f(\mu)\mu^{4}\mathrm{d}\mu\approx 0\end{aligned} \tag{260}$$

3)

$$\left|I_{1}+I_{2}+I_{3}\right|\ll\left|\int_{0}^{\mu_{\text{eff}}}f(\mu)\mu^{4}(\ln\mu)\mathrm{d}\mu\right|. \tag{261}$$

5.2. Zeropoint Energy Density Corresponding to a Non-Singular Gliner Cosmology

We assume now that

$$\int_{0}^{\mu_{\text{eff}}}f(\mu)\mathrm{d}\mu=0,\int_{0}^{\mu_{\text{eff}}}f(\mu)\mu^{4}\mathrm{d}\mu<0,\int_{0}^{\mu_{\text{eff}}}f(\mu)\mu^{2}\mathrm{d}\mu>0,p_{*}\gg\mu_{\text{eff}}. \tag{262}$$

From Equation (250), Equation (256) and (262) we obtain

$$\begin{aligned}\varepsilon &\triangleq \varepsilon\left(D^{+},D^{-},\mu_{\text{eff}},p_{*}\right)\\ &=\frac{1}{4}p_{*}^{2}\int_{0}^{\mu_{\text{eff}}} f(\mu)\mu^{2}\mathrm{d}\mu-\left(C_{1}-\frac{1}{8}\ln p_{*}\right)\left|\int_{0}^{\mu_{\text{eff}}} f(\mu)\mu^{4}\mathrm{d}\mu\right|\\ &\quad+\frac{1}{8}\int_{0}^{\mu_{\text{eff}}} f(\mu)\mu^{4}(\ln\mu)\mathrm{d}\mu-\left(\frac{1}{p_{*}^{2}}\right)\frac{1}{32}\int_{0}^{\mu_{\text{eff}}} f(\mu)\mu^{6}\mathrm{d}\mu\\ &\quad+O\left(\int_{0}^{\mu_{\text{eff}}} f(\mu)\mu^{8}\right)p_{*}^{-5}+O\left(p_{*}^{D^{-}+D^{+}+2}\right),\end{aligned}\tag{263}$$

and

$$\begin{aligned}p &\triangleq p\left(D^{+},D^{-},\mu_{\mathbf{eff}},p_{*}\right)\\ &=-\frac{1}{12}p_{*}^{2}\int_{0}^{\mu_{\text{eff}}} f(\mu)\mu^{2}\mathrm{d}\mu-\left(C_{2}+\frac{1}{8}\ln p_{*}\right)\left|\int_{0}^{\mu_{\text{eff}}} f(\mu)\mu^{4}\mathrm{d}\mu\right|\\ &\quad-\frac{1}{8}\int_{0}^{\mu_{\text{eff}}} f(\mu)\mu^{4}(\ln\mu)\mathrm{d}\mu+\left(\frac{5}{p_{*}^{2}}\right)\frac{1}{32}\int_{0}^{\mu_{\text{eff}}} f(\mu)\mu^{6}\mathrm{d}\mu\\ &\quad+O\left(\int_{0}^{\mu_{\text{eff}}} f(\mu)\mu^{8}\right)p_{*}^{-5}+O\left(p_{*}^{D^{-}+D^{+}+2}\right)\end{aligned}\tag{364}$$

correspondingly. From Equation (263) and Equation (264) we obtain

$$\begin{aligned}3p+\varepsilon &=-\frac{1}{4}p_{*}^{2}\int_{0}^{\mu_{\text{eff}}} f(\mu)\mu^{2}\mathrm{d}\mu-\left(3C_{2}+\frac{3}{8}\ln p_{*}\right)\left|\int_{0}^{\mu_{\text{eff}}} f(\mu)\mu^{4}\mathrm{d}\mu\right|\\ &\quad-\frac{3}{8}\int_{0}^{\mu_{\text{eff}}} f(\mu)\mu^{4}(\ln\mu)\mathrm{d}\mu+\left(\frac{5}{p_{*}^{2}}\right)\frac{3}{32}\int_{0}^{\mu_{\text{eff}}} f(\mu)\mu^{6}\mathrm{d}\mu\\ &\quad+\frac{1}{4}p_{*}^{2}\int_{0}^{\mu_{\text{eff}}} f(\mu)\mu^{2}\mathrm{d}\mu-\left(C_{1}-\frac{1}{8}\ln p_{*}\right)\left|\int_{0}^{\mu_{\text{eff}}} f(\mu)\mu^{4}\mathrm{d}\mu\right|\\ &\quad+\frac{1}{8}\int_{0}^{\mu_{\text{eff}}} f(\mu)\mu^{4}(\ln\mu)\mathrm{d}\mu-\left(\frac{1}{p_{*}^{2}}\right)\frac{1}{32}\int_{0}^{\mu_{\text{eff}}} f(\mu)\mu^{6}\mathrm{d}\mu\\ &=-\frac{1}{4}\ln p_{*}\left|\int_{0}^{\mu_{\text{eff}}} f(\mu)\mu^{4}\mathrm{d}\mu\right|-(3C_{2}+C_{1})\left|\int_{0}^{\mu_{\text{eff}}} f(\mu)\mu^{4}\mathrm{d}\mu\right|\\ &\quad-\frac{1}{4}\int_{0}^{\mu_{\text{eff}}} f(\mu)\mu^{4}(\ln\mu)\mathrm{d}\mu+\left(\frac{5}{p_{*}^{2}}\right)\frac{1}{16}\int_{0}^{\mu_{\text{eff}}} f(\mu)\mu^{6}\mathrm{d}\mu<0.\end{aligned}\tag{265}$$

Therefore under conditions (262) the inequality

$$-2\varepsilon<3p+\varepsilon<0\tag{266}$$

corresponding to Gliner non-singular cosmology [2] [4] is satisfied.

5.3. Zeropoint Energy Density in Models with Supermassive Physical Ghost Fields

We assume now that:

1) ghost fields corresponding to massive spin-2 particle with mass m_2 and to massive scalar particle with mass m_0 appears (see Subsection 2.2) as real phys-

ical fields in action (91).

Remark 5.3.1. Note that their unphysical behavior may be restricted to arbitrarily high-energy cutoff Λ by an appropriate limitation on the renormalized masses m_2 and m_0.

Actually, it is only the massive spin-two excitations of the field which give the problem with unitarity and thus require a very large mass (see Subsection II.2).

2) Poincaré group is deformed at some fundamental high-energy cutoff Λ_*

$$\Lambda_* = \Lambda_*\left(m_0, m_2\right) \ll m_0c^2 < m_2c^2. \tag{267}$$

The canonical quadratic invariant $\|p\|^2 = \eta^{ab} p_a p_b$ collapses at high-energy cutoff Λ_* and being replaced by the non-quadratic invariant

$$\|p\|^2 = \frac{\eta^{ab} p_a p_b}{\left(1 + l_{\Lambda_*} p_0\right)}. \tag{268}$$

3) The canonical concept of Minkowski space-time collapses at a small distance to fractal space-time with Hausdorff-Colombeau negative dimension and therefore the canonical Lebesgue measure $\mathrm{d}^4 x$ being replaced by the Colombeau-Stieltjes measure

$$\left(\mathrm{d}\eta(x,\varepsilon)\right)_\varepsilon = \left(v_\varepsilon\left(s(x)\right)\mathrm{d}^4 x\right)_\varepsilon, \tag{269}$$

where

$$\left(v_\varepsilon\left(s(x)\right)\right)_\varepsilon = \left(\left(\left|s(x)\right|^{\left|D^-\right|} + \varepsilon\right)^{-1}\right)_\varepsilon, s(x) = \sqrt{x_\mu x^\mu}, \tag{270}$$

4) we assume that

$$f(\mu) = f_{s.m.}(\mu) + f_{g.m.}(\mu), \tag{271}$$

where $f_{s.m.}(\mu)$ corresponds to standard matter and where $f_{g.m.}(\mu)$ corresponds to physical ghost matter.

Remark 5.3.2. We assume now that

$$\left|f(\mu)\right| = \begin{cases} O\left(\mu^{-n}\right), n > 1 & m_0 c \ll \mu_{\text{eff}}^1 \le \mu \le \mu_{\text{eff}}^2 \ll m_2 c \\ 0 & \mu > \mu_{\text{eff}}^2 \end{cases} \tag{272}$$

Thus vacuum energy density $\varepsilon\left(D^+, D^-, \mu_{\text{eff}}^1, \mu_{\text{eff}}^2\right)$ for free quantum fields is

$$\varepsilon\left(D^+, D^-, \mu_{\text{eff}}^1, \mu_{\text{eff}}^2\right) = \varepsilon\left(\mu_{\text{eff}}^1, \mu_{\text{eff}}^2\right) + \breve{\varepsilon}\left(D^+, D^-, \mu_{\text{eff}}^1, \mu_{\text{eff}}^2\right). \tag{273}$$

Here the quantity $\varepsilon\left(\mu_{\text{eff}}^1, \mu_{\text{eff}}^2\right)$ is given by formula

$$\begin{aligned} \varepsilon\left(\mu_{\text{eff}}^1, \mu_{\text{eff}}^2\right) &= \frac{1}{2(2\pi\hbar)^3} \int_{\mu_{\text{eff}}^1}^{\mu_{\text{eff}}^2} \mathrm{d}\mu\, f(\mu) \int_{\|\mathbf{k}\| \le \sqrt{\mu}} \sqrt{\mathbf{k}^2 + \mu^2}\, \mathrm{d}^3\mathbf{k} \\ &= K \int_{\mu_{\text{eff}}^1}^{\mu_{\text{eff}}^2} \mathrm{d}\mu\, f(\mu) \int_{p \le \sqrt{\mu}} \sqrt{p^2 + \mu^2}\, p^2 \mathrm{d}p, \end{aligned} \tag{274}$$

where $K = \dfrac{2\pi}{(2\pi\hbar)^3}, c = 1$. The quantity $\breve{\varepsilon}\left(D^+, D^-, \mu_{\text{eff}}^1, \mu_{\text{eff}}^2\right)$ is given by formula

$$\breve{\varepsilon}\left(D^{+},D^{-},\mu_{\text{eff}}^{1},\mu_{\text{eff}}^{2}\right) = K'\int_{\mu_{\text{eff}}^{1}}^{\mu_{\text{eff}}^{2}}\mathrm{d}\mu f\left(\mu\right)\int\limits_{\|\mathbf{k}\|>\sqrt{\mu}}\left[\frac{\mu^{2}l_{\Lambda}}{1-\mu^{2}l_{\Lambda}^{2}}+\frac{1}{\sqrt{1-\mu^{2}l_{\Lambda_*}^{2}}}\sqrt{\frac{\mu^{4}l_{\Lambda_*}^{2}}{1-\mu^{2}l_{\Lambda_*}^{2}}+\left(\left|\mathbf{k}\right|^{2}+\mu^{2}\right)}\right]\mathrm{d}^{D^{+},D^{-}}\mathbf{k}, \tag{275}$$

where $K'=\dfrac{1}{2\left(2\pi\hbar\right)^{3}},c=1$.

Remark 5.3.2. We assume now that $\mu^2 l_{\Lambda_*}^2 < 1$, and therefore from Equation (5.3.9) we obtain

$$\varepsilon\left(D^{+},D^{-},\mu_{\text{eff}}^{1},\mu_{\text{eff}}^{2}\right) \simeq K'l_{\Lambda}\int_{\mu_{\text{eff}}^{1}}^{\mu_{\text{eff}}^{2}}\mathrm{d}\mu f\left(\mu\right)\mu^{2}\int\limits_{\|\mathbf{k}\|>\sqrt{\mu}}\mathrm{d}^{3,D_-}\mathbf{k}+K'\int_{\mu_{\text{eff}}^{1}}^{\mu_{\text{eff}}^{2}}\mathrm{d}\mu f\left(\mu\right)\int\limits_{\|\mathbf{k}\|>\sqrt{\mu}}\sqrt{\mathbf{k}^{2}+\mu^{2}}\,\mathrm{d}^{D^{+},D^{-}}\mathbf{k}. \tag{276}$$

From Equation (276) and Equation (239) we obtain

$$\begin{aligned}
&\varepsilon\left(D^{+},D^{-},\mu_{\text{eff}}^{1},\mu_{\text{eff}}^{2}\right)\\
&\simeq K'l_{\Lambda}\int_{\mu_{\text{eff}}^{1}}^{\mu_{\text{eff}}^{2}}\mathrm{d}\mu f\left(\mu\right)\mu^{2}\int\limits_{\|\mathbf{k}\|>\sqrt{\mu}}\mathrm{d}^{D^{+},D^{-}}\mathbf{k}+K'\int_{\mu_{\text{eff}}^{1}}^{\mu_{\text{eff}}^{2}}\mathrm{d}\mu f\left(\mu\right)\int\limits_{\|\mathbf{k}\|>\sqrt{\mu}}\sqrt{\mathbf{k}^{2}+\mu^{2}}\,\mathrm{d}^{D^{+},D^{-}}\mathbf{k}\\
&=K'\Delta\left(D^{+}\right)\Delta\left(D^{-}\right)l_{\Lambda}\int_{\mu_{\text{eff}}^{1}}^{\mu_{\text{eff}}^{2}}\mathrm{d}\mu f\left(\mu\right)\mu^{2}\left[\int_{\sqrt{\mu}}^{\infty}\frac{p^{D^{+}-1}\mathrm{d}p}{\left(p^{\left|D^{-}\right|}+\varepsilon\right)_{\varepsilon}}\right]\\
&+K'\Delta\left(D^{+}\right)\Delta\left(D^{-}\right)\int_{\mu_{\text{eff}}^{1}}^{\mu_{\text{eff}}^{2}}\mathrm{d}\mu f\left(\mu\right)\left[\int_{\sqrt{\mu}}^{\infty}\frac{\sqrt{p^{2}+\mu^{2}}\,p^{D^{+}-1}\mathrm{d}p}{\left(p^{\left|D^{-}\right|}+\varepsilon\right)_{\varepsilon}}\right]\\
&=K'\Delta\left(D^{+}\right)\Delta\left(D^{-}\right)l_{\Lambda}\int_{\mu_{\text{eff}}^{1}}^{\mu_{\text{eff}}^{2}}\mathrm{d}\mu f\left(\mu\right)\mu^{2}\left[\int_{\sqrt{\mu}}^{\infty}p^{D^{-}+D^{+}-1}\mathrm{d}p\right]\\
&+K'\Delta\left(D^{+}\right)\Delta\left(D^{-}\right)\int_{\mu_{\text{eff}}^{1}}^{\mu_{\text{eff}}^{2}}\mathrm{d}\mu f\left(\mu\right)\left[\int_{\sqrt{\mu}}^{\infty}\sqrt{p^{2}+\mu^{2}}\,p^{D^{-}+D^{+}-1}\mathrm{d}p\right].
\end{aligned} \tag{277}$$

Note that

$$\begin{aligned}
\sqrt{p^{2}+\mu^{2}}&=\mu\sqrt{1+\frac{p^{2}}{\mu^{2}}}=\mu\left(1+\frac{1}{2}\frac{p^{2}}{\mu^{2}}-\frac{1}{8}\frac{p^{4}}{\mu^{4}}+\frac{1}{16}\frac{p^{6}}{\mu^{6}}+\cdots\right)\\
&=\mu+\frac{1}{2}\frac{p^{2}}{\mu}-\frac{1}{8}\frac{p^{4}}{\mu^{3}}+\frac{1}{16}\frac{p^{6}}{\mu^{5}}+\cdots
\end{aligned} \tag{278}$$

By inserting Equation (278) into Equation (274) we get

$$\begin{aligned}
&\varepsilon\left(\mu_{\text{eff}}^{1},\mu_{\text{eff}}^{2}\right)\\
&=K\int_{\mu_{\text{eff}}^{1}}^{\mu_{\text{eff}}^{2}}\mathrm{d}\mu f\left(\mu\right)\int\limits_{p\le\sqrt{\mu}}\left(\mu+\frac{1}{2}\frac{p^{2}}{\mu}-\frac{1}{8}\frac{p^{4}}{\mu^{3}}+\frac{1}{16}\frac{p^{6}}{\mu^{5}}+\cdots\right)p^{2}\mathrm{d}p\\
&=K\int_{\mu_{\text{eff}}^{1}}^{\mu_{\text{eff}}^{2}}\mathrm{d}\mu f\left(\mu\right)\left[\int\limits_{0}^{\sqrt{\mu}}\left(\mu p^{2}+\frac{1}{2}\frac{p^{4}}{\mu}-\frac{1}{8}\frac{p^{6}}{\mu^{3}}+\frac{1}{16}\frac{p^{8}}{\mu^{5}}+\cdots\right)\mathrm{d}p\right]\\
&=K\int_{\mu_{\text{eff}}^{1}}^{\mu_{\text{eff}}^{2}}\mathrm{d}\mu f\left(\mu\right)\left[\mu\frac{p^{3}}{3}+\frac{1}{2}\frac{p^{5}}{5\mu}-\frac{1}{8}\frac{p^{7}}{7\mu^{3}}+\frac{1}{16}\frac{p^{9}}{9\mu^{5}}+\cdots\right]_{0}^{\sqrt{\mu}}
\end{aligned}$$

$$= K\int_{\mu_{\text{eff}}^1}^{\mu_{\text{eff}}^2} \mathrm{d}\mu\, f(\mu)\left[\mu\frac{\mu^{\frac{3}{2}}}{3}+\frac{1}{2}\frac{\mu^{\frac{5}{2}}}{5\mu}-\frac{1}{8}\frac{\mu^{\frac{1}{2}}}{7\mu^3}+\frac{1}{16}\frac{\mu^{\frac{9}{2}}}{9\mu^5}+\cdots\right]$$

$$= K\int_{\mu_{\text{eff}}^1}^{\mu_{\text{eff}}^2} f(\mu)\mathrm{d}\mu\left[\frac{1}{3}\mu^{\frac{5}{2}}+\frac{1}{10}\mu^{\frac{3}{2}}-\frac{1}{56}\mu^{\frac{1}{2}}+\frac{1}{144}\mu^{-\frac{1}{2}}+\cdots\right] \tag{279}$$

$$= K\int_{\mu_{\text{eff}}^1}^{\mu_{\text{eff}}^2} f(\mu)\mathrm{d}\mu\left[\frac{1}{3}\mu^{\frac{5}{2}}+\frac{1}{10}\mu^{\frac{3}{2}}-\frac{1}{56}\mu^{\frac{1}{2}}+\frac{1}{144}\mu^{-\frac{1}{2}}\right]+o\left(\left(\mu_{\text{eff}}^1\right)^{-n+1/2}\right).$$

The pressure $p\left(D^+,D^-,\mu_{\text{eff}}^1,\mu_{\text{eff}}^2\right)$ for free quantum fields is

$$p\left(D^+,D^-,\mu_{\text{eff}}^1,\mu_{\text{eff}}^2\right)=p\left(\mu_{\text{eff}}^1,\mu_{\text{eff}}^2\right)+\breve{p}\left(D^+,D^-,\mu_{\text{eff}}^1,\mu_{\text{eff}}^2\right). \tag{280}$$

Here the quantity $p\left(\mu_{\text{eff}}^1,\mu_{\text{eff}}^2\right)$ is given by formula

$$\begin{aligned} p\left(\mu_{\text{eff}}^1,\mu_{\text{eff}}^2\right) &= \frac{1}{2(2\pi\hbar)^3}\int_{\mu_{\text{eff}}^1}^{\mu_{\text{eff}}^2} \mathrm{d}\mu\, f(\mu)\int_{\|\mathbf{k}\|\le\sqrt{\mu}}\frac{\|\mathbf{k}\|^2}{\sqrt{\mathbf{k}^2+\mu^2}}\mathrm{d}^3\mathbf{k} \\ &= \frac{K}{3}\int_{\mu_{\text{eff}}^1}^{\mu_{\text{eff}}^2} \mathrm{d}\mu\, f(\mu)\int_{p\le\sqrt{\mu}}\frac{p^4}{\sqrt{p^2+\mu^2}}\mathrm{d}p. \end{aligned} \tag{281}$$

The quantity $\breve{p}\left(D^+,D^-,\mu_{\text{eff}}^1,\mu_{\text{eff}}^2\right)$ is given by formula

$$\breve{p}\left(D^+,D^-,\mu_{\text{eff}}^1,\mu_{\text{eff}}^2\right)\simeq\frac{K'}{3}\int_{\mu_{\text{eff}}^1}^{\mu_{\text{eff}}^2} \mathrm{d}\mu\, f(\mu)\int_{\|p\|>\sqrt{\mu}}\frac{\|\mathbf{k}\|^2}{\sqrt{\mathbf{k}^2+\mu^2}}\mathrm{d}^{D^+,D^-}\mathbf{k}, \tag{282}$$

where $K'=\dfrac{1}{2(2\pi\hbar)^3}, c=1$. Note that

$$\begin{aligned} \frac{1}{\sqrt{p^2+\mu^2}} &= \mu^{-1}\left(\sqrt{1+\frac{p^2}{\mu^2}}\right)^{-1} \\ &= \mu^{-1}\left(1-\frac{1}{2}\frac{p^2}{\mu^2}+\frac{3}{8}\frac{p^4}{\mu^4}-\frac{5}{16}\frac{p^6}{\mu^6}+\cdots\right) \\ &= \frac{1}{\mu}-\frac{1}{2}\frac{p^2}{\mu^3}+\frac{3}{8}\frac{p^4}{\mu^5}-\frac{5}{16}\frac{p^6}{\mu^7}+\cdots \end{aligned} \tag{283}$$

By inserting Equation (283) into Equation (281) we get

$$\begin{aligned} & p\left(\mu_{\text{eff}}^1,\mu_{\text{eff}}^2\right) \\ &= \frac{K}{3}\int_{\mu_{\text{eff}}^1}^{\mu_{\text{eff}}^2} \mathrm{d}\mu\, f(\mu)\int_{p\le\sqrt{\mu}}\left[\frac{1}{\mu}-\frac{1}{2}\frac{p^2}{\mu^3}+\frac{3}{8}\frac{p^4}{\mu^5}-\frac{5}{16}\frac{p^6}{\mu^7}+\cdots\right]p^4\mathrm{d}p \\ &= \frac{K}{3}\int_{\mu_{\text{eff}}^1}^{\mu_{\text{eff}}^2} \mathrm{d}\mu\, f(\mu)\int_{p\le\sqrt{\mu}}\left[\frac{p^4}{\mu}-\frac{1}{2}\frac{p^6}{\mu^3}+\frac{3}{8}\frac{p^8}{\mu^5}-\frac{5}{16}\frac{p^{10}}{\mu^7}+\cdots\right]\mathrm{d}p \\ &= \frac{K}{3}\int_{\mu_{\text{eff}}^1}^{\mu_{\text{eff}}^2} \mathrm{d}\mu\, f(\mu)\left[\frac{p^5}{5\mu}-\frac{1}{2}\frac{p^7}{7\mu^3}+\frac{3}{8}\frac{p^9}{9\mu^5}-\frac{5}{16}\frac{p^{11}}{10\mu^7}+\cdots\right]_0^{\sqrt{\mu}} \end{aligned}$$

$$
\begin{aligned}
&= \frac{K}{3}\int_{\mu_{\text{eff}}^1}^{\mu_{\text{eff}}^2} \mathrm{d}\mu\, f(\mu)\left[\frac{\mu^{\frac{5}{2}}}{5\mu} - \frac{1}{2}\frac{\mu^{\frac{7}{2}}}{7\mu^3} + \frac{3}{8}\frac{\mu^{\frac{9}{2}}}{9\mu^5} - \frac{5}{16}\frac{\mu^{\frac{11}{2}}}{10\mu^7} + \cdots\right] \\
&= \frac{K}{3}\int_{\mu_{\text{eff}}^1}^{\mu_{\text{eff}}^2} \mathrm{d}\mu\, f(\mu)\left[\frac{1}{5}\mu^{\frac{3}{2}} - \frac{1}{14}\mu^{\frac{1}{2}} + \frac{1}{24}\mu^{-\frac{1}{2}} - \frac{1}{32}\mu^{-\frac{3}{2}} + \cdots\right] \\
&= \frac{K}{3}\int_{\mu_{\text{eff}}^1}^{\mu_{\text{eff}}^2} \mathrm{d}\mu\, f(\mu)\left[\frac{1}{5}\mu^{\frac{3}{2}} - \frac{1}{14}\mu^{\frac{1}{2}} + \frac{1}{24}\mu^{-\frac{1}{2}} - \frac{1}{32}\mu^{-\frac{3}{2}}\right] + o\left(\left(\mu_{\text{eff}}^1\right)^{-n-1/2}\right).
\end{aligned}
\tag{284}
$$

6. Discussion and Conclusion

We will now briefly review the canonical assumptions that are made in the usual formulation of the cosmological constant problem.

The canonical assumptions:

1) The physical dark matter.

Dark matter is a hypothetical form of matter that is thought to account for approximately 85% of the matter in the universe, and about a quarter of its total energy density. The majority of dark matter is thought to be non-baryonic in nature, possibly being composed of some as-yet-undiscovered subatomic particles. Its presence is implied in a variety of astrophysical observations, including gravitational effects that cannot be explained unless more matter is present than can be seen. For this reason, most experts think dark matter to be ubiquitous in the universe and to have had a strong influence on its structure and evolution. The name dark matter refers to the fact that it does not appear to interact with observable electromagnetic radiation, such as light, and is thus invisible (or 'dark') to the entire electromagnetic spectrum, making it extremely difficult to detect using usual astronomical equipment. Because dark matter has not yet been observed directly, it must barely interact with ordinary baryonic matter and radiation. The primary candidate for dark matter is some new kind of elementary particle that has not yet been discovered, in particular, weakly-interacting massive particles (WIMPs), or gravitationally-interacting massive particles (GIMPs). Many experiments to directly detect and study dark matter particles are being actively undertaken, but none has yet succeeded.

2) The total effective cosmological constant λ_{eff} is on at least the order of magnitude of the vacuum energy density generated by zero-point fluctuations of the standard particle fields.

3) Canonical QFT is an effective field theory description of a more fundamental theory, which becomes significant at some high-energy scale Λ_*.

4) The vacuum energy-momentum tensor is Lorentz invariant.

5) The Moller-Rosenfeld approach [34] [35] to semiclassical gravity by using an expectation value for the energy-momentum tensor is sound.

6) The Einstein equations for the homogeneous Friedmann-Robertson-Walker metric accurately describes the large-scale evolution of the Universe.

Remark 6.1.1. Note that obviously there is a strong inconsistency between Assumptions 2 and 3: the vacuum state cannot be Lorentz invariant if modes are ignored above some high-energy cutoff Λ_*, because a mode that is high energy in one reference frame will be low energy in another appropriately boosted frame. In this paper Assumption 3 is not used and this contradiction is avoided.

Remark 6.1.2. Note that also, Assumptions 1, 3, 4 and 5 is modified, which we denote as Assumptions 4 and 5 respectively.

Modified assumptions

1') The physical dark matter.

2') The total effective cosmological constant λ_{eff} is on at least the order $|\mu_{\text{eff}}|^{-n+5}\ln|\mu_{\text{eff}}|$ of magnitude of the *renormalized* vacuum energy density generated by zero-point fluctuations of standard particle fields and ghost particle fields, see subsection 1.2.

3') The vacuum energy-momentum tensor is not Lorentz invariant.

6.1. The Physical Ghost Matter and Dark Matter Nature

In the contemporary quantum field theory, a ghost field, or gauge ghost is an unphysical state in a gauge theory. Ghosts are necessary to keep gauge invariance in theories where the local fields exceed a number of physical degrees of freedom. For example in quantum electrodynamics, in order to maintain manifest Lorentz invariance, one uses a four-component vector potential $A_\mu(x)$, whereas the photon has only two polarizations. Thus, one needs a suitable mechanism in order to get rid of the unphysical degrees of freedom. Introducing fictitious fields, the ghosts, is one way of achieving this goal. Faddeev-Popov ghosts are extraneous fields which are introduced to maintain the consistency of the path integral formulation. Faddeev-Popov ghosts are sometimes referred to as "good ghosts".

"Bad ghosts" represent another, more general meaning of the word "ghost" in theoretical physics: states of negative norm, or fields with the wrong sign of the kinetic term, such as Pauli-Villars ghosts, whose existence allows the probabilities to be negative thus violating unitarity.

(VI.1) In contrary with standard Assumption 1 in the case of the new approach introduced in this paper we assume that:

(VI.1.1.a) The ghosts fields and ghosts particles with masses at a scale less then a fixed scale m_{eff} really exist in the universe and formed dark matter sector of the universe, in particular:

(VI.1.1.b) these ghosts fields give additive contribution to a full zero-point fluctuation (*i.e.* also to effective cosmological constant λ_{eff} [5], see subsection 1.2).

(VI.1.1.c) Pauli-Villars renormalization of zero-point fluctuations (see subsection 1.2) is no longer considered as an intermediate mathematical construct but obviously has rigorous physical meaning supported by assumption **(VI.1.1.a-b).**

(VI.1.2) The physical dark matter formed by ghosts particles;

(VI.1.3) The standard model fields do not to couple directly to the ghost sector in the ultraviolet region of energy at a scale less then a fixed large energy scale Λ_*, in particular:

(VI.1.3.a) The "bad" ghosts fields with masses at a scale less then a fixed scale m_{eff}, where $m_{\text{eff}}c^2 \ll \Lambda_*$, cannot appear in any effective physical lagrangian which contains also the standard particles fields.

In additional though not necessary we assume that:

(VI.1.4) The "bad" ghosts fields with masses at a scale m_*, where $m_*c^2 \gg \Lambda_*$ can appear in any effective physical lagrangian which contains also the standard particles fields, in particular:

(VI.1.4.a) Pauli-Villars finite renormalization with masses of ghosts fields at a scale m_* of the S-matrix in QFT (see Subsection 2.1-2) is no longer considered as an intermediate mathematical construct but obviously has rigorous physical meaning supported by assumption (**IV1.4**).

(VI.1.4.b) If the "bad" ghosts fields coupled to matter directly, it gives rise to small and controllable violation of the unitarity condition.

Remark 6.1.3. We emphasize that in universe standard matter coupled with a *physical* ghost matter has the equation of state [3]:

$$\varepsilon_{\text{vac}}\left(\mu_{\text{eff}}\right) = -p\left(\mu_{\text{eff}}\right) = \frac{1}{8}\int_{0}^{\mu_{\text{eff}}} f\left(\mu\right)\mu^4\left(\ln\mu\right)\mathrm{d}\mu = \frac{c^4\lambda_{\text{vac}}}{8\pi G}, \tag{285}$$

where

$$\left|f\left(\mu\right)\right| = \begin{cases} O\left(\mu^{-n}\right), n>1 & \mu \le \mu_{\text{eff}} \\ 0 & \mu > \mu_{\text{eff}} \end{cases} \tag{286}$$

and where $\mu_{\text{eff}} = m_{\text{eff}}c$ (see subsection I.2, Equation (46)) and therefore gives rise to a de Sitter phase of the universe even if bare cosmological constant $\lambda = 0$.

(**VI.1.5**) In order to obtain QFT description of the dark component of matter in natural way we expand the standard model of particle physics on a sector of ghost particles, see [12], Section 2.3.2. QFT in a ghost sector developed in [12], Section 3.1-3.4 and Section 4.1-4.8.

6.2. Different Contributions to λ_{eff}.

The total effective cosmological constant λ_{eff} is on at least the order of magnitude of the vacuum energy density generated by zero-point fluctuations of *standard* particle fields.

Assumption 2 is well justified in the case of the traditional approach, because the contribution from zero-point fluctuations is on the order of 1 in Planck units and no other known contributions are as large thus, assuming no significant cancellation of terms (e.g. fine tuning of the bare cosmological constant λ), the total λ_{eff} should be at least on the order of the largest contribution [15].

(VI.2) In contrary with standard Assumption 1 in the case of the new approach introduced in this paper we assume that:

(VI.2.1) For simplicity though not necessary bare cosmological constant $\lambda = 0$.

(VI.2.2) The total effective cosmological constant λ_{eff} depends only on mass distribution $f\left(\mu\right)$ and constant $\mu_{\text{eff}} = m_{\text{eff}}c$ but cannot depend on large energy scale $\sim \Lambda_*$

Remark 6.2.1. Note that in subsection we pointed out that under Assumption **VI.1** if bare cosmological constant $\lambda = 0$ the total cosmological constant λ_{vac} is on at least the order $|\mu_{\text{eff}}|^{-n+5}$ of magnitude of the *renormalized* vacuum energy density generated by zero-point fluctuations of standard particle fields and ghost particle fields

$$\begin{aligned}\varepsilon_{\text{vac}}(\mu_{\text{eff}}) &= \frac{1}{8}\int_0^{\mu_{\text{eff}}} f(\mu)\mu^4(\ln\mu)\,\mathrm{d}\mu + O(\Lambda_*^{-2}),\\ p_{\text{vac}}(\mu_{\text{eff}}) &= -\frac{1}{8}\int_0^{\mu_{\text{eff}}} f(\mu)\mu^4(\ln\mu)\,\mathrm{d}\mu + O(\Lambda_*^{-2}).\end{aligned} \tag{287}$$

6.3. Effective Field Theory and Lorentz Invariance Violation

To prevent the vacuum energy density from diverging,the traditional approach also assumes that performing a high-energy cutoff is acceptable. This type of regularization is a common step in renormalization procedures, which aim to eventually arrive at a physical, cutoff-independent result. However, in the case of the vacuum energy density, the result is inherently cutoff dependent, scaling quartically with the cutoff Λ_*.

Remark 6.3.1. By restricting to modes with particle energy a certain cutoff energy $\omega_{\mathbf{k}} \le \Lambda_*$ a finite, regularized result for the energy density can be obtained. The result is proportional to Λ_*^4. Any other fields will contribute similarly, so that if there are n_b bosonic fields and n_f fermionic fields, the density scales with $(n_b - 4n_f)$ Λ_*^4. Typically, the cutoff is taken to be near = 1 in Planck units (*i.e.*the Planck energy), so the vacuum energy gives a contribution to the cosmological constant on the order of at least unity according to Equation (6.2.4). Thus we see the extreme ne-tuning problem: the original cosmological constant λ must cancel this large vacuum energy density $\varepsilon_{\text{vac}} \simeq 1$ to a precision of 1 in 10^{120}—but not completely—to result in the observed value $\lambda_{\text{eff}} = 10^{-120}$ [5].

Remark 6.3.2. As it pointed out in this paper that a high-energy theory, *i.e.* QFT in fractal space-time with Hausdorff-Colombeau negative dimension would not display the zero-point fluctuations that are characteristic of QFT, and hence that the divergence caused by oscillations above the corresponding cutoff frequency is unphysical. In this case, the cutoff Λ_* is no longer an intermediate mathematical construct, but instead a physical scale at which the smooth, continuous behavior of QFT breaks down.

Poincaré group of the momentum space is deformed at some fundamental high-energy cutoff Λ_* The canonical quadratic invariant $\|p\|^2 = \eta^{ab}p_a p_b$ collapses at high-energy cutoff Λ_* and being replaced by the non-quadratic invariant:

$$\|p\|^2 = \frac{\eta^{ab}p_a p_b}{(1 + l_{\Lambda_*}p_0)}. \tag{288}$$

Remark 6.3.3. In contrary with canonical approach the total effective cosmological constant λ_{eff} depends only on mass distribution $f(\mu)$ and constant $\mu_{\text{eff}} = m_{\text{eff}} c$ but cannot depend on large energy scale $\sim \Lambda_*$.

6.4. Semiclassical Möller-Rosenfeld Gravity

Assumption 5 means that it is valid to replace the right-hand side of the Einstein equation $T_{\mu\nu}$ with its expectation $\langle T_{\mu\nu} \rangle$. It requires that either gravity is not in fact quantum, and the Moller-Rosenfeld approach is a complete description of reality, or at least a valid approximation in the weak field limit. The usual argument states that the vacuum state $|0\rangle$ should be locally Lorentz invariant so that observers agree on the vacuum state. This means that the expectation value of the energy-momentum tensor on the vacuum, $\langle 0|\hat{T}_{\mu\nu}|0\rangle$, must be a scalar multiple of the metric tensor $g_{\mu\nu}$ which is the only Lorentz invariant rank $(0,2)$ tensor. By using Moller-Rosenfeld approach the Einstein field equations of general relativity, a term representing the curvature of spacetime $R_{\mu\nu}$ is related to a term describing the energy-momentum of matter $\langle 0|\hat{T}_{\mu\nu}|0\rangle$, as well as the cosmological constant λ and metric tensor $g_{\mu\nu}$ reads:

$$R_{\mu\nu} - \frac{1}{2} R_{\upsilon}^{\upsilon} g_{\mu\nu} + \lambda g_{\mu\nu} = 8\pi \langle 0|\hat{T}_{\mu\nu}|0\rangle. \tag{289}$$

The $\hat{T}_{00}$ component is an energy density, we label $\langle 0|\hat{T}_{\mu\nu}|0\rangle = \varepsilon_{\text{vac}}$, so that the vacuum contribution to the right-hand side of Equation (289) can be written as

$$8\pi \langle 0|\hat{T}_{\mu\nu}|0\rangle = 8\pi \varepsilon_{\text{vac}} g_{\mu\nu}. \tag{290}$$

Subtracting this from the right-hand side of Equation (289) and grouping it with the cosmological constant term replaces with an "effective" cosmological constant [5]:

$$\lambda_{\text{eff}} = \lambda + 8\pi \varepsilon_{\text{vac}}. \tag{291}$$

Note that in flat spacetime, where $g_{\mu\nu} = diag(-1,+1,+1,+1)$, Eq. (290) implies $\varepsilon_{\text{vac}} = -p_{\text{vac}}$, where $p_{\text{vac}} = \langle 0|\hat{T}_{ii}|0\rangle$ for any $i = 1,2,3$ is the pressure. Obviously this implies that if the energy density is positive as is usually assumed, then the pressure must be negative, a conclusion which extends to any metric $g_{\mu\nu}$ with a $(-1,+1,+1,+1)$ signature.

Remark 6.4.1. In this paper we assume that the vacuum state $|0\rangle$ should be locally invariant under modified Lorentz boost (17)-(18) but not locally Lorentz invariant. Obviously this assumption violate the Equation (290). However modified Lorentz boosts (17)-(18) becomes Lorentz boosts for sufficiently small energies and therefore in IR region one obtain in a good approximation

$$8\pi \langle 0|\hat{T}_{\mu\nu}|0\rangle \approx 8\pi \varepsilon_{\text{vac}} g_{\mu\nu} \tag{292}$$

and

$$\lambda_{\text{eff}} \approx \lambda + 8\pi \varepsilon_{\text{vac}}. \tag{293}$$

Thus Möller-Rosenfeld approach holds in a good approximation.

6.5. Quantum Gravity at Energy Scale $\Lambda \leq \Lambda_*$. Controllable Violation of the Unitarity Condition

Gravitational actions which include terms quadratic in the curvature tensor are renormalizable. The necessary Slavnov identities are derived from Becchi-Rouet-Stora (BRS) transformations of the gravitational and Faddeev-Popov ghost fields. In general, non-gauge-invariant divergences do arise, but they may be absorbed by nonlinear renormalizations of the gravitational and ghost fields and of the BRS transformations [14]. The geneic expression of the action reads

$$I_{sym} = \int -\mathrm{d}^4 x\sqrt{-g}\left(\alpha R_{\mu\nu}R^{\mu\nu} - \beta R^2 + 2\kappa^{-2}R\right), \tag{294}$$

where the curvature tensor and the Ricci is defined by $R^{\lambda}_{\mu\alpha\nu} = \partial_\nu \Gamma^{\lambda}_{\mu\alpha}$ and $R_{\mu\nu} = R^{\lambda}_{\mu\lambda\nu}$ correspondingly, $\kappa^2 = 32\pi G$. The convenient definition of the gravitational field variable in terms of the contravariant metric density reads

$$\kappa h^{\mu\nu} = g^{\mu\nu}\sqrt{-g} - \eta^{\mu\nu}. \tag{295}$$

Analysis of the linearized radiation shows that there are eight dynamical degrees of freedom in the field. Two of these excitations correspond to the familiar massless spin-2 graviton. Five more correspond to a massive spin-2 particle with mass m_2. The eighth corresponds to a massive scalar particle with mass m_0. Although the linearized field energy of the massless spin-2 and massive scalar excitations is positive definite, the linearized energy of the massive spin-2 excitations is negative definite. This feature is characteristic of higher-derivative models, and poses the major obstacle to their physical interpretation.

In the quantum theory, there is an alternative problem which may be substituted for the negative energy. It is possible to recast the theory so that the massive spin-2 eigenstates of the free-fieid Hamiltonian have positive-definite energy, but also negative norm in the state vector space. These negative-norm states cannot be excluded from the physical sector of the vector space without destroying the unitarity of the $\mathbf{S}$ matrix. The requirement that the graviton propagator behaves like p^{-4} for large momenta makes it necessary to choose the indefinite-metric vector space over the negative-energy states. The presence of massive quantum states of negative norm which cancel some of the divergences due to the massless states is analogous to the Pauli-Villars regularization of other field theories. For quantum gravity, however, the resulting improvement in the ultraviolet behavior of the theory is sufficient only to make it renormalizable, but not finite.

Remark 6.5.1. (I) The renormalizable models which we have considered in this paper many years mistakenly regarded only as constructs for a study of the ultraviolet problem of quantum gravity. The difficulties with unitarity appear to preclude their direct acceptability as canonical physical theories in locally Minkowski space-time. In canonical case they do have only some promise as phenomenological models.

(II) However, for their unphysical behavior may be restricted to *arbitrarily large energy scales* Λ_* mentioned above by an appropriate limitation on the renormalized masses m_2 and m_0. Actually, it is only the massive spin-two excitations of the field which give the trouble with unitarity and thus require a very large mass. The limit on the mass m_0 is determined only by the observational constraints on the static field.

6.6. Pauli-Villars Masses Distribution Corresponding to Ghost Matter Sector above High Energy Cutoff Λ_* A Common Origin of the Dark Energy and Dard Matter Phenomena

Dark matter is a hypothetical form of matter that is thought to account for approximately 85% of the matter in the universe, and about a quarter of its total energy density. The majority of dark matter is thought to be non-baryonic in nature, possibly being composed of some as-yet undiscovered subatomic particles. Its presence is implied in a variety of astrophysical observations, including gravitational effects that cannot be explained unless more matter is present than can be seen. For this reason, most experts think dark matter to be ubiquitous in the universe and to have had a strong influence on its structure and evolution. Dark matter is called dark because it does not appear to interact with observable electromagnetic radiation, such as light, and is thus invisible to the entire electromagnetic spectrum, making it extremely difficult to detect using usual astronomical equipment [36] [37] [38].

Figure 8 Analysis of a giant new galaxy survey, made with ESO's VLT Survey Telescope in Chile, suggests that dark matter may be less dense and more smoothly distributed throughout space than previously thought. An international team used data from the Kilo Degree Survey (KiDS) to study how the light from about 15 million distant galaxies was affected by the gravitational influence of matter on the largest scales in the Universe. The results appear to be in disagreement with earlier results from the Planck satellite. This map of dark matter in the Universe was obtained from data from the KiDS survey, using the VLT Survey Telescope at ESO's Paranal Observatory in Chile. It reveals an expansive web of dense (light) and empty (dark) regions. This image is one out

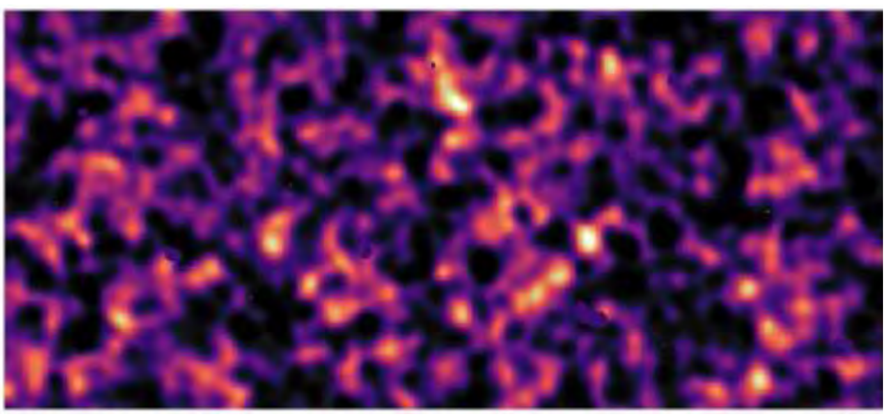

Figure 8. Dark matter map for a patch of sky based on gravitational lensing analysis [38] Hilderbrandt 16.

of five patches of the sky observed by KiDS. Here the invisible dark matter is seen rendered in pink, covering an area of sky around 420 times the size of the full moon. This image reconstruction was made by analyzing the light collected from over three million distant galaxies more than 6 billion light-years away. The observed galaxy images were warped by the gravitational pull of dark matter as the light traveled through the Universe. Some small dark regions, with sharp boundaries, appear in this image. They are the locations of bright stars and other nearby objects that get in the way of the observations of more distant galaxies and are hence masked out in these maps as no weak-lensing signal can be measured in these areas [38]. The luminous (light-emitting) components of the universe only comprise about 0.4% of the total energy. The remaining components are dark. Of those, roughly 3.6% are identified: cold gas and dust, neutrinos, and black holes. About 23% is dark matter, and the overwhelming majority is some type of gravitationally self-repulsive dark energy.

Remark 6.6.1. In order to explain physical nature of the dark matter sector we assume that the main part of dark matter, *i.e.*, $\simeq 23\% - 4.6\% = 18\%$ (see **Figure 9**) formed by supermassive ghost particles with masses such that $mc^2 > \Lambda_*$, see ref. [13], Subsection 2.3.

Remind that vacuum energy density for free scalar quantum field with a wrong statistic is:

$$\varepsilon(\mu) = -\frac{1}{2}\frac{1}{(2\pi\hbar)^3}\int_0^\infty 4\pi c\sqrt{p^2+\mu^2}\,p^2\mathrm{d}p = K'\int_0^\infty \sqrt{p^2+\mu^2}\,p^2\mathrm{d}p = K'I(\mu), \quad (296)$$

where $\mu = mc$. From the basic definitions [1]

$$p = T_{xx}, p(\mu) = -\frac{1}{2}\frac{1}{(2\pi\hbar)^3}\int_0^\infty u_x p_x 4\pi p^2\mathrm{d}p, \mathbf{u} = \frac{c\mathbf{p}}{\sqrt{p^2+\mu^2}}, \overline{u_x p_x} = \frac{1}{3}\langle \mathbf{u},\mathbf{p}\rangle \quad (297)$$

one obtains

$$p(\mu) = \frac{K'}{3}\int_0^\infty \frac{p^4\mathrm{d}p}{\sqrt{p^2+\mu^2}} = K'F(\mu). \quad (298)$$

Remark 6.6.2. Note that the integral in RHS of Equation (297) and in Equation (298) is divergent and ultraviolet cutoff is needed. Thus in accordance with [1] we set

$$\varepsilon(\mu, p_0) = K'I(\mu, p_0), p(\mu, p_0) = K'F(\mu, p_0), \quad (299)$$

where

$$I(\mu, p_0) = \int_0^{p_0}\sqrt{p^2+\mu^2}\,p^2\mathrm{d}p, F(\mu, p_0) = \int_0^{p_0}\frac{p^4\mathrm{d}p}{\sqrt{p^2+\mu^2}}, \quad (300)$$

where $p_0 \le \Lambda_*/c$. For fermionic quantum field with a wrong statistic, similarly one obtains

$$\varepsilon(\mu, p_0) = -4K'I(\mu, p_0), p(\mu) = -4K'F(\mu, p_0). \quad (301)$$

Thus from Equations. (300)-(301) by using formally Pauli-Villars regularization [7] [8] and regularization by high-energy cutoff the expression for

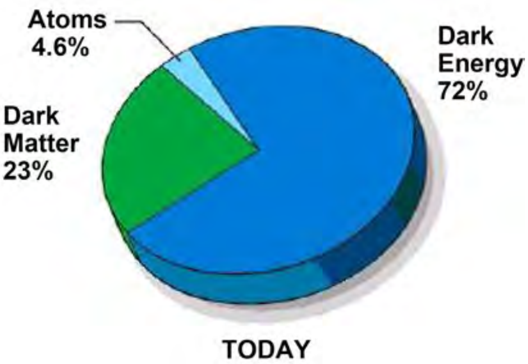

Figure 9. Matter and energy distribution in the universe today. The luminous (light-emitting) components of the universe only comprise about 0.4% of the total energy. The remaining components are dark.

free vacuum energy density ε reads

$$\varepsilon_{\text{vac}} = \sum_{i=0}^{2M} f_i I(\mu_i, p_0) \tag{302}$$

and the expression for pressure p reads

$$p_{\text{vac}} = \sum_{i=0}^{2M} f_i F(\mu_i, p_0). \tag{303}$$

Definition 6.6.1. We define now discrete distribution $f_{PV}: \mathbb{R}_+ \to \mathbb{R}$ by formula

$$f_{PV}(\mu_i) = f_i, \tag{304}$$

and we will call it as a full discrete Pauli-Villars masses distribution.

Remark 6.6.3. We assume now that in Equations (302)-(303): 1) the quantities $\mu_i^{s.m} = \mu_i, i = 1, 2, \cdots, M$ are masses of physical particles corresponding to standard matter and 2) the quantities $\mu_i^{g.m} = \mu_i, i = M+1, 2, \cdots, 2M$ are masses of ghost particles with a wrong kinetic term and wrong statistics corresponding to physical dark matter.

Remark 6.6.5. We recall that the Euler-Maclaurin summation formula reads

$$\begin{aligned} &\textstyle\sum_{i=1}^{2M} g(\mu_1 + (i-1)h) \\ &= \int_{\mu_1}^{\mu_{2M}} f(\mu)\mathrm{d}\mu + A_1[g(\mu_{2M}) - g(\mu_1)] \\ &\quad + A_2 h[g'(\mu_{2M}) - g'(\mu_1)] + O(h^2),\ f(\mu) = \frac{1}{h} g(\mu). \end{aligned} \tag{305}$$

Let $g(\mu)$ be an appropriate continuous function such that: 1)
$g(\mu_i) = f_i, i = 1, 2, \cdots, 2M$,
2) $g'(\mu_{2M}) = 0, g'(\mu_1) = 0$.

Thus from Equations (302)-(303) and Equations (305) we obtain

$$\begin{aligned} \varepsilon_{\text{vac}} &= \sum_{i=0}^{2M} f_i I(\mu_i, p_0) = \int_{\mu_1}^{\mu_{2M}} f(\mu) I(\mu, p_0)\mathrm{d}\mu \\ &\quad + A_1 h[f(\mu_{2M}) I(\mu_{2M}, p_0) - f(\mu_1) I(\mu_1, p_0)] + O(h^2) \end{aligned} \tag{306}$$

and

$$p_{\text{vac}} = \sum_{i=0}^{2M} f_i F(\mu_i, p_0) = \int_{\mu_1}^{\mu_{2M}} f(\mu) F(\mu, p_0) \mathrm{d}\mu + A_1 h\left[f(\mu_{2M}) F(\mu_{2M}, p_0) - f(\mu_1) F(\mu_1, p_0)\right] + O\left(h^2\right). \tag{307}$$

Definition 6.6.2. We will call the function $f_{PV}(\mu)$ as a full continuous Pauli-Villars masses distribution.

Definition 6.6.3. We define now: 1) discrete distribution $f_{PV}^{b.g.m} : \mathbb{R}_+ \to \mathbb{R}$ by formula

$$f_{PV}^{b.g.m}\left(\mu_i^{s.m}\right) = f_i, i = 1, 2, \cdots, M \tag{308}$$

and we will call it as discrete Pauli-Villars masses distribution of the bosonic ghost matter and

2) discrete distribution $f_{PV}^{f.g.m} : \mathbb{R}_+ \to \mathbb{R}$ by formula

$$f_{PV}^{f.g.m}(\mu_i) = f_i, i = M+1, 2, \cdots, 2M \tag{309}$$

and we will call it as discrete Pauli-Villars masses distribution of the fermionic ghost matter.

Remark 6.6.4. We rewrite now Equations (306)-(307) in the following equivalent form

$$\varepsilon_{\text{vac}} = \sum_{i=1}^{M} f_{PV}^{b.g.m}\left(\mu_i^{s.m}\right) I\left(\mu_i^{b.g.m}, p_0\right) + \sum_{j(i)=M+1}^{2M} f_{PV}^{f.g.m}\left(\mu_{j(i)}^{f.g.m}\right) I\left(\mu_{j(i)}^{f.g.m}, p_0\right) \tag{310}$$

and

$$p_{\text{vac}} = \sum_{i=1}^{M} f_{PV}^{b.g.m}\left(\mu_i^{b.g.m}\right) F\left(\mu_i^{b.g.m}, p_0\right) + \sum_{j(i)=M+1}^{2M} f_{PV}^{f.g.m}\left(\mu_{j(i)}^{f.g.m}\right) F\left(\mu_{j(i)}^{f.g.m}, p_0\right), \tag{311}$$

where $j(i) = i + M, i = 1+1, 2, \cdots, M$.

Remark 6.6.6. We assume now that:1) $\mu_i^{b.g.m} \approx \mu_{j(i)}^{f.g.m}$,

2) $\left| f_{PV}^{b.g.m}\left(\mu_i^{b.g.m}\right) + f_{PV}^{f.g.m}\left(\mu_{j(i)}^{f.g.m}\right)\right| \ll 1$, *i.e.*,

$$f_{PV}^{b.g.m}\left(\mu_i^{b.g.m}\right) \approx -f_{PV}^{f.g.m}\left(\mu_{j(i)}^{f.g.m}\right). \tag{312}$$

Note that Equation (312) meant highly symmetric discrete Pauli-Villars masses distribution between bosonic ghost matter and fermionic ghost matter above that scale Λ_*.

Thus from Equations (310)-(311) and Equations (312) we obtain

$$\begin{aligned}\varepsilon_{\text{vac}} &= \sum_{i=1}^{M} f_{PV}^{b.g.m}\left(\mu_i^{b.g.m}\right) I\left(\mu_i^{b.g.m}, p_0\right) + \sum_{j(i)=M+1}^{2M} f_{PV}^{f.g.m}\left(\mu_{j(i)}^{f.g.m}\right) I\left(\mu_{j(i)}^{f.g.m}, p_0\right) \\ &= \sum_{i=1}^{M}\left[f_{PV}^{b.g.m}\left(\mu_i^{b.g.m}\right) + f_{PV}^{f.g.m}\left(\mu_{j(i)}^{f.g.m}\right)\right] I(\mu_i, p_0)\end{aligned} \tag{313}$$

and

$$\begin{aligned}p_{\text{vac}} &= \sum_{i=1}^{M} f_{PV}^{b.g.m}\left(\mu_i^{b.g.m}\right) F\left(\mu_i^{b.g.m}, p_0\right) + \sum_{j(i)=M+1}^{2M} f_{PV}^{f.g.m}\left(\mu_{j(i)}^{f.g.m}\right) F\left(\mu_{j(i)}^{f.g.m}, p_0\right) \\ &= \sum_{i=1}^{M}\left[f_{PV}^{b.g.m}\left(\mu_i^{b.g.m}\right) + f_{PV}^{f.g.m}\left(\mu_{j(i)}^{f.g.m}\right)\right] F(\mu_i, p_0).\end{aligned} \tag{314}$$

From Equations (313)-(314) and Equations (305) finally we obtain

$$\begin{aligned}\varepsilon_{\text{vac}} &= \sum_{i=1}^{M}\left[f_{PV}^{b.g.m}\left(\mu_i^{b.g.m}\right)+f_{PV}^{f.g.m}\left(\mu_{j(i)}^{f.g.m}\right)\right]I\left(\mu_i, p_0\right)\\ &= \int_{\mu_1}^{\mu_{\text{eff}}}\left[f_{PV}^{b.g.m}\left(\mu\right)+f_{PV}^{f.g.m}\left(\mu\right)\right]I\left(\mu, p_0\right)\mathrm{d}\mu\end{aligned} \tag{315}$$

and

$$\begin{aligned}p_{\text{vac}} &= \sum_{i=1}^{M}\left[f_{PV}^{b.g.m}\left(\mu_i^{s.m}\right)+f_{PV}^{f.g.m}\left(\mu_{j(i)}^{f.g.m}\right)\right]F\left(\mu_i, p_0\right)\\ &= \int_{\mu_1}^{\mu_{\text{eff}}}\left[f_{PV}^{b.g.m}\left(\mu\right)+f_{PV}^{f.g.m}\left(\mu\right)\right]F\left(\mu, p_0\right)\mathrm{d}\mu,\end{aligned} \tag{316}$$

where obviously

$$f_{PV}^{b.g.m}\left(\mu\right)+f_{PV}^{f.g.m}\left(\mu\right)=f_{PV}^{g.m.}\left(\mu\right)\approx 0. \tag{317}$$

Thus finally we obtain

$$\varepsilon^{g.m.}\left(\mu_{\text{eff}}^{(1)},\mu_{\text{eff}}^{(2)},p_0\right)=\int_{\mu_{\text{eff}}^{(1)}}^{\mu_{\text{eff}}^{(2)}} f_{PV}^{g.m.}\left(\mu\right)I\left(\mu, p_0\right)\mathrm{d}\mu, \tag{318}$$

and

$$p^{g.m.}\left(\mu_{\text{eff}}^{(1)},\mu_{\text{eff}}^{(2)},p_0\right)=\int_{\mu_{\text{eff}}^{(1)}}^{\mu_{\text{eff}}^{(2)}} f_{PV}^{g.m.}\left(\mu\right)F\left(\mu, p_0\right)\mathrm{d}\mu, \tag{319}$$

where $\mu_{\text{eff}}^{(1)},\mu_{\text{eff}}^{(2)} \gg p_0$. In order to calculate $\varepsilon^{g.m.}\left(\mu_{\text{eff}}^{(1)},\mu_{\text{eff}}^{(2)},p_0\right)$ and $p^{g.m.}\left(\mu_{\text{eff}}^{(1)},\mu_{\text{eff}}^{(2)},p_0\right)$ let us evaluate now the following quantities defined above by Equations (300)

$$I\left(\mu, p_0\right)=\int_0^{p_0} p^2\sqrt{p^2+\mu^2}\,\mathrm{d}p=\int_0^{p_0}\mu p^2\sqrt{1+\frac{p^2}{\mu^2}}\,\mathrm{d}p \tag{320}$$

and

$$F\left(\mu, p_0\right)=\frac{1}{3}\int_0^{p_0}\frac{p^4\mathrm{d}p}{\sqrt{p^2+\mu^2}}=\frac{1}{3}\int_0^{p_0}\frac{p^4\mu^{-1}\mathrm{d}p}{\sqrt{1+\frac{p^2}{\mu^2}}}, \tag{321}$$

where $p_0/\mu \ll 1$. Note that

$$\begin{aligned}&\sqrt{1+\frac{p^2}{\mu^2}}=1+\frac{1}{2}\frac{p^2}{\mu^2}-\frac{1}{8}\frac{p^4}{\mu^4}+\frac{1}{16}\frac{p^6}{\mu^6}+\cdots\\ &p^2\sqrt{p^2+\mu^2}=p^2\mu\sqrt{1+\frac{p^2}{\mu^2}}=p^2\mu\left(1+\frac{1}{2}\frac{p^2}{\mu^2}-\frac{1}{8}\frac{p^4}{\mu^4}+\frac{1}{16}\frac{p^6}{\mu^6}+\cdots\right)\\ &\qquad=p^2\mu+\frac{1}{2}\frac{p^4}{\mu}-\frac{1}{8}\frac{p^6}{\mu^3}+\frac{1}{16}\frac{p^8}{\mu^5}+\cdots\end{aligned} \tag{322}$$

By inserting Equation (322) into Equation (320) one obtains

$$\begin{aligned}I\left(\mu, p_0\right)&=\int_0^{p_0}\left(p^2\mu+\frac{1}{2}\frac{p^4}{\mu}-\frac{1}{8}\frac{p^6}{\mu^3}+\frac{1}{16}\frac{p^8}{\mu^5}+\cdots\right)\mathrm{d}p\\ &=\frac{1}{3}p_0^3\mu+\frac{1}{10}\frac{p_0^5}{\mu}-\frac{1}{7\times 8}\frac{p_0^7}{\mu^3}+\frac{1}{9\times 16}\frac{p_0^9}{\mu^5}+\cdots\end{aligned} \tag{323}$$

Note that

$$\left(1+\frac{p^2}{\mu^2}\right)^{-1/2}=1-\frac{1}{2}\frac{p^2}{\mu^2}+\frac{3}{8}\frac{p^4}{\mu^4}+\cdots$$
$$p^4\mu^{-1}\left(1+\frac{p^2}{\mu^2}\right)^{-1/2}=\frac{p^4}{\mu}-\frac{1}{2}\frac{p^6}{\mu^3}+\frac{3}{8}\frac{p^8}{\mu^5}+\cdots \tag{324}$$

By inserting Equation (324) into Equation (321) one obtains

$$F(\mu,p_0)=\frac{1}{3}\int_0^{p_0}\frac{p^4\mu^{-1}\mathrm{d}p}{\sqrt{1+\frac{p^2}{\mu^2}}}=\frac{1}{3}\int_0^{p_0}\left(\frac{p^4}{\mu}-\frac{1}{2}\frac{p^6}{\mu^3}+\frac{3}{8}\frac{p^8}{\mu^5}+\cdots\right)\mathrm{d}p$$
$$=\frac{p_0^5}{3\times 5\mu}-\frac{1}{2\times3\times7}\frac{p_0^7}{\mu^3}+\frac{1}{8\times 9}\frac{p_0^9}{\mu^5}+\cdots \tag{325}$$

By inserting Equation (323) into Equation (318) one obtains

$$\begin{aligned}&\varepsilon^{g.m.}\left(\mu_{\text{eff}}^{(1)},\mu_{\text{eff}}^{(2)},p_0\right)\\&=\int_{\mu_{\text{eff}}^{(1)}}^{\mu_{\text{eff}}^{(2)}}f_{PV}^{g.m.}(\mu)I(\mu,p_0)\mathrm{d}\mu\\&=\int_{\mu_{\text{eff}}^{(1)}}^{\mu_{\text{eff}}^{(2)}}f_{PV}^{g.m.}(\mu)\left(\frac{1}{3}p_0^3\mu+\frac{1}{10}\frac{p_0^5}{\mu}-\frac{1}{7\times 8}\frac{p_0^7}{\mu^3}+\frac{1}{9\times 16}\frac{p_0^9}{\mu^5}+\cdots\right)\mathrm{d}\mu\\&=\frac{p_0^3}{3}\int_{\mu_{\text{eff}}^{(1)}}^{\mu_{\text{eff}}^{(2)}}f_{PV}^{g.m.}(\mu)\mu\mathrm{d}\mu+\frac{p_0^5}{10}\int_{\mu_{\text{eff}}^{(1)}}^{\mu_{\text{eff}}^{(2)}}\frac{f_{PV}^{g.m.}(\mu)\mathrm{d}\mu}{\mu}-\frac{p_0^7}{7\times 8}\int_{\mu_{\text{eff}}^{(1)}}^{\mu_{\text{eff}}^{(2)}}\frac{f_{PV}^{g.m.}(\mu)\mathrm{d}\mu}{\mu^3}+\cdots\end{aligned} \tag{326}$$

By inserting Equation (325) into Equation (319) one obtains

$$\begin{aligned}&p^{g.m.}\left(\mu_{\text{eff}}^{(1)},\mu_{\text{eff}}^{(2)},p_0\right)\\&=\int_{\mu_{\text{eff}}^{(1)}}^{\mu_{\text{eff}}^{(2)}}f_{PV}^{g.m.}(\mu)F(\mu,p_0)\mathrm{d}\mu\\&=\int_{\mu_{\text{eff}}^{(1)}}^{\mu_{\text{eff}}^{(2)}}f_{PV}^{g.m.}(\mu)\left(\frac{p_0^5}{3\times 5\mu}-\frac{1}{2\times3\times7}\frac{p_0^7}{\mu^3}+\frac{1}{8\times 9}\frac{p_0^9}{\mu^5}+\cdots\right)\mathrm{d}\mu\\&=\frac{p_0^5}{3\times 5}\int_{\mu_{\text{eff}}^{(1)}}^{\mu_{\text{eff}}^{(2)}}\frac{f_{PV}^{g.m.}(\mu)\mathrm{d}\mu}{\mu}-\frac{p_0^7}{2\times3\times7}\int_{\mu_{\text{eff}}^{(1)}}^{\mu_{\text{eff}}^{(2)}}\frac{f_{PV}^{g.m.}(\mu)\mathrm{d}\mu}{\mu^3}+\frac{p_0^9}{8\times 9}\int_{\mu_{\text{eff}}^{(1)}}^{\mu_{\text{eff}}^{(2)}}\frac{f_{PV}^{g.m.}(\mu)\mathrm{d}\mu}{\mu^5}+\cdots\end{aligned} \tag{327}$$

Remark 6.6.7. We assume now that

$$\left|f_{PV}^{g.m.}(\mu)\right|=\begin{cases}O\left(\left(\mu_{\text{eff}}^{(1)}\right)^{-n}\right),n>7 & \mu_{\text{eff}}^{(1)}\le\mu\le\mu_{\text{eff}}^{(2)}\\ 0 & \mu>\mu_{\text{eff}}^{(2)}\end{cases} \tag{328}$$

Note that under assumption (328) the quantities $\varepsilon^{g.m.}\left(\mu_{\text{eff}}^{(1)},\mu_{\text{eff}}^{(2)},p_0\right)$ and $p^{g.m.}\left(\mu_{\text{eff}}^{(1)},\mu_{\text{eff}}^{(2)},p_0\right)$ cannot contribute in the value of the cosmological constant.

7. Conclusion

We argue that a solution to the cosmological constant problem is to assume that there exists hidden physical mechanism which cancels divergences in canonical QED_4, QCD_4, Higher-Derivative-Quantum-Gravity, etc. In fact, we argue that corresponding supermassive Pauli-Villars ghost fields, etc. really exist. New theory of elementary particles which contain hidden ghost sector is proposed. In accordance with Zel'dovich hypothesis [1] we suggest that physics of elementary particles is separated into low/high energy ones, the standard notion of smooth spacetime is assumed to be altered at a high energy cutoff scale Λ_* and a new treatment based on QFT in a fractal spacetime with negative dimension is used above that scale. This would fit in the observed value of the dark energy needed to explain the accelerated expansion of the universe if we choose highly symmetric masses distribution below that scale Λ_*, *i.e.*,

$f_{s.m}(\mu) \simeq f_{g.m}(\mu), \mu \le \mu_{\text{eff}}, \mu_{\text{eff}} c^2 < \Lambda_*$

Acknowledgements

We thank the reviewers for their comments.

Conflicts of Interest

The authors declare no conflicts of interest regarding the publication of this paper.

References

[1] Zel'dovich, Ya.B. (1968) The Cosmological Constant and the Theory of Elementary Particles. *Soviet Physics Uspekhi*, **11**, 381-393. https://doi.org/10.1070/PU1968v011n03ABEH003927

[2] Gliner, É.B. (2002) Inflationary Universe and the Vacuumlike State of Physical Medium. *Physics-Uspekhi*, **45**, 213-220. https://doi.org/10.1070/PU2002v045n02ABEH001108

[3] Gliner, É.B. (1966) Algebraic Properties of the Energy-Momentum Tensor and Vacuum-Like States of Matter. *Journal of Experimental and Theoretical Physics* (*JETP*), **22**, 378-382.

[4] Gliner, E.B. and Dimnikova, I.G. (1975) Nonsingular Fridman Cosmology. *Astronomy Letters*, **1**, 7-9.

[5] Weinberg, C.S. (1989) The Cosmological Constant Problem. *Reviews of Modern Physics*, **61**, 1-23. https://doi.org/10.1103/RevModPhys.61.1

[6] Zel'dovich, Y.B. (1967) Cosmological Constant and Elementary Particles. *JETP Letters*, **6**, 316-317.

[7] Nagy, L. (1966) State Vector Spaces with Indefinite Metric in Quantum Field Theory. Akadémiai Kiadó, Budapest.

[8] Bogoljubov, N.N. and Shirkov, D.V. (1984) Quantenfelder. VEB Deutscher Verlag der Wissenschaften, Berlin.

[9] Maguejo, J. and Smolin, L. (2002) Lorentz Invariance with an Invariant Energy Scale. *Physical Review Letters*, **88**, Article ID: 190403. https://doi.org/10.1103/PhysRevLett.88.190403

[10] Maguejo, J. and Smolin, L. (2003) Generalized Lorentz Invariance with an Invariant Energy Scale. *Physical Review D*, **67**, Article ID: 044017. https://doi.org/10.1103/PhysRevD.67.044017

[11] Bouda, A. and Foughali, T. (2012) On the Fock Transformation in Nonlinear Relativity. *Modern Physics Letters A*, **27**, Article ID: 1250036.

https://doi.org/10.1142/S0217732312500368

[12] Foukzon, J., Menkova, E.R., Potapov, A.A. and Podosenov, S.A. (2019) Quantum Field Theory in Fractal Space-Time with Negative Hausdorff-Colombeau Dimensions. The Solution Cosmological Constant Problem.
https://arxiv.org/abs/1004.0451
https://doi.org/10.2139/ssrn.3324024

[13] Arkani-Hamed, N., Cheng, H.-C., Luty, M.A. and Mukohyama, S. (2004) Ghost Condensation and a Consistent Infrared Modification of Gravity. *Journal of High Energy Physics*, **0405**, 074. https://doi.org/10.1088/1126-6708/2004/05/074

[14] Stelle, K.S. (1977) Renormalization of Higher Derivative Quantum Gravity. *Physical Review D*, **16**, 953. https://doi.org/10.1103/PhysRevD.16.953

[15] Cree, S.S., Davis, T.M., Ralph, T.C., Wang, Q., Zhu, Z. and Unruh, W.G. (2018) Can the Fluctuations of the Quantum Vacuum Solve the Cosmological Constant Problem? *Physical Review D*, **98**, Article ID: 063506.
https://arxiv.org/pdf/1805.12293.pdf
https://doi.org/10.1103/PhysRevD.98.063506

[16] Hiller, J.R. (2010) Pauli-Villars Regularization of Field Theories on the Light Front. *AIP Conference Proceedings*, **1317**, 156-161. https://doi.org/10.1063/1.3536550

[17] Ramond, P. (1990) Field Theory: A Modern Primer. Westview Press, Boulder.

[18] Pimentel, B.M. and Tomazelli, J.L. (1996) What Is Wrong with Pauli-Villars Regularization in QED_3? *Progress of Theoretical Physics*, **95**, 1217-1222.
https://doi.org/10.1143/PTP.95.1217

[19] Svozil, K. (1987) Quantum Field Theory on Fractal Spacetime: A New Regularisation Method. *Journal of Physics A*: *Mathematical and General*, **20**, 3861-3875.
https://doi.org/10.1088/0305-4470/20/12/033

[20] Colombeau, J.F. (1984) New Generalized Functions and Multiplication of Distributions. North Holland, Amsterdam.

[21] Vernaeve, H. (2010) Ideals in the Ring of Colombeau Generalized Numbers. *Communications in Algebra*, **38**, 2199-2228. https://doi.org/10.1080/00927870903055222

[22] Falconer, K.J. (1985) The Geometry of Fractal Sets. Cambridge University Press, Cambridge. https://doi.org/10.1017/CBO9780511623738

[23] Manin, Y.I. (2005) The Notion of Dimension in Geometry and Algebra.

[24] Maslov, V.P. (2006) Negative Dimension in General and Asymptotic Topology.

[25] Maslov, V.P. (2007) General Notion of a Topological Space of Negative Dimension and Quantization of Its Density. *Mathematical Notes*, **81**, 140-144.
https://doi.org/10.4213/mzm3530

[26] Maslov, V.P. (2006) Negative Asymptotic Topological Dimension, a New Condensate, and Their Relation to the Quantized Zipf Law. *Mathematical Notes*, **80**, 806-813. https://doi.org/10.4213/mzm3362

[27] Mandelbrot, B.B. (1890) Random Multifractals: Negative Dimensions and the Resulting Limitations of the Thermodynamic Formalism. *Proceedings*: *Mathematical and Physical Sciences*, **434**, 79-88. https://doi.org/10.1098/rspa.1991.0081

[28] Eyink, G. (1989) Quantum Field-Theory Models on Fractal Spacetime. I. Introduction and Overview. *Communications in Mathematical Physics*, **125**, 613-636.
https://doi.org/10.1007/BF01228344

[29] Eyink, G. (1989) Quantum Field-Theory Models on Fractal Spacetime. II. Hierarchical Propagators. *Communications in Mathematical Physics*, **126**, 85-101.

https://doi.org/10.1007/BF02124332

[30] Calcagni, G.J. (2010) Quantum Field Theory, Gravity and Cosmology in a Fractal Universe. *Journal of High Energy Physics*, **2010**, 120. https://link.springer.com/article/10.1007%2FJHEP03%282010%29120 https://doi.org/10.1007/JHEP03(2010)120

[31] Calcagni, G. (2010) Fractal Universe and Quantum Gravity. *Physical Review Letters*, **104**, Article ID: 251301. https://arxiv.org/abs/0912.3142 https://doi.org/10.1103/PhysRevLett.104.251301

[32] Dunne, G.V. and Halliday, I.G. (1988) Negative Dimensional Oscillators. *Nuclear Physics B*, **308**, 589. https://doi.org/10.1016/0550-3213(88)90579-2

[33] Dunne, G.V. (1989) Negative-Dimensional Groups in Quantum Physics. *Journal of Physics A*, **22**, 1719-1736. https://doi.org/10.1088/0305-4470/22/11/014

[34] Parker, L. and Toms, D. (2009) Quantum Field Theory in Curved Spacetime: Quantized Fields and Gravity. Cambridge University Press, Cambridge. https://doi.org/10.1017/CBO9780511813924

[35] Birrell, N. and Davies, P. (1984) Quantum Fields in Curved Space. Cambridge Monographs on Mathematical Physics, Cambridge University Press, Cambridge.

[36] Bauer, M. and Plehn, T. (2018) Yet Another Introduction to Dark Matter.

[37] Lisanti, M. (2016) Lectures on Dark Matter Physics. *Proceedings of the* 2015 *Theoretical Advanced Study Institute in Elementary Particle Physics*, Boulder, 1-26 June 2015, 399-446. https://doi.org/10.1142/9789813149441_0007

[38] Hildebrandt, H. and Viola, M. (2016) KiDS-450: Cosmological Parameter Constraints from Tomographic Weak Gravitational Lensing.

Journal of Modern Physics, 2019, 10, 795-823
http://www.scirp.org/journal/jmp
ISSN Online: 2153-120X
ISSN Print: 2153-1196

Space-Time Properties as Quantum Effects. Restrictions Imposed by Grothendieck's Scheme Theory

Leonid Lutsev

Ioffe Physical-Technical Institute, Russian Academy of Sciences, St. Petersburg, Russia
Email: l_lutsev@mail.ru

How to cite this paper: Lutsev, L. (2019) Space-Time Properties as Quantum Effects. Restrictions Imposed by Grothendieck's Scheme Theory. *Journal of Modern Physics*, **10**, 795-823.
https://doi.org/10.4236/jmp.2019.107054

Received: May 14, 2019
Accepted: June 21, 2019
Published: June 24, 2019

Abstract

In this paper we consider properties of the four-dimensional space-time manifold $\mathcal{M}$ caused by the proposition that, according to the scheme theory, the manifold $\mathcal{M}$ is locally isomorphic to the spectrum of the algebra $\mathcal{A}$, $\mathcal{M} \cong \mathrm{Spec}(\mathcal{A})$, where $\mathcal{A}$ is the commutative algebra of distributions of quantum-field densities. Points of the manifold $\mathcal{M}$ are defined as maximal ideals of density distributions. In order to determine the algebra $\mathcal{A}$, it is necessary to define multiplication on densities and to eliminate those densities, which cannot be multiplied. This leads to essential restrictions imposed on densities and on space-time properties. It is found that the only possible case, when the commutative algebra $\mathcal{A}$ exists, is the case, when the quantum fields are in the space-time manifold $\mathcal{M}$ with the structure group $SO(3,1)$ (Lorentz group). The algebra $\mathcal{A}$ consists of distributions of densities with singularities in the closed future light cone subset. On account of the local isomorphism $\mathcal{M} \cong \mathrm{Spec}(\mathcal{A})$, the quantum fields exist only in the space-time manifold with the one-dimensional arrow of time. In the fermion sector the restrictions caused by the possibility to define the multiplication on the densities of spinor fields can explain the chirality violation. It is found that for bosons in the Higgs sector the charge conjugation symmetry violation on the densities of states can be observed. This symmetry violation can explain the matter-antimatter imbalance. It is found that in theoretical models with non-abelian gauge fields instanton distributions are impossible and tunneling effects between different topological vacua $|n\rangle$ do not occur. Diagram expansion with respect to the $\mathcal{A}$-algebra variables is considered.

Keywords

Space-Time Properties, Quantum Field, Arrow of Time, Chirality, Algebra of

Distributions, Symmetry Violation

1. Introduction

The origin of the arrow of time, the possibility of physics in multiple time dimensions, the violation of the parity principle, and the matter-antimatter imbalance are ones of the most exciting and difficult challenges of physics.

Physics in multiple time dimensions leads to new insights and, at the same time, contains theoretical problems. According to the assertion written in [1] [2] [3], extra time dimensions give new hidden symmetries that conventional one time physics does not capture, implying the existence of a more unified formulation of physics that naturally supplies the hidden information. At the same time, it notes that all but the $(3+1)$-dimensional one might correspond to "dead worlds", devoid of observers, and we should find ourselves inhabiting a $(3+1)$-dimensional space-time [4]. The natural description of the $(3+1)$-space-time with the one-dimensional time can be provided on the base of the Clifford geometric algebra [5]. In the opposite case of multidimensional time, the violation of the causal structure of the space-time and the movement backwards in the time dimensions are possible [6]. A particle can move in the causal region faster than the speed of light in vacuum. This leads to contradictoriness of the multidimensional time theory and, at present, these problems have not been solved.

The arrow of time is the one-way property of time which has no analogue in space. The asymmetry of time is explained by large numbers of theoretical models—by the Second law of thermodynamics (the thermodynamic arrow of time), by the direction of the universe expansion (the cosmological arrow), by the quantum uncertainty and entanglement of quantum states (the quantum source of time), and by the perception of a continuous movement from the known (past) to the unknown (future) (the psychological time arrow) [7]-[13]. At present, there is not a satisfactory explanation of the arrow of time and this problem is far from being solved.

The discrete symmetry of the space reflection P of the space-time and the charge conjugation C may be used to characterize the properties of chiral systems. The violation of the space reflection P exhibits as the chiral symmetry breaking—only left-handed particles and right-handed anti-particles could be observed [14] [15] [16]. The cause of the parity violation is not clear.

The matter-antimatter imbalance remains as one of the unsolved problems. The amount of CP violation in the Standard Model is insufficient to account for the observed baryon asymmetry of the universe. At present, the hope to explain the matter-antimatter imbalance is set on the CP violation in the Higgs sector [17] [18] [19] [20] [21].

In this paper we consider the above-mentioned space-time properties (the arrow of time, multiple time dimensions, and the chirality violation), the violation of the charge conjugation, and find that in the framework of the scheme theory these properties can be determined by the spectrum of the commutative algebra $\mathcal{A}$ of distributions of quantum-field densities. Points of the space-time manifold $\mathcal{M}$ are defined as maximal ideals of quantum-field density distributions. The scheme theory imposes restrictions on space-time properties. Schemes were introduced by Alexander Grothendieck with the aim of developing the formalism needed to solve deep problems of algebraic geometry [22]. This led to the evolution of the concept of space [23]. The space is associated with a spectrum of a commutative algebra or, in other words, with a set of all prime ideals. In the case of the classical physics, the commutative algebra is the commutative ring of functions. In contrast with the classical physics, quantum fields are determined by equations on functionals [24] [25] [26] [27]. Quantum-field densities are linear functionals of auxiliary fields and, consequently, are distributions. There are many restrictions to construct the commutative algebra of distributions. In the common case, multiplication on distributions cannot be defined and depends on their wavefront sets. In the microlocal analysis the wavefront set $\mathrm{WF}(u)$ characterizes the singularities of a distribution *u*, not only in space, but also with respect to its Fourier transform at each point. The term wavefront was coined by Lars Hörmander [28]. It should be noted that the microlocal analysis has resulted in the recent progress in the renormalized quantum field theory in curved space-time [29] [30] [31] [32]. In our case, the possibility to define multiplication on distributions leads to essential restrictions imposed on densities forming the algebra $\mathcal{A}$. The spectrum of the algebra $\mathcal{A}$ is locally isomorphic to the space-time manifold $\mathcal{M}$, $\mathcal{M} \cong \mathrm{Spec}(\mathcal{A})$, and characterizes its properties such as the one-dimensional arrow of time, the chirality violation and the structure group of the space-time manifold $\mathcal{M}$. One can say that the space-time is determined by matter.

The principal assertion of the paper is the proposition that, according to the scheme theory, the manifold $\mathcal{M}$ is locally isomorphic to the spectrum of the algebra $\mathcal{A}$, $\mathcal{M} \cong \mathrm{Spec}(\mathcal{A})$, where $\mathcal{A}$ is the commutative algebra of distributions of quantum-field densities. So, the paper is organized as follows. In order to find distributions of quantum-field densities, in Section II we derive differential equations for the densities of quantum fields from the Schwinger equation and find that wavefronts of the quantum-field density distributions are determined by characteristics of the matrix differential operator and by wavefronts of distributions of composite fields (higher order functional derivatives defined at a point). The quantum fields contain fermion, boson (Higgs), and gauge field components. Multiplication on the quantum-field densities and the commutative algebra $\mathcal{A}$ of distributions of fermion and boson densities are considered in Section III. It is found that the only possible case, when the commutative algebra $\mathcal{A}$ of distributions of quantum-field densities exists, is the case, when the quantum fields are in the space-time manifold $\mathcal{M}$ with the structure group $SO(3,1)$ (Lorentz group) and the time is one-dimensional. The asymmetry of time, the chirality violation of spinor fields, and the charge conjugation symmetry violation in the boson sector are the necessary conditions for the existence of the algebra $\mathcal{A}$. The quantum fields exist only in the space-time manifold with the one-dimensional arrow of time and with chirality and charge conjugation symmetry violations. In Section IV we consider possibility to define a multiplication operation on instanton density distributions in theoretical models with non-abelian gauge fields. It is found that instanton distributions are impossible and, therefore, tunneling effects between different topological vacua $|n\rangle$ do not occur. This leads to the zero value of the Pontryagin index Q and to the zero neutron electric dipole moment. Fermion, boson (Higgs) and gauge field density distributions satisfying the restriction requirements considered in Sections III and IV are generators of the algebra $\mathcal{A}$. Ideals, localization, the spectrum of the density distribution algebra $\mathcal{A}$ and the scheme $(\mathcal{M}, \mathcal{A}_{\mathcal{M}})$ are considered in Section V. If the algebra $\mathcal{A}$ can be determined and is the component of the scheme, then the space-time manifold $\mathcal{M}$ with quantum fields exists. Otherwise, the space-time manifold is devoid of matter and, consequently, does not exist. In Section VI we consider diagram expansion with respect to auxiliary fields and find that wavefronts of distributions of composite fields at a point introduced in Section II are included in the characteristics of the matrix differential operator and wavefront sets of quantum-field density distributions are located on the light cone. Diagram expansion with respect to the $\mathcal{A}$-algebra variables are considered in Section VII.

2. Quantum-Field Equations

Quantum fields are determined by equations on functionals. In this section we consider singularities of the linear components $w^{\zeta}(x)$ (densities) of the functional solution

$$Z(q) = \sum_{\zeta} \int w^{\zeta}(x) q^{\zeta}(x) \mathrm{d}x + \sum_{n>1} \sum_{\zeta_1 \cdots \zeta_n} \int \cdots \int G^{\zeta_1 \cdots \zeta_n}(x_1 \cdots x_n) q^{\zeta_1}(x_1) \cdots q^{\zeta_n}(x_n) \mathrm{d}x_1 \cdots \mathrm{d}x_n, \tag{1}$$

where $q^{\zeta}(x)$ is the auxiliary fields, $G^{\zeta_1 \cdots \zeta_n}(x_1 \cdots x_n)$ are the higher order distributions $(n>1)$. For this purpose, we derive differential equations for the densities of quantum fields from the Schwinger equation. Let us consider fields Ψ on the 4-dimensional space-time manifold $\mathcal{M}$

$$\Psi(x) = \{\Psi^{\zeta}(x)\} = \{\psi^{\alpha}(x), \bar{\psi}^{\alpha}(x), \varphi^{n}(x), \varphi^{+n}(x), A_{\mu}^{a}(x)\}, \tag{2}$$

where $\psi^{\alpha}(x)$, $\bar{\psi}^{\alpha}(x)$ are the fermion (spinor) fields, $\varphi^{n}(x)$, $\varphi^{+n}(x)$ are the bosons (for example, Higgs bosons), and $A_{\mu}^{a}(x)$ are the gauge field potentials. In relation (2) and in the all following relations Greek letter indices α and β enumerate types of fermions, μ, ν and ρ are indices of the space-time variables, Latin letters n, m, l enumerate types of bosons, and a, b, c are the gauge indices, respectively. $\zeta = \{\alpha, n, a\}$ is the multiindex.

Since wavefronts of distributions can be localized [33] and a differential manifold locally resembles Euclidian space near each point, we consider the case when the space-time manifold $\mathcal{M}$ is the 4-dimensional Euclidian (pseudo-Euclidian) space with the Euclidian metric tensor $g^{\mu\nu}$. In order to derive quantum-field equations, we consider the action of the fields Ψ on the manifold $\mathcal{M}$ [14] [15] [34]

$$S(\Psi)=\int_{\mathcal{M}} L(\Psi(x))\mathrm{d}x$$

with the Lagrangian

$$\begin{aligned} L(\Psi(x)) = & -\frac{1}{4}F^{a}_{\mu\nu}(x)F^{\mu\nu a}(x)+i\bar{\psi}^{\alpha}(x)\gamma^{\mu}\nabla^{\alpha}_{\mu\beta}\psi^{\beta}(x) \\ & -m^{(\alpha)}c\bar{\psi}^{\alpha}(x)\psi^{\alpha}(x)-\mu_{\alpha\beta n}\bar{\psi}^{\alpha}(x)\varphi^{n}(x)\psi^{\beta}(x) \\ & -\mu^{*}_{\alpha\beta n}\bar{\psi}^{\alpha}(x)\varphi^{+n}(x)\psi^{\beta}(x)+\bar{\nabla}^{l}_{\mu n}\varphi^{+n}(x)\nabla^{\mu l}_{m}\varphi^{m}(x) \\ & -m^{(n)2}c^{2}\varphi^{+n}(x)\varphi^{n}(x)+\nu\left(\varphi^{+n}(x)\varphi^{n}(x)\right)^{2}, \end{aligned} \tag{3}$$

where

$$F^{a}_{\mu\nu}=\partial_{\mu}A^{a}_{\nu}-\partial_{\nu}A^{a}_{\mu}+e_{j(a)}C^{a}_{bc}A^{b}_{\mu}A^{c}_{\nu},$$

$$F^{a\mu\nu}=g^{\mu\rho}g^{\nu\sigma}F^{a}_{\rho\sigma},$$

are the intensity of the gauge fields,

$$\gamma^{\mu}\gamma^{\nu}+\gamma^{\nu}\gamma^{\mu}=2g^{\mu\nu}$$

are Dirac matrices. $\mu_{\alpha\beta n}$ and $\mu^{*}_{\alpha\beta n}$ are the Yukawa interaction constants. ν is the boson interaction constant. $m^{(\alpha)}$ and $m^{(n)}$ are masses of fermions and bosons, respectively. c is the light velocity.

$$\nabla^{\alpha}_{\mu\beta}=\hbar\partial_{\mu}\delta^{\alpha}_{\beta}-ie_{j(a)}T^{\alpha}_{a\beta}A^{a}_{\mu},$$

$$\nabla^{l}_{\mu m}=\hbar\partial_{\mu}\delta^{l}_{m}-ie_{j(a)}\tau^{l}_{am}A^{a}_{\mu},\quad \nabla^{\mu l}_{m}=g^{\mu\nu}\nabla^{l}_{\nu m},$$

$$\bar{\nabla}^{l}_{\mu m}=\hbar\partial_{\mu}\delta^{l}_{m}+ie_{j(a)}\tau^{*l}_{am}A^{a}_{\mu},$$

$T_{a}=\left\|T^{\alpha}_{a\beta}\right\|$ is the gauge matrix with the commutation relation $[T_a,T_b]=iC^{c}_{ab}T_c$ acting on spinors as $\psi'=\exp(i\sigma^{a}T_{a})\psi$, σ^{a} is an arbitrary real number. $\tau_{a}=\left\|\tau^{m}_{an}\right\|$ is the gauge matrix with the commutation relation $[\tau_a,\tau_b]=iC^{c}_{ab}\tau_c$ acting on bosons as $\varphi'=\exp(i\sigma^{a}\tau_{a})\varphi$. It is supposed that the summation in relation (3) and in the all following relations is performed over all repeating indices. $e_{j(a)}$ is the charge corresponding to the j factor of the direct decomposition of the gauge group $\mathcal{G}=\prod_{j}\mathcal{G}_{j}$ $(=SU(3)\times SU(2)\times U(1))$. If the index a of operators T_a and τ_a belongs to the subgroup $\mathcal{G}_j$, then in the charge $e_{j(a)}$ $j(a)=j$.

For derivation of the quantum-field Schwinger equation it needs to add the linear term (q,Ψ) with auxiliary fields $q(x)=\{q^{\zeta}(x)\}=\left\{q^{\alpha}_{(\psi)}(x),q^{\alpha}_{(\bar{\psi})}(x),q^{n}_{(\varphi)}(x),q^{n}_{(\varphi^{+})}(x),q^{a}_{(A)\mu}(x)\right\}$ to the action $S(\Psi)$

$$\bar{S}(\Psi,q)=S(\Psi)+(q,\Psi),$$

where

$$(q,\Psi)=\int_{\mathcal{M}}\Big(q^{\alpha}_{(\psi)}(x)\psi^{\alpha}(x)+q^{\alpha}_{(\bar\psi)}(x)\bar\psi^{\alpha}(x)+q^{n}_{(\varphi)}(x)\varphi^{n}(x)$$
$$+q^{n}_{(\varphi^+)}(x)\varphi^{+n}(x)+q^{a}_{(A)\mu}(x)A^{a}_{\mu}(x)\Big)\mathrm{d}x.$$

For fields $\varphi^{n}(x)$, $\varphi^{+n}(x)$, and $A^{a}_{\mu}(x)$ the auxiliary fields $q^{\zeta}(x)$ are simple variables and for fields $\psi^{\alpha}(x)$ and $\bar\psi^{\alpha}(x)$ the auxiliary fields are Grassmanian ones, respectively. Then, the Schwinger equation is written in the form [24] [25]

$$\left\{\frac{\vec\delta S(\Psi)}{\delta\Psi^{\zeta}(x)}\bigg|_{\Psi^{\zeta}(x)=\hbar\vec\delta/\delta iq^{\zeta}(x)}+q^{\zeta}(x)\right\}Z(q)=0, \tag{4}$$

where $\vec\delta/\delta\Psi$ is the functional derivative on the left, $Z(q)$ is the generating functional. The derivatives $\vec\delta S(\Psi)/\delta\Psi^{\zeta}(x)$ have been written as

$$\frac{\vec\delta S}{\delta\bar\psi^{\alpha}(x)}=i\gamma^{\mu}\nabla^{\alpha}_{\mu\beta}\psi^{\beta}(x)-m^{(\alpha)}c\psi^{\alpha}(x)-\mu_{\alpha\beta n}\varphi^{n}(x)\psi^{\beta}(x)$$
$$-\mu^{*}_{\alpha\beta n}\varphi^{+n}(x)\psi^{\beta}(x),$$

$$\frac{\vec\delta S}{\delta\psi^{\alpha}(x)}=i\bar\psi^{\beta}(x)\gamma^{\mu}\left(\hbar\overleftarrow{\partial}_{\mu}\delta^{\beta}_{\alpha}+ie_{j(a)}T^{\beta}_{a\alpha}A^{a}_{\mu}(x)\right)+m^{(\alpha)}c\bar\psi^{\alpha}(x)$$
$$+\mu_{\beta\alpha n}\varphi^{n}(x)\bar\psi^{\beta}(x)+\mu^{*}_{\beta\alpha n}\varphi^{+n}(x)\bar\psi^{\beta}(x),$$

$$\frac{\delta S}{\delta\varphi^{m}(x)}=-\bar\nabla^{m}_{\mu k}\bar\nabla^{\mu k}_{n}\varphi^{+n}(x)-m^{(m)2}c^{2}\varphi^{+m}(x)$$
$$+2\nu\varphi^{m}(x)\varphi^{+m2}(x)-\mu_{\alpha\beta m}\bar\psi^{\alpha}(x)\psi^{\beta}(x),$$

$$\frac{\delta S}{\delta\varphi^{+n}(x)}=-\nabla^{n}_{\mu k}\nabla^{\mu k}_{m}\varphi^{m}(x)-m^{(n)2}c^{2}\varphi^{n}(x)$$
$$+2\nu\varphi^{n2}(x)\varphi^{+n}(x)-\mu^{*}_{\alpha\beta n}\bar\psi^{\alpha}(x)\psi^{\beta}(x),$$

$$\begin{aligned}\frac{\delta S}{\delta A^{a}_{\mu}(x)}=&\left(\partial_{\nu}\delta^{a}_{b}+e_{j(a)}C^{a}_{cb}A^{c}_{\nu}(x)\right)F^{b\nu\mu}(x)+\bar\psi^{\alpha}(x)\gamma^{\mu}T^{\alpha}_{a\beta}\psi^{\beta}(x)\\&-i\left(-\tau^{*k}_{an}\varphi^{+n}(x)\nabla^{\mu k}_{m}\varphi^{m}(x)+\bar\nabla^{\mu k}_{n}\varphi^{+n}(x)\tau^{k}_{am}\varphi^{m}(x)\right).\end{aligned} \tag{5}$$

In order to get the Schwinger equation we should substitute of derivatives $\hbar\vec\delta/\delta iq^{\zeta}(x)$ for $\Psi^{\zeta}(x)$ in relations (5). The formal solution of the Schwinger Equation (4) is the functional integral

$$Z(q)=\int\exp\left[\frac{i}{\hbar}\big(S(\Psi)+(q,\Psi)\big)\right]D\Psi. \tag{6}$$

We consider densities of the quantum fields $\psi^{\alpha}(x)$, $\bar\psi^{\alpha}(x)$, $\varphi^{n}(x)$, $\varphi^{+n}(x)$, and $A^{a}_{\mu}(x)$ in the expansion (1)

$$w^{\zeta}(x)=\frac{\vec\delta Z(q)}{\delta q^{\zeta}(x)}\bigg|_{q\to 0}.$$

Taking into account the form of the functional $Z(q)$ (1) and the form of the Lagrangian (3), from the Schwinger Equation (4) we can obtain differential equations for the densities

$$w(x)=\left\{w^{\zeta}(x)\right\}=\left\{w_{(\psi)}^{\alpha}(x),w_{(\bar{\psi})}^{\alpha}(x)),w_{(\varphi)}^{n}(x),w_{(\varphi^{+})}^{n}(x),w_{(A)\mu}^{a}(x)\right\},$$

which can be written in the form

$$\begin{gathered}w_{(\bar{\psi})}^{\alpha}(x)\left(i\hbar\gamma^{\mu}\overleftarrow{\partial}_{\mu}+m^{(\alpha)}c\right)=B_{(\bar{\psi})}^{\alpha}\left(w^{\zeta_{(n)}(\mathrm{comp})}(x)\right)\\ \left(i\hbar\gamma^{\mu}\vec{\partial}_{\mu}-m^{(\alpha)}c\right)w_{(\psi)}^{\alpha}(x)=B_{(\psi)}^{\alpha}\left(w^{\zeta_{(n)}(\mathrm{comp})}(x)\right)\\ \left(\hbar^{2}\Box+m^{(n)2}c^{2}\right)w_{(\varphi)}^{n}(x)=B_{(\varphi)}^{n}\left(w^{\zeta_{(n)}(\mathrm{comp})}(x)\right)\\ \left(\hbar^{2}\Box+m^{(n)2}c^{2}\right)w_{(\varphi^{+})}^{n}(x)=B_{(\varphi^{+})}^{n}\left(w^{\zeta_{(n)}(\mathrm{comp})}(x)\right)\\ \Box w_{(A)\mu}^{a}(x)=B_{(A)\mu}^{a}\left(w^{\zeta_{(n)}(\mathrm{comp})}(x)\right),\end{gathered}\tag{7}$$

where

$$\Box(\cdot)=g^{\mu\nu}\frac{\partial^{2}(\cdot)}{\partial x^{\mu}x^{\nu}}$$

is the d'Alembert operator; $B^{\zeta}=\left\{B_{(\psi)}^{\alpha},B_{(\bar{\psi})}^{\alpha},B_{(\varphi)}^{n},B_{(\varphi^{+})}^{n},B_{(A)\mu}^{a}\right\}$ are polynomials of distributions $w^{\zeta_{(n)}(\mathrm{comp})}(x)$ of composite fields $\bar{\psi}^{\alpha}(x)\psi^{\beta}(x)$, $\varphi^{n}(x)\psi^{\beta}(x)$, $\varphi^{+n}(x)\varphi^{m}(x)$, $A_{\mu}^{a}(x)A_{\nu}^{b}(x)$, $\cdots$. Distributions $w^{\zeta_{(n)}(\mathrm{comp})}(x)$ ($\zeta_{(n)}=\{\zeta_1,\cdots,\zeta_n\}$, $n\geq 2$) are defined as higher order functional derivatives at a point

$$w^{\zeta_{(n)}(\mathrm{comp})}(x)=\left.\frac{\delta^{n}W}{\underbrace{\delta q^{\zeta_1}(x_1)\cdots\delta q^{\zeta_n}(x_n)}_{n}}\right|_{x_1,\cdots,x_n\to x}$$

Equations (7) can be written in the form

$$\mathcal{N}_{\zeta}^{\eta}w^{\zeta}(x)=B^{\eta}\left(w^{\zeta_{(n)}(\mathrm{comp})}(x)\right),\tag{8}$$

where $\mathcal{N}_{\zeta}^{\eta}=\sum_{p=0}^{k}a_{p\zeta}^{\eta}\partial_{x}^{p}$ is the matrix differential operator. Solutions of the Schwinger equation (4) determined the generating functional $Z(q)$ and solutions of Equations (7), (8) can be found in the approximate form by the diagram technique [25] [26] [27], which will be considered in Sections VI and VII. In the common case, solutions of Equations (7) and (8) are distributions and have singularities. The question is: which distributions of the densities $w^{\zeta}(x)$ can be multiplied and, therefore, form a commutative algebra? We consider the densities $w^{\zeta}(x)$ expressed in the oscillatory--integral form [33] [35] [36]

$$w^{\zeta}(x)=\int_{T^{*}\mathcal{M}}F^{\zeta}(x,\chi)\exp\left[i\sigma^{\zeta}(x,\chi)\right]\mathrm{d}\chi,\tag{9}$$

where $T^{*}\mathcal{M}$ is the cotangent bundle over the space-time manifold $\mathcal{M}$, $\sigma^{\zeta}(x,\chi)$ is the phase function, $F^{\zeta}(x,\chi)$ is the amplitude, χ is the covector, and $(x,\chi)\in T^{*}\mathcal{M}$. It should be noted that relation (9) defines Lagrangian distributions, which form the subset of the space of all distributions $D'(\mathcal{M})$.

Any Lagrangian distribution can be represented locally by oscillatory integrals [36]. Conversely, any oscillatory integral is a Lagrangian distribution. We consider the case of the real linear phase function of χ

$$\sigma^{\zeta}(x,\chi)=k^{\zeta}\chi_{\nu}x_{\nu}, \tag{10}$$

where k^{ζ} is a coefficient. Our consideration of the case of Lagrangian distributions is motivated by the statement that, if the multiplication cannot be defined on the Lagrangian distribution subset, then this operation cannot be defined on the space $D'(\mathcal{M})$.

The wavefront set $\mathrm{WF}(u)$ of a distribution u can be defined as [28] [33] [35]

$$\mathrm{WF}(u)=\left\{(x,\xi)\in T^{*}\mathcal{M}\mid \xi\in\Gamma_{x}(u)\right\},$$

where the singular cone $\Gamma_{x}(u)$ is the complement of all directions ξ such that the Fourier transform of u, localized at x, is sufficiently regular when restricted to a conical neighborhood of ξ. The wavefront of the distributions $\mathrm{WF}(w^{\zeta})$ characterizes the singularities of solutions and is determined by the wavefront of $w^{\zeta(n)(\mathrm{comp})}(x)$ and by the characteristics of the matrix operator $\mathcal{N}_{\zeta}^{\eta}$ [33] [35]

$$\mathrm{WF}(w^{\zeta})\subset \mathrm{Char}(\mathcal{N}_{\zeta}^{\eta})\cup \mathrm{WF}\left(B^{\eta}\left(w^{\zeta(n)(\mathrm{comp})}\right)\right), \tag{11}$$

where the characteristics $\mathrm{Char}(\mathcal{N}_{\zeta}^{\eta})$ is the set $\left\{(x,\xi)\in T^{*}M\setminus 0\right\}$ defined by linear algebraic equations of highest power orders in the unknown Fourier transforms $\tilde{w}^{\zeta}(\xi)$

$$\sum_{\zeta,\,p=\max k} a_{p\zeta}^{\eta}(-i\xi)^{p}\,\tilde{w}^{\zeta}(\xi)=0,$$

where coefficients $a_{p\zeta}^{\eta}$ are defined by the matrix differential operator $\mathcal{N}_{\zeta}^{\eta}=\sum_{p=0}^{k}a_{p\zeta}^{\eta}\partial_{x}^{p}$ in Equation (8) and are equal to coefficients of linear differential operators acted on the densities $w(x)$ in equation (7). The covector $\xi\in T^{*}(x)$ lies in the cotangent cone Γ_{x} at the point x. Taking into account Equations (7), we can find that

$$\mathrm{Char}(\mathcal{N}_{\zeta}^{\eta})\Big|_{x}=g^{\mu\nu}\xi_{\mu}\xi_{\nu},$$

consequently, singularities of solutions are located on this cone. The wavefronts $\mathrm{WF}\left(w^{\zeta(n)(\mathrm{comp})}\right)$ of composite fields are considered in Sections III and VI. In Section VI we find that in the framework of the diagram expansion wavefronts $\mathrm{WF}\left(w^{\zeta(n)(\mathrm{comp})}\right)$ are determined by $\mathrm{Char}(\mathcal{N}_{\zeta}^{\eta})$.

Starting from the proposition that properties of the space-time manifold $\mathcal{M}$ are defined by the quantum fields $\Psi^{\zeta}(x)$ and, consequently, by the commutative algebra $\mathcal{A}$ of distributions $w^{\zeta}(x)$, in the next section we find that this statement results in essential restrictions imposed on the space-time manifold $\mathcal{M}$.

3. Algebra of Distributions of Quantum-Field Densities. Fermion and Boson Sectors

In order to determine points of the space-time manifold $\mathcal{M}$ by means of the densities $w^{\xi}(x)$, it is necessary to define multiplication on densities, to construct the commutative algebra $\mathcal{A}$ of distributions of densities, and to find maximal ideals of this algebra. According to Ref. [33] [35], multiplication on distributions $u, v \in D'(M)$ with wavefronts $\mathrm{WF}(u) = \{(x,\xi)\}$ and $\mathrm{WF}(v) = \{(x,\eta)\}$ is determined, if and only if

$$\mathrm{WF}(u) \cap \mathrm{WF}'(v) = \varnothing, \tag{12}$$

where $\mathrm{WF}'(v)$ is the image of $\mathrm{WF}(v)$ in the transformation $(x,\eta) \mapsto (x,-\eta)$ in the cone subset Γ of the cotangent bundle T^*M. The wavefront of the product is defined as

$$\begin{aligned} \mathrm{WF}(uv) \subset \{(x,\xi+\eta) \mid (x,\xi) \in \mathrm{WF}(u) \text{ or } \xi = 0, \\ (x,\eta) \in \mathrm{WF}(v) \text{ or } \eta = 0; \xi + \eta \neq 0\}. \end{aligned} \tag{13}$$

Taking into account the linear form of the phase function (10), from relations (12) and (13) we obtain restrictions on the densities $w^{\xi}(x)$. For this purpose, we consider wavefronts of densities for the case of the 4-dimensional space-time manifold $\mathcal{M}$, when the structure group of the cotangent bundle $T^*\mathcal{M}$ is the Lie group $SO(4-p,p)$ with $p=0$, $p=1$, and $p>1$.

The fields Ψ (2) are observed relative to inertial frames of reference in the space-time manifold $\mathcal{M}$. Rectilinear motion transforms the fields Ψ and, consequently, their densities $w^{\xi}(x)$ and wavefronts. This transformation can be considered as a diffeomorphism of $\mathcal{M}$ and is described by the arcwise connected part of the $SO(4-p,p)$ group. More precisely, if $f:\Omega \to \Omega'$ is the diffeomorphism of open subsets $\Omega, \Omega' \subset M$, $f_+ : T^*\Omega \to T^*\Omega'$ is the diffeomorphism induced by *f*, and $f_* : D'(\Omega) \to D'(\Omega')$ is the isomorphism, then for the distribution $u \in D'(\Omega)$ [33] [35]

$$\mathrm{WF}(f_* u) = f_+ \mathrm{WF}(u). \tag{14}$$

Thus, rectilinear motion results in the transformation f_* of the field densities $w^{\xi}(x)$ induced by the arcwise connected part of the structure group and the transformation f_+ of density wavefronts (14). If, as a result of these transformations, the covector $\xi \in \mathrm{WF}(w^{\xi}) \subset T^*M$ changes its orientation $\xi \mapsto -\xi$, then the multiplication (13) on the density $w_1^{\xi}(x)$ with the covector ξ and the density $w_2^{\xi}(x)$ with the covector $-\xi$ is impossible. We consider transformations of density wavefronts induced by the arcwise connected part of the structure group (14) and by discrete symmetry transformations—the time reversal and the space reflection.

3.1. Time Reversal

We assume that the co-ordinate variables of the space-time manifold $\mathcal{M}$ can be divided by time *ct* and space *r* variables, $x = \{ct_1, \cdots, ct_p, r_{p+1}, \cdots\}$ $(p = 0,1,2,\cdots)$. The structure group of the space-time manifold is $SO(4-p,p)$. We consider the time reversal *T* on the manifold $\mathcal{M}$ and the possibility of embedding of the time reversal into the arcwise connected part of the group

$SO(4-p,p)$.

Euclidian space-time manifold with the structure group $SO(4,0)$. Let us consider the case of the time reversal on the Euclidian space-time manifold M with the structure group $SO(4,0)$ of the cotangent bundle $T^*\mathcal{M}$. The signature of the space-time metric is $(----)$. In this case, $p=0$ and the time variable *ct* is identical to the space one (for example, r_1). The image of the inversion $\xi \mapsto -\xi$ in relation (14) on wavefronts of densities can be reached by the transformation induced by the arcwise connected part of the group $SO(4,0)$ (**Figure 1(a)**). Thus, we always can find densities with covectors ξ and η in relation (13) such that $\xi+\eta=0$. Consequently, multiplication on distributions in the Euclidian space-time manifold with the signature of the space-time metric $(----)$ is impossible. One can only say about a partial multiplication operation on a subset of the distribution space. The analogous consideration can be carried out for manifold $\mathcal{M}$ with the structure group $SO(0,4)$ and with the signature of the space-time metric $(++++)$.

Pseudo-Euclidian space-time manifold with the structure group $SO(3,1)$. The signature of the space-time metric is $(+---)$. In accordance with relation $g^{\mu\nu}\xi_\mu\xi_\nu=0$ defining boundaries of a singular cone, the space-time manifold is separated by three regions: the future light cone $\Gamma^{(f)}$, the past light cone $\Gamma^{(p)}$, and the space-like region $\Gamma^{(s)}$ (**Figure 1(b)**). The multiplication of distributions with singularities in the region $\Gamma^{(s)}$ is impossible because of the existence of the inversion $\xi \mapsto -\xi$ reached by the arcwise connected part of the group $SO(3,1)$. Therefore, singularities can exist only in the cone $\Gamma^{(f)}$ or in the cone $\Gamma^{(p)}$. The time reversal T inverts the covector $\xi \in \mathrm{WF}(w^\zeta) \subset T^*\mathcal{M}$ from the future light cone $\Gamma^{(f)}$ to the past light cone $\Gamma^{(p)}$ (**Figure 1(b)**). The Lorentz transformation $SO(3,1)$ acts on future and past light cones separately. Consequently, the arcwise connected part of the group $SO(3,1)$ does not contain the time inversion. So, if we exclude field density distributions $w^\zeta(x)$ with singularities in the past light cone $\Gamma^{(p)}$ and consider only density distributions with singularities in the future light cone $\Gamma^{(f)}$, then for these distributions the multiplication can be defined. Correspondingly, densities of states $T\Psi^\zeta(x)$ are forbidden. In this case, we have the one-way direction of time and there is not the symmetry of time on density distributions. The arrow of time is pointing towards the future. According to (13), the wavefront of the product of quantum-field densities in the future light cone $\Gamma^{(f)}$ is given by

$$\mathrm{WF}\left(w^{\zeta_1}\cdots w^{\zeta_n}\right) \subset \left\{\left(x, \sum_i^n \xi^{\zeta_i}\right) \mid \xi^{\zeta_i} \in \Gamma^{(f)}, \sum_i^n \xi^{\zeta_i} \neq 0\right\},$$

where $\xi^{\zeta_i}=\beta^{\zeta_i}\chi^{(i)}$ is the covector associated with the density w^{ζ_i}, β^ζ is a function of field invariants, such as chirality, charge signs, charge parity, etc. Taking into account that for the Dirac adjoint spinor density $w^\alpha_{(\bar\psi)}(x)$ and for the density $w^n_{(\varphi^+)}(x)$ the exponent term in the integral in relation (9) must have opposite sign than for densities $w^\alpha_{(\psi)}(x)$ and $w^n_{(\varphi)}(x)$, respectively, and, therefore, is transformed as $i\sigma^\zeta(x,\chi) \to -i\sigma^\zeta(x,\chi)$ (for $w^\alpha_{(\psi)}(x) \to w^\alpha_{(\bar\psi)}(x)$, $w^n_{(\varphi)}(x) \to w^n_{(\varphi^+)}(x)$), we find that in the cone $\Gamma^{(f)}$

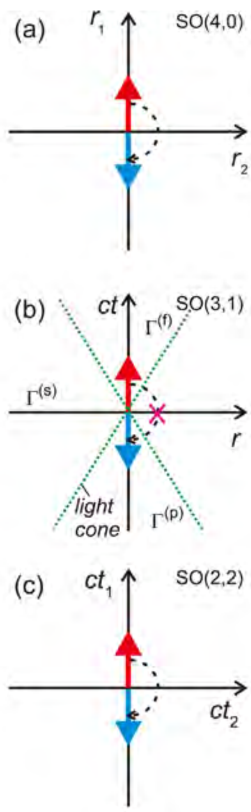

Figure 1. Transformation of the covector $\xi \mapsto -\xi$ at the time reversal of the space-time manifold $\mathcal{M}$ with the structure groups (a) $SO(4,0)$, (b) $SO(3,1)$, and (c) $SO(2,2)$. The image of the transformation $\xi \mapsto -\xi$ can be reached by means of a transformation of the arcwise connected part of groups $SO(4,0)$ and $SO(2,2)$ and is not attainable for the case of the arcwise connected part of the $SO(3,1)$ group.

$$\beta_{(\psi)} > 0, \quad \beta_{(\bar{\psi})} < 0$$
$$\beta_{(\varphi)} > 0, \quad \beta_{(\varphi^+)} < 0. \tag{15}$$

Pseudo-Euclidian space-time manifold with the structure group $SO(4-p,p)$ ($p>1$). The signatures of the space-time metric are $(++--)$ ($p=2$) and $(+++-)$ ($p=3$). If the time dimension is equal to 2 or higher ($p>1$), then the image of the time inversion of densities in the time plane $(ct_1,\cdots,ct_p)$ is attained by means of a transformation of the arcwise connected part of the group $SO(4-p,p)$ (Figure 1(c)). In this case, one can find densities with covectors ξ and η in relation (13) such that $\xi+\eta=0$. Multiplication on distributions in this space-time manifold is impossible.

3.2. Space Reflection and Charge Conjugation in the Fermion Sector

Another restriction to define multiplication on the density distribution algebra is caused by the chirality of fermions and by the charge conjugation. Since, according to the above-mentioned subsection the pseudo-Euclidian space-time manifold with the Lorentz group $SO(3,1)$ and the arrow of time are necessary conditions for definition of multiplication on density distributions, we consider fermion distributions with singularities in the future light cone $\Gamma^{(f)}$. Right-handed and left-handed states of the Dirac fields $\psi^{\alpha}(x)$ and $\bar{\psi}^{\alpha}(x)$ are defined by projective operators $(1\pm\gamma^5)/2$ acting on a spinor [14] [15] [37]

$$\psi_R^{\alpha}(x)=\frac{1+\gamma^5}{2}\psi^{\alpha}(x)$$

$$\psi_L^{\alpha}(x)=\frac{1-\gamma^5}{2}\psi^{\alpha}(x).$$

The space reflection P converts the right-handed spinor into the left-handed one, and vice versa

$$P\psi_R^{\alpha}(x)=iL_p\psi_L^{\alpha}(x)$$

$$P\psi_L^{\alpha}(x)=iL_p\psi_R^{\alpha}(x),$$

where in the Weyl (chiral) basis

$$L_p=\begin{pmatrix}0 & I\\ I & 0\end{pmatrix}$$

and I is the identity 2-matrix. $\psi_R^{\alpha}(x)$ and $\psi_L^{\alpha}(x)$ are eigenvectors of the operator γ^5 with the chirality $\lambda=1$ (the right-handed state) and the chirality $\lambda=-1$ (the left-handed state), respectively. Double space reflection P^2 can be regarded as 360° rotation. It transforms spinors as

$$P^2\psi_{\rho}^{\alpha}(x)=-\psi_{\rho}^{\alpha}(x),$$

where $\rho=\{R,L\}$.

For fulfilment of relations (15) the coefficients $\beta_{(\psi)}$ and $\beta_{(\bar{\psi})}$ must contain a charge factor κ_c such that $\beta(\psi)=1$ and $\beta(\bar{\psi})=-1$. We consider two cases, (1) $\beta=\lambda\kappa_c$ with the chirality λ and (2) $\beta=\kappa_c$ without chirality. In order to fulfil multiplication on densities $w_{(\psi_R)}^{\alpha}(x)$, $w_{(\psi_L)}^{\alpha}(x)$, $w_{(\bar{\psi}_R)}^{\alpha}(x)$, $w_{(\bar{\psi}_L)}^{\alpha}(x)$ in the first case, for right-handed and left-handed states of the fermion fields we should get

$$\kappa_c\left(\psi_R^{\alpha}(x)\right)=1,\quad \kappa_c\left(\psi_L^{\alpha}(x)\right)=-1,$$

$$\kappa_c\left(\bar{\psi}_R^{\alpha}(x)\right)=-1,\quad \kappa_c\left(\bar{\psi}_L^{\alpha}(x)\right)=1,$$

$$\lambda\left(\psi_R^{\alpha}(x)\right)=1,\quad \lambda\left(\psi_L^{\alpha}(x)\right)=-1,$$

$$\lambda\left(\bar{\psi}_R^{\alpha}(x)\right)=1,\quad \lambda\left(\bar{\psi}_L^{\alpha}(x)\right)=-1.$$

The charge conjugation C transforms κ_c: $C\kappa_c\left(\psi_R^{\alpha}(x)\right)=\kappa_c\left(\bar{\psi}_R^{\alpha}(x)\right)=-1$, $C\kappa_c\left(\bar{\psi}_R^{\alpha}(x)\right)=\kappa_c\left(\psi_R^{\alpha}(x)\right)=1$, $C\kappa_c\left(\psi_L^{\alpha}(x)\right)=\kappa_c\left(\bar{\psi}_L^{\alpha}(x)\right)=1$, and $C\kappa_c\left(\bar{\psi}_L^{\alpha}(x)\right)=\kappa_c\left(\psi_L^{\alpha}(x)\right)=-1$. The commutative algebra $\mathcal{A}$ of distributions contains densities $w^{\zeta}(x)$ of states $\psi_R^{\alpha}(x)$, $\psi_L^{\alpha}(x)$, $\bar{\psi}_R^{\alpha}(x)$, $\bar{\psi}_L^{\alpha}(x)$,

$CP\psi_R^{\alpha}(x)$, $CP\psi_L^{\alpha}(x)$, $CP\bar{\psi}_R^{\alpha}(x)$, $CP\bar{\psi}_L^{\alpha}(x)$, their sums and products. Densities $w^{\zeta}(x)$ of states $P\psi_R^{\alpha}(x)$, $P\psi_L^{\alpha}(x)$, $P\bar{\psi}_R^{\alpha}(x)$, $P\bar{\psi}_L^{\alpha}(x)$, $C\psi_R^{\alpha}(x)$, $C\psi_L^{\alpha}(x)$, $C\bar{\psi}_R^{\alpha}(x)$, $C\bar{\psi}_L^{\alpha}(x)$ are forbidden and are not contained in the algebra $\mathcal{A}$. This version of the theoretical model contains particles and antiparticles and can explain the chirality violation. Quantum states of a particle and an antiparticle can be interchanged by applying the *CP*-operation.

In the second case, the fulfilment of the relation $\beta = \kappa_c$ with $\kappa_c\left(\psi_R^{\alpha}(x)\right) = \kappa_c\left(\psi_L^{\alpha}(x)\right) = 1$ and $\kappa_c\left(\bar{\psi}_R^{\alpha}(x)\right) = \kappa_c\left(\bar{\psi}_L^{\alpha}(x)\right) = -1$ results in forbidden densities $w^{\zeta}(x)$ of states $C\psi_R^{\alpha}(x)$, $C\psi_L^{\alpha}(x)$, $C\bar{\psi}_R^{\alpha}(x)$, and $C\bar{\psi}_L^{\alpha}(x)$. Wavefronts of these densities are in the past light cone $\Gamma^{(p)}$: $\mathrm{WF}\left(w^{\alpha}_{(C\psi_R)}\right)$, $\mathrm{WF}\left(w^{\alpha}_{(C\psi_L)}\right)$, $\mathrm{WF}\left(w^{\alpha}_{(C\bar{\psi}_R)}\right)$, and $\mathrm{WF}\left(w^{\alpha}_{(C\bar{\psi}_L)}\right) \in \Gamma^{(p)}$. At the same time, the commutative algebra $\mathcal{A}$ of distributions contains densities $w^{\zeta}(x)$ of states $\psi_R^{\alpha}(x)$, $\psi_L^{\alpha}(x)$, $\bar{\psi}_R^{\alpha}(x)$, $\bar{\psi}_L^{\alpha}(x)$, $P\psi_R^{\alpha}(x)$, $P\psi_L^{\alpha}(x)$, $P\bar{\psi}_R^{\alpha}(x)$, and $P\bar{\psi}_L^{\alpha}(x)$. In this case, the theoretical model does not contain antiparticles and the chirality is not violated. In the experiment this case of the theoretical model is not observed.

3.3. Charge Conjugation in the Boson Sector

We consider the common case of the boson (Higgs) sector containing the quantum fields $\varphi^{n}(x)$ and $\varphi^{+n}(x)$. We assume that $\varphi^{n}(x) \neq \varphi^{+n}(x)$. By analogy with the fermion case, the covector of singularity of the density of $\varphi^{n}(x)$ is $\beta_{(\varphi)}\chi$ and the analogous covector of the density of $\varphi^{+n}(x)$ is $-\beta_{(\varphi^{+})}\chi$, respectively. In order to fulfil relations (15) and the requirement that $\beta_{(\varphi)}\chi$, $-\beta_{(\varphi^{+})}\chi \in \Gamma^{(f)}$, we must write the coefficient β in the form $\beta_{(\varphi)} = \kappa_c\left(\varphi^{n}(x)\right) = 1$ and $\beta_{(\varphi^{+})} = \kappa_c\left(\varphi^{+n}(x)\right) = -1$. The charge conjugation C changes the sign of the factor κ_c: $C\kappa_c\left(\varphi^{n}(x)\right) = \kappa_c\left(\varphi^{+n}(x)\right) = -1$ and $C\kappa_c\left(\varphi^{+n}(x)\right) = \kappa_c\left(\varphi^{n}(x)\right) = 1$. Thus, densities of $\varphi^{n}(x)$ and $\varphi^{+n}(x)$ can be multiplied and are included in the algebra $\mathcal{A}$. On the contrary, wavefronts of densities of states $C\varphi^{n}(x)$ and $C\varphi^{+n}(x)$ are in the past light cone $\Gamma^{(p)}$ and must be excluded. This leads to the charge conjugation symmetry violation in the boson sector.

It should be noted that in the modified theoretical models of the Higgs boson sector [17] [18] [19] [20] [21] [41] [42] [43] [44] extending the BEH model [38] [39] [40] some particles in the Higgs sector have negative charge parities and are charged. In this case, the above-mentioned *C*-violation on density distributions in the Higgs sector can explain the observed matter-antimatter imbalance.

Thus, as a result of this section, we define the multiplication on distributions of the fermion and boson (Higgs) quantum-field densities. Fermion and boson density distributions with singularities in the future light cone $\Gamma^{(f)}$ are generators of the algebra $\mathcal{A}$, which is commutative for boson densities and supercommutative for fermion ones (Grassmanian variables). The asymmetry of time (*T*-violation), the chiral asymmetry (*P*-violation) and the charge (*C*) conjugation symmetry violation are caused by singularities of density distributions and these space-time manifold properties are local. In the next section we consider restrictions imposed by fulfilment of the density multiplication operation for gauge fields.

4. Gauge Fields and the Density Distribution Algebra

Multiplication on distributions in the density distribution algebra $\mathcal{A}$ imposes restrictions on theoretical models with non-abelian gauge fields. In this section we demonstrate that instantons ensured tunneling between different topological vacua cannot be included in the algebra $\mathcal{A}$. Let us consider the gauge fields A_μ^a with the non-abelian gauge group $\mathcal{G}$ in the pseudo-Euclidian space-time manifold $\mathcal{M}$ (the Minkowski space-time) with the structure group $SO(3,1)$ and discuss the generally accepted instanton model, in which instantons are functions. At the given time t the space variables form the Euclidian space $\mathbb{R}^3$. Adjoining the single point ∞, we can form the compact topological space $\mathbb{R}^3 \cup \{\infty\}$. This one-point compactification of the 3-dimensional Euclidean space $\mathbb{R}^3$ is homeomorphic to the 3-sphere $\mathbb{S}^3$. If the local transformation $U(x,t) \in G$ of the gauge Lie group $\mathcal{G}$ is trivial at $|x| \to \infty$

$$\lim_{|x|\to\infty} U(x,t) = 1,$$

then the gauge potential $A_\mu = A_\mu^a T_a$ (T_a is the gauge matrix belonging to the Lie algebra of the group $\mathcal{G}$) at $|x| \to \infty$ is the pure gauge

$$A_\mu = U^{-1}(x,t)\partial_\mu U(x,t). \tag{16}$$

and the gauge fields $F_{\mu\nu}^a$ are vanishing. The map on the gauge group $\mathcal{G}$

$$f : \mathbb{S}^3 \to \mathcal{G}$$

defines the homotopy group $\pi_3(\mathcal{G})$. If $G = SU(N)$, then, using the Bott periodicity theorem for unitary groups $SU(N)$ ($N \geq 2$), one can find that [45] [46]

$$\pi_3(SU(N)) = \mathbb{Z}. \tag{17}$$

In this case, the gauge potential A_μ (16) is characterized by homotopy classes $n \in \mathbb{Z}$ of the group $\pi_3(SU(N))$ (17) and can be classified by the topological index [47]

$$n = \frac{1}{24\pi^2} \oint_{\mathbb{S}^3} \varepsilon_{\mu\nu\rho\sigma} \mathrm{tr}\left[A_\nu A_\rho A_\sigma\right] \mathrm{d}\sigma_\mu, \tag{18}$$

where $\varepsilon_{\mu\nu\rho\sigma} = (-1)^p$, p is the parity of the permutation $\{\mu\nu\rho\sigma\}$. If the Minkowski space-time $\mathcal{M}$ can be substituted by the Euclidian space-time manifold, then the topological index (18) can be written via the Pontryagin index

$$Q = \frac{-1}{16\pi^2} \int \mathrm{tr}\left[\tilde{F}_{\mu\nu} F^{\mu\nu}\right] \mathrm{d}^4 x, \tag{19}$$

where $\tilde{F}_{\mu\nu} = \varepsilon_{\mu\nu\rho\sigma} F^{\rho\sigma}/2$ is the dual fields in Euclidean space, $F^{\mu\nu} = F^{a\mu\nu} T^a$, and $\tilde{F}_{\mu\nu} = \tilde{F}_{\mu\nu}^a T^a$.

Taking into account (16), (17), and (18), one can find that vacuum states are characterized by the topological index n. The gauge operator U_m with the topological index m transforms the vacuum state [47] [48] [49]

$$U_m |n\rangle = |n+m\rangle. \quad (20)$$

According to [14] [15] [47] [48] [49] [50] an instanton is a gauge field configuration fulfilling the classical equations of motion in Euclidean space-time, which is interpreted as a tunneling effect between different topological vacua $|n\rangle$. Instantons are labeled by its Pontryagin index Q (19). If $Q=1$, the instanton solution is written as [14] [15] [47] [48] [49] [50]

$$A_\mu = \left(\frac{\rho^2}{\rho^2+\lambda^2}\right) U_1^{-1}(x,t)\partial_\mu U_1(x,t), \quad (21)$$

where λ is the scale parameter giving the instanton size, $\rho = \left|x^2+(ct)^2-|a|^2\right|^{1/2}$, a is the instanton center point. One can imagine that the instanton (21) ensures tunneling between the topological vacuum $|n\rangle$ at $t\to-\infty$ and the vacuum $|n+1\rangle$ at $t\to\infty$. Taking into account that topological vacua $|n\rangle$ are connected by instanton tunneling and requiring the physical vacuum state to be stable against gauge transformations (20), one can find that the physical vacuum is

$$|\theta\rangle = \sum_n \mathrm{e}^{-in\theta}|n\rangle, \quad (22)$$

where θ is the phase angle. In this case, $U_m|\theta\rangle = \mathrm{e}^{im\theta}|\theta\rangle$. The gauge theory with θ-vacuum ($\theta\neq 0$) (22) can be regarded as the theoretical model with the additional term proportional to θQ in the action (3) [14] [15] [47]

$$S \to S - i\theta Q$$

in the case of the Euclidean space-time and

$$S \to S + \theta Q \quad (23)$$

in the case of the Minkowski space-time. Q is the Pontryagin index (19). The additional term θQ breaks P and CP invariance [14] [15] [47] [51].

In the instanton solution $A_\mu = A_\mu^a T_a$ (21) the gauge potentials A_μ^a are functions. Can the instanton solution (21) be generalized on the distribution space $D'(\mathcal{M})$? And can instanton density distributions are multiplied? In order to answer these questions, we consider theoretical models, in which Euclidean instanton solutions have been found and the tunneling behavior has been transfered on the Minkowski space by the Wick rotation [47] [49] [50] [52] [53], and models, in which vacuum tunneling has been studied directly in the Minkowski space [54] [55].

Euclidean instanton solutions.

In order to look for a tunneling path in gauge theory which connects topologically different classical vacua $|n\rangle$, one performs an analytic continuation of the action $S(\Psi)$ (3) to imaginary (Euclidean) time $\tau = it$ [47] [49] [50] [52] [53]. In this case, instanton solutions (21) are functions and the analytic continuation is correct. In contrast with function spaces, the analytic continuation of density distributions of quantum fields $w^a_{(A)\mu}(x)\in A\in D'(\mathcal{M})$ to imaginary time

$\tau = it$ changes their singularities. The changes in singularities are due to changes in the functional integral (6)

$$Z(q) = \int \exp\left[\frac{i}{\hbar}\left(S(\Psi)+(q,\Psi)\right)\right]D\Psi$$
$$\rightarrow \int \exp\left[\frac{-1}{\hbar}\left(S(\Psi)+(q,\Psi)\right)\right]D\Psi.$$

Let us consider these changes in distributions $w^{a}_{(A)\mu}(x)$ in detail. Suppose that a gauge field has the topological vacuum $|n\rangle$ at $t \to -\infty$. In order to find a tunneling path, we consider $t > -\infty$ and perform the complexification $t^{c} \to t + i\tau$ ($t, \tau \in \Re$). In this case, the time is 2-dimensional. According to Figure 1(c) (Section III), one can find densities $w^{a}_{(A)\mu}(x)$ with covectors ξ and η in relation (13) such that $\xi + \eta = 0$ and multiplication on distributions in this space-time manifold is impossible. If we consider the restriction of distributions on the imaginary time τ, then the space-time manifold is Euclidean. As in the above-mentioned case, we always can find densities with covectors ξ and η in relation (13) such that $\xi + \eta = 0$ (Figure 1(a)). Consequently, multiplication on distributions $w^{a}_{(A)\mu}(x)$ is impossible, too. Thus, instanton density distributions are not contained in the algebra $\mathcal{A}$.

Vacuum tunneling in the Minkowski space.

Vacuum tunneling of non-abelian gauge theory directly in the Minkowski space has been studied in [54]. In order to connect vacua of different topological indices and to obtain the potential-energy barrier in winding-number space, through which tunneling occurs, the authors introduce a family of intermediate field configurations as

$$A_0 = 0,$$
$$\vec{A}(x,t) = \vec{f}\left(x, \lambda(t)\right), \tag{24}$$

where λ is a parameter describing the field configuration within the family. The initial potential is $\vec{A}^{(1)} = \vec{f}\big|_{\lambda=\lambda_1}$ and the terminal potential is $\vec{A}^{(2)} = \vec{f}\big|_{\lambda=\lambda_2}$. The function $\vec{f}$ varies continuously from $\vec{A}^{(1)}$ to $\vec{A}^{(2)}$ as λ varies from λ_1 to λ_2. The WKB vacuum-tunneling amplitude has been found from differential equations in which the parameter $\lambda(t)$ is the dynamical variable.

But, the attempt to generalize the above-mentioned family of intermediate field configurations on density distributions $w^{a}_{(A)\mu}(x)$ of quantum fields results in impossibility to define multiplication on these densities. Indeed, the motion along the curve $\lambda(t)$ (24) in the winding-number space is possible in forward and backward directions. Consequently, the time reversal T inverts the covector $\xi \in \mathrm{WF}\left(w^{a}_{(A)\mu}\right) \subset T^{*}\mathcal{M}$ and one can always find densities $w^{a(1)}_{(A)\mu}(x)$ and $w^{a(2)}_{(A)\mu}(x)$ with covectors ξ and η, relatively, in relation (13) such that $\xi + \eta = 0$. Multiplication is only partial defined and, therefore, one can conclude that instanton density distributions must be excluded from the algebra $\mathcal{A}$. As it is shown in Section V, these distributions cannot define ideals and points of the space-time manifold $\mathcal{M}$.

The additional term θQ in the action S (23) breaks P and CP invariance and contributes directly to the neutron electric dipole moment [51] [56]. According to the above-mentioned consideration, instanton distributions are impossible and, therefore, tunneling effects between different topological vacua $|n\rangle$ do not occur. This leads to a degeneration of the energy density of the θ-vacuum (22) with respect to the phase θ. The vacuum energy density becomes θ-invariant. In order to achieve the θ-invariance in the action S (23), one should require that the Pontryagin index Q is equal to zero. This leads to the zero value of the neutron electric dipole moment.

Thus, in Sections III and IV, we define the multiplication on distributions of the quantum-field densities and construct the commutative density distribution algebra $\mathcal{A}$. Multiplication is well-defined operation for all elements of the algebra. Fermion, boson (Higgs) and gauge field density distributions with singularities in the future light cone $\Gamma^{(f)}$ satisfying the restriction requirements are generators of the algebra $\mathcal{A}$. Spectrum of the density distribution algebra $\mathcal{A}$ and the scheme $(\mathcal{M}, \mathcal{A}_{\mathcal{M}})$ are considered in the next section.

5. Ideals and Spectrum of the Density Distribution Algebra. Scheme $(\mathcal{M}, \mathcal{A}_{\mathcal{M}})$

For definition of the scheme $(\mathcal{M}, \mathcal{A}_{\mathcal{M}})$ contained the spectrum of the commutative density distribution algebra $\mathcal{A}$ isomorphic to the space-time manifold $\mathcal{M}$, it needs to carry out localization and to determine the sheaf of structure algebras and the spectrum of the algebra $\mathcal{A}$. To this end, we define prime and maximal ideals of this algebra. The algebra $\mathcal{A}$ consists of density distributions $w^{\zeta}(x)$ with singularities in the closed future light cone subset, $\mathrm{WF}(w^{\zeta}) \subset \Gamma^{(f)} \subset T^{*}\mathcal{M}$. The complement of the future light cone subset $\Gamma^{(f)}$ is the open cone subset $\bar{\Gamma}^{(f)}$. In the cone subset $\bar{\Gamma}^{(f)}$ the densities $w^{\zeta}(x)$ are C^{∞}-smooth functions. We define the maximal ideal at the point x_0 as the set of distributions equal to zero at the point x_0 in the cone subset $\bar{\Gamma}^{(f)}$ (**Figure 2**)

$$m_{x_0} = \left\{ w^{\zeta}(x) \mid \lim_{x \to x_0} w^{\zeta}(x) = 0 \text{ in } \bar{\Gamma}^{(f)} \right\}.$$

p is called a prime ideal if for all distributions $w_1(x)$ and $w_2(x) \in A$ with $w_1(x) w_2(x) \in p$ we have $w_1(x) \in p$ or $w_2(x) \in p$ [57] [58]. Every maximal ideal m_x is prime.

In the process of localization of the algebra $\mathcal{A}$ we find a local algebra contained only information about the behavior of density distributions $w^{\zeta}(x)$ near the point x of the space-time manifold $\mathcal{M}$. We consider the case of maximal ideals. Then, the local algebra $\mathcal{A}_x$ is defined as the commutative algebra consisting of fractions of density distributions $w_1(x)$ and $w_2(x)$

$$\mathcal{A}_x = \left\{ \frac{w_1(x)}{w_2(x)} \middle| w_1(x), w_2(x) \in \mathcal{A}, w_2(x) \notin m_x \right\}, \tag{25}$$

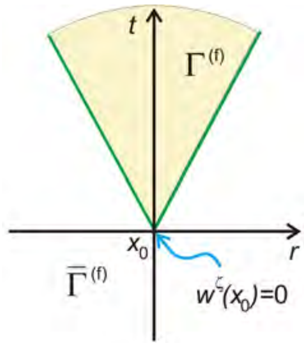

Figure 2. Maximal ideal is defined as the set of distributions equal to zero at the point x_0 in the cone subset $\overline{\Gamma}^{(f)}$, which is complement of the future light cone.

where m_x is the maximal ideal at the point *x*. The fraction $w_1(x)/w_2(x)$ is the equivalence class defined as

$$\frac{w_1(x)}{w_2(x)} = \frac{w_1'(x)}{w_2'(x)},$$

if there exists the distribution $v(x) \in \mathcal{A}$, $v(x) \notin m_x$ such that

$$v(x)\big(w_1(x)w_2'(x) - w_2(x)w_1'(x)\big) = 0.$$

Operations on the local algebra $\mathcal{A}_x$ (25) look identical to those of elementary algebra

$$\frac{w_1(x)}{w_2(x)} + \frac{w_1'(x)}{w_2'(x)} = \frac{w_1(x)w_2'(x) + w_1'(x)w_2(x)}{w_2(x)w_2'(x)}$$

and

$$\frac{w_1(x)}{w_2(x)} \cdot \frac{w_1'(x)}{w_2'(x)} = \frac{w_1(x)w_1'(x)}{w_2(x)w_2'(x)}.$$

Algebras $\mathcal{A}_{U_i}$ on open sets $U_i \subset M$

$$\mathcal{A}_{U_i} = \bigcap_{x \in U_i} \mathcal{A}_x$$

determine the structure sheaf [59] $\mathcal{A}_M = \{\mathcal{A}_{U_i}\}$ on the space-time manifold $\mathcal{M}$. The inverse limit of the structure sheaf $\mathcal{A}_M$ coincides with the algebra $\mathcal{A}$

$$\mathcal{A} = \varprojlim_{U_i \in M} \mathcal{A}_{U_i},$$

where $\{U_i\}$ is the open covering of $\mathcal{M}$.

The spectrum of the algebra $\mathcal{A}$, denoted by $\mathrm{Spec}(A)$, is the set of all prime ideals of $\mathcal{A}$, equipped with the Zariski topology [22] [59] [60]. The prime ideals correspond to irreducible subvarieties of the space $\mathrm{Spec}(A)$. Maximal ideals of the algebra $\mathcal{A}$ correspond to points.

The structure sheaf and the spectrum of the algebra $\mathcal{A}$ are used in definition of schemes [22] [59] [60]. In our case, the scheme over the algebra $\mathcal{A}$ is the pair $(\mathcal{M}, \mathcal{A}_{\mathcal{M}})$ such that there exists an open covering $\{U_i\}$ of $\mathcal{M}$ for which each pair $(U_i, \mathcal{A}_{U_i})$ is isomorphic to $(V_i, \mathcal{O}_{V_i})$, where $\{V_i\}$ is the open covering of $\mathrm{Spec}(A)$ and $\mathcal{O}_{V_i}$ is the restriction of the structure sheaf $\mathcal{O}_{\mathrm{Spec}(A)}$ to each V_i. As a result, one can say that the local isomorphism $\mathcal{M} \cong \mathrm{Spec}(\mathcal{A})$ imposed by the theory of schemes and by restrictions on multiplication on the quantum-field-density distributions in the algebra $\mathcal{A}$ lead to the dependence of the space-time properties on the matter. The arrow of time, the chirality violation of spinor fields, and the charge conjugation symmetry violation in the boson sector are consequences of this dependence.

6. Densities of Composite Fields in the Framework of the Diagram Expansion

Let us consider approximations of Schwinger equation solutions expressed by the diagram expansion and find singularities and wavefronts of composite field densities $w^{\zeta(n)(\mathrm{comp})}$ in relation (11). For this purpose, it needs to define the generating functional of connected Green's functions W. In the abridged notation, the action in the exponent of the formal solution $Z(q)$ (6) of the Schwinger equation can be written in the form

$$\begin{aligned}\frac{i}{\hbar}\left(S(\Psi)+(q,\Psi)\right) &= \sum_{p=1}^{4}\frac{1}{p!}\lambda_p \Psi^p \\ &\equiv \sum_{p=1}^{4}\frac{1}{p!}\sum_{\zeta_1\cdots\zeta_p}\int\cdots\int \lambda_p^{\zeta_1\cdots\zeta_p}\left(x_1\cdots x_p\right)\Psi^{\zeta_1}\left(x_1\right)\cdots\Psi^{\zeta_p}\left(x_p\right)\mathrm{d}x_1\cdots\mathrm{d}x_p,\end{aligned} \tag{26}$$

where $\lambda_1 = \bar{q} = \{\bar{q}^\zeta(x)\} = \{iq^\zeta(x)/\hbar\}$ are the auxiliary fields, λ_2 are the operator variables $-\gamma^\mu\vec{\partial}_\mu - im^{(\alpha)}c/\hbar$, $-i\hbar\Box - im^{(n)2}c^2/\hbar$, and $-i\Box/\hbar$ acted on fermions, bosons and gauge field potentials, respectively. These operators are defined by Equations (7). λ_3 are constants of the three-particle interactions defined by the Lagrangian terms (3) $\bar{\psi}^\alpha\gamma^\mu e_{j(a)}T^\alpha_{a\beta}A^a_\mu\psi^\beta$, $\mu_{\alpha\beta n}\bar{\psi}^\alpha\varphi^n\psi^\alpha$, $\mu^*_{\alpha\beta n}\bar{\psi}^\alpha\varphi^{+n}\psi^\alpha$, by terms with $A^a_\mu A^b_\nu A^c_\rho$, and by terms with $A^a_\mu\varphi^{+n}\varphi^n$. The four-particle constants λ_4 are originated from the Lagrangian terms $\nu\left(\varphi^{+n}\varphi^n\right)^2$ and $e^2_{j(a)}g^{\mu\rho}g^{\nu\sigma}C^a_{bc}C^a_{de}A^b_\mu A^c_\nu A^d_\rho A^e_\sigma$.

By definition, the generating functional of connected Green's functions is written as

$$W(\lambda_1,\lambda_2,\lambda_3,\lambda_4) = \ln Z(\lambda_1,\lambda_2,\lambda_3,\lambda_4) = \ln Z(\bar{q},\lambda_2,\lambda_3,\lambda_4), \tag{27}$$

where Z is defined by relation (1). The Schwinger Equation (4) for the functional W can be written in the form [25]

$$\lambda_1 + \sum_{p=2}^{4}\frac{1}{(p-1)!}\lambda_p H_{p-1} = 0, \tag{28}$$

where

$$H_p = \left(\frac{\delta W}{\delta\lambda_1} + \frac{\delta}{\delta\lambda_1}\right)^p \cdot 1.$$

Solution of the Schwinger Equation (28) can be found by iterations in the form of the power series expansion for the functional W with respect to the vertices λ_3, λ_4. In the zero approximation $(\lambda_3 = \lambda_4 = 0)$ the formal solution (28) of the functional W is written as

$$W^{(0)} = \frac{\kappa}{2} \operatorname{tr} \ln\left(-\lambda_2^{-1}\right),$$

where $\kappa = 1$ for bosons and $\kappa = -1$ for fermions, respectively. $-\lambda_2^{-1}(x_1 - x_2)$ is the kernel of the inverse operator $-\lambda_2$ called the propagator. The next iteration can be found by the substitution of $W^{(0)}$ for W in terms H_{p-1} in Equation (28) and so on. The third order vertex approximation of the functional $W(\lambda_1, \lambda_2, \lambda_3, \lambda_4)$ is presented in Figure 3. We assign solid lines to the propagators $-\lambda_2^{-1}$. Propagators $-\lambda_2^{-1}$ connected to single (λ_1), triple (λ_3) and quadruple (λ_4) vertices must be integrated over space-time variables and must be summed over indices ζ.

Taking into account the causality, which means that an effect cannot occur from a cause that is not in the back (past) light cone of that event [61] [62], we use causal Green's functions and propagators. Thus, propagators $-\lambda_2^{-1} = \left\{S_\beta^{c\alpha}(x), D_{nl}^c(x), D_0^c(x)\right\}$ can be written in the following form [61].

For fermions

$$S_\beta^{c\alpha}(x) = \left(i\gamma^\mu \partial_\mu + m^{(\alpha)} c/\hbar\right) \delta_\beta^\alpha D^c(x),$$

for bosons

$$D_{nl}^c(x) = D^c(x)\delta_{nl},$$

and for gauge field potentials

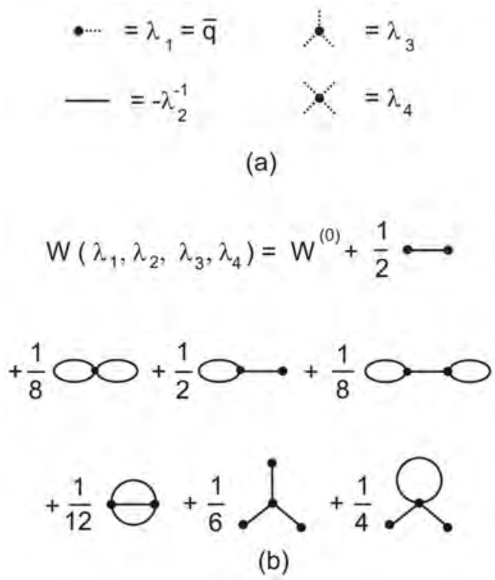

Figure 3. (a) Propagators $-\lambda_2^{-1}$, vertices λ_1, λ_3 and λ_4. (b) The third order vertex approximation of the functional $W(\lambda_1, \lambda_2, \lambda_3, \lambda_4)$. $W^{(0)} = \frac{\kappa}{2} \operatorname{tr} \ln\left(-\lambda_2^{-1}\right)$.

$$D_0^c(x) = D^c(x)\Big|_{m=0}, \tag{29}$$

where

$$D^c(x) = \theta(t)D^-(x) - \theta(-t)D^+(x),$$

$$D^\pm(x) = \frac{1}{4\pi}\varepsilon(t)\delta(\rho) \mp \frac{mi}{8\pi\sqrt{\rho}}\theta(\rho)\Big[N_1\big(m\sqrt{\rho}\big) \mp i\varepsilon(t)J_1\big(m\sqrt{\rho}\big)\Big]$$
$$\mp \frac{mi}{4\pi^2\sqrt{-\rho}}\theta(-\rho)K_1\big(m\sqrt{-\rho}\big),$$

$$\rho = (ct)^2 - x^2$$
$$\varepsilon(t) = \theta(t) - \theta(-t).$$

$N_1(x)$, $J_1(x)$, $K_1(x)$ are Neumann, Bessel and Hankel functions, respectively. Propagators $-\lambda_2^{-1}$ (29) are equal to zero in the light-cone exterior and have singularities on the light cone. Taking this into account, we find singularities and wavefronts of composite field densities $w^{\zeta(n)(\mathrm{comp})}$, which can be written as a derivative of the functional W

$$\begin{aligned} w^{\zeta(n)(\mathrm{comp})}(x) &= \left(\frac{i}{\hbar}\right)^n \bar{w}^{\zeta_1,\cdots,\zeta_n(\mathrm{comp})}(x) \\ &= \left(\frac{i}{\hbar}\right)^n \frac{\delta^n W}{\underbrace{\delta\bar{q}^{\zeta_1}(x_1)\cdots\delta\bar{q}^{\zeta_n}(x_n)}_{n}}\Bigg|_{x_1,\cdots,x_n\to x} \\ &= \left(\frac{i}{\hbar}\right)^n \lim_{x_1,\cdots,x_n\to x}\sum_p \int\cdots\int\left(-\lambda_2^{\zeta_1}\right)^{-1}(x_1 - z_1) \\ &\quad \cdots\left(-\lambda_2^{\zeta_n}\right)^{-1}(x_n - z_n)A^{(p)}(z_1,\cdots,z_n)\mathrm{d}z_1\cdots\mathrm{d}z_n, \end{aligned} \tag{30}$$

where n is the number of fields, $A^{(p)}(z_1,\cdots,z_n)$ is the residual part of the diagram which is depicted by the index p. Summation is drawn out over all diagrams. Differentiation of the functional W with respect to auxiliary fields $\bar{q}^{\zeta}$ results in the removal of the corresponding λ_1-vertices in diagrams. In **Figure 4** hollow single vertices denote the removed λ_1-vertices and, therefore, the corresponding differentiation operation. For these vertices the integration over space-time variables and the summation over indices ζ must be dropped out. In this case, singularities of derivations of the functional W (30) are determined by propagators $-\lambda_2^{-1}$ (29) connected with hollow single vertices and the composite field densities $w^{\zeta(n)(\mathrm{comp})}$ have singularities on the light cone. Thus, wavefronts $\mathrm{WF}\left(w^{\zeta(n)(\mathrm{comp})}\right)$ in relation (11) are included in the characteristics $\mathrm{Char}\left(\mathcal{N}_\zeta^\eta\right)$ and wavefront sets of quantum-field density distributions are located on the light cone.

Now we return to relation (11) and consider a possible extension of the wavefront set $\mathrm{WF}\left(w^\zeta\right)$ formed by wavefronts $\mathrm{WF}\left(w^{\zeta(n)(\mathrm{comp})}\right)$ of composite fields. In other words, can wavefronts $\mathrm{WF}\left(w^{\zeta(n)(\mathrm{comp})}\right)$ of composite fields vary the wavefront set $\mathrm{WF}\left(w^\zeta\right)$ without loss of multiplication in the algebra $\mathcal{A}$?

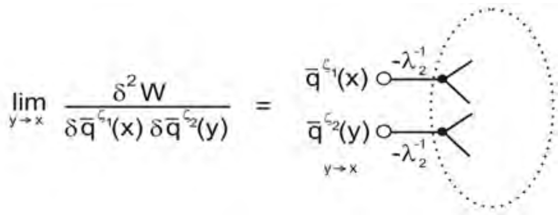

Figure 4. Differentiation of the functional W with respect to the auxiliary fields $\bar{q}^{\zeta_1}(x)$ and $\bar{q}^{\zeta_2}(y)$. Hollow single vertices denote the differentiation operation. The dotted line bounds residual part of the diagram.

According to the above-mentioned, one can see that the only possible case, in which the multiplication of distributions of quantum-field densities can be defined, is the case, when the quantum fields are in the space-time manifold $\mathcal{M}$ with the structure group $SO(3,1)$. Let us assume that wavefronts of $w^{\zeta(n)(\text{comp})}(x)$ are in the space-like region $\Gamma^{(s)}$ (**Figure 1(b)**) and wavefronts $\text{WF}\left(w^{\zeta(n)(\text{comp})}\right)$ take part to the wavefront $\text{WF}\left(w^{\zeta}\right)$. The transformation f of the space-time manifold $\mathcal{M}$ induced by a rectilinear motion transforms the wavefront of densities $\text{WF}\left(w^{\zeta}\right)$ in relation (14) such that in the space-like region $\Gamma^{(s)}$ the covector inversion $\xi \mapsto -\xi \in \text{WF}\left(w^{\zeta}\right)$ can be reached by the arcwise connected part of the group $SO(3,1)$. Consequently, the extension of the wavefront set $\text{WF}\left(w^{\zeta}\right)$ on the space-like region $\Gamma^{(s)}$ should be ignored because the multiplication on these distributions is impossible. The extension on the past light cone $\Gamma^{(p)}$ should be ignored too because one can find covectors $\xi_1 \in \Gamma^{(f)}$ and $\xi_2 \in \Gamma^{(p)}$ such that $\xi_1 + \xi_2 = 0$. Thus, the multiplication on the densities $w^{\zeta}(x)$ can be defined in the only case, in which the densities are distributions with the wavefront set $\text{WF}\left(w^{\zeta}\right) \in \Gamma^{(f)}$.

7. Diagram Expansion with Respect to the *A*-Algebra Variables

The multiplication on the commutative density distribution algebra $\mathcal{A}$ gives us possibility to define differentiation of functionals of $\mathcal{A}$-algebra variables and to construct diagram expansion with respect to densities. Let us assume that functionals can be given in the form of power series with respect to the densities $w = \left\{w^{\zeta_1}(x), \cdots, w^{\zeta_m}(x)\right\} \in \mathcal{A}$

$$R(w) = \sum_{n=0}^{\infty} \sum_{\zeta_1 \cdots \zeta_n} \int \cdots \int F^{\zeta_1 \cdots \zeta_n}(x_1 \cdots x_n) w^{\zeta_1}(x_1) \cdots w^{\zeta_n}(x_n) \mathrm{d}x_1 \cdots \mathrm{d}x_n. \quad (31)$$

The differentiation of the functional $R(w)$ with respect to the density $w^{\xi_p}(x_p)$ is reduced to the elimination of the density $w^{\xi_p}(x_p)$ and to the dropping out the integral over variables x_p in the power series (31)

$$\begin{aligned} \frac{\delta R(w)}{\delta w^{\xi_p}(x_p)} &= \sum_{n=0}^{\infty} \sum_{\zeta_1, \cdots, \hat{\xi}_p, \cdots, \zeta_n} \int \cdots \int F^{\zeta_1 \cdots \zeta_n}(x_1 \cdots x_n) \\ &\times \prod_{k=0}^{p-1} \kappa_{pk} \underbrace{w^{\zeta_1}(x_1) \cdots \hat{w}^{\xi_p}(x_p) \cdots w^{\zeta_n}(x_n)}_{n-1} \mathrm{d}x_1 \cdots \mathrm{d}\hat{x}_p \cdots \mathrm{d}x_n, \end{aligned} \quad (32)$$

where the mark $\hat{}$ points out that the given variable must be dropped. The summation over indices $\zeta_1,\cdots,\hat{\xi}_p,\cdots,\zeta_n$ in relation (32) is performed over all sets $\{\hat{\xi}_p,\zeta_2,\cdots,\zeta_n\}$, $\cdots$, $\{\zeta_1,\cdots,\zeta_{n-1},\hat{\xi}_p\}$. Since the densities $w^{\zeta_i}(x_i)$ can be Grassmanian variables, we define the differentiation as left one. The term $\prod_{k=0}^{p-1}\kappa_{pk}$ appears from permutations between densities $w^{\zeta_i}(x_i)$ during the differentiation. $\kappa_{pk}=(-1)^{\deg w^p\cdot\deg w^k}$ depends on parity degrees $\deg w^p$, $\deg w^k$ of densities $w^{\xi_p}(x_p)$, $w^{\zeta_k}(x_k)$.

In order to construct diagram expansion of Schwinger equation solutions with respect to densities $w^{\zeta}(x)$ belonging to the $\mathcal{A}$-algebra, we use the first Legendre transform of the generating functional W. The technique of Legendre transforms makes it possible to find anomalous solutions of the Schwinger equations (4) and (28). Anomalous solutions contain nonperturbative information about quantum field models at spontaneous symmetry breaking and at phase transitions [25] [63] [64] [65]. Furthermore, the use of the diagram expansion of the Legendre transform greatly reduces the number of diagrams. The first Legendre transform Y of the functional W is defined as [25]

$$Y(\overline{w};\lambda_2,\lambda_3,\lambda_4)=W(\overline{q},\lambda_2,\lambda_3,\lambda_4)-\sum_{\zeta}\int\overline{w}^{\zeta}(x)\overline{q}^{\zeta}(x)\mathrm{d}x, \tag{33}$$

where the functional W is defined by relation (27) and

$$\overline{w}^{\zeta}(x)=\frac{\hbar}{i}w^{\zeta}(x)=\frac{\vec{\delta}W(\overline{q})}{\delta\overline{q}^{\zeta}(x)}. \tag{34}$$

Taking into account relations (33) and (34), one can obtain the variable $\overline{q}^{\zeta}(x)$ as the functional of the density $\overline{w}^{\zeta}(x)$

$$\frac{\vec{\delta}Y(\overline{w})}{\delta\overline{w}^{\zeta}(x)}=-\overline{q}^{\zeta}(x). \tag{35}$$

The Schwinger Equation (4) for the functional Y can be written in the form [25]

$$\frac{\vec{\delta}Y}{\delta\overline{w}}=\lambda_2\overline{w}+\sum_{p=3}^{4}\frac{1}{(p-1)!}\lambda_p H_{p-1}, \tag{36}$$

where in the abridged notation

$$H_p=\left[\overline{w}-\left(\frac{\vec{\delta}^2Y}{\delta\overline{w}^2}\right)^{-1}\frac{\vec{\delta}}{\delta\overline{w}}\right]^{p-1}\overline{w}$$

and

$$\left(\frac{\vec{\delta}^2Y}{\delta\overline{w}^2}\right)^{-1}$$

is the kernel of the inverse operator of

$$\int\frac{\vec{\delta}^2Y}{\delta\overline{w}(x)\delta\overline{w}(y)}f(y)\mathrm{d}y.$$

By analogy with solutions of Equation (28), solution of the Schwinger equation (36) can be found by iterations in the form of the power series expansion for the functional Y with respect to the vertices λ_3, λ_4. In the zero approximation $(\lambda_3=\lambda_4=0)$ the formal solution (36) is the Gaussian functional integral and the functional Y is written as

$$Y^{(0)}(\bar{w};\lambda_2)=\frac{\kappa}{2}\operatorname{tr}\ln\left(-\lambda_2^{-1}\right)+\frac{1}{2}\bar{w}\lambda_2\bar{w},$$

where $\kappa=1$ for bosons and $\kappa=-1$ for fermions, respectively. The next iteration can be found by the substitution of $Y^{(0)}$ for Y in the term H_2 in equation (36) and so on. In diagrams describing these iterations propagators $-\lambda_2^{-1}$, vertices λ_3 and λ_4 remain the same as shown in diagrams in Section VI. The λ_1 -vertices should be removed from diagrams and the variables $\bar{w}$ should be included. The first order vertex approximation of the functional $Y(\bar{w};\lambda_2,\lambda_3,\lambda_4)$ is presented in **Figure 5**. We assign wavy lines to the variables $\bar{w}$. Propagators $-\lambda_2^{-1}$ and variables $\bar{w}$ connected to triple (λ_3) and quadruple (λ_4) vertices must be integrated over space-time variables and must be summed over indices ζ.

The anomalous solution is found as an extremum

$$\left.\frac{\delta\Phi}{\delta\bar{w}^{\zeta}(x)}\right|_{\bar{w}_0^{\zeta}}=0$$

at the stationarity point $\bar{w}_0^{\zeta}(x)$ of the functional

$$\Phi(\bar{w};\lambda_1,\lambda_2,\lambda_3,\lambda_4)=Y(\bar{w};\lambda_2,\lambda_3,\lambda_4)+\sum_{\zeta}\int\bar{w}^{\zeta}(x)\bar{q}^{\zeta}(x)\mathrm{d}x.$$

In order to find the anomalous solution, the Legendre transform Y should be given in the relevant diagram approximation.

The natural next step should be to go from bare to dressed lines in diagrams, which requires analysis based on the second Legendre transform of the functional W. But, it should be noted that in the generating functional W (27) coefficients λ_2 are operator variables. Since, differential operators and density distributions $w^{\zeta}(x)$ form a noncommutative algebra, the differentiation of the functional W with respect to λ_2 may be incorrect. This is required accurate definition of the functional derivative $\delta W/\delta\lambda_2$ and, consequently, the second Legendre transform. This problem is planed to consider in the next study. In contrast with this case, in models in statistical physics (for example, for the classical non-ideal gas and for the Ising model) coefficients λ_2 are not operator variables and the second Legendre transform is well defined [25].

8. Conclusions

In summary, in this paper in the framework of the scheme theory we describe the dependence between quantum fields and properties of the 4-dimensional space-time manifold $\mathcal{M}$. Contrary to algebras of smooth functions, densities of quantum fields, which can be found from the Schwinger equation, are distributions and, in the common case, do not form an algebra. In order to determine

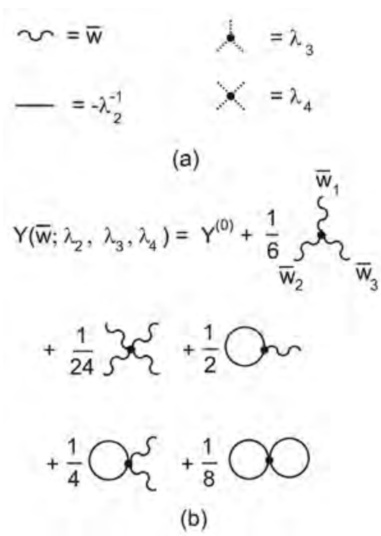

Figure 5. (a) Propagators $-\lambda_2^{-1}$, vertices λ_3, λ_4, and variables $\bar{w}$. (b) The first order vertex approximation of the functional $Y\left(\bar{w};\lambda_2,\lambda_3,\lambda_4\right)$. $Y^{(0)}=\frac{\kappa}{2}\operatorname{tr}\ln\left(-\lambda_2^{-1}\right)+\frac{1}{2}\bar{w}\lambda_2\bar{w}$.

the commutative algebra $\mathcal{A}$ of distributions of quantum-field densities, ideals and its spectrum, it is necessary to define multiplication on densities and to eliminate those densities, which cannot be multiplied. This leads to essential restrictions imposed on densities forming the algebra $\mathcal{A}$. Taking into account that in the framework of the scheme theory the space-time manifold $\mathcal{M}$ is locally isomorphic to the spectrum of the algebra $\mathcal{A}$, $\mathcal{M}\cong\operatorname{Spec}(\mathcal{A})$, and points of the manifold $\mathcal{M}$ are defined as maximal ideals of quantum-field density distributions, the restrictions caused by the possibility to define multiplication on the density distributions result in the following properties of the space-time manifold $\mathcal{M}$.

1) The only possible case, when the commutative algebra $\mathcal{A}$ of distributions of quantum-field densities exist, is the case, when the quantum fields are in the space-time manifold $\mathcal{M}$ with the structure group $SO(3,1)$ (Lorentz group). On account of the local isomorphism $\mathcal{M}\cong\operatorname{Spec}(\mathcal{A})$, the quantum fields exist only in the space-time manifold with the one-dimensional time.

2) We must exclude field density distributions with singularities in the past light cone $\Gamma^{(p)}$. The algebra $\mathcal{A}$ consists of the density distributions $w^{\zeta}(x)$ with wavefronts in the closed future light cone subset, $\mathrm{WF}\left(w^{\zeta}(x)\right)\subset\Gamma^{(f)}\subset T^{*}\mathcal{M}$. In this case, we have the one-way direction of time and there is not the symmetry of time on the density distributions. The arrow of time is pointing towards the future.

3) The restrictions caused by multiplication on the density distributions can explain the chirality violation of spinor fields. The densities of right-handed and left-handed fermion states $P\psi_R^{\alpha}(x)$, $P\psi_L^{\alpha}(x)$, $P\bar{\psi}_R^{\alpha}(x)$, $P\bar{\psi}_L^{\alpha}(x)$, $C\psi_R^{\alpha}(x)$, $C\psi_L^{\alpha}(x)$, $C\bar{\psi}_R^{\alpha}(x)$, $C\bar{\psi}_L^{\alpha}(x)$, where P is the space reflection and C

is the charge conjugation, are forbidden and are not contained in the algebra $\mathcal{A}$. The commutative algebra $\mathcal{A}$ contains densities $w^{\zeta}(x)$ of states $\psi_R^{\alpha}(x)$, $\psi_L^{\alpha}(x)$, $\bar{\psi}_R^{\alpha}(x)$, $\bar{\psi}_L^{\alpha}(x)$, $CP\psi_R^{\alpha}(x)$, $CP\psi_L^{\alpha}(x)$, $CP\bar{\psi}_R^{\alpha}(x)$, $CP\bar{\psi}_L^{\alpha}(x)$, their sums and products.

4) For bosons (for example, in the Higgs sector) the densities of states $C\varphi^{n}(x)$ and $C\varphi^{+n}(x)$, where $\varphi^{n}(x)\neq\varphi^{+n}(x)$, must be excluded from the algebra $\mathcal{A}$. The algebra $\mathcal{A}$ contains densities of $\varphi^{n}(x)$ and $\varphi^{+n}(x)$. This leads to the charge conjugation symmetry violation and can explain the observed matter-antimatter imbalance.

5) Multiplication on distributions in the density distribution algebra $\mathcal{A}$ imposes restrictions on theoretical models with non-abelian gauge fields. In the framework of the scheme theory instanton distributions are impossible and, therefore, tunneling effects between different topological vacua $|n\rangle$ do not occur. This leads to a degeneration of the energy density of the θ-vacuum with respect to the phase θ, to zero value of the Pontryagin index Q and to zero value of the neutron electric dipole moment.

The well-defined multiplication on the density distributions $w^{\zeta}(x)$ and the commutability of the algebra $\mathcal{A}$ give the possibility to construct diagram expansion with respect to the $\mathcal{A}$-algebra variables. The technique of Legendre transforms makes it possible to find anomalous solutions of the Schwinger equation.

Conflicts of Interest

The author declares no conflicts of interest regarding the publication of this paper.

References

[1] Bars, I. (2000) *Physical Review D*, **62**, Article ID: 046007. https://doi.org/10.1103/PhysRevD.62.105018

[2] Bars, I. (2006) *Physical Review D*, **74**, Article ID: 085019. https://doi.org/10.1103/PhysRevD.74.085019

[3] Bars, I., Terning, J. and Nekoogar, F. (2010) Extra Dimensions in Space and Time. Springer, New York. https://doi.org/10.1007/978-0-387-77638-5

[4] Tegmark, M. (1997) *Classical and Quantum Gravity*, **14**, L69-L75. https://doi.org/10.1088/0264-9381/14/4/002

[5] Chappell, J.M., Hartnett, J.G., Iannella, N., Iqbal, A. and Abbott, D. (2006) *Frontiers in Physics*, **4**, Article 44. https://doi.org/10.3389/fphy.2016.00044

[6] Velev, M.V. (2012) *Physics Essays*, **25**, 403-438. https://doi.org/10.4006/0836-1398-25.3.403

[7] Lebowitz, J.L. (1993) *Physics Today*, **46**, 32-38. https://doi.org/10.1063/1.881363

[8] Kiefer, C. and Zeh, H.D. (1995) *Physical Review D*, **51**, 4145-4153. https://doi.org/10.1103/PhysRevD.51.4145

[9] Zeh, H.D. (2010) The Physical Basis of The Direction of Time (The Frontiers Collection). 5th Edition, Springer, Berlin.

[10] Jennings, D. and Rudolph, T. (2010) *Physical Review E*, **81**, Article ID: 061130. https://doi.org/10.1103/PhysRevE.81.061130

[11] Mersini-Houghton, L. and Vaas, R. (2012) The Arrows of Time. A Debate in Cosmology. Springer, Berlin. https://doi.org/10.1007/978-3-642-23259-6

[12] Bousso, R. (2012) *Physical Review D*, **86**, Article ID: 123509. https://doi.org/10.1103/PhysRevD.86.123509

[13] Smolin, L. (2013) Time Reborn: From the Crisis in Physics to the Future of the Universe. Houghton Mifflin Harcourt, New York.

[14] Huang, K. (1982) Quarks, Leptons and Gauge Fields. World Scientific, Singapore. https://doi.org/10.1142/0001

[15] Cheng, T.-P. and Li, L.-F. (1984) Gauge Theory of Elementary Particle Physics. Clarendon Press, Oxford.

[16] Barron, L.D. (2012) *Chirality*, **24**, 957-958. https://doi.org/10.1002/chir.22106

[17] Shu, J. and Zhang, Y. (2013) *Physical Review Letters*, **111**, Article ID: 091801. https://doi.org/10.1103/PhysRevLett.111.091801

[18] Cirigliano, V., Dekens, W., de Vries, J. and Mereghetti, E. (2016) *Physical Review D*, **94**, Article ID: 016002. https://doi.org/10.1103/PhysRevD.94.034031

[19] Carena, M., Ellis, J., Lee, J.S., Pilaftsis, A. and Wagner, C.E.M. (2016) *Journal of High Energy Physics*, **123**, 38. https://doi.org/10.1007/JHEP02(2016)123

[20] Englert, Ch., Nordström, K., Sakurai, K. and Spannowsky, M. (2017) *Physical Review D*, **95**, Article ID: 015018. https://doi.org/10.1103/PhysRevD.95.015018

[21] Goodsell, M.D. and Staub, F. (2017) *The European Physical Journal C*, **77**, 46. https://doi.org/10.1140/epjc/s10052-017-5259-x

[22] Grothendieck, A. (1961-1967) Eléments de Géométrie Algébrique, I-IV. Publications Mathématiques de lIHES, 4, 8, 11, 17, 20, 24, 28 and 32.

[23] Cartier, P. (2001) *Bulletin of the American Mathematical Society*, **38**, 389-408. https://doi.org/10.1090/S0273-0979-01-00913-2

[24] Schwinger, J. (1951) *Proceedings of the National Academy of Sciences*, **37**, 452-459. https://doi.org/10.1073/pnas.37.7.452

[25] Vasiliev, A.N. (1998) Functional Methods in Quantum Field Theory and Statistical Physics. Gordon and Breach, London.

[26] Lutsev, L.V. (2007) *Journal of Physics A*: *Mathematical and Theoretical*, **40**, 11791-11814. https://doi.org/10.1088/1751-8113/40/39/007

[27] Lutsev, L.V. (2009) Diagram Technique for Quantum Models with Internal Lie-Group Dynamics. In: Levy, M.B., Ed., *Mathematical Physics Research Developments*, Nova Science Publishers, New York, 141-188.

[28] Hörmander, L. (1971) *Acta Mathematica*, **127**, 79-183. https://doi.org/10.1007/BF02392052

[29] Radzikowski, M. (1996) *Communications in Mathematical Physics*, **179**, 529-553. https://doi.org/10.1007/BF02100096

[30] Brunetti, R. and Fredenhagen, K. (2000) *Communications in Mathematical Physics*, **208**, 623-661. https://doi.org/10.1007/s002200050004

[31] Strohmaier, A., Verch, R. and Wollenberg, M. (2002) *Journal of Mathematical Physics*, **43**, 5514-5530. https://doi.org/10.1063/1.1506381

[32] Brouder, Ch., Dang, N.V. and Helein, F. (2014) *Journal of Physics A*: *Mathematical and Theoretical*, **47**, Article ID: 443001.

https://doi.org/10.1088/1751-8113/47/44/443001

[33] Treves, F. (1982) Introduction to Pseudo-Differential and Fourier Integral Operators. Plenum Press, New York and London.

[34] Dubrovin, B.A., Fomenko, A.T. and Novikov, S.P. (1992) Modern Geometry—Methods and Applications. Part I. The Geometry of Surfaces, Transformation Groups, and Fields. Second Edition, Springer, New York.

[35] Hörmander, L. (1985) The Analysis of Linear Partial Differential Operators. Volume 1: Distribution Theory and Fourier Analysis. Springer-Verlag, Berlin. https://doi.org/10.1007/978-3-662-30724-3_1

[36] Hörmander, L. (1985) The Analysis of Linear Partial Differential Operators. Volume 4: Fourier Integral Operators. Springer-Verlag, Berlin.

[37] Davydov, A.S. (1976) Quantum Mechanics. Pergamon Press, Oxford.

[38] Englert, F. and Brout, R. (1964) *Physical Review Letters*, **13**, 321-323. https://doi.org/10.1103/PhysRevLett.13.321

[39] Higgs, P.W. (1964) *Physics Letters*, **12**, 132-133. https://doi.org/10.1016/0031-9163(64)91136-9

[40] Higgs, P.W. (1964) *Physical Review Letters*, **13**, 508-509. https://doi.org/10.1103/PhysRevLett.13.508

[41] Gunion, J.F. and Haber, H.E. (2003) *Physical Review D*, **67**, Article ID: 075019. https://doi.org/10.1103/PhysRevD.67.075019

[42] Branco, G.C., Ferreira, P.M., Lavoura, L., Rebelo, M.N., Sher, M. and Silva, J.P. (2012) *Physics Reports*, **516**, 1-102. https://doi.org/10.1016/j.physrep.2012.02.002

[43] Haber, H.E. and Kane, G.L. (1985) *Physics Reports*, **117**, 75-263. https://doi.org/10.1016/0370-1573(85)90051-1

[44] Baer, H. and Tata, X. (2006) Weak Scale Supersymmetry: From Superfields to Scattering Events. Cambridge Univ. Press, Cambridge. https://doi.org/10.1017/CBO9780511617270

[45] Bott, R. (1959) *Annals of Mathematics*, **70**, 313-337. https://doi.org/10.2307/1970106

[46] Dubrovin, B.A., Fomenko, A.T. and Novikov, S.P. (1985) Modern Geometry-Methods and Applications: Part II, the Geometry and Topology of Manifolds. Graduate Texts in Mathematics, Vol. 104, Springer Verlag, New York.

[47] Rajaraman, R. (1982) Solitons and Instantons. An Introduction to Solitons and Instantons in Quantum Field Theory. North-Holland Publishing Company, Amsterdam.

[48] Jackiw, R. and Rebbi, C. (1976) *Physical Review Letters*, **37**, 172-175. https://doi.org/10.1103/PhysRevLett.37.172

[49] Callan, C.G., Dashen, R.F. and Gross, D.J. (1976) *Physics Letters*, **63B**, 334-340. https://doi.org/10.1016/0370-2693(76)90277-X

[50] ‘t Hooft, G. (1976) *Physical Review Letters*, **37**, 8-11. https://doi.org/10.1103/PhysRevLett.37.8

[51] Wilczek, F. (1978) *Physical Review Letters*, **40**, 279-282. https://doi.org/10.1103/PhysRevLett.40.279

[52] Llewellyn Smith, C.H. (1982) *Philosophical Transactions of the Royal Society of London A*, **304**, 5-22.

[53] Schäfer, T. and Shuryak, E.V. (1998) *Reviews of Modern Physics*, **70**, 323-425.

https://doi.org/10.1103/RevModPhys.70.323

[54] Bitar, K.M. and Chang, S.-J. (1978) *Physical Review D*, **17**, 486-497. https://doi.org/10.1103/PhysRevD.17.486

[55] de Vega, H.J., Gervais, J.L. and Sakita, B. (1978) *Nuclear Physics B*, **143**, 125-147. https://doi.org/10.1016/0550-3213(78)90451-0

[56] Crewther, R.J., Di Vecchia, P., Veneziano, G. and Witten, E. (1979) *Physics Letters*, **88B**, 123. https://doi.org/10.1016/0370-2693(79)90128-X

[57] Cox, D., Little, J. and O'Shea, D. (1998) Ideals, Varieties, and Algorithms. Springer-Verlag, New York. https://doi.org/10.1007/978-1-4757-2693-0

[58] Lang, S. (2002) Algebra. Graduate Texts in Mathematics. Springer-Verlag, Berlin. https://doi.org/10.1007/978-1-4613-0041-0

[59] Mumford, D. (1999) The Red Book of Varieties and Schemes. Springer-Verlag, Berlin. https://doi.org/10.1007/b62130

[60] Eisenbud, D. and Harris, J. (1998) The Geometry of Schemes. Springer-Verlag, Berlin.

[61] Bogoliubov, N.N. and Shirkov, D.V. (1980) Introduction to the Theory of Quantized Field. John Wiley & Sons, New York.

[62] Bohm, D. (2005) Causality and Chance in Modern Physics. Taylor and Francis, London.

[63] Vasil'ev, A.N. and Kazanskii (1973) *Theoretical and Mathematical Physics*, **14**, 215-226. https://doi.org/10.1007/BF01029302

[64] De Dominicis, C. and Martin, P.C. (1964) *Journal of Mathematical Physics*, **5**, 14-30. https://doi.org/10.1063/1.1704062

[65] De Dominicis, C. and Martin, P.C. (1964) *Journal of Mathematical Physics*, **5**, 31-59. https://doi.org/10.1063/1.1704064

Journal of Modern Physics, 2019, 10, 824-834
http://www.scirp.org/journal/jmp
ISSN Online: 2153-120X
ISSN Print: 2153-1196

Templates for Quantifying Clay Type and Clay Content from Magnetic Susceptibility and Standard Borehole Geophysical Measurements

David K. Potter[1*], Arfan Ali[2], Salem Abdalah[3]

[1]Department of Physics, University of Alberta, Edmonton, Canada
[2]Brunei Shell Petroleum, Sendirian Berhad, Brunei Darussalam
[3]Institute of Petroleum Engineering, Heriot-Watt University, Edinburgh, UK
Email: *dkpotter@ualberta.ca

How to cite this paper: Potter, D.K., Ali, A. and Abdalah, S. (2019) Templates for Quantifying Clay Type and Clay Content from Magnetic Susceptibility and Standard Borehole Geophysical Measurements. *Journal of Modern Physics*, **10**, 824-834.
https://doi.org/10.4236/jmp.2019.107055

Received: May 13, 2019
Accepted: June 21, 2019
Published: June 24, 2019

Abstract

This paper proposes a rapid means of identifying clay type and quantifying clay content from new template crossplots that compare magnetic susceptibility measurements with standard borehole well log data. The templates are similar in format to standard industry charts, but have a number of advantages over the commonly used charts. Laboratory measurements of magnetic susceptibility on core samples and drill cuttings have recently shown strong correlations with key petrophysical parameters, particularly clay content and fluid permeability [1] [2]. A new template crossplot between magnetic susceptibility and borehole spectral gamma ray log data can firstly help to quickly identify the types of clay present in the formation. Additional new template crossplots between magnetic susceptibility and borehole bulk density data allow the mineral contents and porosities of binary mixtures of clay minerals and matrix minerals (such as illite clay + quartz) to be rapidly quantified. The templates can use ambient (room temperature) magnetic susceptibility data from measurements on core samples or drill cuttings in the laboratory or at the wellsite. Furthermore, the paper shows how the templates can potentially be extended to utilize borehole magnetic susceptibility data for *in situ* estimations of the type and content of clay. This requires accounting for the temperature dependence of the magnetic susceptibility of paramagnetic minerals (such as illite clay), which varies with depth in a borehole. Whilst borehole magnetic susceptibility measurements are rarely part of standard well logging operations, they could be a potentially useful tool for *in situ* clay type and content quantification, which in turn can help predict fluid permeability.

Keywords

Magnetic Susceptibility, Clay, Spectral Gamma Ray, Bulk Density, Borehole

Logs, Temperature Dependence, Core, Drill Cuttings

1. Introduction

Standard industry charts for identifying mineralogy, such as the widely used Schlumberger well logging interpretation charts [3], concentrate on the bulk matrix minerals quartz (SiO_2) for clastic reservoirs, and calcite ($CaCO_3$) and dolomite ($CaMg(CO_3)_2$) for carbonate reservoirs. Small amounts of other minerals are important components of reservoir rocks, and can have key controls on the petrophysical properties. In particular, the type and content of certain clay minerals (such as fibrous illite) can significantly control the fluid permeability of the rock (*i.e.*, the ability of fluids to flow through the rock). There is little in terms of reference charts for identifying clay minerals, apart from some standard charts using borehole data from spectral gamma ray (e.g., potassium versus thorium crossplot [3]) or using the spectral gamma ray log data in combination with photoelectric log (PEF) data [3]. Whilst a combination of the thorium/potassium ratio and PEF log data can identify clay mineral type within relatively narrow ranges, none of these standard charts can give a quantitative estimate of the clay content.

The purpose of the present paper is to show how the new template crossplots, utilizing magnetic susceptibility measurements in combination with certain standard borehole log data, can rapidly quantify the clay content in addition to identifying the clay type. It has been demonstrated that magnetic susceptibility measurements on core samples [1] and more recently on drill cuttings [2] provide a rapid, non-destructive tool for estimating clay content and relating this to fluid permeability, and other special core analysis (SCAL) parameters such as the cation exchange capacity per unit pore volume, Q_v [1]. We now present some new template crossplots, similar in format to standard industry crossplot charts [3], which utilize magnetic susceptibility and some standard wire line log data (specifically spectral gamma ray and bulk density), as a new tool for rapidly estimating clay type and content. The new crossplots use magnetic susceptibility measurements at ambient temperature undertaken in the laboratory on core samples (core plugs, slabbed core or whole core), or at the wellsite on drill cuttings, to estimate clay type and content. Paramagnetic clays in particular, such as illite, can be a major control on fluid permeability and other petrophysical parameters [1]. The clay content derived from the new template crossplots can subsequently help to rapidly estimate fluid permeability, since strong correlations between magnetically derived illite content and fluid permeability have been demonstrated in core samples [1] and drill cuttings [2], and other petrophysical parameters (such as Q_v), via this "quick look" analysis well before the actual core permeability and other data become available. Whilst there are other methods of determining clay type and content, such as by X-ray diffraction (XRD), these methods can be time consuming, expensive and semi-quantitative.

We envisage our proposed template crossplots as a rapid complement to these other techniques, rather than as a replacement.

We also describe how the templates can potentially be extended to utilize borehole magnetic susceptibility data, in combination with other borehole data, to estimate clay type and content *in situ*. This involves incorporating the temperature dependence on magnetic susceptibility of paramagnetic minerals, and extends our earlier work in this area [4]. Whilst borehole magnetic susceptibility devices are rarely used at present in standard well logging tool strings, our new template crossplots indicate the potential usefulness of running such tools to estimate clay type and content *in situ* straight from the well logging data.

2. Methodologies and New Templates

2.1. Determining Clay Type from a Template Utilizing Magnetic Susceptibility and Standard Borehole Spectral Gamma Ray Data

The first step is to identify the clay type. A rapid new potential way of doing this is to plot borehole spectral gamma ray data against magnetic susceptibility from core samples or drill cuttings. **Figure 1** shows a new plot of thorium/potassium (Th/K) ratio from borehole spectral gamma ray data against mass magnetic susceptibility (at ambient temperature) for mixtures of quartz plus different clay minerals. The Th/K data originates from sources such as [5] and has been utilized in standard industry charts [3], whilst the magnetic susceptibility data comes from four main sources [6] [7] [8] [9]. The mass magnetic susceptibility is J/H where J is the magnetization per unit mass and H is the applied field strength.

Figure 1 would be applicable for laboratory or wellsite magnetic susceptibility measurements on core samples or drill cuttings at ambient (room temperature) conditions (20˚C in our case). Each rectangle represents the range of values from 100% quartz to 100% of the relevant mineral indicated. Each rectangle starts at a mass magnetic susceptibility value of -0.619×10^{-8} m^3 kg^{-1} (100% quartz [9]). Most of the clay minerals shown are paramagnetic (with positive magnetic susceptibility), and as the percentage of each mineral increases the mass magnetic susceptibility increases. For these minerals the top of each rectangle represents 100% of the mineral indicated in the rectangle. For example, the 100% quartz to 100% biotite range is from -0.619×10^{-8} m^3 kg^{-1} to 98×10^{-8} m^3 kg^{-1}. The only exception to this in **Figure 1** is kaolinite, which is diamagnetic with low negative magnetic susceptibility [7] [9], and the bottom of that rectangle represents 100% kaolinite. The different types of clay occupy fairly well defined regions of **Figure 1**. There is a small degree of overlap between the Th/K ratios of illite and muscovite, which is difficult to show on the figure, and the muscovite and biotite magnetic susceptibility values overlap in the region -0.619×10^{-8} m^3 kg^{-1} to 15×10^{-8} m^3 kg^{-1}.

The applicability of **Figure 1** can be extended to utilize borehole magnetic susceptibility data for *in situ* clay typing. For diamagnetic clay minerals, such as

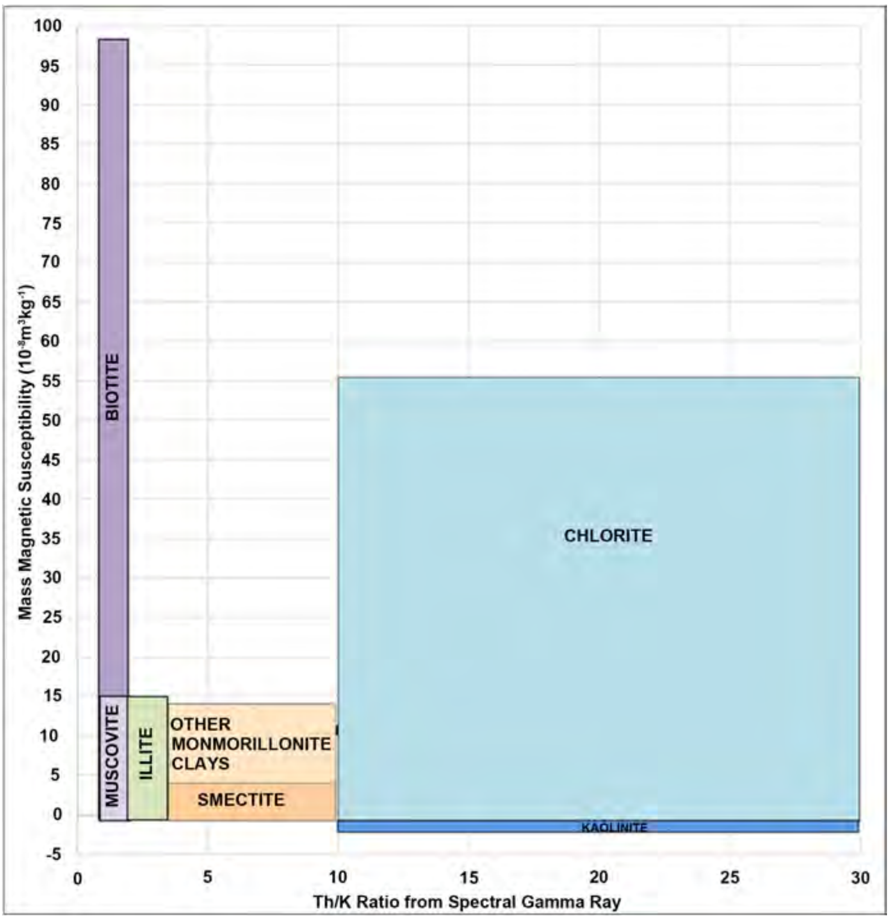

Figure 1. Spectral gamma ray thorium/potassium (Th/K) ratio [5], where Th is in parts per million and K is in per cent, versus mass magnetic susceptibility (at ambient temperature) for mixtures of quartz plus different minerals as indicated. Each rectangle starts at $-0.619 \times 10^{-8}\ m^3\,kg^{-1}$ (100% quartz [9]) on the mass magnetic susceptibility axis, and the rectangles represent the range of values from 100% quartz to 100% of the mineral indicated based on magnetic susceptibility values for those minerals [6] [7] [8] [9]. Note that increasing kaolinite content results in more negative magnetic susceptibility, since kaolinite is diamagnetic [7] [9].

kaolinite, the magnetic susceptibility values for borehole measurements will be identical to those in **Figure 1**, since the magnetic susceptibility of diamagnetic minerals is not dependent on temperature. However, for the paramagnetic clay minerals shown (*i.e.*, illite, chlorite, montmorillonite, smectite, biotite, muscovite) the maximum magnetic susceptibility values shown in **Figure 1** will decrease with increasing temperature according to the Curie Law as follows:

$$J/H = C/T \tag{1}$$

where J is the magnetization per unit mass, H is the strength of the applied magnetic field ($H = B/\mu_0$, where B is the applied field in Tesla and μ_0 is the magnetic permeability of free space), J/H is the mass magnetic susceptibility, C is a mineral specific Curie constant, and T is the absolute temperature in Kelvin. Equation (1) can also be expressed in terms of volume magnetic susceptibility,

M/H, where M is the magnetization per unit volume. Temperature normally increases with depth. If one knows the temperature at any particular depth (most well logging operations include a temperature log), or one knows the depth and the local geothermal gradient (*i.e.*, the variation of temperature with depth at that locality), then the magnetic susceptibility can be calculated. An example of the variation of magnetic susceptibility with temperature for different mixtures of illite clay + quartz is given in our earlier work [4].

Determining clay type from **Figure 1** has a number of advantages as follows:

1) The ranges of the different minerals are much smaller than for charts that use spectral gamma ray data alone, such as standard potassium (in percentage) versus thorium (in parts per million) plots [3].

2) Whilst some standard charts that are derived entirely from borehole data (such as Th/K ratio from the spectral gamma ray log versus PEF from the lithodensity log) also have relatively narrow ranges for the clay minerals, the clay type from **Figure 1** can be obtained via rapid, non-destructive magnetic susceptibility measurements on core samples or drill cuttings without the need to run a PEF log. Furthermore, the use of drill cuttings could be extremely cost effective (compared to core samples which are expensive to obtain) since these are readily available in every drilled well. One might also use portable spectral gamma ray equipment on core or drill cuttings, without the need to run a spectral gamma ray log. Often just the total gamma ray log is run, which is cheaper than running a full spectral gamma ray log.

3) Magnetic susceptibility measurements on core and drill cuttings are much quicker and cheaper than other laboratory techniques for determining clay type and content, such as X-ray diffraction (XRD) [1] [10]. However, if supplementary mineralogical data is available (from XRD, thin sections etc.) then this will help to confirm the binary mineral mixture for the quantification of clay described in Section 2.2 below.

4) Whilst **Figure 1** details binary mixtures of quartz + clay minerals, the figure would be virtually identical (and indistinguishable on the current vertical y-axis scale) if we plotted calcite + clay minerals or dolomite + clay minerals. This is because quartz, calcite and dolomite are all diamagnetic with very similar low, negative magnetic susceptibilities (-0.619×10^{-8} m^3 kg^{-1}, -0.484×10^{-8} m^3 kg^{-1} and -0.480×10^{-8} m^3 kg^{-1} respectively [9]). The advantage of this is that **Figure 1** can be used to identify clay type in clastic (quartz matrix) reservoirs or carbonate (calcite and /or dolomite) reservoirs.

There are, however, some limitations of our proposed clay typing methodology:

1) The method assumes a binary mixture of a matrix mineral (such as quartz or calcite) with a clay mineral. If there is a mixture of more than one clay mineral the point plotted on **Figure 1** will represent the combined effect of all those minerals in the sample, which may make it difficult to identify the individual clay minerals present. Nevertheless, this is also a limitation of the current stan-

dard industry charts based on spectral gamma ray data [3]. Moreover, whilst reservoir rocks can contain several mineral components, there are often two key components that dominate. For example, binary mixtures of quartz + illite are commonly the dominant mineral components in certain conventional reservoirs [1] and unconventional (e.g., shale) reservoirs [11] [12] [13].

2) In some reservoir rocks small amounts of ferrimagnetic minerals (e.g., magnetite, Fe_3O_4) can dominate a low field magnetic susceptibility signal, and obscure the signal from the clays. Any ferrimagnetic minerals in the sample will result in a higher magnetic susceptibility value on **Figure 1** compared to the value from the clay minerals alone. However, this is generally not an issue if one undertakes a high field magnetic susceptibility measurement. At high applied fields (more than about 300 mT) magnetite saturates and no longer contributes to the magnetic susceptibility signal, leaving just the signal from the paramagnetic clays (or other paramagnetic minerals) and the diamagnetic minerals like quartz or calcite [9] [14]. Note that hematite (α-Fe_2O_3) is a rare exception that may need even higher fields to saturate. High field magnetic susceptibility measurements require more specialist equipment than low field measurements, however low field measurements are often sufficient for the present purposes.

2.2. Template Crossplots for Quantifying Clay Content from Magnetic Susceptibility and Standard Borehole Bulk Density Data

The second step in the procedure is to quantify the amount of clay. **Figure 2** shows an example template crossplot of mass magnetic susceptibility (at ambient temperature) versus bulk density for various mixtures of illite clay and quartz, which can be used for quantifying illite (and quartz) by plotting magnetic susceptibility measurements on core samples or drill cuttings in the laboratory or at the wellsite in conjunction with the borehole bulk density data (or core derived bulk density). **Figure 2** assumes a simple mixture of the two components, with the mass magnetic susceptibilities of the end members being 15×10^{-8} m^3 kg^{-1} for 100% illite [8] and -0.619×10^{-8} m^3 kg^{-1} for 100% quartz [9]. The bulk densities were taken as 2.75 g/cm^3 for illite (an average of values given in [15]) and 2.65 g/cm^3 for quartz [3].

Figure 2 also takes account of realistic formation rock porosities ranging from 0% to 40%, and so can also be used as a rapid way to estimate the porosity of the binary mineral mixture. **Figure 2** assumes water filled porosity, as is standard practice for other widely used industry charts [3]. The magnetic susceptibility values will not change significantly if the porosity is filled with water, oil or gas as in most cases these fluids are diamagnetic with quite similar low negative magnetic susceptibilities [16].

Figure 2 has a significant advantage over another commonly used standard industry chart, which uses neutron porosity versus bulk density to estimate porosity and mineralogy of the matrix minerals quartz, calcite and dolomite [3]. If

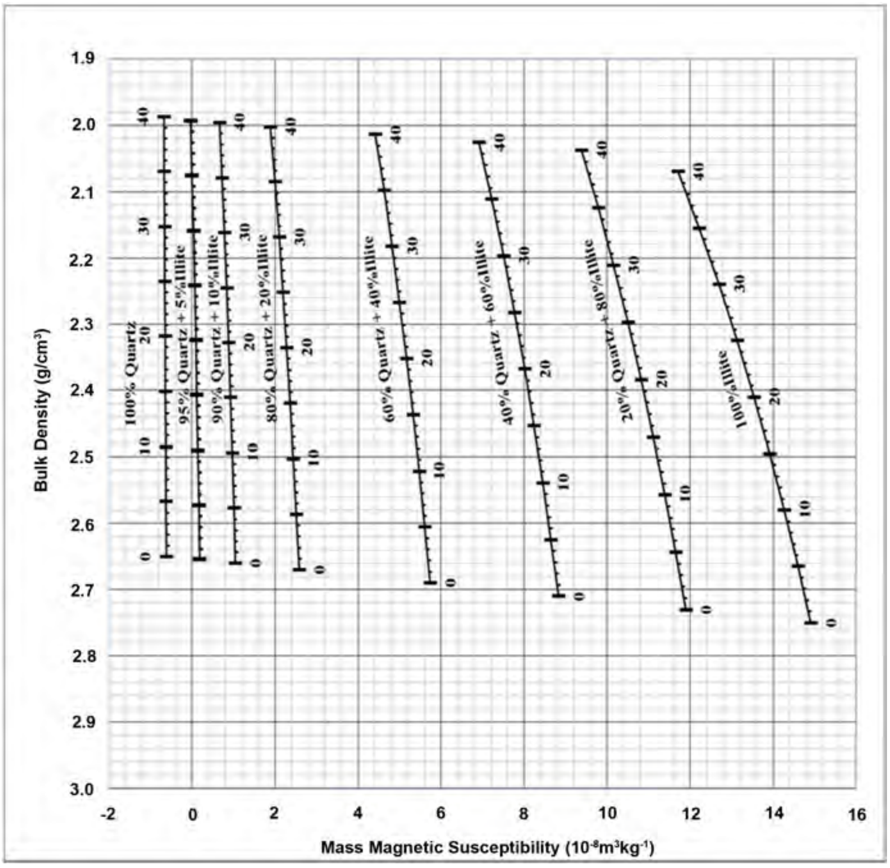

Figure 2. Template crossplot of mass magnetic susceptibility (at ambient temperature) versus bulk density for mixtures of quartz and illite as indicated. The numbers 0, 10, 20, 30 and 40 represent the percentage porosity of the mixture (*i.e.*, 0% to 40%).

there is any clay in the sample the "apparent" neutron porosity increases due to bound water in the clay, and does not reflect the real (lower) porosity of the sample. The neutron tool sees all of the hydrogen in the sample, and it can't distinguish hydrogen in bound water in clay from hydrogen in fluid (*i.e.*, liquid water, hydrocarbons) filled porosity. Our Figure 2, in contrast, utilizes magnetic susceptibility rather than neutron porosity, and the porosities derived from our magnetic susceptibility versus bulk density values will not be adversely affected by the clay present in the samples, and will better reflect the actual porosities of the samples.

Figure 3 is a similar plot to Figure 2, but gives a template for much lower illite contents. Very low percentages of illite clay can have a dramatic effect on a sample's fluid permeability [1], and so it is useful to have a template that is capable of quantifying very small percentages of illite.

2.3. Extending the Templates for Quantifying Clay Content *in Situ* from Borehole Magnetic Susceptibility Measurements Combined with Borehole Bulk Density Data

As discussed in Section 2.1 the magnetic susceptibility of a paramagnetic mineral such as illite clay decreases with increasing temperature (and therefore also

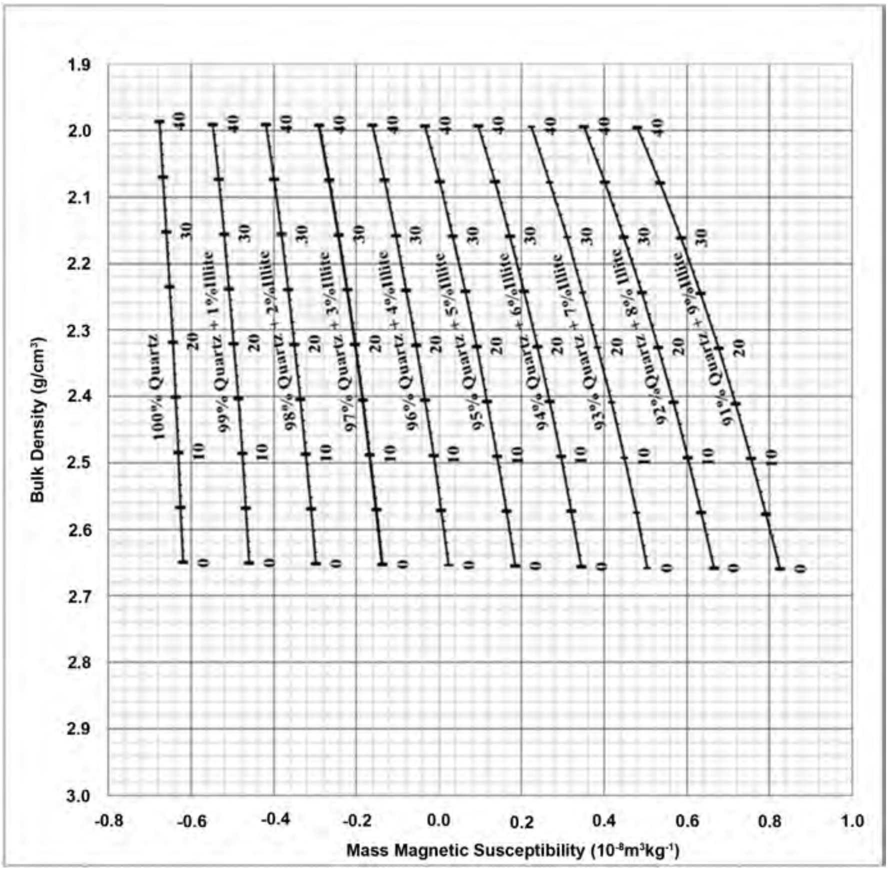

Figure 3. Template crossplot of mass magnetic susceptibility (at ambient temperature) versus bulk density for further mixtures of quartz and illite where the illite content is low (0% - 10%). The numbers 0, 10, 20, 30 and 40 represent the percentage porosity of the mixture (*i.e.*, 0% to 40%).

generally with depth) according to the Curie Law (Equation (1)). Therefore similar plots to **Figure 2** and **Figure 3** at different temperatures could be used to quantify illite content from *in situ* borehole magnetic susceptibility and bulk density data. The binary mineral mixture lines would merely be shifted by varying amounts to the left (*i.e.*, to lower magnetic susceptibilities), dependent upon the temperature, for any temperature above ambient (room temperature) used for **Figure 2** and **Figure 3**. However, that would require many plots similar to **Figure 2** and **Figure 3**, each at a different temperature. A better and simpler approach to quantify clay content from *in situ* borehole measurements would be to just use the borehole magnetic susceptibility data alone (without the bulk density data). The clay content could be quantified from a single magnetic susceptibility versus temperature plot for several different percentage mixtures of a particular binary mineral combination. An example of such a plot for illite + quartz mixtures is given by us in [4].

Alternatively, if the bulk density data were to be included, then the temperature dependence of the magnetic susceptibility could be shown on 3D plots. **Figure 4** shows one such example of a 3D plot of mass magnetic susceptibility

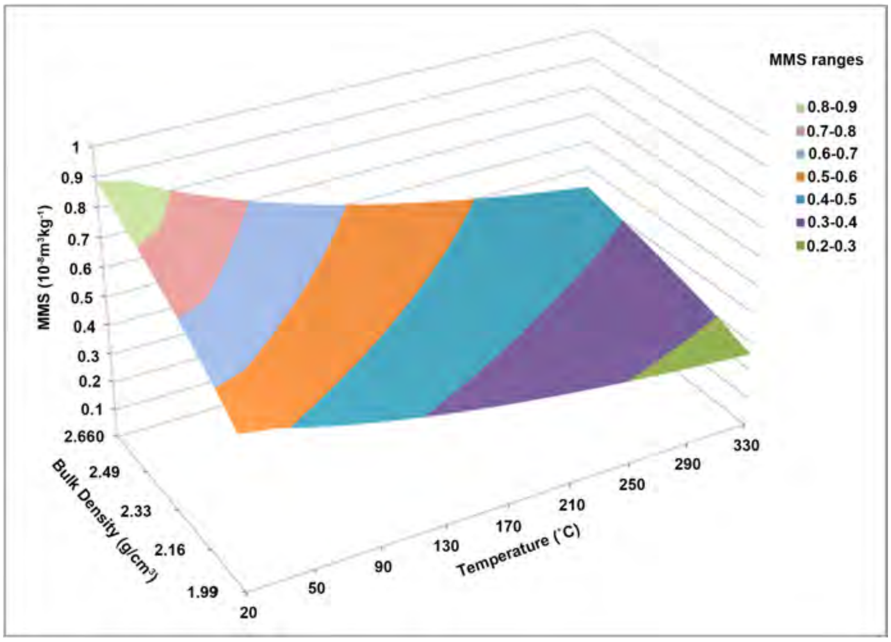

Figure 4. 3D plot of mass magnetic susceptibility (MMS) versus bulk density as a function of temperature for a mixture of 9.5% illite and 90.5% quartz. The MMS ranges in the legend have units of 10^{-8} m^3 kg^{-1}.

versus bulk density as a function of temperature for a binary mixture comprising 9.5% illite and 90.5% quartz. The decrease in mass magnetic susceptibility with increasing temperature is clearly shown. For mixtures with a higher illite content than those shown in Figure 4 the magnetic susceptibility values at any temperature would be higher (likewise mixtures with a lower illite content will have lower magnetic susceptibility values), and would decrease with increasing temperature according to Equation (1). 3D plots like Figure 4 have the advantage of being able to include an additional parameter (in this case bulk density), but the disadvantage in that a separate plot is required for each binary mineral mixture.

3. Conclusions

A methodology to rapidly and non-destructively identify clay type and quantify clay content is proposed, which utilizes some new template crossplots of magnetic susceptibility versus standard borehole data (or core data) involving spectral gamma ray and bulk density. The binary mineral mixture (e.g., illite clay + quartz) can first be identified from Figure 1, and then the individual mineral contents of the binary mixture, together with the mixture porosity, can be quantified from plots like Figure 2 and Figure 3. The new plots have a number of advantages over other more traditional plots and techniques as we detailed.

The new plots can utilize magnetic susceptibility measurements at ambient temperatures in the laboratory or at the wellsite using core samples or drill cuttings. The use of drill cuttings would be particularly cost effective, since these are produced for any drilled well at essentially no extra cost (unlike expensive core samples).

The methodology can also utilize borehole magnetic susceptibility measurements to identify the clay type (in conjunction with spectral gamma ray data), and quantify the clay content, *in situ* using the borehole magnetic susceptibility data alone or in combination with borehole bulk density data. For these *in situ* applications from borehole measurements, the plots need to take account of the temperature dependence of the magnetic susceptibility of paramagnetic minerals, since reservoir temperatures vary with depth in boreholes.

Acknowledgements

D. K. P. thanks the Natural Sciences and Engineering Research Council of Canada (NSERC) for a Discovery Grant.

Conflicts of Interest

The authors declare no conflicts of interest regarding the publication of this paper.

References

[1] Potter, D.K. (2007) *Petrophysics*, **48**, 191-201.

[2] Banks, J.Y., Tugwell, A.G. and Potter, D.K. (2018) Constraining Uncertainty in Complex Reservoir Description—A Case History Applying Magnetic Susceptibility to Estimate Permeability from Core Samples and Cuttings. 59*th Annual Logging Symposium*, London, 2-6 June 2018, 11 p.

[3] Log Interpretation Charts (2005) Schlumberger. 279.

[4] Ali, A. and Potter, D.K. (2012) *Geophysics*, **77**, WA211-WA221. https://doi.org/10.1190/geo2011-0282.1

[5] Fertl, W.H. (1979) *The Log Analyst*, **20**, 3-37.

[6] Borradaile, G.J., MacKenzie, A. and Jensen, E. (1990) *Journal of Geophysical Research* (*Solid Earth*), **95**, 8447-8451. https://doi.org/10.1029/JB095iB06p08447

[7] Dearing, J.A. (1994) Environmental Magnetic Susceptibility: Using the Bartington MS2 System. Chi Publishing, Kenilworth.

[8] Hunt, C.P., Moskowitz, B.M. and Banerjee, S.K. (1995) Magnetic Properties of Rocks and Minerals. In: Ahrens, T.J., Ed., *Rock Physics and Phase Relations*: *A Handbook of Physical Constants*, AGU Reference Shelf Vol. 3, American Geophysical Union, Washington DC, 189-204. https://doi.org/10.1029/RF003p0189

[9] Potter, D.K., AlGhamdi, T.M. and Ivakhnenko, O.P. (2011) *Petrophysics*, **52**, 50-57.

[10] Potter, D.K., Corbett, P.W.M., Barclay, S.A. and Haszeldine, R.S. (2004) *Journal of Sedimentary Research*, *Research Methods Papers Section*, **74**, 730-735. https://doi.org/10.1306/021304740730

[11] Ross, D.J.K. and Bustin, R.M. (2008) *AAPG Bulletin*, **92**, 87-125. https://doi.org/10.1306/09040707048

[12] Dehghanpour, H., Zubair, H.A., Chhabra, A. and Ullah, A. (2012) *Energy Fuels*, **26**, 5750-5758. https://doi.org/10.1021/ef3009794

[13] Makhanov, K.K. (2013) An Experimental Study of Spontaneous Imbibition in Horn River Shales. MSc Thesis, University of Alberta, Edmonton, 109.

https://doi.org/10.2118/162650-MS

[14] Potter, D.K. and Ivakhnenko, O.P. (2008) *Petrophysics*, **49**, 57-66.

[15] Deer, W.A., Howie, R.A. and Zussman, J. (1983) An Introduction to the Rock Forming Minerals. Longman Group Limited, London, 528.

[16] Ivakhnenko, O.P. and Potter, D.K. (2004) *Physics and Chemistry of the Earth*, **29**, 899-907. https://doi.org/10.1016/j.pce.2004.06.001

Journal of Modern Physics, 2019, 10, 835-860
http://www.scirp.org/journal/jmp
ISSN Online: 2153-120X
ISSN Print: 2153-1196

A Physical Explanation for Particle Spin

Dirk J. Pons[1*], **Arion D. Pons**[2], **Aiden J. Pons**[3]

[1]Department of Mechanical Engineering, University of Canterbury, Christchurch, New Zealand
[2]University of Cambridge, Cambridge, UK
[3]University of Canterbury, Christchurch, New Zealand
Email: *dirk.pons@canterbury.ac.nz, arion.pons@gmail.com, aidenpons@gmail.com

How to cite this paper: Pons, D.J., Pons, A.D. and Pons, A.J. (2019) A Physical Explanation for Particle Spin. *Journal of Modern Physics*, **10**, 835-860.
https://doi.org/10.4236/jmp.2019.107056

Received: May 3, 2019
Accepted: June 22, 2019
Published: June 25, 2019

Abstract

CONTEXT The spin of a particle is physically manifest in multiple phenomena. For quantum mechanics (QM), spin is an intrinsic property of a point particle, but an ontological explanation is lacking. In this paper we propose a physical explanation for spin at the sub-particle level, using a non-local hidden-variable (NLHV) theory. **APPROACH** Mechanisms for spin were inferred from the Cordus NLHV theory, specifically from theorised structures at the sub-particle level. **RESULTS** Physical geometry of the particle can explain spin phenomena: polarisation, Pauli exclusion principle (Einstein-Podolsky-Rosen paradox), excited states, and selective spin of neutrino species. A quantitative derivation is provided for electron spin g-factor g = 2, and a qualitative explanation for the anomalous component. **IMPLICATIONS** NLHV theory offers a candidate route to new physics at the sub-particle level. This also implies philosophically that physical realism may apply to physics at the deeper level below QM. **ORIGINALITY** The electron g-factor has been derived using sub-particle structures in NLHV theory, without using quantum theory. This is significant as the g-factor is otherwise considered uniquely predicted by QM. Explanations are provided for spin phenomena in terms of physical sub-structures to the particle.

Keywords

Non-Local Hidden-Variable Theory, Cordus, g Factor, Fundamental Physics, Spin

1. Introduction

The spin of a particle is a key concept for particle physics, and is physically manifest in multiple phenomena such as entanglement, [1] [2] [3] [4] Pauli pairs, photon polarisation, superconductivity, selective spin of neutrino species, and electron spin g-factor [5]. Despite spin having physical effects, it has no ontological explanation. Quantum mechanics (QM) instead treats it as an intrinsic parameter. This paper offers a physical explanation for spin using non-local hidden-variable (NLHV) theory, specifically the variant called the Cordus theory [6]. It is shown that, under the assumptions of this theory, spin parameters arise naturally as properties of the physical structures at the sub-particle level. This is then used to provide physical explanations of the Pauli Exclusion Principle and the selective spin of neutrino species. The electron g-factor is derived and it is shown quantitatively that g = 2 for this NLHV theory.

2. Context: Orbital and Spin Angular Momentum

2.1. Background

In classical mechanics angular momentum is rotation of a body around an axis. The classical regime gives way to the Fermi-Dirac probability distribution when the separation between particles is much smaller than the de Broglie wavelength of the particles.

In particle physics there are two types of angular momentum, orbital and spin. The sum of orbital angular momentum and spin is the total angular momentum for the particle. The total is conserved, though momentum can be transferred between the orbital and spin components, hence spin-orbit interaction.

The *orbital* angular momentum is generally believed to involve a particle moving in a circular locus, such as an electron moving round the nucleus, or two quarks spinning around each other. It is quantized, as opposed to being a continuous variable, and takes on integer values. The *spin* angular momentum (or simply 'spin') is analogous to a quantized rotation of the particle, e.g. the electron, about its own axis. Quantum mechanics disfavors an interpretation of rotation, and instead considers spin to be an intrinsic property. QM also rejects the idea that spin could arise from smaller internal particles rotating around a spin axis, as in a bag or plum-pudding model. The confirmatory evidence appears in the electron spin g-factor. At the particle level the quantum spin is measured with respect to a direction set by the observer, and the outcomes are represented by probabilities of finding the particle with spin in that direction (projection). Under QM the particle has no physical orientation either.

Spin is a vector with a total value and a direction. The fermions take spin values of odd half-integer increments (1/2, 3/2, 5/2, etc.). The spin of the electron, proton, and neutron is 1/2 and this applies to the leptons and quarks generally. These particles are subject to the Pauli Exclusion principle, that two co-located particles are unable to be in the same spin state and instead take different spin directions, e.g. +1/2 and −1/2 to achieve this. In contrast bosons have integer spin. These include the photon, mesons (quark plus antiquark), and Higgs boson. These bosons follow Bose-Einstein statistics, *i.e.* there is no interaction between multiple particles, and they can co-locate. It also applies to some atoms, hence condensed states of 2He2 in superfluidity, and electron Cooper-pairs in superconductivity. Atomic nuclei with even mass number have integer spin, and odd have ½ spin.

These attributes of particles are well quantified but no deeper explanation is available.

2.2. Application

Spin is an important property that is often used in entanglement experiments [1] [2] [3] [4] and interferometry [7]. It is also a key feature in the further development of quantum theory, e.g. the Higgs mechanism and muon properties. The table of nuclides also shows that spin is key to understanding the properties of the nucleus [8]. Other phenomena where spin is important are annihilation [9] [10] [11], including of muons [12], proton size anomaly [13], and aspects of cosmology such as leptogenesis [14]. Spin is also practically important in optical tweezers [15].

2.3. Ontological Challenges

There are several conceptual problems with spin. The first is explaining how spin arises at the fundamental level, why particles have the values they do, and what underpins the Pauli Exclusion principle and Bose-Einstein behavior. For example, QM does not offer any deeper explanation of why spin numbers prevent fermions from co-locating.

A second problem is the lack of explanation for why the *type of assembly of particles* should affect the spin. For example, individual electrons are fermions, whereas a pair of electrons (Cooper pair) is a boson. Likewise, why are nuclides with odd total of nucleons fermions, while those with even totals are bosons?

Third, there is no satisfactory explanation why *multiple* 2He2 nuclei and Cooper-pairs do not also physically co-locate like the photons. They do not contract to a singularity. Given that all are bosons, one expects a consistent behaviour from the same spin property. A related question is why should spin be exclusively 1/2 for elementary fermions, yet merely predominately 1 for bosons? What is the basis of this differentiation?

A fourth issue is that, though quantized, the spin of a particle is nonetheless functionally linked to classical angular momentum, as shown in the empirical Einstein-de Haas effect (an electric current in a coil causes a magnet to rotate), and the complementary Barnett effect (an object becomes magnetized when spun). Why is this?

2.4. Contrasting Perspectives

It is undisputed that the spin property can be *formalized* within quantum mechanics. However QM does not provide an *ontological* explanation of how these behaviors arise. Attempts to provide physical interpretation have been undertaken from the outset of quantum theory, e.g. by Dirac [5], but spin remains resistant to such description within QM. It is generally accepted that there is no explanation, that the properties are merely intrinsic, that QM is complete as a theory as it is, e.g. [16].

It is understandable that QM would construct spin this way. After all QM is premised on particles being zero-dimensional points, hence internal structures are disallowed. Nonetheless, from a NLHV perspective there ought in principle be an underlying mechanics or sub-structure to the particle, but in practice such explanations have been elusive. While the simpler classes of NLHV theory have been excluded by the Bell-type inequalities [17] [18] [19], it has not been possible to rule them all out [20]. Hence it is not impossible that an NLHV theory may provide a solution, but in practice it has been difficult to find workable variants, and hence this branch of physics has become obscure. Historically the main NLHV theory was the de Broglie-Bohm [21] [22]. There has continued to be interested therein [23] [24] [25], but it has not yet progressed to a comprehensive theory of physics. More recently the Cordus variant of NLHV theory [6] has been shown to explain multiple physical phenomena.

2.5. Brief Summary of the Cordus Theory

The Cordus theory [6] postulates the existence of specific physical structures at the sub-particle level, and functional behaviors thereof. Philosophically the theory is premised on physical realism that observable phenomena have underlying physical mechanisms [26]. Design principles were used to construct the theory, hence the features are not arbitrary conjectures [6]. The theory predicts that particles have internal structures and externally emitted discrete forces [5] [26]. See **Figure 1** for the predicted structure of the electron, and **Figure 2** for the photon.

The figures show the sub-strutures and internal mechanisms that are inferred for these particles, and a brief explanation follows based on [27] [28]. The particle is proposed to have an *inner structure* comprising two *reactive ends*, which are a small finite distance apart (span), and each behaves like a particle in their interaction with the external environment, when they are energized. The reactive ends are proposed to emit discrete forces, which react with external fields, matter, and photons. A *fibril* joins the reactive ends and provides instantaneous connectivity and synchronicity between the two reactive ends. It is a persistent and dynamic structure but does not interact with matter. There is also an *external structure* whereby the reactive ends periodically energize (at the de Broglie frequency), and in doing so emit *discrete forces* that have components in three orthogonal directions. These discrete forces are connected in a flux tube and emitted into the external environment. The whole is sometimes termed a *particule* where it is necessary to differentiate from the point particle of QM. For further details of the internal structures see [26] [29].

One of the implications is that particles are linear structures of finite length they have size. They also have orientation determined by discrete force emission. It is also not relevant to think of the particle as a solid volume of material, or a

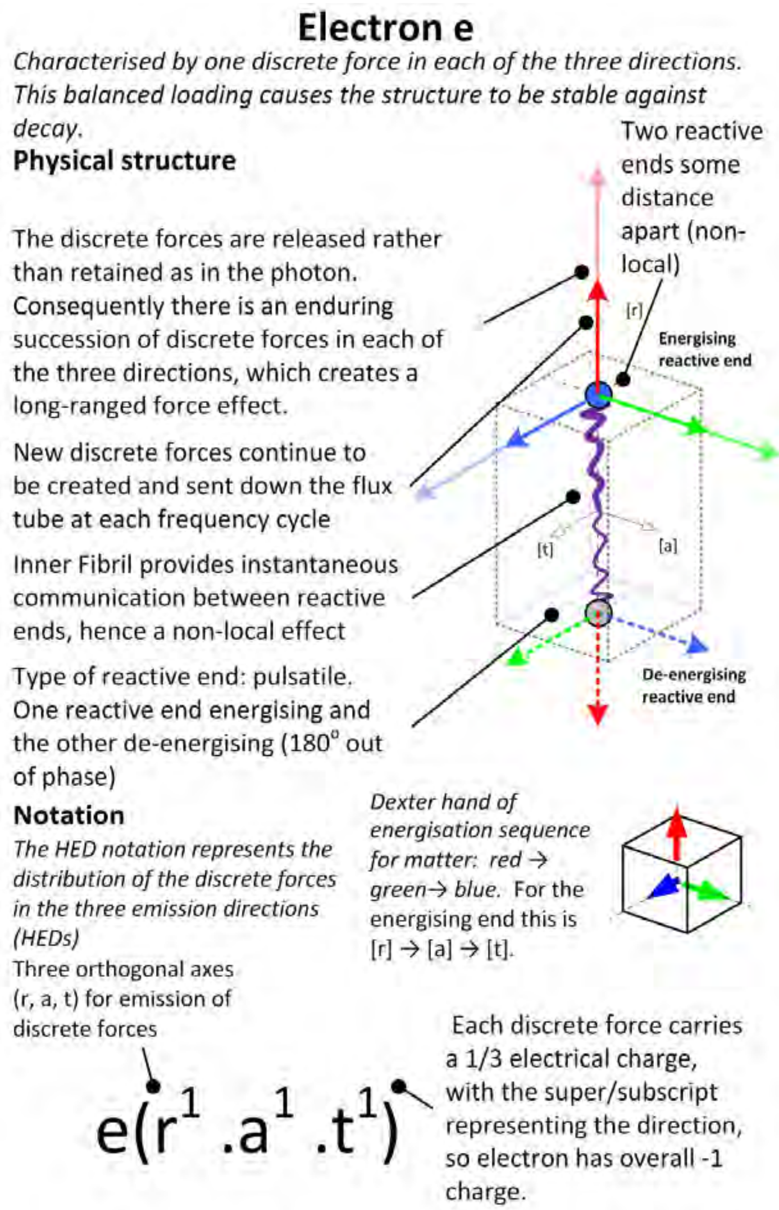

Figure 1. The Cordus design for the electron, showing the reactive ends, fibril, and discrete force emissions. Adapted from [27].

spinning ball of charge. This is especially relevant later when considering the electron spin g-factor.

In this theory, an important difference between the electron and photon is the nature of the emissions. The electron and all massy particles are proposed to emit discrete forces and release them into the external environment to contribute to a fabric of discrete forces. The reactive ends are energized in turn. In contrast the photon is proposed to shunt its discrete force in and out of the fabric, without releasing them. Also both reactive ends are simultaneously active, in opposite directions of transmission. This is important later when considering the Pauli principle.

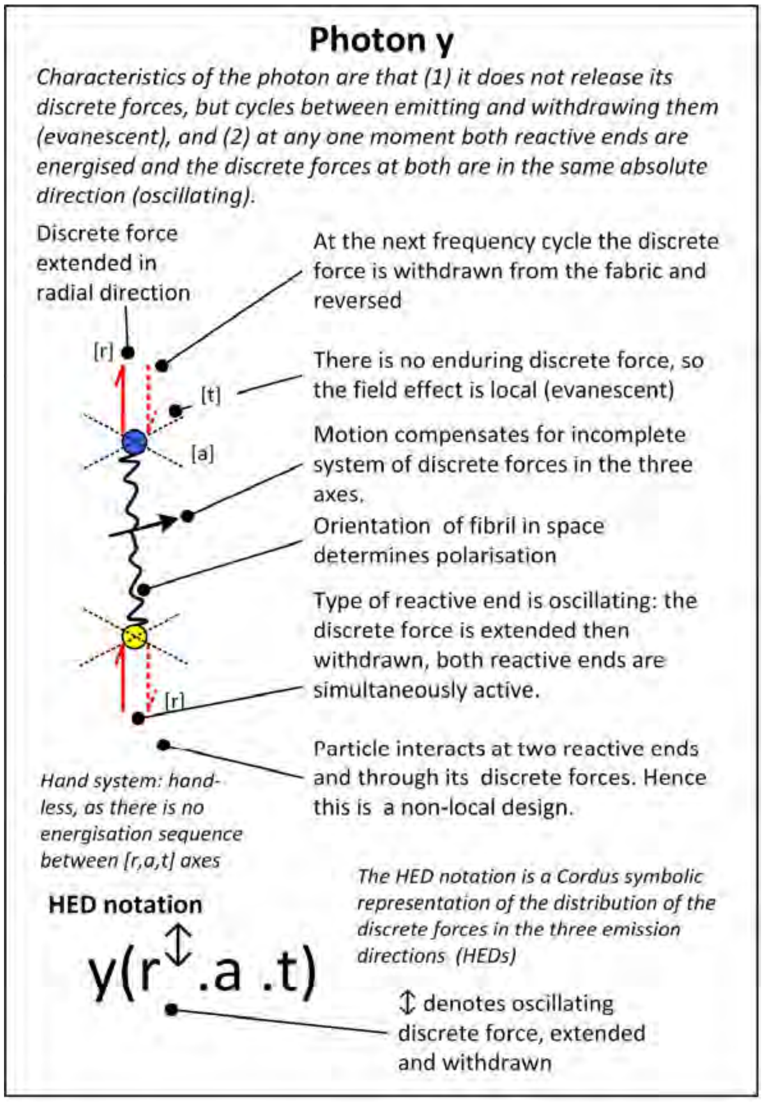

Figure 2. Proposed internal structure of the photon, showing the dual-energization of the reactive ends, and the shunting arrangement of the discrete forces. Adapted from [28].

The theory has been used to explain the following phenomena:

- Wave-particle duality in the double slit device [6], in terms of each reactive end passing through one of the slits.
- Derivation of optical laws from a particle perspective [6], in terms of components of the discrete forces and the effects thereof at reflection and refraction. This includes derivation of critical angle, Snell's law and Brewster's angle.
- Explanation of the decay processes [30] [31] in terms of a contribution by fabric density and loading of neutrino species.
- Prediction of a deeper unified decay model [32] where all the nucleon decay processes (forward, inverse, and induced) may be represented in a single unified decay equation: p + 2y + z <=> n + $\underline{e}$ + v with proton p, photon y, addi-

tional photons z where necessary for mass difference, neutron n, electron e, and antimatter species denoted with underscore. Particles, other than photons, change matter-antimatter species when transferred over the equality. This equation may be rearranged to represent $\beta-$, $\beta+$, and EC in the conventional forward directions, and the induced decays too.

- Explanation for the selective spin characteristics of neutrinos whereby the direction of spin is correlated with the matter-antimatter species [30], in terms of the interaction of the incomplete discrete force structures of these particles with the handedness of the background fabric of discrete forces from other particles.
- Explanation for the annihilation process including a conceptual explanation of the difference between otho- and para-positronium decay rates (ortho and para refer to spin combinations of the bound electron and anti-electron/positron) [33], in terms of the differences in mutual orientations of the two spin states and the effect of the resulting discrete forces on stability.
- Provision of a mechanics for pair production [34] and likewise photon emission [29] [35], in terms of mechanisms that change the particles.
- Structure of atomic nuclei and explanation of stability for nuclides H to Ne [36] [37], in terms of a nuclear polymer comprising protons and neutrons in cisphasic and transphasic relationships, neutrons that bridge the polymer, and a predicted morphology of polymer shapes.
- Prediction of a mechanism for asymmetrical baryogenesis in terms of remanufacture of the antielectron (ex pair production) to the proton 8y + z => e + p + 2v [38].
- Explanation of entropy in terms of geometric irreversibility of particles, hence a group property at the bulk level, not a characteristic of the individual particle, which can be reversed at an energy cost at the particle level (Maxwell's agent) [39].
- Nature of the vacuum and the cosmological horizon [40]. In this theory the vacuum comprises a fabric of discrete forces generated by matter particles. The cosmological boundary is the expanding surface where the fabric colonizes the void outside the universe. This theory identifies the infeasibility of placing a physical agent at the boundary of the universe, and also predicts there is no practical way to control the universe from its outer boundary as the holographic principle suggests.
- A theory for time as an emergent property of matter [41], wherein time for a matter particle originates with the frequency cycles of the re-energization of the particle's reactive ends, with relativistic velocity, acceleration, and high gravitation, affecting the energization process. Discrete forces of different particles affect each other via the fabric providing a temporal connectedness of phenomena that are at different geometric locations. The piece-wise communication, via discrete field interactions of the fabric, between adjacent

volumes of space applies spatial consistency to time, hence space time is discrete.

- Origin of the finite speed of light [42]. On conceptual grounds the density of the fabric determines the electrical and magnetic constants of the vacuum, and gives the speed of light a particular value. A variable speed of light (VSL) is predicted, depending on the fabric density hence the proximity and spatial distribution of matter. Results disfavor the universal applicability of the cosmological principle of homogeneity and isotropy of the universe.
- The time dilation, Lorentz and relativistic Doppler formulations are derivable from the Cordus NLHV particle perspective [43]. The equations contain an unexpected dependency on the fabric density. For a homogenous fabric, which is the assumption of general relativity, the conventional formulations are recovered.

3. Method

The purpose of the current work was to prospect for deeper explanations for spin from the Cordus NLHV theory. The present work extends the theory for superposition and entanglement [26].

We used this theory to infer candidate physical structures for spin. We did not find it necessary to change the fundamentals of the theory, though we did identify specific dimensions that were tacit in the original theory. We show that spin may be understood as a geometric attribute of the internal structure of a Cordus particle.

The resulting theory provides a description of spin that is quantized and does not involve orbits. We found that the theory predicts additional spin properties beyond those recognized by QM. The distinction between these properties is lost when one reduces the structure to a point particle, hence the QM perspective is able to be recovered.

We tested the theory for logical congruence against known phenomena of Pauli exclusion, excited states, and selective spin of neutrino species. For the later see also prior work [30]. Explanations were found for these effects, and did not require new assumptions in conflict with the original premises.

We then applied the theory to determine the electron spin g-factor, and quantitatively recovered the Dirac g-factor. We explored the anomalous dipole moment, and found a qualitative explanation for it, but a quantitative derivation was elusive at this time.

4. Results: A proposed Physical Basis for Spin

4.1. Orientation Angles for Spin

Since Cordus particles have span, they consequently have angular orientation relative to a reference frame. Their frequency behavior means they also have a phase property [44]. We propose these as the basis for spin.

The key spin variables in this theory are the orientation angles of the fibril, and the energization phase. If the fibril is orientated with the axis of measurement, then there is only one variable, which is the energization phase, see the electron model above. However in the more general situation the number of dimensions (variables) required to define a Cordus particle is three linear dimensions [x, y, z] for location of a reactive end, one for the length of the span (related to type and energy of the particle), up to three polarisation angles for the orientation of the discrete forces, one composite variable to denote the discrete force content (this differentiates the type of particle) [29], another for the degree of overloading of discrete forces, and one phase variable to indicate which reactive end is energizing. The matter/antimatter hand, which is identified as the hand of energization sequence, requires another variable [33] [45].

Depending on how they are counted, that gives a total of 11 independent variables to fully define a Cordus particle. Not all these dimensions are simple numbers: some like the number and charge of discrete forces are sets, though this is not apparent in the case of the electron but instead becomes evident in say the neutron [31]. The photon has a still simpler discrete force structure and does not need all these variables.

The dimensions of particularly interest for spin are those of orientation. In this theory the spatial orientation of one particle relative to another is defined by several angles: the phase of energization θ, and three orientation angles for the fibril and system of discrete forces A_1, A_2, A_3, see **Figure 3** and text following.

4.2. Predicted Sub-Types of Spin

We identify several different *types of spin* within the Cordus theory. It is proposed that not all these are manifest in every situation, and some are predicted only to be evident at a finer scale. Several of these spin variables are naturally inaccessible to representation in quantum theory because it assumes particles are 0-D points.

Number of Reactive ends (E)

The number of reactive ends in the particle, which is two rather than say three, indicates the *energization frequency model* of the particle. For the Cordus theory E = 2 for a single particle. For QM, and any theory built on a 0-D point construct, the number of reactive ends is E = 1. For electromagnetic wave theory, where a dipole construct is sometimes used, E = 2.

Intra-Energisation state (*s*)

This indicates the energization state of the reactive end at the moment under examination. The *s* variable denotes the energization state of a reactive end at the moment in question. For matter particles like the electron, one reactive end is energizing s(1) while the other is de-energizing s(0), *i.e.* the two reactive ends are 180˚ out of phase, hence an s(1,0) structure. The reactive ends thus pulse with discrete force emissions. There is no emission of discrete forces at the de-energized state. At each ½ frequency cycle the state of any one reactive end changes.

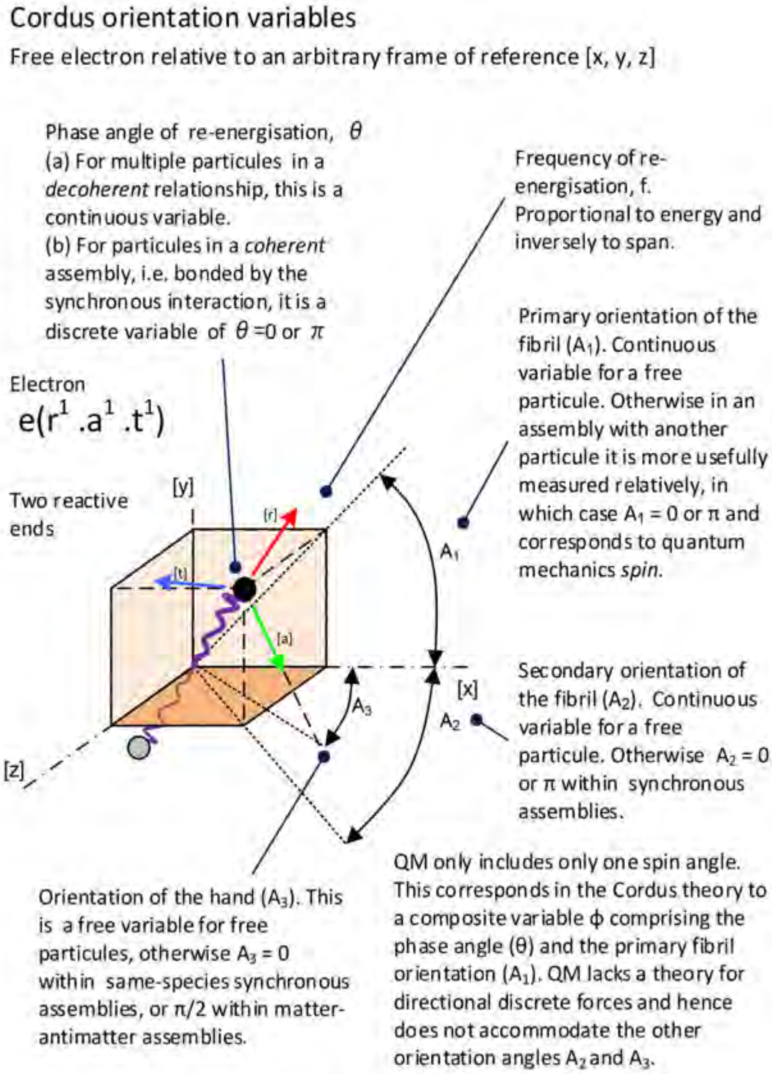

Figure 3. Definition of Cordus orientation variables that define spin.

For the photon, both reactive ends are simultaneously active. At any one moment, one reactive end is emitting a discrete force and the other is retracting its emission, s(+½, −½). The photon oscillates its emissions. The reactive ends are simultaneously active, though in different directions. At the next ½ frequency cycle the state of the reactive ends changes.

Nuclides with even numbers of nucleons and symmetrical polymers emit discrete forces simultaneously in all directions, though from different locations in the polymer [36]. At a sufficient coarse scale of observation, where the span of the polymer is considered to be zero, this would appear to be a particle with simultaneous emissions in all directions, *i.e.* s(1,1). This, we propose, is the basis of the bosonic attribute of nuclides with even numbers of nucleons.

Fibril orientation angle ($A_{1\text{-}3}$)

This measure of spin refers to the orientation of the fibril of a single particle, relative to another particle or frame of reference. The necessary parameters are two angles A_1 andA_2 describing the orientation of the span, and a third angle A_3 for the alignment of the [a] axis. These apply to massy particles and the photon. They correspond to polarisation angles for the photon in electromagnetic wave theory.

Inter Phase angle (θ) *– cis and transphasic*

There is a relative phase angle θ of energisation between two neighboring particles. If the particles are in a *coherent* relationship, which requires synchronization of discrete forces and a common frequency of the energization ω, then the only options are $\theta = 0$ (*cisphasic*) or $\theta = \pi$ (*transphasic*) energization [33] [44]. In the more general case of a *discoherent* relationship then there are no restrictions on θ. In this way the Cordus theory provides a means to differentiation coherent and discoherent (discord) states of matter. This is difficult to explain with other theories.

Discrete force pairs

The difference in orientation of matter-antimatter discrete force pairs is interpreted as a form of spin at a deeper level within the particle. The Cordus notation for these is $x^{1}_{\underline{1}}$ and $x^{\underline{1}}_{1}$ [30] [33]. This concept is not needed for the present discussion, but is included for completeness as it is important in the proposed Cordus processes for decay and the weak interaction [31], photon emission [35] and pair production [34]. It is also relevant in the solution for asymmetrical baryogenesis [38].

Angular momentum (*M*)

This spin refers to angular momentum. The interpretation is of a free Cordus particle rotating about an axis. For an individual particle or decoherent assemblies of particles this spin may be a continuous value. However in coherent systems it is quantized due to the synchronicity of the interactions between the particles [44]. Hence it is proposed that the quantized nature of spin arises from the coherent assembly of particles, specifically from their mutual alignment of emission directions.

Handed motion (*H*)

Spin hand refers to the direction of the angular momentum relative to the direction of motion, and may be clockwise or anticlockwise. This is a geometrically simple concept but it has potentially profound implications because it explains the selective spin characteristics of the neutrino matter-antimatter species, see below and [30]. Hence it is possible with this theory to explain why neutrinos spin the one way, and anti-neutrinos the other. This has otherwise not been explained with conventional QM.

Having proposed the origins of spin variables at the sub-particle level, we next apply these principles to explain several phenomena.

5. Applications of Cordus Theory to Quantum Phenomena

5.1. Empirical Measurement of Spin

The Cordus theory proposes that measured spin corresponds to phase and an-

gular orientation of the fibril of the particle.

This is consistent with how spin is measured empirically. In a coherent light source the photons are produced with a certain orientation, and this occurs either at emission or by subsequent filtering using polarizers to exclude non-compliant orientations. Also the component of electric field, hence component of spin, may be measured in an axis set by the observer. These light sources produce many photons and the probabilities measured by quantum mechanics represent these components and the underlying stochastic variability. A number of photons are sacrificed for measurement purposes, and used to infer the properties of the wider ensemble. Hence also, a decoherent light source produces photons with uncontrolled orientations, and this is represented in quantum mechanics as indeterminate spin. The Cordus theory is consistent with these results, but explains them as arising from the geometric properties of the particle. Thus it is proposed that the aligned molecules within polarising filters really do selectively obstruct photons that have orientation that is non-compliant with the filter.

5.2. Coherence and Decoherence

The Cordus theory proposes that coherence arises when adjacent particles synchronize the phase of emission of their discrete forces.

Within the Cordus explanation for spin there is a differentiation between coherent and decoherent assemblies of particles [44]. This is not a distinction explainable with quantum theory. The Cordus theory proposes that the formation of coherence between two or more matter particles requires their acceptance of a common (or harmonic) *frequency*, and a common *phase* of emissions. This is because the bonding is via the synchronous interaction (strong force), which as the name implies requires synchronous emission of discrete forces [44]. This fixes the frequency ω of the particle to a common or harmonic value.

The synchronous interaction also makes the three orientation angles A_1, A_2 and A_3 into local constants, so they are no longer variables. The only remaining variable is the phase angle θ, which in the coherent case is either cisphasic ($\theta = 0$) or transphasic ($\theta = \pi$). Consequently for coherent assemblies of matter, both frequency and phase are no longer variables for an individual particle but are instead group properties. We propose this as the physical mechanism underpinning superfluidity, superconductivity, and Bose-Einstein condensates (see below).

Multiple particles that are in *decoherent* assembly have their own independent parameters for all these variables. Such assemblies are predicted to interact via the electro-magneto-gravitational (EMG) forces instead of the synchronous force.

As this shows, physically meaningful definitions of spin are provided in this NLHV design. However there are more spin variables here than provided in quantum theory. This can be explained as follows. QM assumes that all particles are in a coherent assembly state, which means that all the angles of polarisation are fixed, and the frequency too. Consequently the only spin variable left in a coherent body is the phase θ, which can only take two values (since the particle has two reactive ends). This explains why spin is discrete in quantum mechanics. QM does not extend to describe ensembles of decoherent particles, which is what the other Cordus variables are used for.

5.3. Pauli Exclusion Principle

The Cordus theory proposes that pairs of electrons can share a common space by arranging to have transphasic (opposite phase) inter-particle relationships.

This theory may be applied to understand the interaction between electron Pauli pairs in orbitals. The two electrons in an orbital are known to have opposite spin when measured, hence the Einstein-Podolsky-Rosen paradox. This is considered a paradox because it is unclear how the two particles interacted to communicate their states to each other to contrive such a result.

The Cordus theory explains the situation as follows. The two electrons share locations for reactive ends but in opposite (transphasic) re-energisation phase, see **Figure 4**. This transphasic interaction protects the emission directions of the assembly, and is thus energetically favourable for the individual participants. This also explains why there are *only two* electrons in each orbital, not more, hence the Pauli Exclusion Principle. Hence the two electrons are always found to be in complementary states when measured. The fact that the electrons are sharing the orbital means that they have pre-arranged with each other (and the nucleus) to be in this complementary state even before the Observer started the interrogation, so to the Observer the outcome of the experiment looks like an act of contrivance by the particles. However that is merely an artefact of observation.

Note that it is not the *absolute* orientation of the particle that is proposed to be important, but the *relative* orientation between the two particles. In a coherent system, the two particles can *only* be either in phase with each other or out of phase, hence only two spin states are possible for Pauli pairs. In the more general case where two electrons are *not* in coherence with each other, there are infinitely many orientations that the fibril may take. This is proposed as the reason why the Pauli exclusion principle only applies in special situations like orbitals.

In this context the Cordus particle concept can also be extended to larger assemblies such as atomic nuclei [46]. It is able to explain why each of the nuclides H to Ne are stable, unstable, or non-existent [37]. It does this by proposing that the protons and neutrons are also linear structure like the electron, and that these form closed chains or *nuclear polymers* [36]. The polymers are stabilised by bridge neutrons, which accommodates the empirical observation that heavier elements need more neutrons for stability.

5.4. Excited States and Photon Emission

The Cordus theory proposes that excited states comprise one electron in a set adopting a higher harmonic frequency, while still retaining synchronous interactions with the basal particle(s).

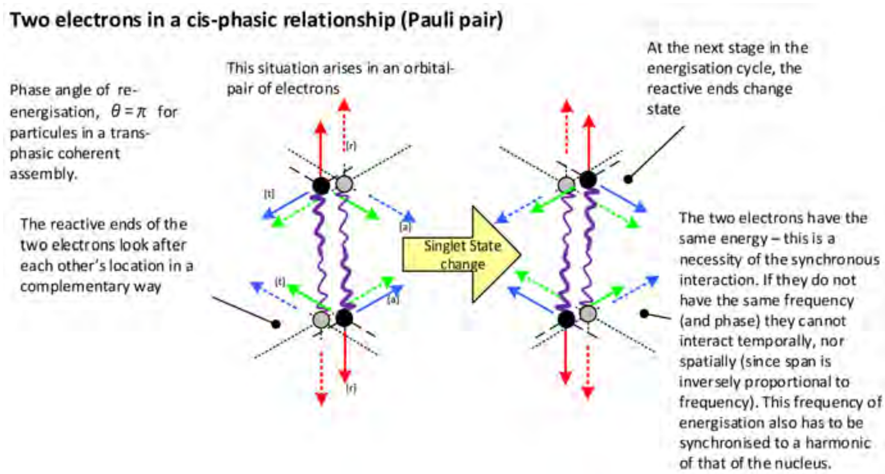

Figure 4. The Cordus explanation for the spin arrangements for a Pauli electron pair.

The behaviour of excited states can also be understood in terms of this Cordus theory. In an excited state one of the electrons (B) in a Pauli pair absorbs energy. In the Cordus explanation, this energy causes the B electron to increase its frequency and decrease its span. It therefore moves into partial temporal and spatial de-synchronisation with electron A (which remains in the ground state). B can persist in this state by finding a harmonic frequency with which to interact with A, a type of spin gearing. However the interaction is also, via A, with the rest of the nucleus. The nucleus has a large resistance to changing its spin attributes, due to its large mass.

Electron B may transfer some energy into electron A and the nucleus, as part of the process of negotiating a mutually acceptable set of harmonic frequencies. Or it may emit the energy as a photon. Emission is also covered by this theory [29] [35]. This is a precise interaction and any excess energy above that needed for the relevant frequencies is a hindrance, and is discarded. Thus the orbital system takes only certain discrete energy states. Hence the quantum nature of discrete energy levels can also be qualitatively explained using this NLHV theory. This negotiation process takes frequency cycles, hence time, and thus the transitions are not instantaneous.

The relationship between electrons A and B thereby changes from the direct 1:1 synchronicity of the ↑↓ state (this notation refers to the discrete forces, see **Figure 1**), to one where electron B is at a higher harmonic frequency. B is then trapped in this state. Subsequently an external perturbation means that B is no longer in an energetically sustainable position. It is expected that B will more easily revert back to the ground state when it and A are momentarily in a cisphasic relationship ↑↑ (or ↓↓). For it to make the transition back to the transphasic state ↑↓ it needs to change its frequency to that of A, and move into the opposite phase. The Cordus theory separately identifies mechanisms whereby a particle can skip half a frequency cycle by emitting a photon [29]. If this photon also carries away the energy difference, then the spin adjustment is complete, and the intersystem crossing occurs. Hence this is a phosphorescence emission.

5.5. Selective Spin of Neutrino Species

This theory proposes that the physical mechanism for the matter-antimatter species differentiation is the handedness of the energisation sequence of the discrete forces [45]. Given three axes, there are only two such sequences, which are dexter and sinister (right and left). Expansion of this concept has been used to explain annihilation [33], pair production [34], and asymmetrical baryogenesis [38]. When coupled with the concept of spin described above, the theory also explains the unique spin characteristics of the neutrino species [30]. The physical evidence is that the neutrino always spins one way relative to its motion (left handed), and the antineutrino the other (right handed).

The proposed mechanism is that the neutrino species have incomplete discrete force emission and hence must recruit discrete forces from the fabric. This results in reactive translational and rotary motions. The direction of spin motion is determined by the energisation sequence, and this is also the matter-antimatter species differentiation, see **Figure 5** and **Figure 6**.

Up to here the explanations for spin phenomena have been quantitative. We now demonstrate that the theory quantitatively recovers the principle component of the electron g-factor.

6. Electron Spin G-Factor

Thompson's plum-pudding model of the atom proposed electrons in a matrix of positive charge, making up a solid ball. That concept of solidity was disproved by Rutherford [47] in the gold-foil experiments. This led to the modern idea of quantum mechanics, with a nucleus and electrons in orbitals. Even though quantum mechanics treats particles as 0D points, there is still an acceptance that particles occupy space stochastically such that macroscopic matter has volume. For example the proton has an empirically known charge radius. It is invariably assumed that such particles occupy the whole of their volume, even if non-uniformly and not continuously in time. This assumption is important in what follows.

Dirac explored the assumption that the electron had its charge on an outer conductive spherical surface [48]. If particles like the electron were solid spheres, or comprised sub-particles in a *solid spherical* matrix, and if the same sub-particles contributed fractionally to both charge and mass, then it would be expected that the moments of charge and mass would be the same.

Empirical evidence shows this not to be the case, and suggests that the internal sub-charges would need to be distributed differently to the sub-masses. More specifically, the *g-factor* represents the constant of proportionality between the magnetic dipole moment μ_s which measures spin of a charge, relative to the spin angular momentum S which measures the moment distribution of mass. The

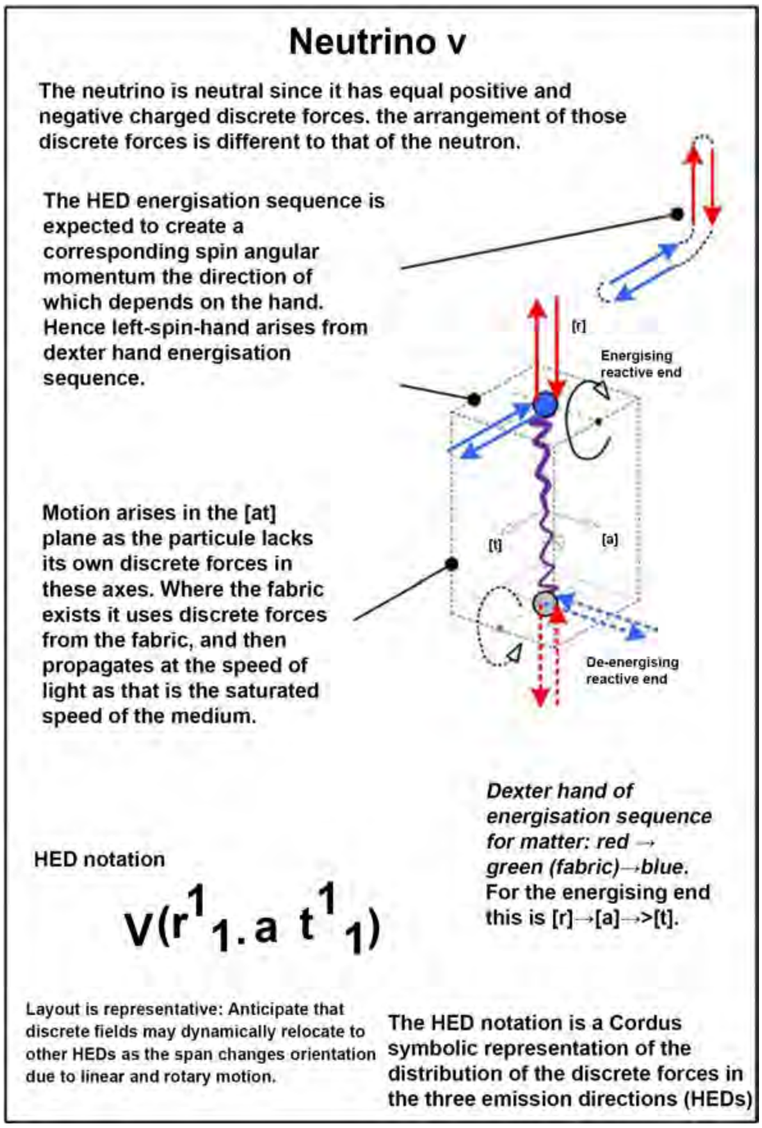

Figure 5. Proposed structure of the neutrino, including internal structure and external discrete force structure. The imbalance of the discrete forces results in linear and spin motions. The latter is uniquely determined by the energisation sequence, hence matter-antimatter species. Image adapted with permission from [30].

Dirac electron spin g-factor is approximate twice the spin, more accurately 2.00231930436153. That this is about 2 rather than 1 is evidence that the charge of the particle is distributed very differently to its mass. This is considered one of the key characteristics of QM, since no other theory of physics has been able to explain why $g = 2$. There is a further triumph for QM, since the anomalous magnetic dipole moment (the discrepancy from 2) can be calculated to high accuracy by quantum electrodynamics [49].

Explanation of electron g-factor with Cordus particle theory

In what follows we show that the new theory is able to derive $g = 2$. In the Cordus theory the electrostatic field strength of an electric charge is determined

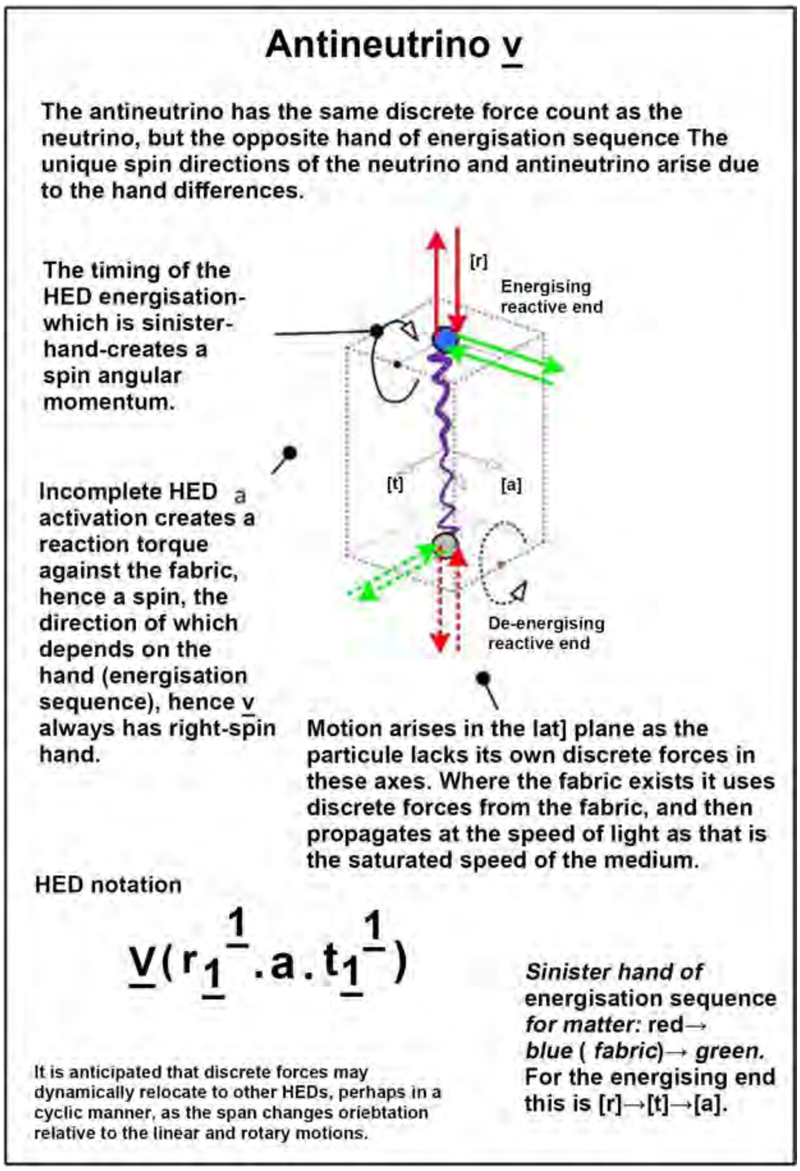

Figure 6. Proposed structure of the antineutrino, including internal structure and external discrete force structure. This particle spins in the opposite direction to the neutrino, because of the difference in energization sequence of the discrete forces. Image adapted with permission from [30].

by the *signed sum of discrete forces* emitted by that charge. The theory predicts, in contrast, that *mass* is determined by the *total number of discrete forces*, irrespective of their charge. Hence some particles (e.g. the neutron) emit *charge-neutral* pairs of discrete forces that contribute to mass but not to charge [31]. This is an important difference. In neutral particles, such as the neutron, it is proposed that both positive and negative discrete forces are emitted so the net electrostatic field strength is zero, but there are still discrete forces contributing to the mass and gravitational effect. In other particles, like the proton, both effects exist: there is a net external charge and a neutral part. These are the overt and implicit (or covert) parts respectively [32]. Thus the implicit discrete forces contribute to mass, and hence to spin angular momentum. In this theory, mass is also determined by the energisation frequency, whereas charge is not. Hence higher frequencies cause more discrete forces to be emitted in unit time, hence greater mass.

Hence the Cordus theory predicts different mechanisms for the electric field and mass. In contrast the classical perspective is of a spherical solid body with a radial dispersion of both charge and gravitational field. For the electron, in the Cordus theory, the discrete forces are identified as a complete set of one emission in each of the three axes, hence e = [r^1, a^1, t^1] without covert discrete forces [34]. This sums to one unit of charge and one unit of mass. We show that the electron g-factor for this arrangement is 2.

Start by noting that the electron spin g-factor is a constant included in the Dirac particle equation:

$$\mu_e = g_e \cdot \frac{\mu_B}{\hbar} S_e \tag{1}$$

where μ_e is the electron magnetic moment which measures the distribution of charge, g_e is the electron spin g-factor, μ_B is the Bohr magneton, e is the electron charge, $\hbar$ is the reduced Planck constant, and S_e is the spin angular momentum which measures the distribution of mass.

Identify the Bohr magneton, where m_e is the electron mass:

$$\mu_B = \frac{e\hbar}{2m_e} \tag{2}$$

Hence by substitution and rearrangement:

$$g_e = 2\frac{\mu_e/e}{S_e/m_e} \tag{3}$$

The term μ_e/e is the *moment of charge per unit charge*, and S_e/m_e is the *moment of mass per unit of mass*.

In the Cordus theory the mass and charge interactions occur at the reactive ends, since the discrete forces provide the underlying mechanisms of causality. Hence it is *at the ends of the span* that the discrete forces act. Furthermore, the frequency of emission for the charge and the mass is the same, since both are serviced by the underlying energisation process: the electrostatic force is proposed to be from the linear action of the discrete forces, and the mass & gravitation from the torsional action of the same complex of discrete forces. Both effects originate at the reactive ends. Thus the Cordus theory predicts that the moment arm for charge is the same as that for mass, hence:

$$\mu_e/e = S_e/m_e \tag{4}$$

The above moment arm considerations are important. In contrast the classical perspective is that the mass is contained uniformly *inside* a spherical volume whereas the charge is distributed on the *surface* of that volume, hence different moment arms for the two effects.

Substituting Eqnation (5) into Eqnation (4) gives the electron spin g-factor per the Cordus NLHV theory:

$$g_e = 2 \tag{5}$$

This recovers the Dirac electron spin g-factor. This finding disconfirms the classical idea of a particle being a simple spherical solid body. The finding is consistent with QM but independent thereof and derived from a NLHV basis.

This is novel as the derivation is from a NLHV particle theory. Previously the only theory of physics to explain this result has been quantum theory. Providing a derivation using the Cordus particle theory shows that the phenomenon is not a uniquely quantum effect. We have shown this may be accomplished assuming a particle structure with two reactive ends, in contrast to classical mechanics that assumes a spherical particle, and QM a 0-D point particle. Note that this Cordus particle structure was originally derived for a different phenomenon [6], rather than being specifically designed to explain spin, and hence there is coherence across the range of phenomena explained by the theory.

Anomalous magnetic dipole moment

The empirical evidence is that g_e is slightly more than 2, *i.e.* that the moment of charge is larger than the moment of mass, g = 2.00231930436153. This small difference is called the anomalous magnetic dipole moment. It is explained by quantum electrodynamics as an interaction between the electron and one or more virtual photons. QED is able to calculate g_e to high precision, which is one of the great successes of the standard model.

The Cordus theory explains the anomalous magnetic dipole moment as an interaction between the electron and the fabric. The fabric in this theory comprises the volume of space containing the discrete forces emitted by all the particles in the observable universe [40] [42]. The energisation of a reactive end creates and emits a new discrete force into this fabric. There will exist random events when a discrete force in the fabric happens to be co-located and aligned (cis) or anti-aligned (trans) with this new emission, and the response of the particle is slightly asymmetrical.

Where the discrete forces of the electron and the fabric are *aligned* the effect is to momentarily retard the emission of the discrete force, *i.e.* postpone the effect of the charge into the future. This fractionally reduces the strength of the charge in the present moment. For the case where the discrete forces are *anti-aligned*, the combination creates the structure of a photon [29]. This new photon has a brief existence in the fabric. The brevity is due to the two discrete forces, one from the fabric and the other from the electron, being members of separate flux tubes with spatially diverging commitments. Consequently the created photon is merely a temporary random alignment. This is similar to the QM concept of 'virtual photon'. The temporary photon moves a small distance in its brief existence, and then separates into its constituent discrete forces. However we propose that it can occasionally be absorbed by a third particle, such as a passing neutrino. Hence the anti-aligned pairing fractionally neutralises charge, hence *reduces* effective charge while preserving charge moment. The effect is less pronounced for mass, because of the greater statistical improbability of three discrete forces from the fabric having the necessary coincidence. Inspection of Eqnation (4) shows that the effect of these two asymmetries is to increase the g factor above 2. This is not inconsistent with the Schwinger radiative correction [49].

Likewise other fortuitous alignments of discrete forces may mimic the discrete force structure of other particles, such as electron-antielectron, or quark-antiquark pairs, and thereby create virtual particles of these types too. These will also make a small contribution to fractionally decreasing the effect of charge. However these other particles have more complex discrete force structures, and hence the probability of these structures being correctly presented by the randomness in the fabric are smaller. Hence heavier virtual particles will be rarer and make a smaller overall contribution. This is similar to the QED prediction of a secondary contribution by hadronic vacuum polarisation [50].

Muon g-factor

The g factor effect is not proportional to mass, within a family of particles, because the spin angular momentum scales proportionally with increased mass, e.g. for the muon $S_\mu \propto m_\mu$. Nonetheless the muon g factor is not identical to that of the electron, but is instead slightly greater with $g_\mu = 2.0023318414$. Our explanation is that the higher energisation frequency of the muon causes it to emit discrete forces more often, and hence a greater exposure to forming a virtual photon with a discrete force from the fabric. These interactions decrease the effective charge and increase the g factor. In contrast the standard model imputes this to greater access to heavier virtual particles.

The implication is that the fabric density affects the production of virtual photons. The Cordus theory predicts that the production of virtual photons will be proportional to the fabric density, and the alignment thereof with the particle. We make the falsifiable prediction that the anomalous magnetic dipole moment is not universally constant. Instead we predict g_e will be greater in situations of higher fabric density (e.g. regions of higher gravitational field strength or denser galaxies or relativistic velocities), and should display a correlation with orientation (e.g. spin relative to alignment towards charged objects or large bodies of coherent matter). Since the fabric density is temporally and spatially variable in the universe, this further implies that the anomalous magnetic dipole moment changes with epoch and location in the universe. An interesting future research question is whether the anomalous moment might be used to determine the absolute value of the local fabric density.

It makes sense that the production process of virtual photons should depend on the fine structure constant α. This is because α is interpreted in this theory as 'a measure of the transmission efficacy of the fabric, *i.e.* it determines the relationship between the electric constant of the vacuum fabric, and the speed of propagation c through the fabric' [29]. Hence α relates to electrical forces and propagation of fields, which includes electron bonding.

7. Discussion

7.1. Commentary

Starting from first principles of geometry, we have shown that physical structures at the sub-particle level can explain multiple spin phenomena including polarisation, features of coherent-decoherent assemblies, Pauli exclusion principle (Einstein-Podolsky-Rosen paradox), excited states, and selective spin of neutrino species. We finished by recovering the electron spin g-factor $g \approx 2$, and explaining why the anomalous magnetic dipole moment and muon g-factor are greater.

7.2. Implications

We have shown that phenomena considered to be uniquely quantum may be explained by theories other than QM. The conventional interpretation is that the electron g-factor precludes the possibility of fundamental particles having internal structure. Hence QM asserts that spin truly is an intrinsic property. The present work falsifies this by deriving the g-factor using NLHV structures without recourse to quantum theory.

We have achieved this by departing from the conventional assumption that any hidden variable solution would comprise smaller particles rotating about a central mass, somewhat like planets orbiting the sun, the defunct plum-pudding model, or the extant bag models of nuclear structure. Such designs would indeed not explain the g-factor. However there is no need to limit the design of a NLHV solution to an orbital arrangement. By conceptualising a radically different arrangement, we have shown that the g-factor may be recovered.

The g-factor result is more than an interesting curiosity, because it does not stand alone. The same theory has been applied to many other phenomena. It derives from first principles the laws of optical reflection and refraction [6], explains the stability of the atomic nucleus [36] [37], derives the Lorentz factor [43], explains asymmetrical baryogenesis [38]. Other parts of the work address time [41], entropy [39], and the strong force (synchronous interaction) [44]. The theory is logically consistent across all these explanations. This strengthens the case for a new physics based on hidden variables.

The wider implication is that the next deeper level of physics would be based on particles having sub-structures. While the possibility of a non-point structure has been considered from the outset of quantum theory [51], up to now the difficulty has being devising an alternative structure. This is especially as the Bell type inequality tests precluded many types of internal structure [17]. However the specific structure predicted by the Cordus theory is not precluded by the Bell tests [26]. The new theory implies that there is a deeper determinism to particle behaviour, which is approximated by the stochastic representation of quantum mechanics. As shown in the above references, a unification between features of particle behaviour and general relativity is conceptually feasible at this deeper level. This is another attractive feature of the theory.

7.3. Limitations

The limitation of the theory is the lack of a mathematical formalism. In this regard quantum mechanics is much superior. We derived the basic form of the electron g-factor using a mathematical approach, but not the anomalous part. We have yet to find a form of mathematics to represent the Cordus theory – this is an open problem. The number of geometric variables in the Cordus particle is broadly consistent with string/M theory, though the theories come at the problem with different approaches. Possibly this hints at a correspondence, in which case some of the string theories might be formulated to create a mathematical representation of the Cordus particle structure.

7.4. Implications for Future Research

We have only addressed the first of the questions identified at the outset: how does spin arise at the fundamental level? The other questions remain: Why are nuclides with odd total of nucleons fermions, while those with even totals are bosons? Why do some bosons (photons) stack, whereas other bosons like 2He2 nuclei do not co-locate? Why only ½ spin for elementary fermions and predominately 1 for bosons? What is the physical mechanism for the Einstein–de Haas and Barnett effects?

8. Conclusions

This work makes several original conceptual contributions. We propose that the spin property arises from the internal structure of particles, and this is new. We have predicted what those structures are, and how they relate to spin. Consequently, the work provides a physical explanation for spin, which has not been achieved before.

The new spin theory provides a conceptual explanation for a variety of observed spin behaviors. Existing quantum based theories already provide quantitative formalisms in some cases, but an ontological explanation has been lacking.

Another contribution is the advancement of the non-local hidden-variable branch of physics. By addressing the spin behaviors and deriving the electron g-factor, the comprehensiveness of the Cordus theory has been enlarged. The theory provides a single coherent framework that explains spin (this paper), photon absorption & emission [29] [35], matter/antimatter & annihilation [33] [45], nuclide structures and stability (to at least Ne) [36] [37], strong interaction [44], weak interaction [31], decay sequences [30] [32] [52], asymmetrical genesis (baryogenesis and leptogenesis) [34] [38], time dilation [41] [43], aspects of cosmology [40] [42], entropy [39], and wave-particle duality [6] [26]. This is original as it provides wider coverage than other NLHV theories.

This theory explains multiple spin phenomena that are held to be uniquely quantum effects: Pauli electron pairs, excited states, and the electron spin g-factor $g \approx 2$. An explanation, albeit qualitative, is also offered for the anomalous component. Explaining these using a theory of physics other than QM is original.

Another accomplishment is offering an explanation of the selective spin characteristics of the neutrino species. This has not been explained with other theories.

In summary the work demonstrates that a physical basis can be conceived for spin, and that the electron g-factor can be explained by NLHV theory. Consequently, we reject as unnecessary simplification the QM premise that particles are 0D points and particle properties merely intrinsic, and instead we propose the principle of physical realism applies. We suggest the idea that particles do have internal structure is a promising concept for advancing fundamental physics.

Acknowledgements

Parts of this paper are based on an earlier unpublished work [53]. We acknowledge the contribution of Ariel Pons to those early ideas.

Contribution Statement

All authors contributed to the general development of the theory. DP led the development of the specific explanations provided here. DP wrote the first draft of the paper and all authors contributed to its finalisation.

Conflicts of Interest

The authors declare no conflicts of interest regarding the publication of this paper.

References

[1] Xiang, S.-H., Deng, X.-P., Song, K.-H., Wen, W. and Shi, Z.-G. (2011) *Physica Scripta*, **84**, Article ID: 065010. https://doi.org/10.1088/0031-8949/84/06/065010

[2] Julsgaard, B., Kozhekin, A. and Polzik, E.S. (2001) *Nature*, **413**, 400-403. https://doi.org/10.1038/35096524

[3] Hasegawa, Y., Loidl, R., Baron, M., Badurek, G. and Rauch, H. (2006) *Physica B: Condensed Matter*, **385-386**, 1377-1380. https://doi.org/10.1016/j.physb.2006.05.208

[4] Chen, W., Shen, R., Sheng, L., Wang, B.G. and Xing, D.Y. (2012) *Physical Review Letters*, **109**, Article ID: 036802. https://doi.org/10.1103/PhysRevLett.109.036802

[5] Dirac, P.A.M. (1942) *Royal Society of London—Proceeding*, **180**, 1-40. https://doi.org/10.1098/rspa.1942.0023

[6] Pons, D.J., Pons, A.D., Pons, A.M. and Pons, A.J. (2012) *Physics Essays*, **25**, 132-140. https://doi.org/10.4006/0836-1398-25.1.132

[7] Hasegawa, Y., Loidl, R., Badurek, G., Baron, M. and Rauch, H. (2003) *Nature*, **425**, 45-48. https://doi.org/10.1038/nature01881

[8] Stone, N.J. (2014) Table of Nuclear Magnetic Dipole and Electric Quadrupole Moments. International Atomic Energy Agency, Wien, INDC(NDS)-0658. http://www.iaea.org/inis/collection/NCLCollectionStore/_Public/45/029/45029196.

pdf

[9] Samsonenko, N.V. and Katchat Chkhotu, L. (1986) *Soviet Physics Journal*, **29**, 562-565. https://doi.org/10.1007/BF00895504

[10] Saglam, M. and Sahin, G. (2009) *International Journal of Modern Physics B*, **23**, 4977-4985. https://doi.org/10.1142/S0217979209053862

[11] Pei, Y.-J. (1996) *Zeitschrift für Physik C: Particles and Fields*, **72**, 39-46. https://doi.org/10.1007/s002880050221

[12] Lyuboshitz, V. (2009) *Physics of Atomic Nuclei*, **72**, 311-318. https://doi.org/10.1134/S1063778809020173

[13] Barger, V., Chiang, C.-W., Keung, W.-Y. and Marfatia, D. (2011) *Physical Review Letters*, **106**, Article ID: 153001. https://doi.org/10.1103/PhysRevLett.106.153001

[14] Ho, C.M. (2011) *Physics Letters B*, **702**, 398-401. https://doi.org/10.1016/j.physletb.2011.07.035

[15] Parkin, S., Knoner, G., Singer, W., Nieminen, T.A., Heckenberg, N.R. and Rubinsztein-Dunlop, H. (2007) Optical Torque on Microscopic Objects. In: Berns, M.W. and Greulich, K.O., Eds., *Laser Manipulation of Cells and Tissues*, Academic Press, Cambridge, 525-561. https://doi.org/10.1016/S0091-679X(06)82019-4

[16] Colbeck, R. and Renner, R. (2011) *Nature Communications*, **2**, 5. https://doi.org/10.1038/ncomms1416

[17] Bell, J.S. (1964) *Physics*, **1**, 195-200. https://doi.org/10.1103/PhysicsPhysiqueFizika.1.195

[18] Leggett, A. (2003) *Foundations of Physics*, **33**, 1469-1493. https://doi.org/10.1023/A:1026096313729

[19] Groblacher, S., Paterek, T., Kaltenbaek, R., Brukner, C., Zukowski, M., Aspelmeyer, M., *et al.* (2007) *Nature*, **446**, 871-875. https://doi.org/10.1038/nature05677

[20] De Zela, F. (2008) *Journal of Physics A*: *Mathematical and Theoretical*, **41**, Article ID: 505301. https://doi.org/10.1088/1751-8113/41/50/505301

[21] De Broglie, L. (1925) *Annales de Physique*, **3**, 3-109. http://tel.archives-ouvertes.fr/docs/00/04/70/78/PDF/tel-00006807.pdf https://doi.org/10.1051/anphys/192510030022

[22] Bohm, D. and Bub, J. (1966) *Reviews of Modern Physics*, **38**, 453-469. https://doi.org/10.1103/RevModPhys.38.453

[23] Holland, P.R. (1993) *Physics Reports*, **224**, 95-150. https://doi.org/10.1016/0370-1573(93)90095-U

[24] Medina, R. (1999) *Annales de la Fondation Louis de Broglie*, **24**, 129-157.

[25] Egg, M. (2013) *Foundations of Physics*, **43**, 872-880. https://doi.org/10.1007/s10701-013-9723-7

[26] Pons, D.J., Pons, A.D. and Pons, A.J. (2017) *Journal of Modern Physics*, **8**, 1257-1274. https://doi.org/10.4236/jmp.2017.88082

[27] Pons, D.J. (2015) Internal Structure of the Electron (Image Licence Creative Commons Attribution 4.0). Wikimedia Commons, (Creative Commons Attribution 4.0 International License). https://commons.wikimedia.org/wiki/File:Internal_structure_of_the_electron.jpg

[28] Pons, D.J. (2015) Internal Structure of the Photon (Image Licence Creative Commons Attribution 4.0). Wikimedia Commons, Creative Commons Attribution 4.0 International License. https://commons.wikimedia.org/wiki/File:Internal_structure_of_the_photon.jpg

[29] Pons, D.J. (2015) *Applied Physics Research*, **7**, 14-26. https://doi.org/10.5539/apr.v7n4p24

[30] Pons, D.J., Pons, A.D. and Pons, A.J. (2014) *Applied Physics Research*, **6**, 50-63. https://doi.org/10.5539/apr.v6n3p50

[31] Pons, D.J., Pons, A.D. and Pons, A.J. (2015) *Applied Physics Research*, **7**, 1-11. https://doi.org/10.5539/apr.v7n1p1

[32] Pons, D.J., Pons, A.D. and Pons, A.J. (2015) *Applied Physics Research*, **7**, 1-13. https://doi.org/10.5539/apr.v7n2p1

[33] Pons, D.J., Pons, A.D. and Pons, A.J. (2014) *Applied Physics Research*, **6**, 28-46. https://doi.org/10.5539/apr.v6n2p28

[34] Pons, D.J., Pons, A.D. and Pons, A.J. (2015) *Journal of Nuclear and Particle Physics*, **5**, 58-69.

[35] Pons, D.J., Pons, A.D. and Pons, A.J. (2016) *Journal of Modern Physics*, **7**, 1049-1067. https://doi.org/10.4236/jmp.2016.710094

[36] Pons, D.J., Pons, A.D. and Pons, A.J. (2015) *Physics Research International*, **2015**, Article ID: 651361. https://doi.org/10.1155/2015/651361

[37] Pons, D.J., Pons, A.D. and Pons, A.J. (2013) *Applied Physics Research*, **5**, 145-174. https://doi.org/10.5539/apr.v5n6p145

[38] Pons, D.J., Pons, A.D. and Pons, A.J. (2014) *Journal of Modern Physics*, **5**, 1980-1994. https://doi.org/10.4236/jmp.2014.517193

[39] Pons, D.J., Pons, A.D. and Pons, A.J. (2016) *Journal of Modern Physics*, **7**, 1277-1295. https://doi.org/10.4236/jmp.2016.710113

[40] Pons, D.J. and Pons, A.D. (2013) *The Open Astronomy Journal*, **6**, 77-89. https://doi.org/10.2174/1874381101306010077

[41] Pons, D.J., Pons, A.D. and Pons, A.J. (2013) *Applied Physics Research*, **5**, 23-47. https://doi.org/10.5539/apr.v5n6p23

[42] Pons, D.J., Pons, A.D. and Pons, A.J. (2016) *Applied Physics Research*, **8**, 111-121. https://doi.org/10.5539/apr.v8n3p111

[43] Pons, D.J., Pons, A.D. and Pons, A.J. (2018) *Journal of Modern Physics*, **9**, 500-523. https://doi.org/10.4236/jmp.2018.93035

[44] Pons, D.J., Pons, A.D. and Pons, A.J. (2013) *Applied Physics Research*, **5**, 107-126. https://doi.org/10.5539/apr.v5n5107

[45] Pons, D.J., Pons, A.D. and Pons, A.J. (2014) *Physics Essays*, **27**, 26-35. https://doi.org/10.4006/0836-1398-27.1.26

[46] Pons, D.J., Pons, A.D. and Pons, A.J. (2013) Proton-Neutron Bonds in Nuclides: Cis and Trans-Phasic Assembly with the Synchronous Interaction.

[47] Rutherford, E. (1911) *Philosophical Magazine*, **6**, 669-688. https://doi.org/10.1080/14786435.2011.617037

[48] Dirac, P.A.M. (1962) *Royal Society—Proceedings Series A*, **268**, 57-67. https://doi.org/10.1098/rspa.1962.0124

[49] Schwinger, J. (1948) *Physical Review*, **73**, 416-417. http://journals.aps.org/pr/abstract/10.1103/PhysRev.73.416 https://doi.org/10.1103/PhysRev.73.416

[50] Miller, J.P., de Rafael, E. and Roberts, B.L. (2007) *Reports on Progress in Physics*, **70**, 795. https://arxiv.org/abs/hep-ph/0703049 https://doi.org/10.1088/0034-4885/70/5/R03

[51] Einstein, A., Podolsky, B. and Rosen, N. (1935) *Physical Review*, **47**, 777. http://link.aps.org/doi/10.1103/PhysRev.47.777 https://doi.org/10.1103/PhysRev.47.777

[52] Pons, D.J., Pons, A.D. and Pons, A.J. (2015) *Applied Physics Research*, **7**, 18-29. https://doi.org/10.5539/apr.v7n3p18

[53] Pons, D.J., Pons, A.D., Pons, A.M. and Pons, A.J. (2011) Special States of Matter. http://vixra.org/abs/1104.0025

Journal of Modern Physics, 2019, 10, 861-880
http://www.scirp.org/journal/jmp
ISSN Online: 2153-120X
ISSN Print: 2153-1196

Negative Mass: Part One

Edward Tannous

Jaffa, Israel
Email: Etannouss@gmail.com

How to cite this paper: Tannous, E. (2019) Negative Mass: Part One. *Journal of Modern Physics*, **10**, 861-880.
https://doi.org/10.4236/jmp.2019.107057

Received: May 16, 2019
Accepted: June 27, 2019
Published: June 30, 2019

Abstract

This article presents a physical model, which describes the ideas of special relativity, in a rational, logical, simple and understandable manner, while using basic mathematical tools. The model is based on Albert Einstein's formula, which describes the "rest" energy of a body with mass (m), given by the formula $E = mc^2$. Based on this formula, and in accordance with the theory of special relativity, we present here a model of a body, moving at a constant velocity in space (at high speeds, close to the speed of light), with speed equal to the speed of light in space-time, determined with an "energy angle" and negative mass. This model offers a method for creating negative mass, a calculating method for the relative velocity, and a method for calculating energy and momentum, in a completely elastic collision and plastic collision, different than in the contemporary nowadays method found in classical and modern physics. In addition, the new model solves problems and paradoxes known in special relativity physics, such as the Twin Paradox and others.

Keywords

Negative Mass, Energy Angle, Frame of Reference, Speed of Light, Special Relativity

1. Introduction

As known today in modern physics, and especially in the theory of special and general relativity, in quantum physics and cosmology, the Albert Einstein's formula describes the "rest" energy of a body with mass (m), by the formula $E = mc^2$, which means that a body with mass m has a proportional amount of energy and vice versa [1]. This formula determines that this energy E can be calculated as the mass m multiplied by the squared speed of light ($c = 3\times10^8\ \text{m/s}$). The equation claims that if the body is stationary, it has an inner energy, which is its "rest" energy, in accordance with its rest mass. When the body is in motion, its total energy is greater than its rest energy, that is, its total mass is greater than its rest mass. Another assumption is regarding the speed of light. When the body moves, it can obtain momentum and energy, but when it approaches the speed of light, it cannot overpass it, regardless of the additional energy it receives [1].

Moreover, regarding the transition from one inertial frame of reference to another, Galileo's relativity assumption requires the principle of equivalence that the laws of motion are the same in all inertial reference frames [2].

Lorentz transformations, appearing in the theory of special relativity, are linear transformations of coordinates between two reference frames moving at a relative constant velocity and showing how time and space change when moving from one reference frame to an inertial reference frame which moves relatively to it at a constant velocity in a straight line [3]. Minkowski's diagrams [4] describe the space-time dynamics from a perspective of relativity, and make it possible to draw graphically and quite easily how a particular event (or collection of events) will be labeled in different frames.

It is well known that there are a few problems in the theory of special relativity, problems without a solution or with a solution which is not intuitively understood. For example, the Twin Paradox is a thought experiment in which a difference of age between a pair of twins is created: the first twin departs from his brother in space at a very high velocity and returns to Earth, while the second remains on Earth. When they meet again, the twin who left and returned back will be younger than his brother. The reason for the different period of time experienced by the twins is that they have undergone different paths in space-time between these two events. The "self-time" between two events depends on the path that connects them. Therefore, each of them measures another self-time. The solution to the Twin Paradox is difficult to understand and is explained by special relativity.

Another conceptual problem in physics, in general and in special relativity in particular, is that mass, energy, and time must have positive values and cannot have a negative value. As a result, there is currently no way to create a negative mass, there is no way to go back in time, and there is no way to produce gravitational repulsion forces.

Furthermore, the current cosmological measurements support the observation that the universe is expanding and its expansion rate is even increasing. The expansion of the universe is a term that describes the growth of distances between different points in the universe in time. One of the explanations for the expansion of the accelerating universe is based on the speculation of a dark unobserved energy, whose origins and properties are still not known.

The purpose of this paper is to provide a model of a body that explains in a deeper way the problems mentioned above. The model gives the same results of the special relativity in classical and modern physics, but in a simpler and easier way to understand, including Lorentz transformations [5], the Minkowsky time interval [6], the Doppler relativity effect, the Twin paradox, energy formulas, elastic and plastic collisions. Moreover, this article shows the existence of the concepts of the "energy angle" and negative mass, which can change the understanding of laws of physics as known today. The model makes the theory of special relativity understood in a more comprehensive way than before.

The new model and its definitions are described in Section 2. The building of the model and the application of the model formulas in the various fields are described in Section 3, including the solution of the problems mentioned above. Discussion, summary and conclusions are given in Section 4.

2. A body Model Moving in the Space-Time

The basic premise of this new theory is that each body or particle moves in space-time at the speed of light, which is derived from the formula $E = mc^2$. A body with mass m_1 in space observes the universe in a different way, with different dimensions and times as compared to another body with a mass m_2, moving at a different velocity. Moreover, each body feels at rest even if its speed is close to the speed of light relative to another body.

The proposed theory is also based on the Galilean equivalence principle, which claims that the laws of physics are the same in all inertial reference frames. However, instead of the assumption of the constancy of the speed of light, the theory here states that the energy of each mass m in any reference frame is constant, *i.e.* $E = mc^2$, and each mass m measured in any spatial-temporal reference frame of four dimensions is already moving at the speed of light c.

When the body is at rest in the Euclidean space (x, y, z), it can be said that it moves in the fourth dimension which is the time axis (t), and its speed is the speed of light. This time axis is called "Light Time Axis" and we mark it as (ct). The "light time axis" is orthogonal to the three axes in the Euclidean space (x, y, z).

The speed of light is the only absolute speed, to all bodies in the universe, and any other speed is actually the projection of the speed of light on the spatial axes, or the difference between the speeds of light in different directions in the frame axes of space-time.

Each body will be have "self-speed of light vector" $\boldsymbol{C}$, where each body with mass has its own self-speed of light vector in its four-dimensional space $\boldsymbol{C} = (c, 0, 0, 0)$ and each body has a different direction of the 'self-speed of light vector' if we observe it from a common frame of reference, unless they are at the same speed and in the same direction, *i.e.*, the two bodies are at rest relative to each other. In this case, their "self-speed of light vector" will be equal, regardless of the magnitude of the mass.

The 'self-speed of the light vector' has the following properties:

1) The modulus of the "self-speed of light vector" is always equal to the speed of light: $|\boldsymbol{C}| = |\boldsymbol{C}'| = c$

2) At any given time t, "the light distance" measured in the frame of reference is equal for all the masses in any frame: $|\boldsymbol{C}_1 \Delta t| = |\boldsymbol{C}_2 \Delta t| = \cdots$

3) The projection of the "self-speed light vector" on the Euclidean space velocity axis (x, y, z) gives a velocity $\boldsymbol{v}'$ and the projection on the time axis

gives its self-time velocity $\boldsymbol{v}_t'$, wherein $c^2 = v_t'^2 + v_x'^2 + v_y'^2 + v_z'^2$.

4) When the body moves in a Euclidean frame of reference (x, y, z) at a velocity $\boldsymbol{v}' = (v_x', v_y', v_z')$, the "self-speed light vector" is $\boldsymbol{C}' = (v_t', v_x', v_y', v_z')$. The "self-time Velocity" $v_t' = \frac{\mathrm{d}(ct')}{\mathrm{d}t}$ of the moving body in a frame of reference can be calculated, as: $v_t'^2 = c^2 - (v_x'^2 + v_y'^2 + v_z'^2)$, or by the projection of the vector $\boldsymbol{C}'$ on the self-speed light vector $\boldsymbol{C}$ of the frame of reference $v_t' = \frac{\boldsymbol{C} \cdot \boldsymbol{C}'}{c}$

5) The "energy angle" α is the angle between two self-speed light vectors of the reference frame with respect to the moving one, therefore: $\sin\alpha = \frac{v}{c}$ where $v = |\boldsymbol{v}'| = \sqrt{v_x'^2 + v_y'^2 + v_z'^2}$ or $v_t' = c \cdot \cos\alpha$.

The properties of the self-speed of the light vector are obtained as a result of simple basic mathematics, *i.e.* it is based on its definition as a vector representing velocity.

3. Evolution of a Body Moving in the Space-Time

In this section the evolution of a body moving at the speed of light in the space-time, in accordance with this new theory and the model derived from it will be shown. The formulas derived from this new theory, and its implications and applications in the various branches of physics, including solutions of special problems in physics will be detailed.

3.1. Development of Equations According to the Model

This sub-section presents the equations which are derived from this new theory. At first we refer to one body and its relation to other bodies will be discussed later. The evolution of the body in terms of speed, energy, energetic angle, and from there how to obtain a negative mass will be treated. From there it will be shown how to obtain known formulas in physics via this new theory, which include energy formulas, specifically for completely elastic collision and plastic collisions.

3.1.1. One-Dimensional Space

Without losing generality, reference will be made to only a one-dimensional spatial frame (1D) in x and x' axes, orthogonal to ct and ct', respectively. The 1D choice is only to ease the understanding of the theory. The theory applies to 3D models as well.

Figure 1(a) describes the velocity frame of reference of a body moving in relation to a frame of reference at speed v in direction x, showing a self-speed light vector of the moving body, consisting of two elements, the velocity v in the direction of x $v = v_x = \mathrm{d}x/\mathrm{d}t$ and the velocity along the time axis v_t' of the mass in the direction of the axis of the self-speed of light vector of the reference frame. $\boldsymbol{C}$ is the "self-speed light vector" in the frame of reference and $\boldsymbol{C}'$ is the "self-speed light vector" of another moving body. The angle α describes the rotation angle between the two frames. The projection of the self-speed light of the moving body $\boldsymbol{C'}$ on the horizontal axis v_x gives the velocity v in the x direction. Its projection on axis $\boldsymbol{C}$ gives the self-time speed $v'_t = \mathrm{d}(ct')/\mathrm{d}t$, which is the speed of light time of the moving body measured in the frame of reference.

The x or x' axis is determined perpendicularly to the "self-speed of light vector" of each frame separately. Thus, we obtain that the angle α between the two "self-speed light vectors" is the same angle between the two axes x and x'.

Figure 1(b) describes a model called "Integral Couple Frame" (**ICF**), a time integration frame with the following meaning:

An integral on v_x creates the x-axis and its direction.

An integral on $\boldsymbol{C'}$ creates the ct axis and its direction.

An integral on v'_t creates the ct' axis and its direction.

It should be noted that the x' axis is normalized to the "self-speed light vector" of the moving body $\boldsymbol{C'}$.

The result gives two frames with distances x', ct and x, ct' wherein the ct time axis is not normal to the x axis, and the ct' axis is not normal to the x' axis.

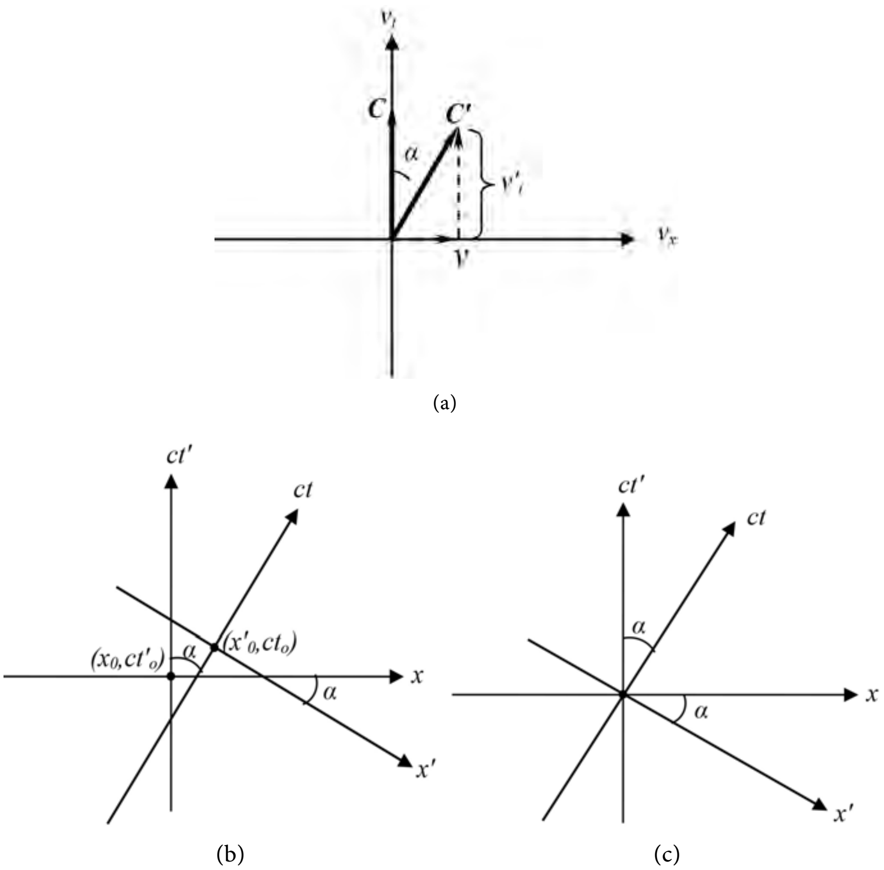

Figure 1. (a) The velocities plot of the moving body model relative to a frame of reference, with $\boldsymbol{C}$ "self-speed of light vector" in the body frame of reference and $\boldsymbol{C'}$ the "self-speed of light vector" of the moving body. The angle α describes the rotation angle between the two frames;. (b) "Integral Couple Frame" Model (ICF), which is a time integra-

tion. The angle α is the same angle as in **Figure 1(a)**; (c) The body's initial condition.

The parameters x_0, x'_0, ct_0, ct'_0 are the constants obtained from the integration operation and have values that can be calculated according to the boundary values, *i.e.* the initial conditions. The main axes can be placed one over the other and can be reset in time and space as shown in **Figure 1(c)**. The ICF model, which describes the intersection between x' and ct axes, shows the motion in the frame with time progression, while the point of $x' = 0$ will always be attached to the ct value.

3.1.2. Lorentz Transformation

As mentioned above, the value of the angle α depends proportionally on the magnitude of the speed v:

$$v = c \sin \alpha \tag{1}$$

The parameter β can be found from Equation (1), that is the ratio between the speed v and the speed of light c:

$$\beta = \frac{v}{c} = \sin \alpha \tag{2}$$

The Lorentz factor defined in Einstein's theory of relativity and its relation to the energetic angle α can also be identified here as:

$$\gamma = \frac{1}{\sqrt{1 - \frac{v^2}{c^2}}} = \frac{1}{\sqrt{1 - \sin^2 \alpha}} = \frac{1}{\cos \alpha} \tag{3}$$

Figure 2 describes the changes in distances and light time in the moving frame and their projections in the stationary frame. The differences in the moving frame measured in the reference frame are:

$$\begin{aligned} \Delta x &= \cos \alpha \cdot \Delta x' \\ \Delta t &= \frac{1}{\cos \alpha} \cdot \Delta t' \end{aligned} \quad \text{therefore} \quad \begin{aligned} \Delta x &= \frac{1}{\gamma} \Delta x' \\ \Delta t &= \gamma \Delta t' \end{aligned} \tag{4}$$

In the equations above, two concepts are obtained, Length contraction and Time dilation. That is, the length $\Delta x'$ of the moving frame measured from the reference frame Δx is shorter. In fact, the length and time of light do not change, but their projections from one frame to another are different.

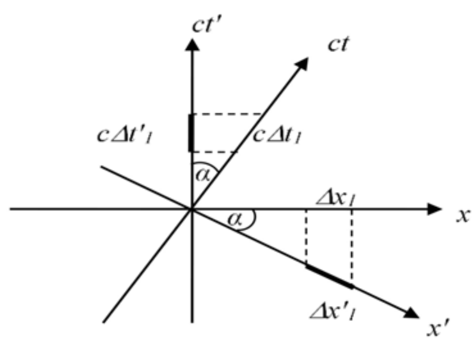

Figure 2. The changes in distance and light time in the moving frame and their projections in the stationary frame.

Figure 3 describes two events, e and k, in the x,ct plane and x',ct' plane and the projections of the coordinates in both frames. The values of the events e and k are obtained by calculating the coordinate's projections of the events in one frame onto the other frame, and the subtraction between them results in the equations of the following differences.

i.e. $\Delta x = x_e - x_k$, $\Delta x' = x'_e - x'_k$, $\Delta ct = ct_e - ct_k$ and $\Delta ct' = ct'_e - ct'_k$.

We obtain thus:

$$\begin{matrix} \Delta x' = \cos\alpha \cdot \Delta x - \sin\alpha \cdot c\Delta t' \\ c\Delta t = \cos\alpha \cdot c\Delta t' + \sin\alpha \cdot \Delta x \end{matrix} \quad \text{and vice versa} \quad \begin{matrix} \Delta x = \cos\alpha \cdot \Delta x' + \sin\alpha \cdot c\Delta t \\ c\Delta t' = \cos\alpha \cdot c\Delta t - \sin\alpha \cdot \Delta x' \end{matrix} \tag{5}$$

We can substitute Equation (1) and (3) into Equation (5), resulting in Lorentz transformation:

$$\begin{matrix} \Delta x' = \gamma\left(\Delta x - v\Delta t\right) \quad \text{and vice versa} \quad \Delta x = \gamma\left(\Delta x' + v\Delta t'\right) \\ \Delta t' = \gamma\left(\Delta t - \dfrac{v}{c^2}\Delta x\right) \qquad \Delta t = \gamma\left(\Delta t' + \dfrac{v}{c^2}\Delta x'\right) \end{matrix} \tag{6}$$

If the distance between the two events e and k is l, Minkowski's interval formula can be obtained directly without using an imaginary time axis:

$$l^2 = (c\Delta t)^2 + \Delta x'^2 = (c\Delta t')^2 + \Delta x^2$$
$$\Downarrow$$
$$\Delta s^2 = (c\Delta t)^2 - \Delta x^2 = (c\Delta t')^2 - \Delta x'^2$$

In the Euclidean space x, y, z:

$$\Delta s^2 = (c\Delta t)^2 - \Delta x^2 - \Delta y^2 - \Delta z^2 = (c\Delta t')^2 - \Delta x'^2 - \Delta y'^2 - \Delta z'^2 .$$

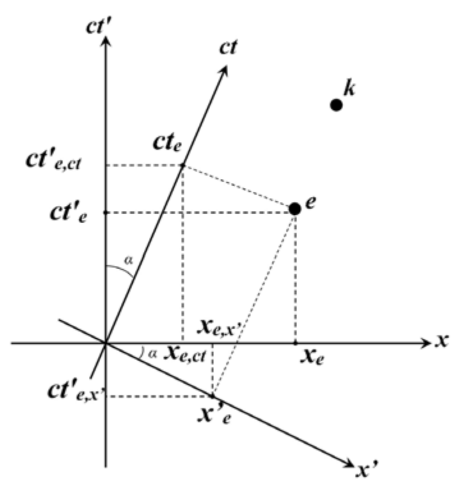

Figure 3. Two events e and k in the x,ct plane and x',ct' plane and coordinates' projections for both frames.

3.1.3. Invariance of the Speed of Light in the 2 Frames

This theory, as we have pointed out, is based on one premise, namely that each body moves in space-time at the speed of light. Here we will demonstrate that

Einstein's premise, which is that the speed of light is equal in all frames, is indeed obtained from our premise regarding the energy of a moving body.

Figure 4(a) describes a photon exiting from the origin of the stationary frame at time $t = t' = 0$ and making its way to point x_1. The angle at which the photon advances in the x, ct plane is β, which is a bisector of the two axes *i.e.*, $\beta = (\pi/4 - \alpha/2)$.

Figure 4(b) describes the photon reaching point x_1, where the stationary frame progresses in time to a value of ct_1. The values of x' and ct' are equal at this point. Both the stationary and moving frames measure a speed of light equal to c, even though the distances and times are not equal. The ratio of the distances that the light travels in the stationary and moving frames is:

$$\frac{x'}{x} = \frac{ct'}{ct} = \tan\beta = \frac{1-\sin\alpha}{\cos\alpha} \quad \text{which shows a Doppler effect for the relativistic case.} \tag{7}$$

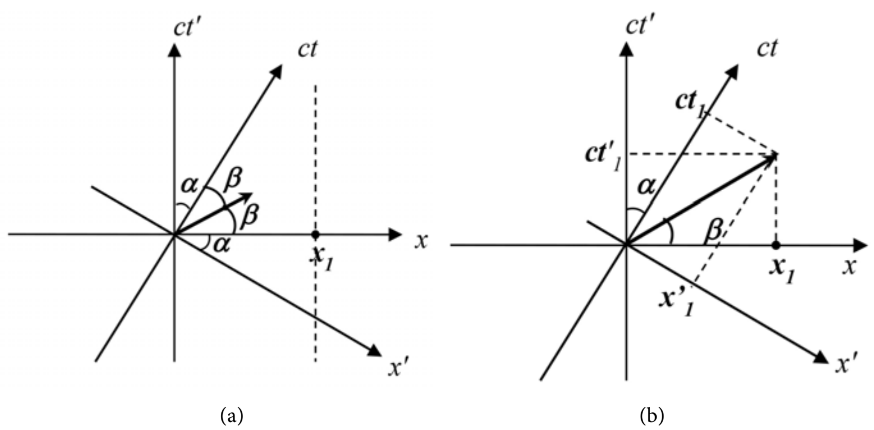

Figure 4. (a): Scheme of a photon exiting from the origin of the stationary frame and the description of distances and times in the frames. (b): The photon reaches point x_1 and the description of the distances and times in the frames.

Figure 5 describes the separation velocity vector $\boldsymbol{V}_{ax}$, the separation of the axes' origin of the moving frame $(x', y', z') = (0,0,0)$ from the axes' origin of the stationary (reference) frame $(x, y, z) = (0,0,0)$ in the space-time plane. The velocity of the moving frame is the vector difference between two vectors of the speed light vectors of both frames with $\boldsymbol{C}_1$ and $\boldsymbol{C}_2$. The vectors in the polar description (r,θ) are: $\boldsymbol{C}_1 = \left(c, \frac{\pi}{2}\right)$ and $\boldsymbol{C}_2 = \left(c, \frac{\pi}{2} - \alpha\right)$, whose representation in Cartesian form is: $\boldsymbol{C}_1 = (0, c) = c\hat{v}_t$ and $\boldsymbol{C}_2 = (v, v'_t) = v\hat{v}_x + v'_t\hat{v}_t$ wherein: $\hat{v}_t$ is a unit vector of the velocity in the direction of the "light time" axis ct, and $\hat{v}_x$ is a unit vector velocity in the direction of the x-axis. $\boldsymbol{V}_{ax}$ is the separation velocity vector, *i.e.*, the separation of the two bodies in the space-time, whose direction is the movement of the axes' origin of the one-dimensional moving frame $(x') = (0)$ relative to the axes' origin of the stationary frame

$(x)=(0)$.

Using $v=c\sin\alpha$ and $v'_t=c\cdot\cos\alpha$ will lead to

$\boldsymbol{V}_{ax}=c\sin\alpha\hat{v}_x+c(\cos\alpha-1)\hat{v}_t$

The use of $\cos\alpha=\cos^2(\alpha/2)-\sin^2(\alpha/2)$ and $\sin\alpha=2\sin(\alpha/2)\cos(\alpha/2)$ will lead to: $\boldsymbol{V}_{ax}=2c\sin(\alpha/2)\cos(\alpha/2)\hat{v}_x+c\left(\cos^2(\alpha/2)-1-\sin^2(\alpha/2)\right)\hat{v}_t$

Finally using $\cos^2(\alpha/2)-1=-\sin^2(\alpha/2)$ will lead to:

$$\boldsymbol{V}_{ax}=2c\sin(\alpha/2)\cos(\alpha/2)\hat{v}_x-2c\sin^2(\alpha/2)\hat{v}_t$$

$$\boldsymbol{V}_{ax}=2c\sin(\alpha/2)\left(\cos(\alpha/2)\hat{v}_x-\sin(\alpha/2)\hat{v}_t\right)$$

In a polar representation the upper expression, gives the following formula:

$$\boldsymbol{V}_{ax}=\boldsymbol{C}_2-\boldsymbol{C}_1=\left(2c\sin\left(\frac{\alpha}{2}\right),-\frac{\alpha}{2}\right) \tag{8}$$

The projection of the velocity vector on the *x*-axis gives the relation for the speed v using Equation (1):

$$\boldsymbol{V}_{ax}\cos\frac{\alpha}{2}=2c\sin\frac{\alpha}{2}\cos\frac{\alpha}{2}=c\sin\alpha=v \tag{9}$$

When the moving frame reaches the speed $v=c$, the value of $\boldsymbol{V}_{ax}$ will be greater than the speed of light, in the space-time, and its angle is -45°. Thus, when $\alpha=\pi/2$, $\boldsymbol{V}_{ax}=\left(\sqrt{2}\cdot c,-\frac{\pi}{4}[\mathrm{rad}]\right)$. This result does not contradict the known laws of physics nowadays, namely that the transfer of energy or mass cannot exceed the speed of light in the Euclidean frame (x,y,z) or (x',y',z'). Indeed, this velocity is in the space-time, and by its projections on each of the three axes, a speed is obtained, which is not greater than the speed of light.

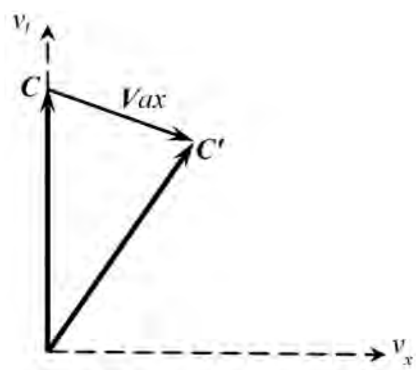

Figure 5. The separation velocity vector, is the separation of the moving frame from the stationary frame.

Figure 6 describes the model for calculating relative velocities of three bodies 1, 2, 3 at different velocities. The first body is treated as a reference frame 1 with x_1, ct_1, *i.e.* $v_{11}=0$, wherein the speed of body number 1 relative to frame 1 is zero, and the self-speed of light vector is $\boldsymbol{C}_1=\left(c,\frac{\pi}{2}\right)$. The second body's frame

x_2, ct_2 moves at a speed v_{12} relative to the first frame and the angle α_{12} is: $\sin\alpha_{12} = v_{12}/c$ with a self-speed of light vector $\boldsymbol{C}_2 = \left(c, \frac{\pi}{2} - \alpha_{12}\right)$, whose projection on the x axis is v_{12}. The velocity of the third body relative to the second frame is v_{23} (we assume that the velocity is in the positive direction of x) with the angle α_{23} according to $\sin\alpha = v_{12}/c$ and gives the self-speed of light vector $\boldsymbol{C}_3 = \left(c, \frac{\pi}{2} - \alpha_{23}\right)$. The velocity of the third body v_{13} by projection of its self-speed of light $\boldsymbol{C}_3$ on the v_{x1} axis of the reference frame is:

$$v_{13} = c\sin\left(\alpha_{12} + \alpha_{23}\right) \tag{10}$$

At speeds much smaller than the speed of light, we obtain $v_{13} = v_{12} + v_{23}$, following Equation (1) since: $\lim\limits_{\alpha_{12},\alpha_{23}\to 0} \sin\left(\alpha_{12} + \alpha_{23}\right) = \sin\alpha_{12} + \sin\alpha_{23}$.

The velocity of the third frame in the reference frame can also be calculated if the velocity v_{23} is in the direction of y_2 axis of the second frame. We therefore obtain the following expression: $\cos\alpha_{13} = \cos\alpha_{12} \cdot \cos\alpha_{23}$. It is possible to calculate v_{13} from Equationn (1) by: $v_{13}^2 = v_{12}^2 + v_{23}^2 - \frac{v_{12}^2 v_{23}^2}{c^2}$. Here, too, at small velocities, we obtain $\lim\limits_{v_{12},v_{23}\ll c} v_{13}^2 = v_{12}^2 + v_{23}^2$ which is a vector addition of speeds according to Pythagoras theorem.

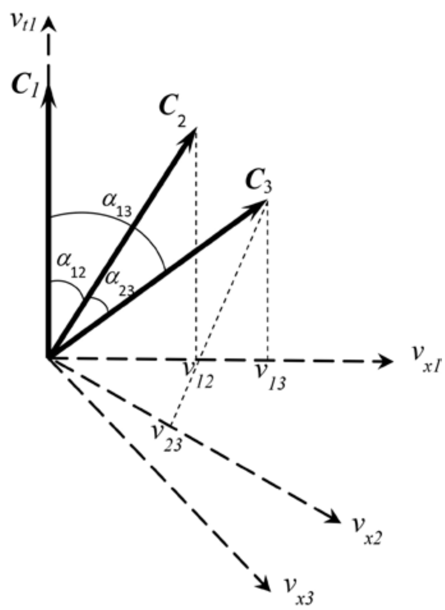

Figure 6. A model presentation for the calculation of relative velocities while describing frames of three bodies at different velocities, and the first body is a reference frame.

Figure 7 describes an array of self-speed of light vectors of three bodies, wherein body 2 moves in the direction of the *x*-axis and body 3 moves in the direction of the *y*-axis.

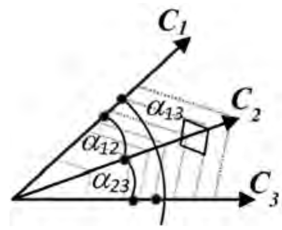

Figure 7. Vector description of self-speed of light vectors of three bodies.

3.1.4. Energy

In this model, the body moves always at the speed of light in space-time, and the velocity of the body in the Euclidean space x, y, z does not change the value of the self-speed of light vector, but only its direction, *i.e.* the angle α. Accordingly, its total energy is $m_0 c^2$ (m_0 is the rest mass of the body). The self-speed light vector in the fourth-dimensional space is: $\boldsymbol{C}' = \left(\frac{\mathrm{d}(ct')}{\mathrm{d}t}, v\right)$, which is composed of two main parts, the self-speed of light $v_t = \frac{\mathrm{d}(ct')}{\mathrm{d}t}$ and the speed of the body relative to the reference frame in the Euclidean space $\boldsymbol{v}$.

The energy consists of the following components:

A) The body self-time energy E_{st}, which determines the **amount of mass left as a result of the movement.**

B) "State" kinetic energy E_α, which is the energy that the body carries in the reference frame, as a result of its speed. (In this case, this energy is kinetic energy, but in other cases, it may also include other energies, therefore here the sign and name are).

The self-time energy E_{st} is the product of the mass m and $\boldsymbol{C}_1$ and $\boldsymbol{C}_2$ that is, the projection of the moving body's self-speed of light vector on the reference frame:

$$E_{st} = m_0 \boldsymbol{C}_1 \cdot \boldsymbol{C}_2 = m_0 c^2 \cos\alpha \equiv \frac{m_0 c^2}{\gamma} \quad (11)$$

i.e., the self-time energy of the mass is smaller than the "rest" energy $E_0 = m_0 c^2$ reaching a value of $m_0 c^2 \cos\alpha$ of the energy in a moving condition, and the difference between them is actually the state kinetic energy E_α, which can also be obtained by the projection of the velocity $\boldsymbol{C}_2$ on the motion direction of the moving frame in the following formula:

$$E_\alpha = m_0 \boldsymbol{C}_2 \cdot \boldsymbol{V}_{ax} = 2 m_0 c^2 \sin^2(\alpha/2) = m_0 c^2 (1 - \cos\alpha) \equiv m_0 c^2 \left(1 - \frac{1}{\gamma}\right) \quad (12)$$

For small values of α (small speeds relative to the speed of light), the state kinetic energy tends to $E_k = \frac{m_0 v^2}{2}$ from $\lim_{\alpha \to 0} \frac{E_\alpha}{\frac{m_0 v^2}{2}} = \frac{m_0 c^2 (1 - \cos\alpha)}{\frac{m_0 c^2 \sin^2\alpha}{2}} = 1$ and when the speed approaches the speed of light, the energy approaches

$E_k = E_\alpha = m_0c^2$.

That is, when $\alpha = \pi/2$, the total energy of the mass is kinetic m_0c^2 and the self-time energy is zero at this point. This model is in contrast to Einstein's result, that the mass increases to infinity as the speed increases and approaches the speed of light, thus the formula he obtained $E = \gamma m_0 c^2$ is incorrect according to our model.

According to the model of the current theory, the energy conservation law is kept and the sum of the two energies E_{st} and E_α is the rest energy of the body $E_0 = m_0c^2$:

$$E_0 = E_{st} + E_\alpha = m_0c^2 \tag{13}$$

3.1.5. Negative Mass

Figure 8 describes quadrant zones of the changes in the energetic state of a moving body for changes of the energetic angle α, in the range of $(-\pi)$ to (π). Quadrant A shows the change in the velocity from 0 to c, quadrant B shows the change in the velocity from 0 to $-c$, quadrant C shows the change in the velocity from c to 0 and quadrant D shows the change in the velocity from $-c$ to 0. Quadrants C and D are areas where the self-time speed is negative, so that the self-time obtained by the integration method (as shown in Figure 1) is negative, and it is a zone of negative mass.

Figure 9 describes the ratio of the speeds and energies of a body as a function of the energetic angle α, in accordance with the measurement of the velocity and its direction in the reference frame. The sum of the body total energy is equal to $E_0 = m_0c^2$. When the energy angle α is $\pi/2$, the speed energy angle of the moving body reaches the speed of light and the state kinetic energy is equal to m_0c^2. With greater energy input, the body's speed will decrease until the energy angle reaches π and the body will be in a rest state with state kinetic energy of $2m_0c^2$ and self-time energy $\left(-m_0c^2\right)$. The figure shows the speed of a moving body normalized to c, the state kinetic energy E_α and the self-time energy E_{st} normalized both to m_0c^2, as a function of the angle α which extends in the range of $-\pi$ and π, from measurements in a stationary frame. Increasing the speed causes the body mass to be reduced. When the speed reaches the speed of light, the body will be completely massless. The self-time energy E_{st} is the amount of energy left in the body after some of it becomes kinetic energy, and its mass decreases by:

$$m = m_0 \cos\alpha = m_0/\gamma \tag{14}$$

As the body reaches $\alpha = \pi/2$, the speed begins to gradually decrease and the body reaches a negative self-time zone. When the body reaches $\alpha = \pi$, the speed is zero, the kinetic energy is $E_k = 2m_0c^2$ and the self-time energy is $E_{st} = -m_0c^2$. The effective mass m of the body (the mass which the reference frame perceives of the same body) is:

$$E_{st(\alpha=\pi)} = -m_0c^2 = m_{(\alpha=\pi)}c^2 \Rightarrow m_{(\alpha=\pi)} = -m_0 \tag{15}$$

The value of the gravitational force is in inverse ratio by:

$$F_{(\alpha=\pi)} = G\frac{m_{(\alpha=\pi)}M}{r^2} = G\frac{-m_0 M}{r^2} < 0$$

where in M is the mass of the gravitational source (in the reference frame), r is the distance between the masses centers and G is the gravitational constant.

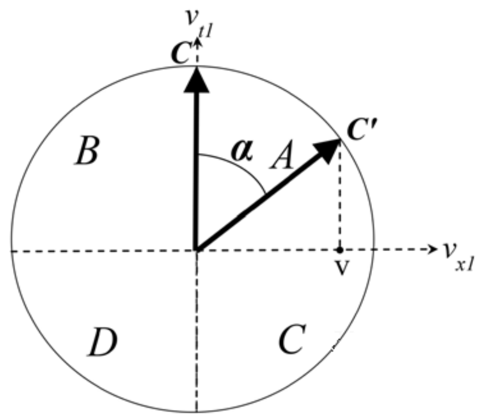

Figure 8. Zones of changes in the energetic state of a moving body with the change of the energetic angle α, in the range of $(-\pi)$ to (π). Quadrants C and D are zones where the self-time speed is negative, so that the self-time is negative, and it is a zone of negative mass.

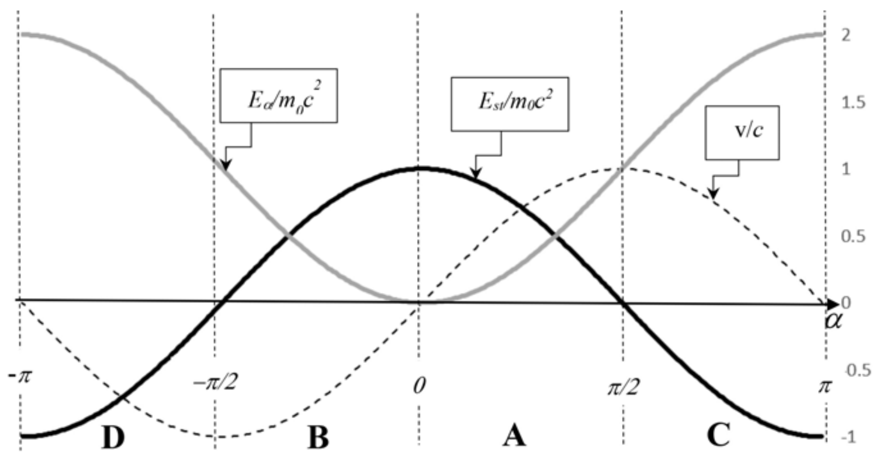

Figure 9. The ratio of the normalized speeds and energies of a body as a function of the energetic angle α. The graph shows the speed of a moving body normalized to c, the kinetic energy E_k normalized to m_0c^2, and the self-time energy E_s normalized to m_0c^2, as a function of the angle α in the range of $-\pi$ and π as measurements from a stationary frame.

Attention is now drawn to **Figure 10(a)** and **Figure 10(b)**, when the body exceeds $\alpha = \pi/2$. **Figure 10(a)** is in the range of $\pi/2 < \alpha < \pi$ and **Figure 10(b)** is in the range of $-\pi < \alpha < -\pi/2$ When the body exceeds the speed-of-light barrier, its speed decreases and its self-time energy receives negative values. The self-time of the moving frame progresses in the negative direction. The projection of a body, moving in the direction of the arrow, in the x-axis is in reverse to its direction, *i.e.* it will move away. Its direction is reversed, therefore its future can be seen, but after a while it moves away and its past can be seen. When the body is in a gravitational field, it will move against gravity, moving from the future to the past.

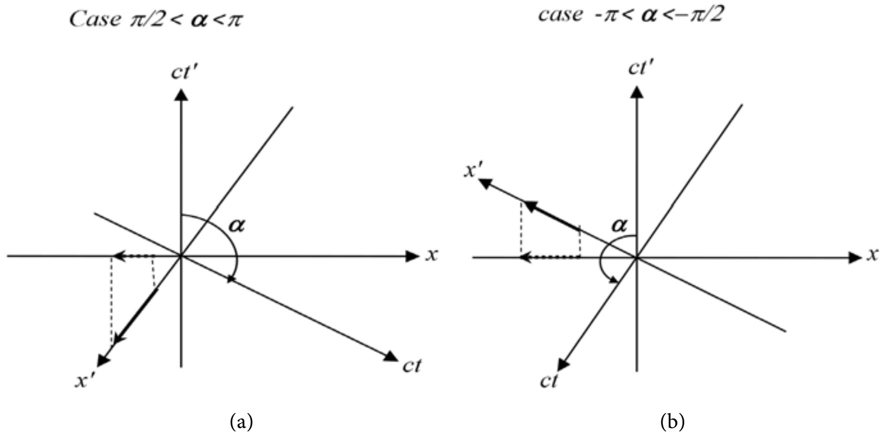

Figure 10. (a) Two frames model for the energy angles in the range of $\pi/2 < \alpha < \pi$; (b) Two frames model for the energy angles in the range of $-\pi < \alpha < -\pi/2$.

Figure 11 shows several bodies K, L, M, N with different self-velocity vectors and the forces of attraction or rejection between them, where body K represents the reference frame. There is an attraction force between the body K and body L and a repulsive force between body K and body N. Also, there is an attraction force between body L and the two bodies, K and N. When body L moves to the right at a speed close to the speed of light and body M moves to the left at a speed close to the speed of light, the speed of body L relative to body M is significantly smaller than the speed of light (it can be seen from the projection of the self-speed of light vector on the x axis of body M), because in relation to it, body L has a negative mass. A negative mass is relative to another mass when the angle between the self-speed vectors between the two masses is greater than $\pi/2$. Negative mass is also obtained for values of velocities smaller than the speed of light, including the zero velocity (a state of rest).

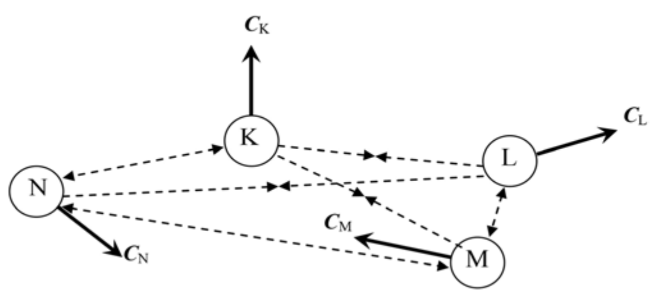

Figure 11. Description of bodies with different self-velocity vectors and the forces of attraction or repulsion between them.

3.1.6. The Amount of Energy Required to Bring a Body to the Speed of Light

The model also provides a method for calculating the amount of energy required to bring a body from a state of rest to the speed of light, according to the following steps:

Applying an F force in order to change the angle of the self-speed of light vector from $\alpha = 0$ to $\alpha = \pi/2$.

Inserting the momentum value $F = \frac{\mathrm{d}p'}{\mathrm{d}t}$ in the formula $\mathrm{d}E_\alpha = F\mathrm{d}x'$ leads to $\mathrm{d}E_\alpha = \mathrm{d}p' \underbrace{\frac{\mathrm{d}x'}{\mathrm{d}t}}_{v'}$

Using the momentum relation $p' = m'v'$ and the differential $\mathrm{d}p' = m'\mathrm{d}v' + v'\mathrm{d}m'$ will lead to $\mathrm{d}E_\alpha = m'v'\mathrm{d}v' + v'^2\mathrm{d}m'$.

Using Equation (1) of the velocity projection value v' on the x axis: $v' = \frac{v}{\cos\alpha}$ will lead to $v' = \frac{c\sin\alpha}{\cos\alpha}$.

Using the differential $\mathrm{d}v' = \frac{c}{\cos^2\alpha}\mathrm{d}\alpha$ and the differential of the mass $m' = m_0\cos\alpha$ is $\mathrm{d}m' = -m_0\sin\alpha\mathrm{d}\alpha$ will lead to the calculation of the energy differential $\mathrm{d}E_\alpha = m_0\cos\alpha\frac{c\sin\alpha}{\cos\alpha}\frac{c}{\cos^2\alpha}\mathrm{d}\alpha - \frac{c^2\sin^2\alpha}{\cos^2\alpha}m_0\sin\alpha\mathrm{d}\alpha$: Finally, using a trigonometric identity leads to $\mathrm{d}E_\alpha = m_0c^2\sin\alpha\mathrm{d}\alpha$.

Since the energy angle needed to bring the body to the speed of light is $\alpha = \pi/2$, the calculation of the energy needed to bring the mass to the speed of light is:

$$E_{\alpha=\pi/2} = \int_0^{\pi/2} m_0c^2\sin\alpha\mathrm{d}\alpha = m_0c^2$$

3.1.7. One-Dimensional Elastic Collision

Attention is now focused on calculating a completely elastic collision in accordance with our model. The coefficient of restitution is equal to 1, meaning that there is no energy loss as a result of the collision. The momentum calculation is based on the equation:

$$m_1\boldsymbol{C}_1 + m_2\boldsymbol{C}_2 = m_1\boldsymbol{C}_1' + m_2\boldsymbol{C}_2' \tag{16}$$

wherein $\boldsymbol{C}_1$ and $\boldsymbol{C}_2$ are the self-speed of light vectors of the two bodies before the collision and $\boldsymbol{C}_1'$ and $\boldsymbol{C}_2'$ are the self-speed light vectors of the two bodies after the collision.

Inserting the value of the self-speed of light vectors $\boldsymbol{C} = c\cdot\cos\alpha\cdot\hat{t} + c\cdot\sin\alpha\cdot\hat{x}$ in this formula will give:

$$\begin{aligned} m_1\sin\alpha_1 + m_2\sin\alpha_2 &= m_1\sin\alpha_1' + m_2\sin\alpha_2' \\ m_1\cos\alpha_1 + m_2\cos\alpha_2 &= m_1\cos\alpha_1' + m_2\cos\alpha_2' \end{aligned} \tag{17}$$

The top equation in this pair of equations is the momentum formula known in classical physics as $m_1 v_1 + m_2 v_2 = m_1 v_1' + m_2 v_2'$, while the second equation is the momentum equation in the time axis. The self-time energies of the two bodies before and after the collision will be $E_{st1} + E_{st2} = E_{st1}' + E_{st2}'$, so that:

$m_1 \cos\alpha_1 + m_2 \cos\alpha_2 = m_1 \cos\alpha_1' + m_2 \cos\alpha_2'$ is obtained, which is the same equation obtained in the last pair of equations. The same formula will be derived from the state kinetic energy conservation law $E_{\alpha_1} + E_{\alpha_2} = E_{\alpha_1'}' + E_{\alpha_2'}'$ (wherein $E_\alpha = m_0 c^2 \left(1 - \cos\alpha\right)$).

3.1.8. Plastic Collision

Attention is now referred to the calculation of a plastic collision, in which two bodies collide and merge into one body. The momentum conservation law will be here according to the following equation:

$$m_1 \boldsymbol{C}_1 + m_2 \boldsymbol{C}_2 = m_3 \boldsymbol{C}_3 \tag{18}$$

wherein $\boldsymbol{C}_2$ and $\boldsymbol{C}_2$ are the self-speed light vectors of the two bodies before the collision and $\boldsymbol{C}_3$ is the self-speed light vector of the body with mass m_3 after the collision. Inserting the self-speed light vector value will lead to the following pair of formulas:

$$\begin{aligned} m_1 \sin\alpha_1 + m_2 \sin\alpha_2 &= m_3 \sin\alpha_3 \\ m_1 \cos\alpha_1 + m_2 \cos\alpha_2 &= m_3 \cos\alpha_3 \end{aligned} \tag{19}$$

The loss of energy $m_1 c^2 + m_2 c^2 > m_3 c^2$ is part of the mass of the two bodies, the mass m_3 will always be smaller than the sum of the two masses m_1 and m_2 and the difference between them is Δm:

$$m_1 + m_2 = m_3 + \Delta m \tag{20}$$

$$\Delta m = \left(m_1 + m_2\right)\left(1 - \sqrt{1 - \frac{4 m_1 m_2}{\left(m_1 + m_2\right)^2} \sin^2 \frac{\alpha_1 + \alpha_2}{2}}\right) \tag{21}$$

Using formulas $\lim\limits_{x \to 0} \left(1 - x\right)^{0.5} = \lim\limits_{x \to 0} \left(1 - 0.5x\right)$ and $\lim\limits_{\alpha \to 0} \sin\alpha = \lim\limits_{\alpha \to 0} a$ will lead for small speeds to the result:

$$\Delta m = \frac{m_1 m_2}{2\left(m_1 + m_2\right)} \left(\sin\alpha_1 - \sin\alpha_2\right)^2 \tag{22}$$

and the loss of energy at small speeds will be:

$$\Delta E = \Delta m c^2 = \frac{m_1 m_2}{2\left(m_1 + m_2\right)} \left(v_1 - v_2\right)^2 \tag{23}$$

This is the same result known from classical physics, in a plastic collision, *i.e.* the loss of energy as a result of the plastic collision ΔE is equal to the value of the energy loss of mass difference m due to collision $\Delta E = \Delta m c^2$.

3.2. Solving Problems According to the Model

In this sub-section, it will be shown how this new theory can be applied to solving complicated and difficult current problems in physics, based on this model, which are simpler and easier solutions to understand. Problems as examples include the Twin Paradox. The expansion of the universe in acceleration and a black hole, which we will explain in the next chapter.

3.2.1. The Twin Paradox

Figure 12 describes a solution to the Twin Paradox in a simple way, by showing the speed of the moving frame in space-time, in two directions. By placing the value $\Delta x' = 0$ (the traveling brother remains at the origin of the axes of the moving frame) from the equations of Lorentz's transformation obtained in Equation (6), the time difference between the two frames is:

$\Delta T = 2\Delta t\left(1-\frac{1}{\gamma}\right) = 2\frac{\Delta x}{v}\left(1-\frac{1}{\gamma}\right)$. The reference frame is of the brother who is left behind, whose self-speed light vector is $\boldsymbol{C}_1 = \left(c, \frac{\pi}{2}\right)$. As soon as the twins separate, the self-speed light vector of the moving frame is $\boldsymbol{C}_{2F} = \left(c, \frac{\pi}{2} - \alpha\right)$, therefore the speed of the moving frame in space-time calculated by Equation (8) is: $\boldsymbol{V}_{axF} = \boldsymbol{C}_{2F} - \boldsymbol{C}_1 = \left(2c\sin\left(\frac{\alpha}{2}\right), -\frac{\alpha}{2}\right)$. When the traveling twin returns, at the same speed but in the opposite direction, the self-speed light vector is $\boldsymbol{C}_{2B} = \left(c, \frac{\pi}{2} + \alpha\right)$, therefore the velocity of the frame in space is

$\boldsymbol{V}_{axB} = \boldsymbol{C}_{2B} - \boldsymbol{C}_1 = \left(2c\sin\left(\frac{\alpha}{2}\right), \pi + \frac{\alpha}{2}\right)$. Using trigonometric identities

$2\cos\frac{\alpha}{2}\sin\frac{\alpha}{2} = \sin\alpha$ and $2\sin^2\frac{\alpha}{2} = 1 - \cos\alpha$ will lead to the value of time difference ΔT by placing it in Equation (3):

$$\Delta T = 2\frac{\Delta x}{v}(1-\cos\alpha) = 2\frac{\Delta x}{v}\left(1-\frac{1}{\gamma}\right) \tag{24}$$

Theoretically, we obtain:

$\Delta T < 2\frac{\Delta x}{v}$ for $0 < \alpha < \frac{\pi}{2}$, when $2\frac{\Delta x}{v}$ is the time which the stationary twin observes. $\Delta T > 2\frac{\Delta x}{v}$ for $\frac{\pi}{2} < \alpha < \pi$, so that the traveling twin seems to be coming back before the beginning of the trip, *i.e.* **movement back in time**.

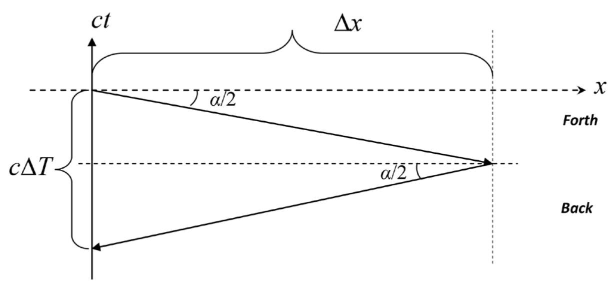

Figure 12. Solving the Twin Paradox by showing the velocity of the frame moving in space-time in two directions, we obtain that the returning twin is younger with a difference of ΔT.

Figure 13 describes the motion of the moving twin relative to his twin brother in the axial frame (using ICF). The ct axis is at an angle $+\alpha$ relative to the ct' axis on the way forth, compared to the way back, when the angle is $-\alpha$. Here as well, we obtain the same time difference between the two frames.

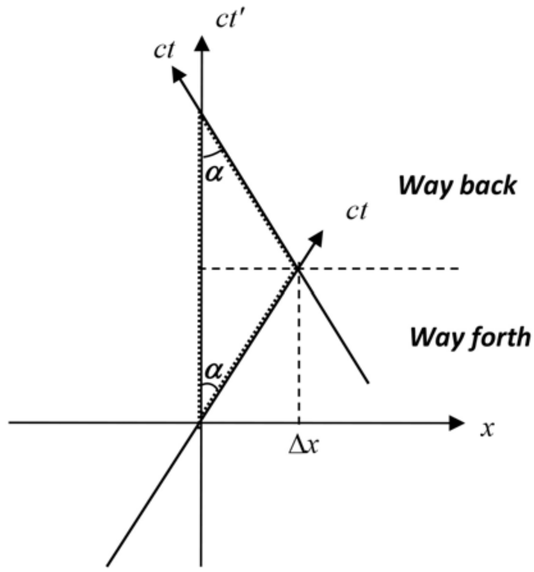

Figure 13. The movement of the traveling brother relative to his twin brother.

4. Discussion and Conclusions

4.1. Comparison with Previous Studies

Many researchers have examined the issue of negative mass, already in 1951, as part of the Gravity Research Foundation. The possibility of negative mass was tested, and how it would behave under gravitational and also other forces [7]. In 2017, researchers at the University of Washington created an inert experimental negative mass by refrigeration of rubidium atoms with lasers, although this was not an entirely real negative mass [8]. In fact, no research has succeeded yet in practice, neither in experiments nor by adequate formulas, to realize or prove the existence of negative mass. The theory here opens thus a door to a new and complete world in physics which will change the laws of physics by showing how a negative mass can be described using the principles of special relativity.

4.2. Summary

It can be seen that the current study provides a solution to a physics problem which encountered nowadays, *i.e.*, that a real body cannot have a negative mass, nor move in a negative space-time. The theory here presents a model which predicts its achievement. Since the model includes a body of a negative mass, forces of repulsion are created between the bodies, and the possibility of creating bodies with negative mass, rejection forces and negative time, which is actually a returning to the past, opens up possibilities and implications in the fields of technology, starting from solving problems, and equations in science, as can be seen in the above description, leading to new inventions of products and processes in many industrial fields. The main results and conclusions are:

1) Each body or particle moves at the speed of light in the fourth dimension, which is the time axis. Each body has a self-speed of light vector of the stationary reference frame $\boldsymbol{C} = (c, 0, 0, 0)$ in the fourth dimension, and a self-speed light vector of the moving Euclidean frame $\boldsymbol{C}' = (v'_t, v'_x, v'_y, v'_z)$. The body has an energy angle a between the two self-speed light vectors of the stationary reference frame and the moving Euclidean frame. When the energy angle is bigger than $\pi/2$, the body mass is negative with negative self-time, and a return to the past becomes possible.

2) Repulsion gravitational forces between bodies, besides the regular attraction forces, can be seen.

3) When the body speed increases, its effective mass decreases.

4) The model solves the Twin Paradox in a simple and easy to understand way.

5) The model describes a method for calculating the amount of energy required to bring a body from a rest state to the speed of light.

6) The model describes a way to calculate energy and momentum, such that in the case of a completely elastic collision, there is no loss of energy as a result of the collision.

7) In the case of a plastic collision, it gives that the energy losses are part of the mass of the two unified bodies.

8) When the energy angle α is equal to $\pi/2$, the speed of the moving body reaches the speed of light and the state kinetic energy is equal to m_0c^2. With greater energy input, the body speed will decrease until the energy angle α reaches π, then the body will be at rest with state kinetic energy of $2m_0c^2$ and self-time energy $(-m_0c^2)$.

The continuation of this study:

9) This model may provide an explanation of how the universe is accelerating and expanding and will avoid the need of the assumption of existence of the dark matter and energy in cosmology.

10) The model may describe the black hole equations in a simpler way.

11) The model may provide more precise formulas even for general relativity.

12) The model will aid research on what happens in quantum physics, and may explain, for example the Heisenberg's uncertainty principle.

Future studies may continue to develop the equations presented in this new model, and may provide experimentally creation of negative mass.

Acknowledgements

To my dear family who believed and supported me for years. To my life teacher Prof. Aharon Peled, who encouraged me and accompanied me all along. Also thanks to Prof. Hashem Zuabi and Dr. David Nir.

Conflicts of Interest

The author declares no conflicts of interest regarding the publication of this paper.

References

[1] Einstein, A. (1905) Zur Elektrodynamik der bewegter Körper. *Ann. Phys.*, **17**, 891. eprint in English (1923) The Principle of Relativity. Dover, New York, 35-65.

[2] Galileo, G. (1967) Dialogue Concerning the Chief World Systems: Ptolemaic and Copernican, Eng. Trans. S. Drake, foreword A. Einstein, 2nd Edition, University of California Press, Berkeley.

[3] Lorentz, H. (1904) *Proc. Acad. Sci.*, **6**, 809.

[4] Minkowski, H. (1909) *Phys. Z.*, **10**, 104.

[5] Rothenstein, B., Popescu, S. and Spix, G.J. (2006) A Brief and Transparent Derivation of Lorentz-Einstein Transformations via Thought Experiments. https://arxiv.org/ftp/physics/papers/0602/0602054.pdf

[6] Minkowski, H. (1908) Space and Time. Cologne Conference, Reprint in English (1923) The Principle of Relativity, Dover, New York, 75-91.

[7] Luttinger, J.M. (1951) On Negative Mass in the Theory of Gravitation. Gravity Research Foundation, University of Wiscosin, Madison, Wis.

[8] Khamehchi, M.A., Hossain, K., Mossman, M.E., Zhang, Y.P., Busch, Th., Forbes, M.M. and Engels, P. (2017) *Physical Review Letters*, **118**, 155301.